

# **Mammalian spermiogenesis and the formation of the sperm head to tail coupling apparatus**

Dissertation  
for the award of the degree  
"Doctor rerum naturalium" (Dr. rer. nat.)  
of the Georg-August-Universität Göttingen

within the doctoral program Biology  
of the Georg-August University School of Science (GAUSS)

submitted by  
**Constanza Tapia Contreras**

from Victoria, Chile

Göttingen, 2021

## **Thesis committee**

Supervisor: Prof. Dr. Sigrid Hoyer-Fender

Department of Developmental Biology - Johann-Friedrich-Blumenbach-Institute of  
Zoology and Anthropology - Georg-August-University of Göttingen

Co-supervisor: Prof. Dr. Rüdiger Behr

Platform Degenerative Diseases

German Primate Center Göttingen

## **Members of the Examination Board**

First reviewer: Prof. Dr. Sigrid Hoyer-Fender

Department of Developmental Biology GZMB - Johann-Friedrich-Blumenbach-Institute of  
Zoology and Anthropology - Georg-August-University of Göttingen

Second reviewer: Prof. Dr. Rüdiger Behr

Platform Degenerative Diseases

German Primate Center Göttingen

Prof. Dr. Ernst Wimmer

Department of Developmental Biology GZMB - Johann-Friedrich-Blumenbach-Institute of  
Zoology and Anthropology - Georg-August-University of Göttingen

Dr. Melina Schuh

Department of Meiosis - Max-Planck-Institute for Biophysical Chemistry

Prof. Dr. Hubertus Jarry

Department of Research Animal Welfare Officer - University Medical Center Göttingen

Prof. Dr. Peter Burfeind

Institute of Human Genetics - University Medical Center Göttingen

Date of the oral examination: 18. 05. 2021

## Declaration

I hereby declare that the Dissertation “Mammalian spermiogenesis and the formation of the sperm head to tail coupling apparatus” was a product of my experimental doctoral project carried out in the Department of Developmental Biology, Georg-August University Göttingen. Further, I confirm that this thesis has been prepared independently and with no other sources and aids than quoted.

Constanza Tapia

Publications that are part of this thesis:

**Tapia Contreras, C. & Hoyer-Fender, S. (2020).** The WD40-protein CFAP52/WDR16 is a centrosome/basal body protein and localizes to the manchette and the flagellum in male germ cells. *Scientific Reports* 10 (1), 14240. <https://doi.org/10.1038/s41598-020-71120-9>

**Tapia Contreras, C. & Hoyer-Fender, S. (2019).** CCDC42 localizes to manchette, HTCA and tail and interacts with ODF1 and ODF2 in the formation of the male germ cell cytoskeleton. *Frontiers in Cell and Developmental Biology*, 7, 151. <https://doi.org/10.3389/fcell.2019.00151>

## **Dedication**

To my Family and Lukas

# Acknowledgment

First and foremost, I would like to express my sincere gratitude to my advisor and mentor, Prof. Dr. Sigrid Hoyer-Fender. I am very grateful to her for giving me the opportunity and allowing me to be her doctoral student. I thank her so much for the valuable scientific training, guidance, encouragement, and assistance throughout my studies, especially for her patience, unconditional support and for being always willing to talk.

Besides my advisor, I would like to thank Prof. Dr. Rüdiger Behr for accepting to be part of my thesis committee, for his help and scientific support. I want to thank Prof. Dr. Ernst Wimmer for letting me be part of the Department of Developmental Biology and providing the scientific environment to carry out this investigation. I am also grateful to Dr. Melina Schuh, Prof. Dr. Ernst Wimmer, Prof. Dr. Hubertus Jarry, and Prof. Dr. Peter Burfeind for taking their time and accepting to be part of my extended committee.

I would like to thank all the people from the Department of Developmental Biology whose assistance was valuable in the fulfillment of this project, including technicians and secretaries. Thanks to Atika, Amel, Diana, Zahra, and Cera for your support and for providing a nice and friendly working atmosphere in our lab. Thanks to Gloribel and Elena for your patience, understanding, advice, and pleasant conversations.

I gratefully acknowledge the scholarship provided by the Chilean National Commission for Scientific and Technological Research (CONICYT), the German Academic Exchange Service (DAAD), and the Department of Developmental Biology, GZMB, Georg-August-Universität Göttingen to undertake my Doctoral degree.

Ich möchte mich auch herzlich bei Frau Frindt bedanken. Vielen Dank dafür, dass Sie an mich geglaubt haben und mir geholfen haben, meine Träume zu erfüllen. "Wo ein Wille ist, ist auch ein Weg". También quisiera agradecer a mi familia, por su amor incondicional. A mis padres Luis y Erika, por darme la vida y estar siempre a mi lado para apoyarme. A mi amado hermano Sebastián, por escucharme, entenderme y siempre recargarme de energía. A mi querida tía Taquitos, por todo su cariño apoyo en cada paso que he dado. A Margarita y abuelitos por su inagotable afecto. Pragnę również podziękować Bogusi i Andrzejowi za przyjęcie mnie w ich domu i za to, że zawsze czuję się jak rodzina. Especialmente quisiera agradecer a Lukas, por todo su amor y apoyo incondicional. Gracias por estar a mi lado, aconsejarme, motivarme y ayudarme a ser la mejor versión de mí misma. Gracias por potenciar cada una de mis habilidades y alentarme a superar mis debilidades. Gracias por ayudarme a ser mejor cada día.

# Table of Contents

List of figures .....	VIII
List of tables .....	X
Abstract .....	1
<b>1. Introduction .....</b>	<b>2</b>
1.1 Mammalian male germ cell differentiation .....	2
1.1.1 Spermatogenesis .....	2
1.1.2 Spermiogenesis .....	3
1.2 The head-tail coupling apparatus, a sophisticated structure that anchors the sperm head to tail .....	6
1.3 Outer dense fiber protein 1 "ODF1" and its role in the formation of the HTCA .....	7
1.4 Centrosome and centrioles during spermatogenesis .....	9
1.5 Overview of the nuclear envelope and LINC complex .....	11
1.6 SUN domain proteins .....	13
1.7 Male infertility due to acephalic spermatozoa syndrome and its genetic etiology .....	16
1.8 Research objectives .....	18
<b>2. Material and methods .....</b>	<b>19</b>
2.1 Material .....	19
2.1.1 Biological material .....	19
2.1.1.1 Bacterial strains .....	19
2.1.1.2 Cell lines .....	19
2.1.2 Vectors .....	19
2.1.3 Oligonucleotides .....	19
2.1.4 Enzymes .....	20
2.1.5 Antibodies .....	21
2.1.5.1 Primary antibodies .....	21
2.1.5.2 Secondary antibodies .....	22
2.1.6 Culture media .....	23
2.1.6.1 Culture media for eukaryotic cells .....	23
2.1.6.2 Culture media for prokaryotic cells .....	23
2.1.7 Buffers and solutions .....	23
2.1.8 Chemicals .....	26

2.1.9 Kits .....	28
2.1.10 Software and web services .....	28
2.2 Methods .....	29
2.2.1. Microbiological methods .....	29
2.2.1.1 Liquid culture of <i>E. coli</i> .....	29
2.2.1.2 Storage of transformed bacteria ( <i>E. coli</i> ) .....	29
2.2.1.3 Transformation .....	29
2.2.2 Molecular biological methods .....	29
2.2.2.1 Plasmid DNA preparation from <i>E.coli</i> .....	29
2.2.2.2 Plasmid construction .....	30
2.2.2.2.1 Subcloning of gene to validate the amber suppression method .....	30
2.2.2.2.2 Subcloning of SUN domain proteins .....	30
2.2.2.2.3 Subcloning of genes for the rapamycin system .....	31
2.2.2.3 Sodium acetate/ethanol DNA precipitation .....	32
2.2.2.4 DNA purification .....	32
2.2.2.5 Measurement of DNA and RNA concentrations .....	32
2.2.2.6 Restriction enzyme digestion of DNA .....	32
2.2.2.7 Vector DNA dephosphorylation .....	33
2.2.2.8 Ligation .....	33
2.2.2.9 DNA sequencing .....	33
2.2.2.10 Total RNA isolation .....	33
2.2.2.11 RNA precipitation .....	33
2.2.2.12 DNase treatment .....	34
2.2.2.13 Phenol: Chloroform DNA/RNA precipitation .....	34
2.2.2.14 cDNA synthesis .....	34
2.2.2.15 RT-PCR .....	34
2.2.2.16 qRT-PCR .....	35
2.2.2.17 PCR .....	35
2.2.2.18 Agarose gel electrophoresis of DNA .....	35
2.2.3 Biochemical methods .....	35
2.2.3.1 Protein extraction from mammalian cells .....	35
2.2.3.2 SDS-Polyacrylamide gel electrophoresis .....	35
2.2.3.3 Western-blot (Immunoblot) .....	36
2.2.3.4 Immunological protein detection .....	36
2.2.3.5 Nitrocellulose membrane stripping .....	37
2.2.3.6 Co-IP (Co-immunoprecipitation) .....	37

2.2.3.7 Crosslinking reaction and harvesting adherent cells .....	37
2.2.4 Cell biological methods .....	38
2.2.4.1 Propagation and subculture of eukaryotic cells .....	38
2.2.4.2 Defrosting and freezing of eukaryotic cells .....	38
2.2.4.3 Transfection .....	38
2.2.4.4 Immunocytology on sperm suspension .....	39
2.2.4.5 Immunocytology .....	39
2.2.5 Generation of <i>Spag4l</i> -deficient mice .....	40
2.2.5.1 Production of the targeting vector .....	40
2.2.5.2 Generation of Sun5 knockout mice .....	40
2.2.5.3 Genomic DNA extraction.....	40
2.2.5.4 Genotyping of mice using PCR .....	41
2.2.5.5 Genotyping of mice using qPCR .....	42
<b>3. Results .....</b>	<b>43</b>
3.1 Mutation screening in patients with acephalic spermatozoon phenotype .....	43
3.1.1 Patients with decapitated spermatozoa carried normal sequence variations of the gene <i>Odf1</i> compared to the reference wild-type sequence .....	44
3.1.2 Patients with decapitated spermatozoa carried normal sequences of exons 10 and 11 of the gene <i>Hook1</i> compared to the reference wild-type sequence.....	47
3.1.3 Patients with decapitated spermatozoa carried normal sequences of exons 6 and 8 of the gene <i>Spag4l</i> compared to the reference wild-type sequence .....	49
3.2 Characterization of the SUN-domain proteins SPAG4 and SPAG4L.....	52
3.2.1 Localization of the SUN domain proteins SPAG4L and SPAG4L2 at the nuclear membrane .....	52
3.2.2 Impact of <i>Spag4</i> - deficiency on gene expression during mouse spermatogenesis .....	57
3.2.3 The amber suppression method and its suitability for the identification of SPAG4 binding proteins .....	60
3.2.4 Reevaluation of the topology of SPAG4 and SPAG4L across the nuclear envelope by drug-induced protein recruitment .....	65
3.3 Generation of <i>Spag4l/Sun5</i> knock out mice .....	72
3.3.1 Genotyping of ES cells .....	72
3.3.2 Genotyping of chimeras .....	75
3.3.3 Genotyping of chimera's offspring .....	75
3.4 Identification of proteins that collaborate in the formation of the HTCA .....	80



3.4.1 CCDC42 localizes to manchette, HTCA and tail and interacts with ODF1 and ODF2 in the formation of the male germ cell cytoskeleton .....	80
3.4.2 The WD40-protein CFAP52/WDR16 is a centrosome/basal body protein and localizes to the manchette and the flagellum in male germ cells .....	98
<b>4. Discussion .....</b>	<b>113</b>
4.1 Relevance and impact of mutations of candidate genes involved in the linkage of sperm tail to its head.....	113
4.2 Topology and localization of SPAG4 and SPAG4L2 at the nuclear membrane might mediate the connection of the sperm nucleus to its tail .....	117
4.3 Identification of proteins that collaborate in the formation of the HTCA.....	121
<b>5. References .....</b>	<b>126</b>
<b>6. Appendix .....</b>	<b>144</b>
6.1 List of Oligonucleotides .....	144
6.2 List of abbreviations .....	149
<b>7. Curriculum vitae .....</b>	<b>153</b>

## List of figures

<b>Figure 1.1.</b> Scheme of spermatogenesis and spermiogenesis in the mouse .....	3
<b>Figure 1.2.</b> Morphogenesis of the spermatozoa during spermiogenesis .....	5
<b>Figure 1.3.</b> Scheme of the neck region and head to tail coupling apparatus (HTCA) .....	7
<b>Figure.1.4</b> Differences of centriolar degeneration in mouse and human .....	11
<b>Figure 1.5.</b> Scheme of the LINC complex .....	13
<b>Figure. 1.6.</b> Schematic localization of human SUN5 mutations .....	15
<b>Figure 3.1.</b> Amino acid sequence alignment of ODF1-exon1 from patient n°17 .....	45
<b>Figure 3.2.</b> Amino acid sequence alignment of ODF1-exon1 from patient n°19 .....	45
<b>Figure 3.3.</b> Amino acid sequence alignment of ODF1-exon2 from patient n°17 .....	46
<b>Figure 3.4.</b> Amino acid sequence alignment of ODF1-exon2 from patient n°19 .....	46
<b>Figure 3.5.</b> DNA sequence alignment of <i>Hook1</i> -exon10 from patient n°17 .....	48
<b>Figure 3.6.</b> DNA sequence alignment of <i>Hook1</i> -exon10 from patient n°19 .....	48
<b>Figure 3.7.</b> DNA sequence alignment of <i>Hook1</i> -exon11 from patient n°17 and 19 .....	49
<b>Figure 3.8.</b> Mutations in TM and coiled-coil domain of the human <i>Spag4l</i> .....	51
<b>Figure 3.9.</b> DNA amplification of exons 6, 8, 11 and 13 of <i>Sun5</i> .....	51
<b>Figure 3.10.</b> DNA sequence alignment of <i>Sun5</i> -exon6 from patient n°17 .....	52
<b>Figure 3.11.</b> DNA sequence alignment of <i>Sun5</i> -exon6 from patient n°19 .....	52
<b>Figure 3.12.</b> Schematic representation of <i>Spag4l2</i> expression plasmids .....	54
<b>Figure 3.13.</b> The protein domain organization of SPAG4L2 and their individual cellular distribution.....	56
<b>Figure 3.14.</b> Schematic representation of the expression of gene markers during spermatogenesis.....	59
<b>Figure 3.15.</b> Gene expression profiling of spermatogenesis marker genes in <i>Spag4</i> -deficient mice .....	60
<b>Figure 3.16.</b> Incorporation of the unnatural amino acid pBpa into LMNC sequences .....	63
<b>Figure 3.17.</b> Evaluation of the amber suppression method by immunoblotting .....	65
<b>Figure 3.18.</b> Schematic representation of the rapamycin system .....	67
<b>Figure 3.19.</b> Rapamycin-induced recruitment of Luciferase-mRFP-FKBP to the nuclear envelope via FRB-ECFP-SUN4 .....	69

<b>Figure 3.20.</b> Rapamycin-induced recruitment of Luciferase-mRFP-FKBP to the nuclear envelope via FRB-ECFP-SPAG4L/SUN5 .....	70
<b>Figure 3.21.</b> Controls for the rapamycin system.....	71
<b>Figure 3.22.</b> Scheme of the <i>Sun5</i> knockout targeting vector .....	72
<b>Figure 3.23.</b> Positive genotyping of ES cells .....	73
<b>Figure 3.24</b> Recombinant Sun5 embryonic stem cells are heterozygous for the wild-type allele .....	74
<b>Figure 3.25.</b> Genotyping of <i>Sun5</i> chimeras .....	75
<b>Figure 3.26.</b> Genotyping of the first generation of <i>Spag4l</i> -deficient mice by nested PCR .....	76
<b>Figure 3.27.</b> Genotyping of the second generation <i>Spag4l</i> -deficient mice.....	77
<b>Figure 3.28.</b> Breeding scheme to generate homozygous-deficient <i>Spag4l</i> <sup>-/-</sup> mice .....	77
<b>Figure 3.29.</b> Relative quantity of exon 7 and 9 of the offspring from heterozygous mice.....	78
<b>Figure 3.30.</b> Genotyping example of the fourth generation .....	79
<b>Figure 4.1.</b> Mapping of HTCA protein interaction network .....	124
<b>Figure 4.2</b> Representative scheme of proteins associated with the HTCA in elongating spermatids.....	125

## List of tables

<b>Table 2.1.</b> Enzymes .....	20
<b>Table 2.2.</b> Primary antibodies .....	21
<b>Table 2.3.</b> Secondary antibodies .....	22
<b>Table 2.4.</b> Culture media for eukaryotic cell culture .....	23
<b>Table 2.5.</b> Culture media for prokaryotic cell culture .....	23
<b>Table 2.6.</b> Buffers and solutions .....	23
<b>Table 2.7.</b> Chemicals .....	26
<b>Table 2.8.</b> Kits .....	28
<b>Table 2.9.</b> Software and services .....	28
<b>Table 2.10.</b> Stacking and separating gel .....	36
<b>Table 2.11.</b> Plasmids and tRNA for UAA incorporation .....	38
<b>Table 2.12.</b> PCR conditions used for genotyping .....	41
<b>Table 2.13.</b> qPCR conditions used for genotyping .....	42
<b>Table 6.1.1</b> Oligonucleotides for mutation screening in patients with acephalic spermatozoon phenotype .....	144
<b>Table 6.1.2</b> Oligonucleotides for RT-PCR in <i>Spag4</i> -deficient mouse .....	145
<b>Table 6.1.3</b> Oligonucleotides for qRT-PCR in <i>Spag4</i> -deficient mouse .....	146
<b>Table 6.1.4</b> Oligonucleotides for amber suppression method .....	146
<b>Table 6.1.5</b> Oligonucleotides for rapamycin system method .....	147
<b>Table 6.1.6</b> Oligonucleotides for <i>Spag4l2</i> investigation .....	147
<b>Table 6.1.7</b> Oligonucleotides for <i>Spag4l2</i> -deficient mice genotyping .....	148
<b>Table 6.1.8</b> Oligonucleotides for qPCR for <i>Spag4l2</i> -deficient mice and ES cells .....	148

## Abstract

The head-tail coupling apparatus (HTCA), also known as connecting piece, provides the physical linkage between the sperm head and its tail. The HTCA morphogenesis initiates during spermiogenesis and is assembled at the posterior area of the spermatid nucleus. The HTCA is built around the proximal and the distal centriole, and consists of the accessory structures, basal plate, capitulum, and segmented columns. These structures are responsible for the tight attachment of the sperm head to the tail, and their disruption leads to acephalic spermatozoa syndrome and male infertility. Thus, the stable connection is essential for moving the sperm nucleus towards the oocyte and successful fertilization. However, its molecular composition is scarcely known.

The outer dense fiber protein 1 (ODF1) is a component of the HTCA and involved in the tight junction of the sperm head to the tail. *Odf1* depletion as well as the partial disruption of *Hook1* and *Spag4l* cause sperm decapitation and male infertility in mice. In humans, however, mutations in these genes remain largely unknown. Thus, the DNA from two patients with the acephalic spermatozoa syndrome was screened for mutations. The screen performed in this study reveals a normal *Odf1* gene sequence. Besides, exons 10 and 11 of *Hook1* and exons 6 and 8 of *Spag4l* were identical to the wild type variant. Therefore, the analyzed regions of the genes *Odf1*, *Hook1*, and *Spag4l* seem not to be implicated in the acephalic syndrome suffered by the two patients here studied.

Beyond that, the interaction between ODF1 and the nuclear membrane protein SPAG4 has been reported as a novel male germ cell-specific linkage complex between the cytoskeletal connecting piece and the nuclear membrane, although their mechanism of interaction is unclear. Thus, the induction of dimerization by rapamycin was explored as a new tool to analyze SUN4 and SUN5 topology. Besides ODF1 or SPAG4 interacting proteins that collaborate in the formation of the HTCA have not been identified. In this study, the coiled-coil domain containing 42 (CCDC42), another essential HTCA component that causes decapitation when missing, and the cilia and flagella associated protein 52 (CFAP52) have been characterized in detail. CCDC42 has been localized to the manchette, perinuclear ring, and tail in male germ cells. CCDC42 interacts biochemically with the outer dense fiber proteins ODF1 and ODF2. These interactions might contribute to the assembly of proteins required for the formation and the stability of the HTCA. CFAP52 localizes to the manchette and sperm tail, indicating that CFAP52 is another promising candidate for the HTCA interacting network.

# 1 Introduction

## 1.1 Mammalian male germ cell differentiation

### 1.1.1 Spermatogenesis

Spermatogenesis is a sophisticated process whereby diploid spermatogonia generate mature haploid spermatozoa. This process consists of three successive phases known as the mitotic or proliferative phase, meiotic phase, and cytodifferentiation phase (Fig. 1.1) (Russell, 1990).

Stem cells multiply during the mitotic phase and undergo differentiation to produce spermatogonia type A. This transformation process continues until spermatogonia type B are generated. Intermediate type B spermatogonia undergo mitosis to give rise to preleptotene spermatocytes (Pl) (Oakberg, 1956; De Rooij & Grootegoed, 1998; Eddy, 1998).

The meiotic phase includes two successive rounds of cell divisions to generate haploid spermatids (Hermo et al., 2010). Spermatocytes undergo two meiotic divisions that include nuclear changes required for chromosome recombination and genetic material exchange. The first meiotic division is characterized by a prolonged prophase which includes leptotene, zygotene, pachytene, diplotene, and diakinesis. Chromatin condensation is initiated during leptotene and is followed by chromosome pairing (synaptonemal complex formation) in zygotene (Clermont, 1972; Russell, 1990). During zygotene-pachytene, the chromosome synapsis is regulated by meiotic proteins of the synaptonemal complex (Meuwissen et al., 1992; Yuan et al., 2000; Costa et al., 2005). After chromosome pairing, homologous chromatids exchange genetic material in pachytene, a process known as crossing-over. Afterward, the synaptonemal complex disintegrates in the diplotene phase. With diakinesis, the first meiotic division is completed, and secondary spermatocytes are generated. Secondary spermatocytes undergo a fast second meiotic division without DNA replication to produce round spermatids (Russell, 1990).

Spermiogenesis, or cytodifferentiation phase, is the final stage of mature spermatozoa production. During this phase, round spermatids experience a dramatic remodeling that includes nuclear shaping and condensation, acrosome and flagellum development, and cytoplasm elimination, which results in a functional spermatozoon (Russell, 1990).

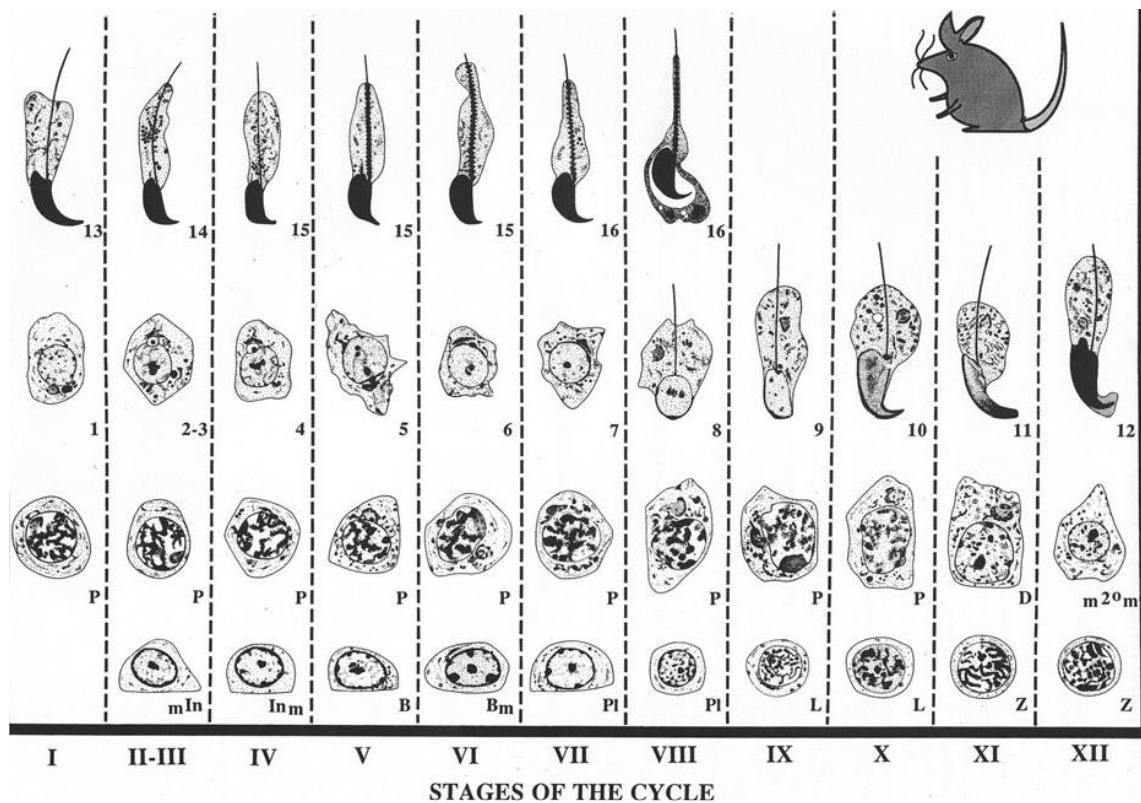


**Figure 1.1** Scheme of spermatogenesis and spermiogenesis in the mouse.  $m^{In}$  (mitosis of intermediate spermatogonia),  $^{In}m$  (intermediate spermatogonia), B (spermatogonia),  $Bm$  (mitosis of spermatogonia), Pl (preleptotene), L (leptotene), Z (zygotene), (P (pachytene), D (diplotene),  $m^{2o}m$  (second meiotic division), 1–8 (round spermatids), 9–11 (elongating spermatids), 16 (late spermatids) (Russell, 1990).

### 1.1.2 Spermiogenesis

Spermiogenesis is the last phase of spermatogenesis, where round spermatids experience a total transformation to evolve into mature spermatozoa (Clermont, 1972). This process starts with the acrosome development which consists of four stages: (1) Golgi phase, (2) cap phase, (3) acrosome phase, and (4) maturation phase. During the Golgi phase (Fig.1.2-A), the Golgi apparatus produces several proacrosomal vesicles. The fusion of these vesicles forms the acrosomal vesicle that afterward attaches to the nuclear envelope by the acroplaxome plate. Moreover, in the first phase of the acrosome development, centrioles localize close to the Golgi apparatus. However, centrioles migrate to the caudal area of spermatids during the Golgi phase, being opposite to the acrosome. Thus, acrosome and centrioles establish the bipolarity of the nucleus (Hermo et al., 2009b; Chemes, 2012). Further, the proximal centriole attaches to the nucleus, articulating the implantation fossa and forming the connecting piece. On the other hand, the distal centriole gives rise to the basal body and initiates the formation of the axoneme (Fawcett, 1975; Chemes & Rawe, 2010; Hoyer-Fender, 2012).

Afterward, during the cap phase (Fig. 1.2-B) the acrosome increases in size and moves anteriorly. The development of the manchette characterizes the acrosomal phase (Fig. 1.2-C). This transient microtubular structure evolves from the perinuclear ring situated in the caudal area of the acrosome-acroplaxome complex (Rattner & Olson, 1973). The manchette extends its microtubules longitudinally to the elongating spermatid. This transient structure provides a platform for intramanchette transport (IMT), where molecular motors transport essential proteins to develop the flagellum. In the late stages of spermiogenesis, the manchette disassembles (MacKinnon et al., 1973; Kierszenbaum et al., 2003; Kierszenbaum & Tres, 2004; O'Donnell & O'Bryan, 2014).

During the maturation phase (Fig. 1.2-D), the manchette disintegrates, and the sperm nucleus condensates by compaction of the chromatin. During condensation, histone and nonhistone proteins are replaced first by transition proteins, which are finally replaced by protamines. Once spermatids have reduced their volume, the excess of cytoplasm (residual body) is eliminated. The residual cytoplasm is phagocytized and digested by the Sertoli cells (Balhorn, 1982; Russell, 1990).

At the end of the maturation phase, spermatozoa are completely formed and are composed of two main structures: the head and the tail. The flagellum is constituted by the axoneme, a central microtubular structure (9+2 arrangement), and is further subdivided into the middle, the principal, and the end piece. The axoneme in the flagellum is encompassed by outer dense fibers (ODFs), which in turn are covered by mitochondria in the midpiece. The principal piece is composed of ODFs, which are surrounded by a fibrous sheath (Russell, 1990; O'Donnell & O'Bryan, 2014). ODFs are responsible for protecting the sperm tail from tensile forces during epididymal passage and ejaculation (Baltz et al., 1990a; Lindemann, 1996).



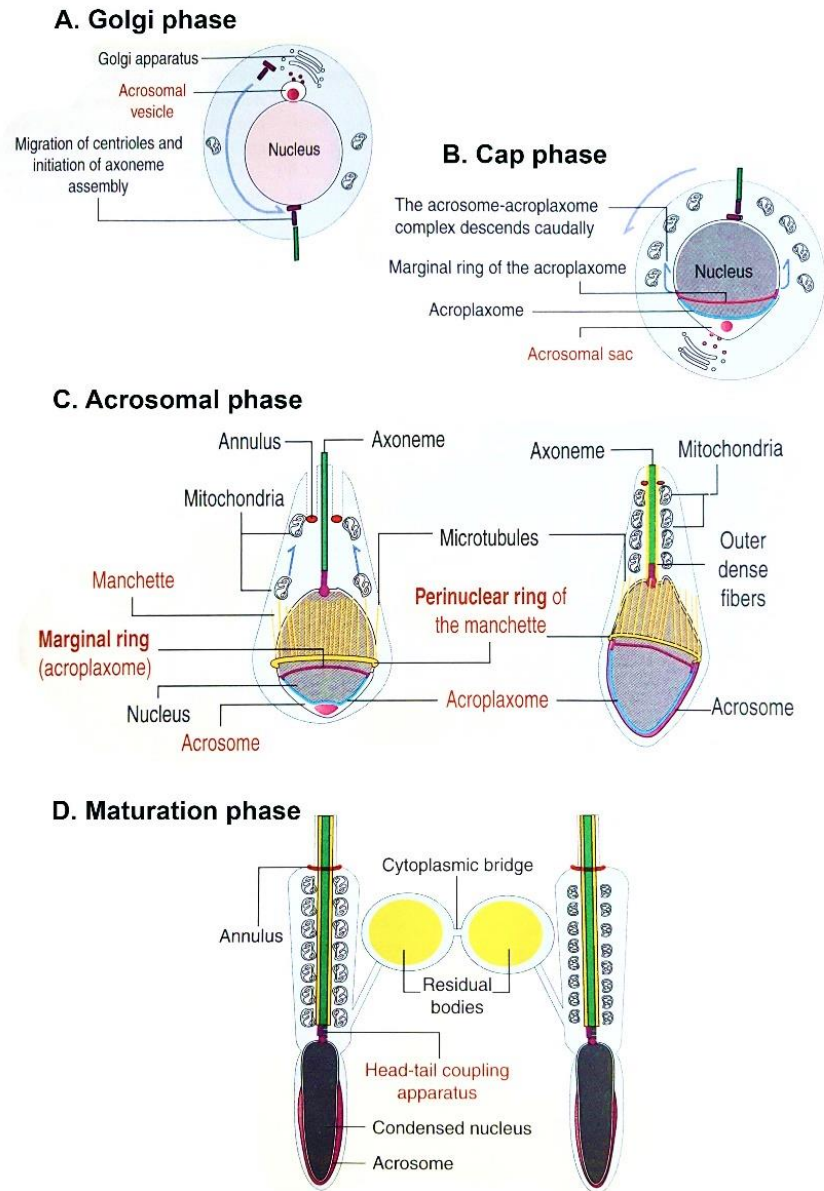


**Figure 1.2. Morphogenesis of the spermatozoa during spermiogenesis.** (A) Golgi phase: Golgi apparatus gives rise to proacrosomal granules, which are transported to the acrosomal vesicle. Centrioles migrate to the caudal area of the nucleus and initiate the axoneme assembly. (B) Cap phase: the acrosome starts to descend to the caudal area and increases its size. (C) Acrosomal phase: the acrosome attaches to the acroplaxome, and the manchette extends its microtubules. Outer dense fibers and mitochondria are aligned around the axoneme. (D) Maturation phase: chromatin is condensed by replacement of transition proteins, manchette is disintegrated, and residual bodies are eliminated (adapted from *Histology and Cell Biology: An Introduction to Pathology* - 4th Edition, ©2016.)

## **1.2 The head-tail coupling apparatus, a sophisticated structure that anchors the sperm head to tail.**

The head-tail coupling apparatus (HTCA), also known as the connecting piece or neckpiece, is a sophisticated structure that anchors the head to the tail in sperm. The HTCA consists of sperm centrioles and several proteins that contribute to building a tight connection between the head and flagellum (Chemes & Rawe, 2010). The connecting piece, a complex dense structure is placed near to centrioles. It starts to organize in striated longitudinal columns and assemble the capitulum (Fawcett & Phillips, 1969). The capitulum is a curved shape structure that conforms to the concavity of the basal plate. Although a narrow space separates both structures, they are bridged by fine filaments. The basal plate further establishes a shallow concave area in the posterior pole of the nucleus, denominated implantation fossa (Fawcett, 1975). In this place, the implantation fossa is in contact with the capitulum, segmented columns of the neckpiece, and the proximal centriole. Thus, these structures assemble the attachment of the sperm head to the tail (Fig. 1.3) (Chemes et al., 1999).

The proper assembly of the HTCA in sperm is required to fertilize oocytes successfully. Therefore, abnormalities in the HTCA lead to acephalic spermatozoa syndrome (Perotti et al., 1981; Chemes et al., 1987). Studies in patients with headless spermatozoa evidence different abnormalities in the head-tail junction, inter alia, loss of the implantation fossa, basal plate, and the presence of nuclear envelope-derived vesicle in the caudal pole. Hence, alterations in these structures lead to either fragility or the total disruption of the tight head-tail conjunction (Baccetti et al., 1989; Chemes et al., 1999; Toyama et al., 2000). Nonetheless, a deeper characterization and comprehension of the morphological and molecular components of the HTCA remains to be elucidated.

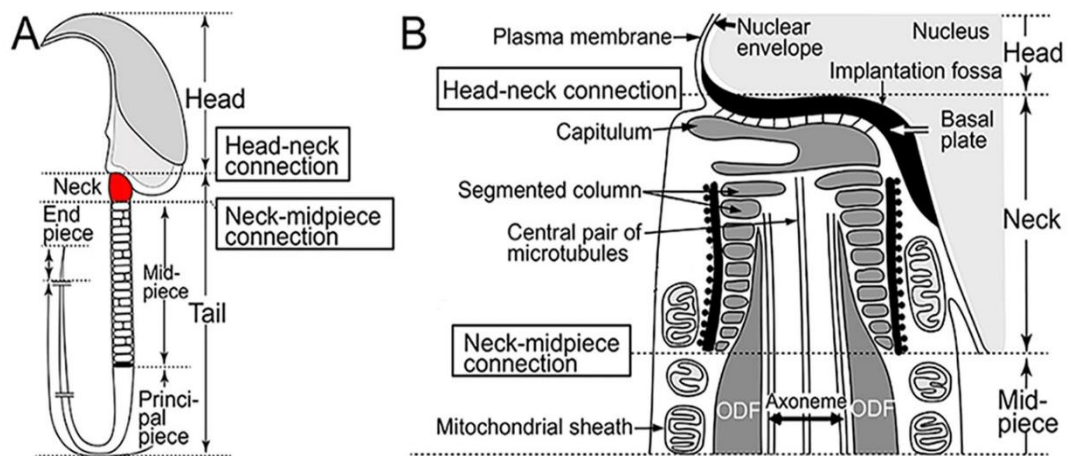


**Figure 1.3. Scheme of the neck region and head to tail coupling apparatus (HTCA).** (A) Neck localization in a mature spermatozoon. (B) A detailed description of the neck components and HTCA. The implantation fossa is a shallow concave area formed by the basal plate in the caudal area of the nucleus. The HTCA structure includes the basal plate that is attached to the capitulum, centrosome and segmented columns connected to the outer dense fibers (ODFs). ODFs are surrounded by the mitochondrial sheath (adapted from Ito et al., 2019).

### 1.3 Outer dense fiber protein 1 "ODF1" and its role in the formation of the HTCA

The sperm flagellum arises from the distal centriole at the posterior region of the nucleus. The centriole gives rise to the axoneme, which consists of two central microtubules surrounded by nine doublet microtubules. In the mid-piece, the axoneme is surrounded by nine outer dense fibers (ODFs). Additionally, the connecting piece and segmented columns are continuous to the capitulum, whereas their posterior area overlaps with the nine ODFs. ODFs in the mature flagellum extend through almost all the length of the principal piece (Fawcett, 1975). Outer dense fibers are indispensable for flagellar movements because they provide elastic recoil and further protection against shearing forces during epididymal transport and ejaculation (Baltz et al., 1990). Moreover, they provide force transmission to the flagellar base during the axonemal beat (Lindemann, 1996).

ODFs are composed of around 14 polypeptides; however, few of them have been described (Vera et al., 1984; Oko, 1988; Petersen, 1999). ODF1 is a spermatid-specific protein of ~27 kDa. It consists of an NH<sub>2</sub>-terminal, which enables self-interaction, and a highly conserved COOH-terminal. The N-terminal domain contains a putative leucine zipper dimerization motif, whereas the C-terminal comprises a high content of cysteine and proline as a repetitive tripeptide

motif CXP (van der Hoorn et al., 1990; Burfeind & Hoyer-Fender, 1991; Morales et al., 1994; Shao & van der Hoorn, 1996). However, the CXP motif variability is not responsible for male infertility in humans (Hofferbert et al., 1993).

ODF1 shares structural features with small heat shock proteins (sHSPs), particularly with the conserved  $\alpha$ -crystalline domain being named HSPB10 for this reason (Fontaine et al., 2003). ODF1/HSPB10 is restricted to the testis and its expression is first detectable in the round spermatid stage (Burmester & Hoyer-Fender, 1996). Given that ODF1 localizes in the sperm connecting piece, this protein acquires relevance regarding its role in the HTCA stability, the formation of the sperm tail, and male fertility. The depletion of ODF1 in mice results in male infertility because of several abnormalities of the HTCA. These disorders include the abnormal structural organization of mitochondrial sheath and ODFs, and destabilization of the connection between the nuclear membrane and capitulum by incrementing their distance, resulting in sperm decapitation. Thus, ODF1 ablation severely affects the stability of the connecting piece and may also cause human male infertility (Yang et al., 2012; 2014).

Although ODF1 is an essential component of the connecting piece, few ODF1 interacting proteins have been identified. ODF1 can self-associate due to its leucine zipper motif in the N-terminal region, albeit this interaction is fragile (Shao & van der Hoorn, 1996). Beyond that, ODF1 leucine zipper enables its interaction with a major ODF protein of the sperm tail accessory fibers, the outer dense fiber protein 2 (ODF2) (Shao et al., 1997). ODF1 and ODF2 reside in the head-connecting piece complex. Therefore, the presence of these two proteins in the connecting piece might be involved in the stable junction of the head to tail in sperm (Schalles et al., 1998).

The stable linkage between the nucleus to the sperm tail is mediated by the HTCA, which is supported by several molecular components that are still unknown. This linkage seems to be assisted by the SUN domain proteins, which tether the centrosome to the nuclear membrane (Malone et al., 2003). The SUN domain protein SPAG4 localizes in the posterior pole of the sperm head in round and elongating spermatids and seems to interact with ODF1 (Shao et al., 1999; Kierszenbaum & Tres, 2002; Pasch et al., 2015). Nevertheless, the disruption of ODF1 does not affect the localization of SPAG4. Although SPAG4 is an essential component for the proper sperm head formation, manchette assembly, and male fertility, its disruption does not prevent the HTCA formation in mice. However, SPAG4 is required for the attachment of the connecting piece to the nucleus. The interaction of ODF1 and SPAG4 may mediate the head-tail connection. In this scenario, the nuclear membrane protein SPAG4, which resides at the posterior pole of spermatids, interacts with ODF1 that localizes in the basal plate and capitulum.

Thus, SPAG4 might recruit ODF1 to the nuclear membrane and arrange the tight linkage of the sperm head to the tail (Calvi et al., 2015; Pasch et al., 2015; Yang et al., 2018). Likewise, the SUN domain protein SPAG4L is expressed in elongating spermatids and strongly associated with the ODF1 leucine zipper (Shao et al., 2001; Fitzgerald et al., 2006). However, the interaction of ODF1 with the SUN domain proteins remains to be investigated.

Furthermore, additional ODF1 interacting proteins might participate in the linkage of the sperm head and tail, inter alia, KLC3 (kinesin light chain 3), which resides in the midpiece of the sperm tail, and OIPI, a member of the RING finger family (Bhullar et al., 2003; Zarsky et al., 2003). Besides that, the coiled-coil domain containing 42 (CCDC42) has a reported function in the HTCA and sperm flagellum development. Mice lacking *Ccdc42* display an abnormal HTCA conformation, prevent sperm flagella formation, and suffer from male infertility (Pasek et al., 2016). Therefore, CCDC42 is an ideal candidate to evaluate its participation in the physical linkage of the sperm head to the tail.

#### **1.4 Centrosome and centrioles during spermatogenesis**

The centrosome is the main microtubule-organizing center (MTOC) and is responsible for generating the mitotic spindle during cell division. It consists of two small organelles, known as centrioles, embedded in a dense pericentriolar matrix (PCM). The PCM is composed of several proteins, although the most abundant components are  $\gamma$ -tubulin and pericentrin (Kellogg et al., 1994; Bornens, 2002; Łuksza et al., 2013).

The centrosome is an example of semi-conservative segregation (Kochanski & Borisy, 1990). Duplication starts in the transition phase G1, where each cell contains a centrosome consisting of two centrioles. This process finishes with the separation of the two centrosomes and their associated PCM. Each centrosome contains a pair of centrioles that consist of a mature or mother centriole and a young or daughter centriole (Urbani & Stearns, 1999; Zimmerman et al., 1999).

Centrioles are short cylindrical structures with  $\sim 0.5 \mu\text{m}$  in length and  $0.2 \mu\text{m}$  in diameter perpendicularly oriented to each other. They are mostly built from  $\alpha$ - and  $\beta$ -tubulin and exhibit an organized structure of nine microtubule triplets with a proximal, middle, and distal tubule (Vorobjev & Chentsov, 1980; Urbani & Stearns, 1999).

The mature or mother centriole consists of distal and subdistal appendages (Vorobjev & Chentsov, 1982; Alvey, 1985; Hoyer-Fender, 2010). The mature centriole in eukaryotic cells

becomes the basal body, which localizes at the base of cilia and flagella (Kellogg et al., 1994; Urbani & Stearns, 1999). In male germinal cells, the centriolar pair migrate from the Golgi apparatus region to the distal pole of the nucleus. There, the proximal centriole participates in the formation of the connecting piece and the anchorage of the sperm nucleus and its tail, whereas the distal centriole acts as a basal body and gives rise to the axoneme (Fawcett & Phillips, 1969; Chemes & Rawe, 2010).

During spermiogenesis, the pericentriolar material (PCM) is remodeled and replaced by striated columns and the capitulum, which connect the sperm head to the tail. The proximal and distal centrioles attach to the nucleus via the HTCA. The proximal centriole is tightly connected with the capitulum, whereas the distal centriole initiates the axoneme formation. In turn, the striated columns connect with the nine outer dense fibers at the lower portion of the neck region (Fawcett & Phillips, 1969; Iwashita & Oura, 1980). During this process the distal centriole that gives rise to the axoneme disintegrates, whereas the proximal centriole goes through a reduction process. The reduction process varies between species. In mice both centrioles are disintegrated, whereas in humans and rhesus monkeys centrosome degeneration is partial (Fig. 1.4) (Schatten et al., 1986; Manandhar & Schatten, 2000).

During the proximal centriole reduction some centriolar proteins are dismissed (Schatten et al., 1986; Manandhar et al., 1998). However, further proteins have been localized in the connecting piece, inter alia, Centrobin, SPATA6, and SPAG4. Beyond that, the depletion of these proteins severely affects the HTCA, and hence they are directly related to the acephalic spermatozoa syndrome (Liška et al., 2009; Yassine et al., 2015; Yuan et al., 2015; Shang et al., 2017; Yang et al., 2018). Therefore, these proteins play an essential role in the development and stabilization of the HTCA. Furthermore, disturbances in the formation of the HTCA are observed, derived from the misalignment or unsuccessful attachment of centrioles to the spermatid nucleus. Besides that, centrosomal defects might interfere with the success of assisted reproduction. In intracytoplasmic sperm injection (ICSI), the sperm is microinjected into the oocyte. However, the microinjection of a sperm with a faulty centriole affects early embryonic development and implantation.

Moreover, centriolar defects may have a genetic cause inherited to the progeny causing male infertility later on. Thus, centriolar impairment seriously affects HTCA stability and weakens the linkage of the sperm head to tail, causing detachment. The sperm head-to-tail linkage comprises centrioles and connecting piece. In some cases of male infertility, decapitated spermatozoa are produced by abnormalities in sperm structure. These include malformation of the midpiece, absence of the implantation fossa or basal plate (Kamal et al., 1999). The

remodeling process of male germ cells during spermiogenesis includes centrosome reduction and protein redistribution. The pericentriolar material surrounding centrioles is transformed into the capitulum and striated columns (Avidor-Reiss et al., 2019). These structures contain specific proteins such as SPATA6, essential for the head-to-tail junction (Yuan et al., 2015). However, the set of proteins involved in the HTCA formation remain to be identified. Abnormalities of the mid-piece in sperm could affect fertilization potential and impair the embryo development after intracytoplasmic sperm injection (Kamal et al., 1999). Hence, identifying the molecular components of the HTCA is of great significance for the development of new diagnostic tools and the treatment of patients with acephalic spermatozoa (Simerly et al., 1995; Schatten & Sun, 2009; Chemes, 2012).

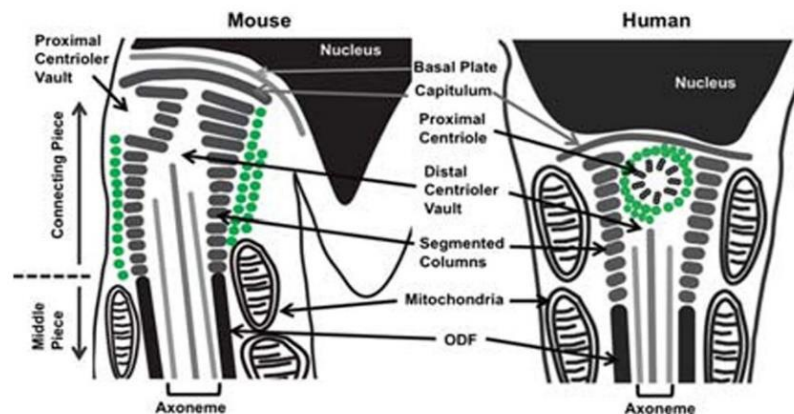


**Figure 1.4 Differences of centriolar degeneration in mice and humans.** In mice, distal and proximal centrioles degenerate, and this area is occupied by dense material. The centriolar vault is surrounded by segmented columns and in the posterior area of the distal vault, the axoneme emerges, which is surrounded by ODFs. In humans and rhesus monkeys only the distal centriole disassembles. The proximal centriole is in close contact with the capitulum and is associated with striated columns. The distal centriole gives rise to the axoneme, which is surrounded by ODFs (Image from Goto et al., 2010).

## 1.5 Overview of the nuclear envelope and the LINC complex

The nuclear envelope is a selective barrier responsible for separating the nucleus from the cytoplasm. It is constituted by an inner and an outer membrane (INM, ONM), enclosing the perinuclear space (PNS). The INM and ONM are fused at the nuclear pores, which are responsible for mediating the traffic of molecules between the cytoplasm and the nucleus (Kite, 1913; Watson, 1955; Gerace & Burke, 1988). The INM is predominantly associated with lamins type A and B, and is involved in chromatin organization. The genes *Lmna*, *Lmnb1*, and *Lmnb2*,

encode lamins. *Lmna* encodes, by alternative splicing, the principal isoforms A and C. *Lmnb1* encodes lamin B1, whereas *Lmnb2* gives rise to the isoforms B2 and B3. Lamin A/C is expressed in later somatic cell differentiation stages, whereas lamins B3 and C2 are shorter splicing variants expressed exclusively in the early stages of spermatogenesis. Furthermore, lamin C2 is exclusively expressed in spermatocytes while lamin B3 is spermatid specific (Watson, 1955; Rober et al., 1989; Furukawa & Hotta, 1993; Alsheimer & Benavente, 1996; Alsheimer et al., 2000; Burke & Stewart, 2002, 2013; Schütz et al., 2005).

On the cytoplasmic side, the ONM is connected to the endoplasmic reticulum (ER). The ONM is characterized by its high content of integral membrane proteins, inter alia, KASH domain proteins (Klarsicht, ANC-1, and Syne homology) that mediate the linkage of the cytoskeleton and the nucleoskeleton (LINC) via interaction with the conserved SUN domain proteins (Watson, 1955; Burke & Stewart, 2002; Zhen et al., 2002; Schirmer et al., 2003; Starr, 2003; Starr & Fridolfsson, 2010).

SUN domain proteins are highly conserved and span the inner nuclear membrane. Their N-terminal region is oriented to the nucleoplasm and interacts with lamins. Their C-terminal region, which contains the SUN domain, interacts with KASH domain proteins in the PNS. Thus, the interaction of SUN-KASH domain proteins forms the LINC complex (Fig. 1.5) (Malone et al., 1999; Burke & Stewart, 2002; Crisp et al., 2006; Starr & Fridolfsson, 2010).

The LINC complex is constituted by the association of several proteins, which include not only SUN and KASH proteins (NESPRIN1/2 and Emerin) but also microtubules, actin filaments, lamins A/C, and chromatin (Starr, 2003; Crisp et al., 2006; Tzur et al., 2006; Wilhelmsen et al., 2006). Emerin resides in large part in the INM, whereas a small fraction localizes in the ONM. It is responsible for binding centrosomes to the ONM via microtubules (Salpingidou et al., 2007).

Besides that, centrosome attachment to the nucleus is mediated by the SUN-KASH complex. The centrosomal and nuclear protein ZYG-12 is a member of the HOOK protein family, which are cytosolic coiled-coil proteins, and mediate the binding to organelles and microtubules. ZYG-12 has been described in *C. elegans* and was characterized as a type II ONM protein. ZYG-12 is recruited to the nuclear envelope by SUN1. Thus, ZYG-12 interacts with SUN1 in the PNS, collaborating in the proper junction of the centrosome to the nucleus. Furthermore, *zyg-12* gene mutations are harmful by disturbing the nucleus to the centrosome junction, affecting the mitotic spindles and DNA segregation (Malone et al., 2003; Minn et al., 2009).



Thus, the SUN-KASH protein complex plays an essential role in diverse cellular processes, inter alia, linking nuclear components to the cytoskeleton, mediating chromosome movements in *S.pombe*, and affecting the migration and location of the nucleus. Further, it mediates the centrosome binding to the nucleus in *C. elegans* (Malone et al., 2003; Starr & Han, 2003; Wilhelmsen et al., 2006; Chikashige et al., 2007).

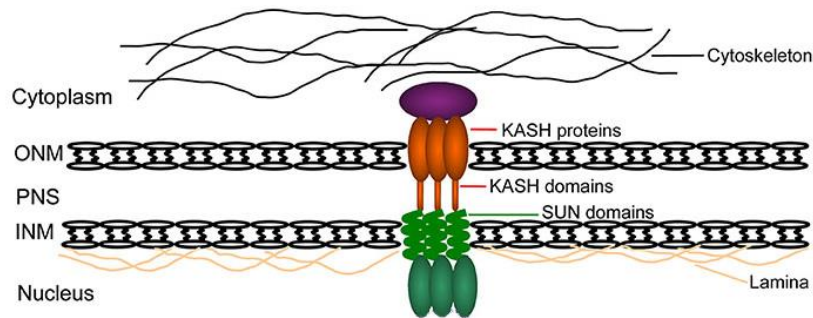


**Figure 1.5. Scheme of the LINC complex.** The N-terminal region of the SUN domain proteins spans the INM, whereas the C-terminal region containing the SUN domain resides in the perinuclear space (PNS). KASH domain proteins span the ONM and interact with the SUN domain in the PNS, forming the LINC complex that connects the cytoplasm with the nucleoplasm (adapted from Zeng et al., 2018).

## 1.6 SUN domain proteins

SUN domain proteins were first described in *Caenorhabditis elegans unc-84*, which are involved in nuclear migration. Thereafter, *sad-1* was described in *S. pombe*. Hence, the comparison between the C-terminal region of UNC-84, Sad1, and human proteins SUN1 and SUN2 revealed the homology of this region defining the name of SUN domain proteins from Sad1 and UNC-84 (Horvitz & Sulston, 1980; Hagan & Yanagida, 1995; Malone et al., 1999).

SUN domain proteins share a common structure which consists of an N-terminal region containing up to three transmembrane domains (TMs), a middle part with up to two coiled-coil regions, and a C-terminal region that contains the conserved SUN domain (Crisp et al., 2006; Haque et al., 2006). The N-terminal region extends into the nucleoplasm, whereas the conserved C-terminal of the SUN domain proteins reside in the perinuclear space (Hodzic et al., 2004; Crisp et al., 2006).

The conserved SUN domain proteins play several roles in different organisms, such as spindle architecture, interaction with lamins, telomere anchorage to the nuclear envelope during meiotic

movements in mice as well as in *S. cerevisiae*. Furthermore, SUN proteins mediate the centrosomal attachment to the nucleus in *C. elegans* (Malone et al., 2003; Conrad et al., 2007; Ding et al., 2007; Schmitt et al., 2007).

In mammals, the SUN domain proteins are encoded by a minimum of five genes (Liu et al., 2007). *Sun1* and *Sun2* are widely expressed in several tissues, and they are crucial in the connection of the cytoskeleton to the nucleoskeleton through giant nesprin and lamins (Hodzic et al., 2004; Padmakumar, 2005; Crisp et al., 2006; Wang et al., 2006). In contrast, SUNC1/SUN3, SPAG4/SUN4, and SPAG4L/SUN5 are expressed predominantly in testes (Göb et al., 2010; Frohnert et al., 2011).

SUN3 is a transmembrane protein with the same topological organization as other SUN domain members. It is expressed in the late stages of spermiogenesis and colocalizes with lamin B3 and lap2 at the posterior pole of spermatids. Moreover, SUN3 overlaps with the manchette in elongating spermatids (Crisp et al., 2006; Göb et al., 2010).

*Spag4*, also known as *Sun4*, is spermiogenesis specific and starts its transcription in round spermatids. During spermiogenesis, SPAG4 exhibits an initial expression in round spermatids where it localizes in the nuclear envelope as well as SUN3 and Nesprin1. Afterward, in elongating spermatids, SPAG4 colocalizes with the transient microtubular manchette. In contrast, in the late stages of spermiogenesis, SPAG4 migrates to the distal pole of the sperm nucleus, specifically where the sperm tail is inserted. Moreover, *Spag4*-deficient mice suffer from severe defects in the manchette structure, chromatin condensation, and sperm head shaping (Calvi et al., 2015; Pasch et al., 2015). Furthermore, *Spag4*-deficiency affects the correct arrangement and docking of the manchette to the spermatid nucleus, perturbs the HTCA tightness by altering the proper junction of the basal plate to the implantation fossa (Yang et al., 2018). Thus, SPAG4 is part of the complex protein network organization that bridges the nucleus to the sperm tail.

*Spag4l*, also called *Sun5*, is highly expressed in testis. The gene SRG4 encodes SUN5 in mouse and its transcription is related to round spermatids (Xing et al., 2004). *Spag4l* and *Spag4l2* are two splice variants of the gene *Sun5*, which differ in 25 amino acids at the N-terminal region. SPAG4L has one transmembrane domain, whereas the longer isoform, SPAG4L2, contains two transmembrane domains at the N-terminus. Although SUN5 was first described to be associated with the apical nuclear envelope of round spermatids facing the acrosome (Frohnert et al., 2011), later analysis revealed that SUN5 resides at the head-to-tail coupling apparatus in mature spermatozoa (Yassine et al., 2015). Moreover, the partial deletion of *Sun5*-gene affects the

HTCA development in mice and causes male infertility due to globozoospermia (Shang et al., 2017).

Furthermore, studies in male patients have identified 12 mutations in the *Sun5*-gene (Fig. 1.6). Zhu et al. (2016) predicted that *Sun5* mutations might cause the acephalic spermatozoa syndrome due to LINC complex alterations. The LINC complex is formed by the interaction of SUN domain proteins with cytoskeletal proteins. Thus, mutations in the SUN domain, as p.Val261Met, p.Thr275Met, p.Ser284, p.Asn348Ile, and p.Arg356Cys, may severely affect their ability to interact with their counterparts. Further, mutations that affect the coiled-coil domain (c.425+1G>A, p.(Leu143Serfs\*30), p.Arg159\*, p.Met162Lys) and the transmembrane domain (p.Gly114Arg and p.Val128Serfs\*7) might disrupt SUN5 localization at the nuclear envelope. Computational prediction and ectopic expression of *Sun5* containing the p.Gly114Arg mutation has shown that the SUN5 protein is not restricted to the NE but also distributes to the cytosol. Moreover, p.Gly114Arg mutation inhibits exon 5 splicing and is responsible for the production of acephalic spermatozoa in humans, whereas the frameshift p.(Leu143Serfs\*30) deletes 5090 base pairs, which includes exon 8 (Elkhatib et al., 2017). Besides that, the mutation p.Arg159\* (c.475C>T) leads to an earlier stop codon that truncates the coiled-coil domain and restrains the transcription of the SUN domain. This mutation is inherited paternally and increases decapitated spermatozoa formation (Shang et al., 2018). (Nomenclature: prefix “p” indicates amino acid change; “c” indicates coding DNA sequence; asterisk indicates translation termination stop-codon)

Among all SUN domain proteins, SUN5 seems to be responsible for the tight linkage of the head to the tail in sperm. *Sun5* impairments may disrupt the LINC complex and thereby be responsible for causing the acephalic spermatozoa syndrome.

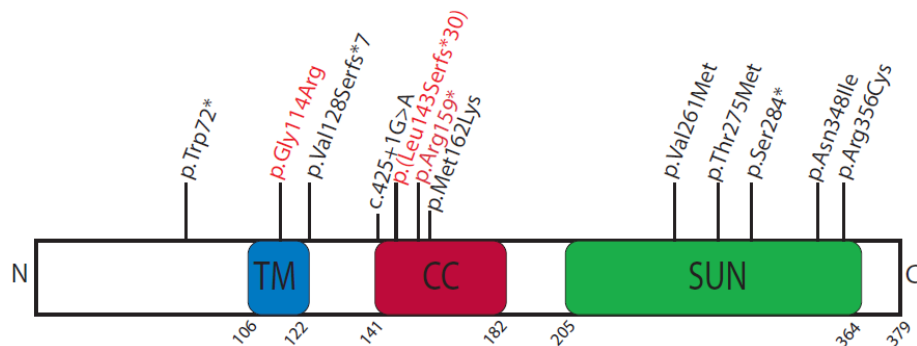


**Figure. 1.6. Schematic localization of human SUN5 mutations.** Transmembrane domain (TM) (blue), coiled-coil domain (red), and SUN domain (green) (adapted from Zhu et al., 2016; Shang et al., 2018).

## 1.7 Male infertility due to acephalic spermatozoa syndrome and its genetic etiology

Several morphological abnormalities of the spermatozoa could cause male infertility. These abnormalities include sperm flagella disorders, impairment in head-neck attachment, irregular acrosome development, and chromatin condensation (Chemes & Rawe, 2003).

In the present work, I focused my attention on abnormalities of the HTCA caused by several defects in the connecting piece and centrioles formation. These aberrations produce acephalic or pinhead spermatozoa, a type of human teratozoospermia (TZI) (WHO, 2010; Chemes & Alvarez Sedo, 2012). HTCA abnormalities lead to a fragile head-tail junction or may severely cause spermatozoa decapitation. Ultra-structural analyses have indicated that the instability of the linkage of the connecting piece to the sperm nucleus caused abnormal alignment of the sperm head to the midpiece. This disorder includes an irregular formation of the basal plate, implantation fossa, and the inability of the proximal centriole to migrate to the posterior area of the sperm nucleus. The proximal centriole attaches to the spermatid nucleus. However, its dysfunction affects its physical contact with the nucleus and causes the separation of sperm head and tail (Chemes et al., 1999; Chemes & Rawe, 2010; Yang et al., 2018). Thus, centriolar and connecting piece dysfunctions seem to have a genetic etiology in humans (Baccetti et al., 1989; Chemes et al., 1999). Yet, molecular components of the HTCA have been scarcely characterized. In humans, solely the gene *Sun5* has been identified to be responsible for the acephalic spermatozoa syndrome. However, in mice models, several genes have been reported to be involved in the head-tail junction, inter alia, *Prss21*, *Oaz3*, *Cntrob*, *Ift88*, *Spata6*, *Odf1*, *Hook1*, *Arl3*, *RIM-BP3*, and *Sun5* (Mendoza-Lujambio, 2002; Netzel-Arnett et al., 2009; Tokuhiro et al., 2009; Zhou et al., 2009; Liška et al., 2013; Qi et al., 2013; Yuan et al., 2015; Zhu et al., 2016).

In mice, the proteins Centrobin (encoded by *Cntrob*), Ift88, RIMBP3, and HOOK1 localize in the manchette, and their disruption affects spermatid elongation. Centrobin resides at the marginal ring of the spermatid acroplaxome, manchette, and HTCA. In mice, the disruption of *Cntrob* affects the manchette assembly and the intramanchette transport, which is responsible for transporting proteins to the HTCA and tail formation. Thus, Centrobin depletion affects the attachment of the HTCA and implantation fossa contributing to sperm decapitation (Liška et al., 2009). Likewise, the intra-flagellar transport protein IFT88 is involved in the formation of the acrosome-acroplaxome complex, HTCA, and the spermatid tail. *Ift88*-disruption affects the intramanchette transport inhibiting the tail development in spermatids (Kierszenbaum et al., 2011).

RIM-BP3 localizes in the manchette of developing spermatids and the gene disruption severely affects the acrosome, acroplaxome, manchette, and nucleus. Moreover, RIM-BP3 interacts with HOOK1, which resides in the manchette (Zhou et al., 2009). HOOK1 belongs to the conserved HOOK protein family, which has a highly conserved NH<sub>2</sub> domain, a coiled-coil domain in the middle part, and a C-terminal domain. These domains are responsible for binding microtubules, promoting the interaction with other proteins, and binding organelles. Moreover, HOOK1 mediates the manchette connection to the nuclear envelope through its C-terminal region. Thus, the truncation of HOOK1 in mice causes abnormal spermatozoon head shape (*azh*) and male infertility (Walenta et al., 2001; Mendoza-Lujambio, 2002).

The proteins PRSS21, OAZ3, SPAT6, and ODF1 contribute to the connection of the head to the tail in sperm and their disruption is related either with a weak connecting piece or total sperm decapitation. Mice lacking PRSS21 (Glycosylphosphatidylinositol-Anchored Serine Protease) demonstrate spermatozoa with abnormal curled tails, decreased motility, abnormal heads and tails orientation, and fragile neck. Thus, during the passage through the epididymis, spermatozoa suffer from decapitation (Netzel-Arnett et al., 2009). Similarly, *Oaz3*-null male mice (Ornithine decarboxylase antizymes) are infertile. They exhibit easy separation of heads from tails due to basal plate and capitulum separation (Tokuhiro et al., 2009). SPATA6 resides exclusively on the connecting piece and *Spata6*-gene disruption in mice disarranges the basal plate connection to the implantation fossa. Thus, *Spata6* mutant mice cause male infertility due to acephalic spermatozoa, which are devoid of the connecting piece, segmented columns, and capitulum (Yuan et al., 2015). ODF1 is a cytoskeletal protein situated in the basal plate, and the ablation of the *Odf1*-gene produces sperm decapitation due to an impairment in the sperm head-to-tail linkage (Yang et al., 2012).

In mice, the disruption of *Sun5* causes male infertility affecting the head-tail coupling apparatus, whereas, in humans, 12 mutations of the gene have been identified. Thus, specific mutations in *Sun5* truncate the translation of the protein affecting its localization at the nuclear envelope. These genetic disorders prevent the centriole attachment to the nucleus, disrupt the HTCA, are responsible for the acephalic spermatozoa syndrome, and cause male infertility (Elkhatib et al., 2017; Shang et al., 2018). The SUN5 protein is described in more detail in chapter 1.6. Thus, identifying the molecular components involved in the acephalic spermatozoa syndrome may contribute to a better understanding of male germ cell differentiation and design diagnostics and treatments in assisted reproduction technology.

## 1.8 Research objectives

ODF1 is an essential component of the HTCA, and its disruption causes sperm decapitation (Yang et al., 2012; 2014). Even though ODF1 is involved in the linkage of the head to the tail in sperm, its interacting partners that mediate this linkage are still unknown. Besides that, *Odf1*-depletion, the partial disruption of *Spag4l* and *Hook1* cause male infertility in mice, suggesting that the acephalic spermatozoa (AS) syndrome has a genetic origin, albeit few mutations have been identified in humans. Given that ODF1 mediate the attachment of the connecting piece to the sperm nucleus and mutations in this gene have not been reported, I explored the *Odf1*-sequence in two patients who exhibited the AS-phenotype. Mutation screening also included regions of the genes *Spag4l* and *Hook1*.

ODF1 interacts with the SUN domain protein SPAG4 (Shao et al., 1999), although this interaction is unusual for SUN-domain proteins. SUN proteins localize at the nuclear envelope (NE), whereas ODF1 localizes in the cytoskeletal area of the HTCA. Hence, this study focused on characterizing the topology of SUN4 and SUN5 to obtain more insights about their orientation in the NE. Thus, I evaluated the topology of *Spag4l* domains by immunocytology. Due to the localization of the SUN-domain proteins at the NE, *Spag4*-depletion might disturb gene transcription during spermatogenesis. Therefore, I evaluated marker genes during spermatogenesis progression in *Spag4*<sup>-/-</sup> mice.

In order to identify additional interactors of SPAG4 apart from ODF1, I explored the amber suppression method, which is based on incorporating a photoreactive unnatural amino acid as a coding codon into a protein. This protein, after photo-activation, cross-links with nearby proteins that afterward can be identified by Western blot. Further, to obtain more insights into the ability of SPAG4 to interact with ODF1, I investigated the orientation of SPAG4 and SPAG4L at the nuclear membrane. For this purpose, recombinant proteins were induced to dimerize by adding the immunosuppressant "rapamycin." To further analyze the function of SPAG4L regarding male fertility, a part of this project was centered on the generation of *Spag4l*-deficient mice.

The last objective was to identify new ODF1 interacting partners that collaborate in the HTCA formation. The focus was centered on CCDC42 due to its reported effect on the formation of the HTCA in mice (Pasek et al., 2016). Besides that, the expression and localization of CFAP52 were analyzed because of its physiological functions, potential role in axoneme stability, and its ability to mediate protein interactions (Li et al., 2001).

## 2 Material and methods

### 2.1 Material

#### 2.1.1 Biological material

##### 2.1.1.1 Bacterial strains

Competent *Escherichia coli* strain DH5 $\alpha$  and D $\alpha$ 10b were used to subclone plasmid DNA.

##### 2.1.1.2 Cell lines

Two different cell lines were cultivated. The cell line derived from mouse embryonic fibroblast (NIH3T3) (Todaro & Green, 1963) and cells derived from human embryonic kidney (HEK293) (Graham et al., 1977).

#### 2.1.2 Vectors

Different vectors were used either for cloning or protein expression in eukaryotic cells. The vectors pCR<sup>TM</sup>II and pJET1.2 were used for cloning, whereas pcDNA3.1 (-) C (Invitrogen) and pEGFP-C1 (Clontech) were used for overexpression in mammalian cells.

#### 2.1.3 Oligonucleotides

Oligonucleotides were designed by NCBI/primer BLAST, whereas primer properties were evaluated using PCR Primer Stats ([https://www.bioinformatics.org/sms2/pcr\\_primer\\_stats.html](https://www.bioinformatics.org/sms2/pcr_primer_stats.html)). Oligonucleotide primers were ordered either from Integrated DNA technologies IDT or Eurofins and dissolved in distilled water to a final concentration of 100  $\mu$ M/  $\mu$ l, according to the manufacturer. Oligonucleotides are listed in 6.1.

## 2.1.4 Enzymes

Enzyme Type	Enzyme	Resource
Restriction Enzyme	AgeI-HF	New England Biolabs
	BamHI-HF	New England Biolabs
	BglII	New England Biolabs
	EcoRI-HF	New England Biolabs
	EcoRV-HF	New England Biolabs
	HindIII-HF	New England Biolabs
	KpnI-HF	New England Biolabs
	NheI-HF	New England Biolabs
	NotI-HF	New England Biolabs
	SacI-HF	New England Biolabs
	SpeI-HF	New England Biolabs
	SpeI-HF	New England Biolabs
	XbaI	New England Biolabs
DNA-polymerase	Taq polymerase	Fermentas
	MangoTaq™ DNA Polymerase	Bioline
	Phusion	Own synthesis
	Advantage 2 Polymerase Mix	Clontech
DNA polymerase mix for qPCR	2X KAPA SYBR® FAST qPCR	KAPA Biosystem
	All-in-One™ qPCR	GeneCopia
	HOT FIREpol® EvaGreen® qPCR Mix Plus (ROX)	Solis BioDyne, Tartu, Estland
Klenow fragment	DNA Polymerase I	Thermo Scientific
DNA ligase	T4 DNA Ligase	New England Biolabs
Proteinase K	Proteinase K	Roth

**Table 2.1. Enzymes**



## 2.1.5 Antibodies

### 2.1.5.1 Primary antibodies

<b>Antibody</b>	<b>Target protein</b>	<b>Host animal</b>	<b>Code</b>	<b>Reference</b>
<b>AntiRedFP</b>	mCherry	rat	5F8	Chromotek
<b>Anti-GFP</b>	pEGFP ECFP	rabbit	An#00002	Own synthesis First bleeding
<b>Anti-GFP</b>	pEGFP ECFP	mouse		Own synthesis Ibrahim Adham
<b>Anti-CCDC42</b>	COILED-COIL DOMAIN CONTAINING 42 (CCDC42) Epitope KHL	rabbit	Bs-8131R ABIN872760	Antibodies Online
<b>Anti-CCDC42</b>	COILED-COIL DOMAIN CONTAINING 42 (CCDC42) Epitope middle region	rabbit	ARP52735_P050 ABIN2785068	Antibodies Online
<b>Anti-ODF1</b>	Outer dense fiber of sperm tails 1 (ODF1)	rabbit		Antibodies online
<b>Anti-Pericentrin</b>	Pericentrin	rabbit	PRB432C	Covance
<b>Anti-gamma Tubulin</b>	$\gamma$ -tubulin	mouse	GTU-88	Sigma-Aldrich
<b>Anti-myc</b>	Myc-tag	rabbit	AA31-80 ABIN1532205	Antibodies Online
<b>Anti-Myc polyclonal</b>	Myc-tag	rabbit		Millipore
<b>Anti-HA</b>	HA-tag	mouse	C5	Abcam
<b>Anti-CFAP52</b>	CFAP52	rabbit	PA839781LA01	Cusabio

**Table 2.2. Primary antibodies**

### 2.1.5.2 Secondary antibodies

Antibody	Target protein	Host animal	Code	Reference
goat anti-mouse HRP-coupled	mouse-HRP	goat		Jackson Immuno Research
goat anti-rabbit HRP-coupled	rabbit-HRP	goat		Jackson Immuno Research
goat anti-rat HRP-coupled	Rat-HPR	goat		Jackson Immuno Research
goat anti rabbit-IgG (H+L)	rabbit IgG	goat	Alexa fluor R 555	Life Technologies
goat anti-mouse-IgG (H+L)	mouse IgG	goat	Alexa fluor R 555	Molecular probes
goat $\alpha$ guinea pig-IgG	guinea pig IgG	goat	Cy3	Dianova
goat $\alpha$ mouse	mouse IgG	goat	MFP590	Mobitec
goat anti-rabbit	rabbit IgG	goat	MFP488	Mobitec
goat $\alpha$ rabbit IgG	rabbit IgG	goat	DyLight 488	Thermo Scientific
goat $\alpha$ mouse IgG	mouse IgG	goat	DyLight 488	Thermo Scientific

**Table 2.3. Secondary antibodies**

## 2.1.6 Culture media

### 2.1.6.1 Culture media for eukaryotic cells

Cell line	Ingredients
NIH3T3 HEK293	Gibco DMEM + Glutamax-I 1x 500 ml (contains 4.5 g/l D-glucose and sodium pyruvate), penicillin-streptomycin 1%, FBS 10%

Table 2.4. Culture media for eukaryotic cells

### 2.1.6.2 Culture media for prokaryotic cells

LB-Medium	10 g Trypton 10 g NaCl 5 g yeast extract *Ampicillin at 100µg/mL or Kanamycin at 50 mg/mL
LB agar plate	1.5% (w/v) agar in LB medium

Table 2.5. Culture media for prokaryotic cell culture

## 2.1.7 Buffers and solutions

Buffer/solution name	Ingredients
Blocking solution (Western-Blot)	5% (w/v) skimmed milk powder diluted in 1X-TBST buffer
Blocking solution (Immunocytology))	1 % (w/v) BSA in PBS 0.5 % (v/v) Tween diluted in 1X-PBS buffer
Denaturation buffer 8X	250 mM Tris-HCl (pH 6.8) 8% (w/v) SDS 40% (w/v) 2-β-Mercaptoethanol 0.004% (w/v) bromophenol blue 60% (w/v) glycerol
Denaturation buffer 2X	62.5 mM Tris-HCl (pH 6,8)

	2% (w/v) SDS 10% (w/v) 2- $\beta$ -Mercaptoethanol 0.001% (w/v) bromophenol blue 10% (w/v) glycerol
DNA loading buffer 6X	0.09% (w/v) xylene cyanol FF 60 mM EDTA 0.09% (w/v) bromophenol blue 60% (w/v) glycine
KHM buffer	110 mM KOAc 20 mM Hepes, pH 7.4 2 mM MgCl <sub>2</sub>
Laemmli electrophoreses buffer (10X)	0.25 M Tris 2 M (w/v) glycine 1% (w/v) SDS
Lysis buffer for eukaryotic cells	150 mM NaCl 2 mM EDTA 1% Triton X-100 1X of protease inhibitors cocktail 100X In PBS (pH 7.2)
Lysis buffer for prokaryotic cells	150 mM NaCl 250 mM Tris-HCl (pH 7.2) 0.1% Triton X-100 1 mM DTT 1 mM PMSF
Lysis buffer for <i>in situ</i> proteinase K digestion	0.4% SDS 2% Triton X-100 400 mM NaCl 50 mM Tris-HCl, pH 7.4 1 mM DTT 2 $\mu$ g/ml pepstatin A 1 $\mu$ g/ml Leupeptin
NID buffer	50 mM KCl 10 mM Tris-HCl (pH 8,3) 2 mM MgCl <sub>2</sub> 0.1 mg/ml gelatine 0.45% (v/v) NP40 0.45% (v/v) Tween 20 Proteinase K 1,6U/300 $\mu$ l

Paraformaldehyde 3.7%	3.7 gr Paraformaldehyde diluted in 1X-PBS
PBS buffer (10X)	140 mM NaCl 7 mM Na <sub>2</sub> HPO <sub>4</sub> 3 mM KH <sub>2</sub> PO <sub>4</sub>
RIPA buffer	150 mM NaCl 1% Nonidet P40 0.5% Sodium Deoxycholate 0.1% SDS 50 mM Tris (pH 7.7) 10 mM PMSF
10X RIPA buffer for crosslinking assay	0.5 M Tris-HCl (pH 7.4) 1.5 M NaCl 2.5% Deoxycholate 10% NP-40 10 mM EDTA
Stripping solution	1.5% (w/v) glycine 0.1% (w/v) SDS 1% Tween 20 Final pH 2.2
TAE buffer (50X)	242 g/l Tris 57.1 ml/l glacial acetic acid 100 ml of 0.5 M EDTA Final pH 8.0
TBST	20 mM Tris-HCl (pH 7.5) 300 mM NaCl 0.2% Triton X-100
Transfer buffer	1 M Tris-HCl (pH 7.5) 20 M glycine 0.4 mM MgCl <sub>2</sub> 0.04% (w/v) SDS 20% methanol

**Table 2.6. Buffers and solutions**

## 2.1.8 Chemicals

Name	Company
2-β- Mercaptoetanol	Sigma-Aldrich
Agarose	Serva
Ampicillin	Serva
APS	Sigma-Aldrich
Bromophenol blue	Sigma-Aldrich
BSA	AppliChem
CaCl <sub>2</sub>	Merk
DAPI	Sigma-Aldrich
DTT	Sigma-Aldrich
EDTA	Roth
Ethanol	VWR Chemicals
Fluoromount-G™	Invitrogen
Glacial acetic acid	ChemSolute
Glucose	Roth
Glycerol	Roth
Glycine	Roth
HCl (37%)	Roth
HEPES	Roth
Imidazole	Roth
IPTG	Sigma-Aldrich
Kanamycin	Sigma-Aldrich
KCl	Merk
KH <sub>2</sub> PO <sub>4</sub>	Merk
KOAc	Roth
Methanol	VWR Chemicals
MgCl <sub>2</sub>	AppliChem
MgSO <sub>4</sub>	AppliChem
Na <sub>2</sub> HPO <sub>4</sub>	Merk
NaCl	AppliChem
NaHCO <sub>3</sub>	Sigma-Aldrich
Nonidet P40	Fluka
PFA	Sigma-Aldrich

Pierce Protein G Agarose	Thermo Fisher Scientific
PL-FITC	PL biochemicals
PMSF	Sigma-Aldrich
PageRuler™ Prestained Protein Ladder #26616	Thermo Scientific
Protease inhibitors cOmplete Ultra tabler mini EDTA-free	Roche
100X Protease inhibitor cocktail	Cell signaling
Rotiphorese gel 40 (29:1)	Roth
Rapamycin	Millipore
SDS	Roth
Serva DNA Stain G	Serva
Skimmed milk powder (slightly soluble)	Difco
Sodium acetate	AppliChem
S.O.C medium	Invitrogen
TEMED	Roth
Tris	Roth
Triton X-100	Roth
Trypsin-EDTA 0,25%	Life technologies
Tween 20	Roth
X-gal	Thermo Fisher Scientific

**Table 2.7. Chemicals**

## 2.1.9 Kits

Ambion® Acid Phenol:Chloroform: IAA	Thermo Fisher Scientific
Antarctic Phosphatase	BioLabs
Clarity Max™ Western ECL Substrate	Bio-Rad
Dual promoter TA Cloning™ Kit	Invitrogen
EndoFectin Max transfection reagent	Genecopoeia
KAPA™ Mouse Genotyping Hot Start Kit	KAPA Biosystem
Maxima first-strand cDNA Synthesis Kit for RT-qPCR	Thermo Fisher Scientific
5X MEGAscript® T7 kit	Invitrogen by Thermo Fisher Scientific
Miniprep kit NucleoSpin® plasmid	Macherey-Nagel GmbH&CoKG
NucleoSpin® Gel and PCR Clean-Up	Macherey-Nagel GmbH&CoKG
peqGold RNA Pure	PEQLAB
Phenol:Chloroform:IAA, 25:24:1	Ambion
Plasmid Midi Kit	QIAGEN
Protein G-Agarose	Thermo Fisher Scientific
Qubit™ dsDNA HS Assay Kit	Invitrogen
Qubit™ RNA HS Assay Kit	Invitrogen
TA Cloning™ Kit, Dual Promoter	Invitrogen
TURBO DNA-free™ Kit	Life technologies
Viagen DirectPCR-Tail	Viagen Biotech

**Table 2.8. Kits**

## 2.1.10 Software and web services

Software or web service	Website
ZEN blue and black	Microscope Software ZEN from ZEISS Microscopy
Adobe Photoshop 7.0	
NCBI	<a href="https://www.ncbi.nlm.nih.gov/">https://www.ncbi.nlm.nih.gov/</a>
ENSEMBL	<a href="https://www.ensembl.org/index.html">https://www.ensembl.org/index.html</a>
BLAST	<a href="https://blast.ncbi.nlm.nih.gov/Blast.cgi">https://blast.ncbi.nlm.nih.gov/Blast.cgi</a>
Expasy	<a href="https://web.expasy.org/translate/">https://web.expasy.org/translate/</a>
SAC multalin	<a href="http://multalin.toulouse.inra.fr/">http://multalin.toulouse.inra.fr/</a>
Clustal Omega	<a href="https://www.ebi.ac.uk/Tools/msa/clustalo/">https://www.ebi.ac.uk/Tools/msa/clustalo/</a>

**Table 2.9. Software and services**



## **2.2 Methods**

### **2.2.1 Microbiological methods**

#### **2.2.1.1 Liquid culture of *E.coli***

Transformed bacteria from a colony or a glycerol stock were cultivated in LB medium (5 ml to 100 ml) containing selective antibiotics, either ampicillin or kanamycin (at either 100µg/mL or 50 mg/mL, respectively). Bacteria were shaken at 225 rpm at 37°C overnight. Bacterial cultures containing a specific plasmid were used to prepare glycerol stocks (2.2.1.2) or purify DNA plasmid (2.2.2.4).

#### **2.2.1.2 Storage of transformed bacteria (*E. coli*)**

For long-term storage of bacterial transformants, glycerol stocks were prepared. Bacteria were grown overnight in media containing the selective antibiotic. Then 800 µl of liquid culture was gently mixed by pipetting with 200 µl of sterile glycerol and stored at -80°C.

#### **2.2.1.3 Transformation**

10 – 50 µl of competent bacteria cells, either DH5α or DH10b, were defrosted on ice and mixed with 20 µl of ligation reaction (2.2.2.8). The mixture was incubated on ice for 30 minutes. The cells were then heat-shocked for 90 seconds at 42°C and chilled for 2 minutes on ice. Afterward, 200 µl of SOC medium was added to the DNA-competent bacteria mixture and incubated for 1 hour at 37°C. Finally, the transformation mix was plated on LB agar plates containing the appropriate selective antibiotic and incubated-overnight at 37°C.

### **2.2.2 Molecular biological methods**

#### **2.2.2.1 Plasmid DNA preparation from *E.coli***

Plasmid DNA was prepared in three quantitative scales. For small-scale plasmid preparation, the–Mini Kit NucleoSpin® Plasmid was used (Tab. 2.8). To obtain a large-scale DNA preparation, either Midiprep Kit NucleoSpin® Plasmid or Maxiprep was used. The procedure was according to the manufacturer's instruction manual.

## 2.2.2.2 Plasmid construction

### 2.2.2.2.1 Subcloning to validate the amber suppression method

First, *LaminC2* and *Lamin B3* were amplified from mice testes cDNA by RT-PCR (Tab. 6.1.4). PCR was performed using Phusion polymerase. Amplified fragments were purified from the agarose gel (2.2.2.4) and subsequently subcloned into the vector pJET1.2-blunt (Fermentas). *LaminC2* and *LaminB3* were excised from vector pJet1.2 using XbaI and KpnI restriction enzymes. After that, each fragment was subcloned into the expression vector pcDNA3.1 (Invitrogen). The successful cloning was verified via sequencing (2.2.2.9).

The *LaminC* coding sequence was subcloned into pEGFP-N1. The *LaminC* coding sequence was site-directed mutated by introducing the Amber stop codon (TAG) at three different positions encoding either the amino acid arginine in position 470 (R470), threonine in position 488 (T488), or threonine in position 534 (T534). The complete constructs containing the site-directed mutations denominated R470, T488, T534, and the aminoacyl-tRNA were kindly provided by Dr. Petra Neumann-Staubitz.

### 2.2.2.2.2 Subcloning of SUN domain proteins

*Sun1* and *Sun3* were amplified from mice testes cDNA (Table 14). PCR was performed using Phusion polymerase. Amplified fragments were purified from the agarose gel and subsequently subcloned into the vector pJET1.2-blunt (Fermentas). *Sun1* was cut out from the pJET1.2 vector using NheI and BamHI, whereas *Sun3* was digested with restriction enzymes NheI and KpnI (2.2.2.6). Both linearized fragments were subcloned into Cherry-pCR3.1. Sequences of expression plasmids were verified via sequencing (2.2.2.9).

The full-length *Spag412* was amplified from mouse testes cDNA as previously described (Frohnert et al., 2010) and used as a template for PCR. *Spag412* contains two transmembrane domains denominated TM1 (TM38-58) and TM2 (TM77-95).

The TM1 (TM 38-58) was first amplified using the primer pair primer1 and primer TM38-58r. The amplified fragment was cloned into pcDNA3.1 myc/His (-) C (Invitrogen, Paisley, UK). Then, the TM1 insert was excised with NheI-EcoRI from the vector pcDNA3.1 myc/His (-) C. The TM1 insert was subcloned into pEGFP-N1 (Clontech, Palo Alto, CA, USA).

The TM2 (TM77-95) was amplified using the primers: primer1, primer2, primer3 TM2, and Spag77-95r EcoRI. The PCR product was digested with NheI-EcoRI and cloned into pEGFP-N1 (Clontech, Palo Alto, CA, USA).

The TM1-TM2 was amplified using the primer pair primer1 and Spag77-95r EcoRI and cloned into pcDNA3.1 myc/His (-) C. The N-terminal region containing the HA tag, TM1 and TM2 were digested with NheI and EcoRI. The digested fragment was cloned into pEGFP-N1 (Clontech, Palo Alto, CA, USA).

The full-length *Spag4l2* sequence was amplified using the primers pair primer1 and primer Spag77-95r EcoRI. Afterward, the fragment was cloned into pcDNA3.1 myc/His (-) C (Invitrogen, Paisley, UK).

The expression plasmid *HA-Spag4l2-myc* containing a frameshift mutation at its C-terminus was generated by PCR using the primers pair Spag4XbaI-for and Spag4KpnI-frameshift. The PCR product was cloned into pCRII and then digested with XbaI and KpnI. Finally, the fragment was subcloned in pcDNA3.1 myc/His (-) C.

*Spag4Lc-EGFP* was generated by PCR amplification using the primer pair Spag4lC-term-F-HindIII and *Spag4l* C-term-rev-EcoRI. Then, the amplified fragment was subcloned into pEGFP-N1. Finally, all clones were verified by DNA sequencing.

#### **2.2.2.2.3 Subcloning of genes for the rapamycin system**

The expression plasmid *FRB-ECFP-Spag4* was prepared by amplifying the fragment *mECFP-FRB* from the construct *mECFP-FRB* in pCRII (Ref: Hoyer-Fender). The primer pair used were ECFP-N-NheI and FIASH-C-NheI (Table 6.1.6). The amplified fragment was subcloned into pCRII. Then, the *pCRII-mECFP-FRB* plasmid was digested with NheI, whereas *HA-Spag4-myc* in pcDNA3.1 (Ref: W. Sura) was linearized with NheI and XbaI. Finally, both fragments were ligated.

The plasmid *Luciferase-mRFP-FKBP* was prepared by amplifying the *Luciferase* gene from pGL-3 (Promega) with primers Luc-NheI-For2 and Luc-AgeI-Rev2 (Tab. 6.1.5). The amplified *Luciferase* fragment was subcloned into pJET1.2 blunt vector (Fermentas). Subsequently, the plasmid was digested with restriction enzymes NheI (at the 5'-end) and AgeI (at the 3'-end). The expression plasmid *mRFP-FKBP* in pEGFP-N1 (Ref: C. Schultz/M. Schifferer) was linearized with the restriction enzyme AgeI (at the 5'-end) and finally fused to the luciferase gene.

The expression plasmid *FRB-ECFP-Sun5* was generated by amplifying *Sun5/Spag4l* from the construct *HA-Spag4l-myc* in pcDNA3.1(Ref: S.Hoyer-Fender). The primers pair used were Sun5-SacI-N-Rap and Sun5-KpnI-C-Rap (Tab.6.1.5). The PCR product was subcloned into pJET1.2 blunt vector (Fermentas). Afterward, *Spag4l* was cut-out with restriction enzymes SacI

(at the 5'-end) and KpnI (at the 3'-end). The plasmid *mECFP-FRB*-in pCRII (Ref: S.Hoyer-Fender) was linearized with the restriction enzymes SacI and KpnI (both at the 3'-end). Ligation of *Spag4l* to *pCRII-mECFP-FRB* resulted in the fusion of *Spag4l* to the C-terminal region of *pCRII-mECFP-FRB*. The coding sequence of *FRB-ECFP-Spag4l* was amplified with the primer pair ECFP-N-NheI and Sun5-KpnI-C-Rap and cloned pcDNA3.1 (-) C (Invitrogen) linearized with the restriction enzymes SacI and KpnI. All constructs were verified by sequencing.

#### **2.2.2.3 Sodium acetate/ethanol DNA precipitation**

Genomic DNA was concentrated and purified by adding 1/10 volumes of 3M sodium acetate and mixing thoroughly. Then, 2 volumes of 100% ethanol were added, mixed, and incubated overnight at -20°C. After incubation, the samples were centrifuged for 30 minutes at 4°C at top speed. The supernatant was discarded, and the DNA pellet was washed 2 times with 70% ethanol. The DNA pellet was air-dried and resuspended in ddH<sub>2</sub>O.

#### **2.2.2.4 DNA purification**

The PCR product of interest was cut-out from the agarose gel and purified with NucleoSpin® Gel and PCR Clean-Up Kit following the manufacturer's instructions.

#### **2.2.2.5 Measurement of DNA and RNA concentrations**

DNA and RNA concentrations were obtained using either photo-spectrometer (Nanodrop, PeqLab) or Qubit™. Nanodrop estimated DNA concentration is based on UV light absorption at a wavelength of 260 nm. A ratio of OD<sub>260</sub>/OD<sub>280</sub> provided information about the purity of nucleic acids. Whereas Qubit™ estimate DNA or RNA concentration by measuring the fluorescence emitted by the binding to a specific dye. Qubit™ quantification reduces noise and gives more accurate results. DNA or RNA quantification was performed using specific Qubit™ fluorometers for dsDNA or RNA, as indicated in the instruction manual.

#### **2.2.2.6 Restriction enzyme digestion of DNA**

Specific restriction endonucleases were used to digest DNA. 1 µg DNA was incubated with 1 unit of restriction enzyme in the appropriate reaction buffer, provided by the manufacturers, at recommended temperatures and time. Then, the DNA-enzyme digestion mix was inactivated at specific temperatures and time recommended for each enzyme. Finally, digested DNA fragments or vectors were analyzed by gel electrophoresis and purified using the NucleoSpin® Gel and PCR Clean-Up kit (2.2.2.4).

### **2.2.2.7 Vector DNA dephosphorylation**

After the restriction enzyme digestion was completed, phosphate groups were removed to prevent vector religation. DNA vector was treated with 1 µl Antarctic Phosphatase (AnP) (5U), 1/10 vol of 10X Antarctic phosphatase reaction buffer, and ddH<sub>2</sub>O up to 50 µl. The dephosphorylation mix was incubated at 37°C for 30 minutes. The reaction was stopped by heat inactivation at 80°C for 2 minutes. Finally, the dephosphorylated vector was used to proceed with ligation.

### **2.2.2.8 Ligation**

The ligation reaction was performed using T4-DNA ligase. The enzymatic activity of the DNA ligase catalyzes the formation of covalent phosphodiester linkages between the 3' hydroxyl end of one DNA fragment and the 5' phosphate end of another DNA fragment. Ligation reaction contained: 50 ng vector DNA, X ng insert DNA, 2 µl T4 (10X) ligation buffer, 1 µl T4 DNA ligase (5U/ µl) in 20 µl of total reaction volume. The ligation reaction was performed with a molar ratio of insert/vector of 3:1 or 1:1 followed by overnight incubation at 4°C.

### **2.2.2.9 DNA Sequencing**

Plasmid or purified DNA was sent to Microsynth Seqlab (Göttingen) for sequencing.

### **2.2.2.10 Total RNA isolation**

Total RNA was extracted either from NIH3T3 cells grown at a monolayer in cell culture dishes or mouse tissues. Mouse tissues include testis, liver, brain, ovary, kidney, epididymides, and spleen. A small piece of each tissue was triturated by using a mortar and continuously adding liquid nitrogen. The pulverized tissue was homogenized in 1 mL of peqGOLD RNAPure™ using a Dounce hand homogenizer (Tab. 2.8). The RNA extraction was essential, as described in the instruction manual. For RNA isolation from NIH3T3 cells, 1 mL of peqGOLD RNAPure™ was directly added to the cell monolayer and the extraction was carried out according to the instruction manual.

### **2.2.2.11 RNA precipitation**

RNA precipitation was done by adding 0.1 volumes of 3M sodium acetate and 2 volumes of 100% ethanol. RNA was mixed thoroughly and incubated for 20 minutes at -80° C. After incubation, the samples were centrifuged for 20 minutes at 4°C, the supernatant was removed, and the RNA pellet was washed 2 times with 75% DEPC-treated ethanol (ice cold). The samples

were centrifuged for 10 minutes at 4°C. The supernatant was removed, the pellet dried and resuspended in nuclease-free water.

#### **2.2.2.12 DNase treatment**

The DNase treatment was performed by adding 5 µl 10X TURBO reaction buffer, 1 µl (2 U) of TURBO DNase (MEGAscript® T7 kit (Tab. 2.8), 10 µg of RNA and nuclease-free water up to 50 µl. The reaction mix was incubated at 37°C for 30 minutes. Thereafter, the DNase was inactivated by adding 0.1 volume ammonium acetate. Samples were stored at -80°C for future cDNA synthesis.

#### **2.2.2.13 Phenol: Chloroform DNA/RNA precipitation**

DNA or RNA samples were treated with one volume of Ambion® Acid Phenol:Chloroform: IAA, premixed with Isoamyl alcohol (IAA) (25:24:1, pH 6.6/ 7.9). The mixture was vortexed for 20 seconds and centrifuged at room temperature for 5 minutes at 16,000 x g. After centrifugation, the upper aqueous phase was transferred into a fresh 1.5 ml tube. DNA or RNA was precipitated by the addition of 0.1 volume of 3M sodium acetate (pH 5.5) and 2.5x volumes of 100% ethanol. Thereafter, samples were incubated at -20°C overnight. Then, samples were centrifuged at 16,000 x g for 30 minutes at 4°C. The supernatant was removed, and the pellet was washed twice with 70% ethanol. After the last wash, ethanol was removed entirely, and the pellet was dried at room temperature for 20-30 minutes. Finally, DNA or RNA pellet was resuspended in nuclease-free water. Samples were stored at -20°C (DNA) or -80°C (RNA) for future experiments.

#### **2.2.2.14 cDNA synthesis**

According to the manufacturer's instructions, the cDNA was synthesized using the Maxima First-Strand cDNA Synthesis Kit (Tab. 2.8). cDNA was used as the template either for RT-PCR or qRT-PCR.

#### **2.2.2.15 RT-PCR**

RT-PCR was performed according to each primer pair parameters and the size of the expected fragments (Tab. 6.1.2). PCR amplification was carried out using either Mango Taq DNA polymerase, Taq polymerase, or Phusion polymerase.

### **2.2.2.16 qRT-PCR**

qRT-PCR was performed either with All-in-One™ qPCR mix or HOT FIREpol® EvaGreen® qPCR using the CFX96™ Real-Time PCR System (Bio-Rad Laboratories, Hercules, CA, USA). cDNA from a wild type mouse was used to calculate primer efficiency. Relative fold gene quantity was calculated by the delta-delta Ct method ( $2^{-\Delta\Delta C_t}$ ) using *mHPRT* as a reference gene. Primer sequences are given in table 6.1.3.

### **2.2.2.17 PCR**

DNA was amplified using MangoTaq™ DNA, Phusion, or Advantage 2 Polymerase. Different reactions were performed following the manufacturer's instructions. PCR products were evaluated by agarose gel electrophoresis.

### **2.2.2.18 Agarose gel electrophoresis of DNA**

PCR products were evaluated by gel electrophoresis using either 1% or 2% agarose dissolved in 1X-TAE buffer and Serva DNA Stain G. Gel was solidified and inserted into a chamber covered with 1X-TAE buffer. DNA samples were mixed with loading dye, loaded onto the gel, and separated at 100V-120V.

## **2.2.3 Biochemical methods**

### **2.2.3.1 Protein extraction from mammalian cells**

Mammalian cells were washed with 1XPBS, trypsinized, and centrifuged for 3min at 2000 x g. The cell pellet was washed with 1X-PBS and cellular concentration was measured using a Neubauer haemocytometry.  $1 \times 10^6$  cells were resuspended in 32  $\mu$ l 1x-PBS. Protein denaturation was performed by adding 4  $\mu$ l of 8X denaturation buffer and heating at 95°C for 10 minutes.

### **2.2.3.2 SDS-Polyacrylamide gel electrophoresis**

Polyacrylamide gel electrophoresis (PAGE) (Laemmli, 1970) was used to separate proteins based on their size. For that purpose, proteins were denatured to avoid protein folding and give them a negative charge. SDS gels were prepared using a stock solution of 40% acrylamide/bisacrylamide in a ratio of 29:1. The acrylamide concentration chosen for resolving gel preparation (10%, 12%, or 15%) was adapted to the expected molecular size range, whereas the stacking gel was prepared at a concentration of 10%.

Protein samples were loaded onto the SDS-PAGE and separated at 80 V for 30 min. When the loading dye has entered the resolving gel, the voltage turned to 100 V for another 1.5 hours.

Stacking gel		Separating gel			
	10 ml		10%	12%	15%
40% AA Bis Mix	1.25 ml	40% AA Bis Mix	5 ml	6 ml	7.5 ml
ddH <sub>2</sub> O	6.3 ml	ddH <sub>2</sub> O	9.6 ml	8.6 ml	7.1 ml
1M Tris-HCl pH 6.8	1.25 ml	1.5 M Tris-HCl pH 8.8	5 ml	5 ml	5 ml
10% SDS	100 µl	10% SDS	200 µl	200 µl	200 µl
10% APS	100 µl	10% APS	200 µl	200 µl	200 µl
TEMED	100 µl	TEMED	20 µl	20 µl	20 µl

**Table 2.10. Volumes needed for the preparation of two stacking and separating gels**

### 2.2.3.3 Western-blot (Immunoblot)

The Western-blot is defined as the transfer of proteins onto a nitrocellulose membrane (Towbin et al., 1979), followed by protein detection using specific antibodies. The nitrocellulose membrane (Amersham Hybond-ECL, GE Healthcare) was placed together with the SDS-gel between two Whatman filter papers. This set was placed between two sponges into a cassette. Finally, the cassette was placed into the blot chamber (Bio-Rad) containing Towbin buffer. Protein transfer was performed by applying 100 V for 1 hour.

### 2.2.3.4 Immunological protein detection

Membranes were used for antibody detection. Membranes were incubated for one hour at room temperature in blocking solution (5% dry milk in TBST). Afterward, membranes were incubated with primary antibodies diluted in blocking solution at 4°C overnight. After incubation with the first antibody, membranes were washed with TBST buffer for 45 minutes and replacing the TBST buffer every 5 minutes. Then, membranes were incubated with horseradish peroxidase-conjugated secondary antibodies diluted in blocking solution for 45 minutes at room temperature. Unbound antibodies were removed by washing the membranes for 30 minutes with TBST buffer, replacing the buffer every 5 minutes. The HRP conjugated secondary antibodies were detected by chemiluminescence (ECL). Light emission from proteins was detected by ChemiDoc™ Imaging System. The optimal exposure time of each membrane was always adapted to the experimental needs.



### **2.2.3.5 Nitrocellulose membrane stripping**

The nitrocellulose membrane was reevaluated. For this purpose, the primary and secondary antibodies were first removed. Nitrocellulose membranes were stripped accordingly: 1. blots were incubated in 1X-PBS for 10 minutes at room temperature with constant agitation, 2. the PBS buffer was exchanged for stripping solution (see 2.1.9) followed by incubation for 8 minutes, 3. the stripping solution was discarded, and membranes were washed twice with 1X-PBS for 10 minutes each. Thereafter, membranes were washed twice with TBST buffer for 5 minutes each, and unspecific binding sites were blocked with 5% dry milk powder in TBST. The nitrocellulose membrane is now ready for the antibody incubation.

### **2.2.3.6 Co-IP (Co-immunoprecipitation)**

Cells were reseeded and transfected, as described above. 18-24 hours post-transfection, cells were harvested by trypsinization, collected and washed twice with ice-cold 1X-PBS. Cellular pellet was resuspended in 1 ml lysis buffer for CoIP, vortexed, and incubated on ice for 20 minutes. After incubation, cell lysate was passed 10 times through a 21.5-gauge needle followed by 3 times sonication for 45 seconds each. Samples were centrifuged at 15,000 x g for 15 minutes and the supernatant was used for CoIP analysis. 50 µl of supernatant was stored as input, whereas the remnant protein lysate was split into equal parts to perform immunoprecipitation with specific and control antibodies. Incubation with fishing antibodies was carried out on a rolling platform for 1 hour at room temperature. Then, protein G beads were washed with lysis buffer for CoIP and subsequently added to the protein lysate-antibody mixture and incubated overnight at 4°C on a rolling platform. After overnight incubation, beads containing proteins and antibodies were washed 4 times with 1 ml lysis buffer. Finally, beads were resuspended in 50 µl 1X denaturation buffer, whereas the supernatant of 50 µl was resuspended in 50 µl 2X denaturation buffer for SDS-PAGE electrophoresis and boiled at 95°C for 10 minutes.

### **2.2.3.7 Crosslinking reaction and harvesting adherent cells**

Twenty-four hours post-transfection, cell culture dishes were placed on ice, and the medium was removed. Adherent cells were washed two times with 1X-PBS. Then, fresh 1X-PBS was added to the cells, followed by incubation at 4°C with concurrent exposition with or without UV-light at 365 nm for 15 min. Subsequently, PBS was removed and 150µl of 1X-RIPA, containing protease inhibitors, was added (Tab. 2.6), followed by incubation on ice for 10 minutes under slow horizontal movements. Thereafter, cells were scratched using a cell scraper. The cell lysate was transferred into a 1.5 ml tube and centrifuged at 11.000 rpm for 10 min at

4°C. After centrifugation, the supernatant was transferred into a new 1.5 ml tube and 25 µl of 5X LPP buffer was added to 100µl of the supernatant. Samples were heated for 15 min at 95°C and stored at -20°C for Western-blot analysis.

<i>pLMNC-T488-3X-FLAG</i>	Amber stop codon TAG 488
<i>pLMNC-T534-3X-FLAG</i>	Amber stop codon TAG 534
<i>pLMNC-R470-3X-FLAG</i>	Amber stop codon TAG 470
<i>p4XtRNA<sub>pBpa</sub></i>	

**Table 2.11. Plasmids and tRNA for UAA incorporation**

## 2.2.4 Cell biological methods

### 2.2.4.1 Propagation and subculture of eukaryotic cells

NIH3T3 and HEK293 cells were cultivated in Dulbecco's Eagle Medium (DMEM) enriched with 10% fetal bovine serum and 1% penicillin/streptomycin (complete DMEM). Cells were maintained at 37°C and 5% CO<sub>2</sub>. Cells were propagated by removing the old medium and washing them with sterile 1X-PBS. Cells were incubated with 0.25% trypsin, followed by incubation for 3 minutes at 37°C. Trypsin was inactivated by adding complete DMEM and a large part of the solution aspirated. The remaining cells were propagated further by adding fresh complete DMEM.

### 2.2.4.2 Defrosting and freezing of eukaryotic cells

For long-term storage, harvested cells were resuspended in freezing medium containing 20% DMSO. Cells were collected in cryo-vials and first incubated for 2 hours at -20°C followed by transfer to -80°C overnight. Finally, cryo-vials were stored in liquid nitrogen. For revitalization, frozen cells in cryo-vials were prewarmed in a water bath for 3 minutes at 37°C and subsequently diluted with prewarmed medium.

### 2.2.4.3 Transfection

NIH3T3 and HEK293 cells were transfected with EndoFectin<sup>TM</sup> Max transfection reagent following the manufacturer's instructions. Thereafter, cells were incubated at 37°C and 5% CO<sub>2</sub> for 18-24 hours.

#### **2.2.4.4 Immunocytology on sperm suspension**

Fresh testes isolated from mice (C57BL/6) were washed with 1X-PBS, the tunica albuginea was removed, and germ cells were suspended by mincing and pipetting in 3.7% PFA. Cell suspensions were spread on Superfrost Plus (Menzel Glas, Braunschweig) followed by incubation in a humid chamber for 20 minutes. Cells were permeabilized with 0.3% Triton X-100 (in 1X-PBS) for 10 minutes at room temperature. After washing the samples with 1X-PBS, they were incubated in PBT blocking solution for 1 hour. Proteins of interest were stained with appropriate primary antibodies overnight at 4°C. Excess of primary antibodies was removed by washing the samples 3 times with 1X-PBS. Thereafter, samples were incubated with appropriate secondary antibodies for 45 minutes at 37°C. Finally, samples were washed three times in 1X-PBS for 5 minutes each, the mounting medium (Fluoromount-G™) was added, and slides were covered with a coverslip and sealed with nail polish. Samples were analyzed by the fluorescence microscope LSM 750 or 980 (ZEISS) and processed using Adobe Photoshop 7.0.

#### **2.2.4.5 Immunocytology**

Transfected or untransfected NIH3T3 cells were cultivated on coverslips in six-well plates containing an initial concentration of  $2.5 \times 10^5$  or  $3 \times 10^5$  cells per well. After 24 hours, cells were washed 3 times with 1X-PBS and fixed in 3.7% PFA in 1X-PBS for 20 minutes at 4°C. Alternatively, cells were fixed with 100% methanol for 10 minutes at -20°C. After 3 times washing with 1X-PBS, specimens were permeabilized in 0.3% Triton X-100 (in 1X-PBS) for 10 minutes at room temperature. Samples were washed 3 times with 1X-PBS. Another fixative option was to fix cells with 3% Glyoxal for 30 minutes at 4°C, followed by incubation with  $\text{NH}_4\text{Cl}$  for 30 minutes at 4°C. Permeabilization was performed using 0.2% Triton X-100 (in 1X-PBS) for 10 minutes at room temperature. After permeabilization, unspecific antibody bindings were blocked with PBT for 1 hour at room temperature. Subsequently, primary antibodies were added to the samples and incubated for 1 hour at 37°C. Thereafter, cells were washed 3 times with 1X-PBS for 5 minutes each. Afterward, secondary antibodies were added, followed by incubation for 45 minutes at 37°C. DNA was counterstained with DAPI. Cells were washed 3 times with 1X-PBS and covered with mounting medium (Fluoromount-G™). To protect samples from drying, coverslip borders were sealed with nail polish. Slides were stored at 4°C until they were analyzed by laser scanning microscopy (Zeiss LSM 750 or LSM 980) and processed using Adobe Photoshop 7.0.

## **2.2.5 Generation of *Spag4l*-deficient mice**

### **2.2.5.1 Production of the targeting vector**

Homologous recombined mouse embryonic stem cells (Sun5tm1(KOMP)VlG, KOMP/Velocigene project: VG16078) in which the insertion of a replacement vector deleted the *Spag4l2/Sun5* gene were purchased from Velocigene Regeneron Pharmaceuticals, Inc (<http://velocigene.com/komp/detail/16078>). The *Sun5* gene comprises in mouse 12 exons which were entirely disrupted in the embryonic stem cell line and replaced by the reporter gene *LacZ* and the resistant gene *Neomycin*. The cassette deleted the region 153856177 to 153870995, which localizes to chromosome 2. The presence of the targeting vector in ES cells was tested by PCR and qPCR.

### **2.2.5.2 Generation of *Sun5* knockout mice**

Recombinant ES cells were propagated by Prof. Dr. Ibrahim Adham (Institute of Human Genetics, University Medical Center Göttingen). Chimeric mice were generated by microinjection of recombinant ES cells into embryos of the C57Bl6 mouse strain by the animal facility of the Max Planck Institute of Experimental Medicine, Göttingen. Heterozygous *Sun5*-deficient mice were generated by breeding of chimeras carrying the replacement cassette and C57Bl6 mice. Chimeras and heterozygous *Sun5*-deficient mice were genotyped by PCR and qPCR.

### **2.2.5.3 Genomic DNA extraction**

Genomic DNA was prepared using either KAPA™ Mouse Genotyping Kit, NID buffer, or Viagen-DirectPCR®-Tail. ES cell pellet, mice tail-tips, or ear punches were incubated in lysis solution containing 1 µl of KAPA express enzyme, 10X KAPA buffer, and PCR-grade water. Lysis was performed by incubation in a heating block for 1 hour at 75°C followed by enzyme inactivation for 5 minutes at 95°C.

To isolate genomic DNA from mice tail-tip biopsies, tails were placed into a 1.5 ml tube containing 300 µl Viagen-DirectPCR®-Tail buffer (Tab. 2.8) and 0.4 mg/ml of proteinase K. Samples were incubated overnight at 55°C under continuous agitation. Afterward, proteinase K was inactivated by incubation at 85°C for 45 minutes.

Alternatively, mice tail-tips or ear punches were incubated 300 µl NID buffer containing proteinase K (Tab. 2.6) followed by incubation at 56°C overnight. Then, proteinase K was inactivated by incubation at 95°C for 15 minutes.

Finally, DNA samples were quickly centrifugated, the supernatant transferred into a new 1.5 ml tube, and DNA was precipitated using sodium acetate/ethanol (2.2.2.3).

#### 2.2.5.4 Genotyping of mice using PCR

gDNA from ES cells or biopsies from chimeras and their progenies were used to investigate the replacement of the gene *Sun5* by the integration cassette. Thus, gDNA was used as a PCR template using different primer pairs combinations (Tab. 6.1.7).

ES cells were genotyped by PCR using two primer pairs. SunUp/LacInRev was used to amplify a fragment of 562 bp comprising the upstream region of the wild-type allele and 132 bp of the recombinant allele. NeoFwd/SunDown was used to amplify 101 bp of the recombinant allele and 406 bp of the 3' region of the wild-type allele.

Several primer sets were used to detect the transmission of the *Sun5* replacement allele in chimeras and heterozygous mice. SunUp/LacInRev is located at the 5' region as described. LacInF/LacInR are located in the reporter gene LacZ. Different set of primers were used to detect the selection marker *neomycin*, inter alia NeoInF/NeoInR, NeomycinFor3/NeoInR, NeomycinFor/NeoSplitRev and NeomycinFor/NeoInR. Alike, NeoFwd/SunDown, Geno2For/Geno2Rev, and NeomycinFor3/Genotype2Rev locate downstream of the targeting vector or in its 3' region (Fig. 3.24).

PCR reactions were performed using Mango Taq DNA polymerase and primer specific conditions as described in table 2.12.

Step	Temperature	Time	Repetitions
Initial denaturation	95°C	3 min	
Denaturation	95°C	30 sec	
Annealing	Primer TM (Appendix 6.1)	30 sec	45 cycles
Extension	72°C	specific to each fragment length	
Final extension	72°C	10 min	

**Table 2.12. PCR conditions used for genotyping**

### 2.2.5.5 Genotyping of mice using qPCR

ES cells and mice tail-tips were genotyped by quantitative Real-Time PCR using CFX96™ Real-Time PCR System (Bio-Rad Laboratories, Hercules, CA, USA). gDNA was isolated as described (2.2.5.3) and used as the template for qPCR using different primer pair combinations. Primer sets (Tab. 6.1.8) were designed for the amplification of either exon 7 or 9. Primer efficiency was evaluated by the generation of a standard curve with wild-type mouse gDNA. The standard curve was obtained by using serial dilutions of the template.

To perform the qPCR, gDNA from a wild-type mouse was used as internal control, whereas *Prm1* and *Odf1* were used as reference genes to calculate the fold change ( $\log_2^{-\Delta\Delta C_t}$ ).

Internal control, samples, and non-template controls were prepared in triplicate and mixed with the following components: 2X KAPA SYBR® FAST qPCR master mix or HOT FIREpol® EvaGreen® qPCR Mix Plus (ROX), 10 µM forward and reverse primers each, gDNA template and ddH<sub>2</sub>O water up to 10 µl total reaction volume. qPCR reactions were performed using the conditions described in table 2.13.

Step	Temperature	Time	Repetitions
Initial denaturation	95°C	3 min	
Denaturation	95°C	3 sec	
Annealing	57°C	20 sec	40 cycles
Extension	72°C	15 sec	

Table 2.13. qPCR conditions used for genotyping

## 3 Results

### 3.1 Mutation screening in patients with acephalic spermatozoon phenotype

Teratozoospermia (TZI) describes sperm malformations that cause male infertility, including abnormalities of the head and middle/principal piece. The syndrome acephalic or pinhead spermatozoa is characterized by a fragile connecting piece disrupting the connection between sperm head and tail. Albeit these disorders have genetic origins, the molecular components have been scarcely described (Perotti et al., 1981; WHO, 2010; Chemes et al., 1999; Chemes, 2000).

Genetic studies in patients and the generation of knock-out mouse models combined with the ultrastructural evaluations of spermatozoa have enabled the identification of essential genes required for the tight junction between sperm head and tail. The disruption of HTCA or manchette has been ascribed to alterations of *Prss21*, *Oaz3*, *Cntrob*, *Ift88*, *Spata6*, *Odf1*, *Hook1*, *Arl3*, *Stk36*, *Rim-bp3*, and *Sun5* (Mendoza-Lujambio, 2002; Netzel-Arnett et al., 2009; Tokuhiro et al., 2009; Zhou et al., 2009; Liška et al., 2013; Qi et al., 2013; Nozawa et al., 2014; Yang et al. 2012; 2014; Yuan et al., 2015; Zhu et al., 2016).

Most of these genes have been identified in mouse models. This is the case of *Odf1* that encodes the ODF1 protein. ODF1 is an essential component of the HTCA, and its disruption in mice induces the detachment of the sperm head to the tail. However, no mutations have been reported in infertile patients suffering from the acephalic spermatozoan syndrome. Thus, it raises the question if *Odf1* mutations might be causative for male infertility in humans. Therefore, I analyzed the DNA of two infertile patients who had been diagnosed with acephalic spermatozoan phenotype. DNA samples were kindly provided by Prof. Dr. med. Héctor Chemes (Center for Research in Endocrinology, Buenos Aires Children's Hospital, Argentina), who also got the informed consent of the patients. The screening for mutations was carried out on the candidate genes *Odf1*, *Hook1*, and *Sun5*. These genes have been previously reported to play a key role in the sperm head-tail junction.

### 3.1.1 Patients with decapitated spermatozoa carried normal sequence variations of the gene *Odf1* compared to the reference wild-type sequence

ODF1 is a component of the sperm tail outer dense fibers (ODFs) situated parallel to the axoneme. They contribute to the tensile forces of the sperm by providing elasticity to the sperm tail during the flagellar beat. The analyses of spermatozoa from *Odf1*-deficient mice have revealed reduced sperm motility and sperm decapitation. Furthermore, the depletion of *Odf1* caused abnormal mitochondrial arrangement and ODF organization and affected the proper attachment of the sperm head and tail (Fawcett, 1975; Baltz et al., 1990a; Yang et al., 2012; 2014).

*Odf1* gene consists of two exons. Exon 1 comprises 492 bp, whereas exon 2 consists of 596 bp (Hofferbert et al., 1993). Thus, the DNA from two unrelated anonymous patients with acephalic spermatozoan syndrome, named P17 and P19, were used to amplify both exons of the human *Odf1* gene. Exons were amplified using the pair of primers Odf1-Homo-Exon1-For/ Odf1-Homo-Exon1-Rev and Odf1-Homo-Exon2-Forward/ Odf1-Homo-Exon2-Reverse (Tab. 6.1.1). The PCR product of exon 1 exhibited a size of 590 bp, and amplification of exon 2 resulted in two different fragments of 590 bp and 635 bp, respectively. All PCR products were cloned into the vector pJET1.2/blunt (Fermentas), and the DNA isolated from 5 up to 9 individual colonies were sequenced. The obtained sequences were aligned to the human reference NG\_028006.1 by using Multiple Sequence Alignment Clustal Omega. Sequences from exon 1 exhibited a normal coding region in both patients, being identical to the reference sequence (Fig.3.1 - 3.2). Regarding exon 2, two slightly different amino acid sequences were detected in each patient, which corresponded to the variations described as CSP and CNP (Fig. 3.3 – 3.4) (Hofferbert et al., 1993). In humans, in its C-terminal region ODF1 possesses conserved cysteine residues in a variable repetitive tripeptide motif of C-X-P. The tripeptide motif variation is either CSP or CNP resulting from two nucleotide exchanges (AGC → AAC) and (CCC → CCG). Thus, humans are either homozygous or heterozygous for the two *Odf1* alleles. Allele I is shorter and less frequent than allele II. Besides that, allele II is encoded by three additional motifs at the COOH-terminal end. However, these variations do not cause a pathologic sperm phenotype (Burfeind & Hoyer-Fender, 1991; Hofferbert et al., 1993; Hoyer-Fender et al., 1995). To conclude, neither patient P17 nor patient P19 carry harmful mutations in the *Odf1* gene. Therefore, in these cases, *Odf1* is not responsible for the acephalic spermatozoa syndrome.



```

Odf1      MAALSCLLDSVRRDIKKVDRELRLQLRCIDFSTRCLCDLYMHPYCCDLHPYPYCLCYSK 60
P17-Clon4 MAALSCLLDSVRRDIKKVDRELRLQLRCIDFSTRCLCDLYMHPYCCDLHPYPYCLCYSK 60
P17-Clon5 MAALSCLLDSVRRDIKKVDRELRLQLRCIDFSTRCLCDLYMHPYCCDLHPYPYCLCYSK 60
P17-Clon6 MAALSCLLDSVRRDIKKVDRELRLQLRCIDFSTRCLCDLYMHPYCCDLHPYPYCLCYSK 60
P17-Clon16 MAALSCLLDSVRRDIKKVDRELRLQLRCIDFSTRCLCDLYMHPYCCDLHPYPYCLCYSK 60
P17-Clon21 MAALSCLLDSVRRDIKKVDRELRLQLRCIDFSTRCLCDLYMHPYCCDLHPYPYCLCYSK 60
P17-Clon23 MAALSCLLDSVRRDIKKVDRELRLQLRCIDFSTRCLCDLYMHPYCCDLHPYPYCLCYSK 60
P17-Clon24 MAALSCLLDSVRRDIKKVDRELRLQLRCIDFSTRCLCDLYMHPYCCDLHPYPYCLCYSK 60
P17-Clon29 MAALSCLLDSVRRDIKKVDRELRLQLRCIDFSTRCLCDLYMHPYCCDLHPYPYCLCYSK 60
P17-Clon30 MAALSCLLDSVRRDIKKVDRELRLQLRCIDFSTRCLCDLYMHPYCCDLHPYPYCLCYSK 60
*****

Odf1      RSRSCGLCDLYPCCLCDYKLYCLRPSLRS LERKAI RAI EDEKRELAK 107
P17-Clon4 RSRSCGLCDLYPCCLCDYKLYCLRPSLRS LERKAI RAI EDEKRELAK 107
P17-Clon5 RSRSCGLCDLYPCCLCDYKLYCLRPSLRS LERKAI RAI EDEKRELAK 107
P17-Clon6 RSRSCGLCDLYPCCLCDYKLYCLRPSLRS LERKAI RAI EDEKRELAK 107
P17-Clon16 RSRSCGLCDLYPCCLCDYKLYCLRPSLRS LERKAI RAI EDEKRELAK 107
P17-Clon21 RSRSCGLCDLYPCCLCDYKLYCLRPSLRS LERKAI RAI EDEKRELAK 107
P17-Clon23 RSRSCGLCDLYPCCLCDYKLYCLRPSLRS LERKAI RAI EDEKRELAK 107
P17-Clon24 RSRSCGLCDLYPCCLCDYKLYCLRPSLRS LERKAI RAI EDEKRELAK 107
P17-Clon29 RSRSCGLCDLYPCCLCDYKLYCLRPSLRS LERKAI RAI EDEKRELAK 107
P17-Clon30 RSRSCGLCDLYPCCLCDYKLYCLRPSLRS LERKAI RAI EDEKRELAK 107
*****

```

**Figure 3.1. Amino acid sequence alignment of ODF1-exon1 from patient n°17.** The nine clones analyzed showed all an amino acid sequence identical to the reference ODF1 (ref. sec NC\_000008.11).

```

Odf1      MAALSCLLDSVRRDIKKVDRELRLQLRCIDFSTRCLCDLYMHPYCCDLHPYPYCLCYSK 60
P19-Clon1 MAALSCLLDSVRRDIKKVDRELRLQLRCIDFSTRCLCDLYMHPYCCDLHPYPYCLCYSK 60
P19-Clon3 MAALSCLLDSVRRDIKKVDRELRLQLRCIDFSTRCLCDLYMHPYCCDLHPYPYCLCYSK 60
P19-Clon7 MAALSCLLDSVRRDIKKVDRELRLQLRCIDFSTRCLCDLYMHPYCCDLHPYPYCLCYSK 60
P19-Clon11 MAALSCLLDSVRRDIKKVDRELRLQLRCIDFSTRCLCDLYMHPYCCDLHPYPYCLCYSK 60
P19-Clon12 MAALSCLLDSVRRDIKKVDRELRLQLRCIDFSTRCLCDLYMHPYCCDLHPYPYCLCYSK 60
P19-Clon19 MAALSCLLDSVRRDIKKVDRELRLQLRCIDFSTRCLCDLYMHPYCCDLHPYPYCLCYSK 60
P19-Clon21 MAALSCLLDSVRRDIKKVDRELRLQLRCIDFSTRCLCDLYMHPYCCDLHPYPYCLCYSK 60
P19-Clon26 MAALSCLLDSVRRDIKKVDRELRLQLRCIDFSTRCLCDLYMHPYCCDLHPYPYCLCYSK 60
P19-Clon36 MAALSCLLDSVRRDIKKVDRELRLQLRCIDFSTRCLCDLYMHPYCCDLHPYPYCLCYSK 60
*****

Odf1      RSRSCGLCDLYPCCLCDYKLYCLRPSLRS LERKAI RAI EDEKRELAK 107
P19-Clon1 RSRSCGLCDLYPCCLCDYKLYCLRPSLRS LERKAI RAI EDEKRELAK 107
P19-Clon3 RSRSCGLCDLYPCCLCDYKLYCLRPSLRS LERKAI RAI EDEKRELAK 107
P19-Clon7 RSRSCGLCDLYPCCLCDYKLYCLRPSLRS LERKAI RAI EDEKRELAK 107
P19-Clon11 RSRSCGLCDLYPCCLCDYKLYCLRPSLRS LERKAI RAI EDEKRELAK 107
P19-Clon12 RSRSCGLCDLYPCCLCDYKLYCLRPSLRS LERKAI RAI EDEKRELAK 107
P19-Clon19 RSRSCGLCDLYPCCLCDYKLYCLRPSLRS LERKAI RAI EDEKRELAK 107
P19-Clon21 RSRSCGLCDLYPCCLCDYKLYCLRPSLRS LERKAI RAI EDEKRELAK 107
P19-Clon26 RSRSCGLCDLYPCCLCDYKLYCLRPSLRS LERKAI RAI EDEKRELAK 107
P19-Clon36 RSRSCGLCDLYPCCLCDYKLYCLRPSLRS LERKAI RAI EDEKRELAK 107
*****

```

**Figure 3.2. Amino acid sequence alignment of ODF1-exon1 from patient n°19.** The nine clones analyzed showed all an amino acid sequence identical to the reference ODF1 (ref. sec NC\_000008.11).

```

Odf1      MNICKEFSLPPCVDEKDVITYSYGLGSCVKIESPCYPCTSPCSPSP CSP CNPCSPCNPCS 60
P17-Clon2 MNICKEFSLPPCVDEKDVITYSYGLGSCVKIESPCYPCTSPCSPSP CSP-----CS 51
P17-Clon5 MNICKEFSLPPCVDEKDVITYSYGLGSCVKIESPCYPCTSPCSPSP CSP-----CS 51
P17-Clon6 MNICKEFSLPPCVDEKDVITYSYGLGSCVKIESPCYPCTSPCSPSP CNPCNFCSPCNPCS 60
P17-Clon8 MNICKEFSLPPCVDEKDVITYSYGLGSCVKIESPCYPCTSPCSPSP CNPCNFCSPCNPCS 60
P17-Clon9 MNICKEFSLPPCVDEKDVITYSYGLGSCVKIESPCYPCTSPCSPSP CNPCNFCSPCNPCS 60
*****
Odf1      PYDPCNFCYPCGSRFSCRK MIL      82
P17-Clon2 PYDPCNFCYPCGSRFSCRK MIL      73
P17-Clon5 PYDPCNFCYPCGSRFSCRK MIL      73
P17-Clon6 PYDPCNFCYPCGSRFSCRK MIL      82
P17-Clon8 PYDPCNFCYPCGSRFSCRK MIL      82
P17-Clon9 PYDPCNFCYPCGSRFSCRK MIL      82
*****

```

**Figure 3.3. Amino acid sequence alignment of ODF1-exon2 from patient n°17.** Two out of five clones showed the variant motif CSP (clones 2 and 5; yellow) that corresponded to the less frequent allele I. Clones 6, 8, and 9 (green) have the variant motif CNP and contain three additional CNP motifs, which corresponds to the allele II (ref. sec NG\_028006.1 ).

```

Odf1      MNICKEFSLPPCVDEKDVITYSYGLGSCVKIESPCYPCTSPCSPSP CSP CNPCSPCNPCS 60
P19_Clon16 MNICKEFSLPPRVDEKDVITYSYGLGSCVKIESPCYPCTSPCSPSP CSP-----CS 51
P19_Clon20 MNICKESSLPPCVDEKDVITYSYGLGSCVKIESPCYPCTSPCSPSP CSP-----CS 51
P19_Clon22 MNICKEFSLPPCVDEKDVITYSYGLGSCVKIESPCYPCTSPCSPSP CNP-----CS 51
P19_Clon23 MNICKEFSLPPCVDEKDVITYSYGLGSCVKIESPCYPCTSPCSPSP CSP-----CS 51
P19_Clon24 MNICKEFSLPPCVDEKDVITYSYGLGSCVKIESPCYPCTSPCSPSP CSP-----CS 51
*****
Odf1      PYDPCNFCYPCGSRFSCRK MIL      82
P19_Clon16 PYDPCNFCYPCGSRFSCRK MIL      73
P19_Clon20 PYDPCNFCYPCGSRFSCRK MIL      73
P19_Clon22 PYDPCNFCYPCGSRFSCRK MIL      73
P19_Clon23 PYDPCNFCYPCGSRFSCRK MIL      73
P19_Clon24 PYDPCNFCYPCGSRFSCRK MIL      73
*****

```

**Figure 3.4. Amino acid sequence alignment of ODF1-exon2 from patient n°19.** Four out of five clones carried the variant motif CSP (clones 16, 20, 23, and 24; yellow) whereas clone 22 has the variant motif CNP (green) (ref.sec NG\_028006.1).

### **3.1.2 Patients with decapitated spermatozoa carried normal sequences of exons 10 and 11 of the gene *Hook1* compared to the reference wild-type sequence**

The murine *Hook1* gene is highly expressed in testis. *Hook1* has 11 splice variants in mice and 6 in humans. The longest *Hook1* transcript in humans and mice comprises 22 exons. In mice, the deletion of exons 10 and 11 affects HOOK1 functionality and perturbs the correct attachment of sperm head and tail (Mendoza-Lujambio, 2002). In humans, a missense mutation affecting the exon 10 has been identified. This mutation localizes in the central region of the coiled-coil domain, where the base pair G is replaced by A, causing a non-synonymous change in p.Q286R (Chen et al., 2018). Therefore, an alteration in the coiled-coil motif might affect the protein's ability to interact with other proteins and bind to organelles. Besides that, HOOK1 localizes to the manchette in mouse spermatids and is involved in the interconnection between the manchette microtubules (Walenta et al., 2001). Thus, HOOK1 is implicated in the manchette's correct positioning and its proper connection to the nuclear envelope. Therefore, a dysfunctional protein might be responsible for decapitated spermatozoa. It proposes *Hook1* as a causative candidate gene for human teratozoospermia or decapitation syndrome (Mendoza-Lujambio, 2002).

I investigated exons 10 and 11 of the *Hook1* gene to figure out whether *Hook1* is involved in the acephalic syndrome represented by these two patients. Exon 10 and 11 were amplified using the primer pairs Hook1-E10-N-for/Hook-Exon10-Rev and Hook1-E11-N-for/Hook1-E11-N-Rev, respectively (Tab. 6.1.1). Both exons were amplified and cloned into the vector pJET1.2/blunt (Fermentas). The DNA isolated from 2 up to 8 individual colonies were sequenced. Sequences of exon 10 and 11 from both patients exhibit the same nucleotide sequence as the reference NC\_000001.11 (Fig. 3.5 – 3.6 – 3.7). Mutations were not found in the regions investigated, including the annotated deletion of exon 10 and 11. Therefore, the possibility was excluded that mutations in exon 10 or 11 might be causative for the acephalic spermatozoan syndrome in the patients studied here.

```

Hook1_ Ex10      CAAGGCTTGAAGCTGCAAAAAGATGATTACCGTGTTCACTGTGAAGAAGCTTGAAAAGCAGC 60
P17_ClonA2      CAAGGCTTGAAGCTGCAAAAAGATGATTACCGTGTTCACTGTGAAGAAGCTTGAAAAGCAGC 60
P17_ClonA3      CAAGGCTTGAAGCTGCAAAAAGATGATTACCGTGTTCACTGTGAAGAAGCTTGAAAAGCAGC 60
P17_ClonB4      CAAGGCTTGAAGCTGCAAAAAGATGATTACCGTGTTCACTGTGAAGAAGCTTGAAAAGCAGC 60
P17_ClonB6      CAAGGCTTGAAGCTGCAAAAAGATGATTACCGTGTTCACTGTGAAGAAGCTTGAAAAGCAGC 60
P17_ClonG19     CAAGGCTTGAAGCTGCAAAAAGATGATTACCGTGTTCACTGTGAAGAAGCTTGAAAAGCAGC 60
P17_ClonG21     CAAGGCTTGAAGCTGCAAAAAGATGATTACCGTGTTCACTGTGAAGAAGCTTGAAAAGCAGC 60
P17_ClonH23     CAAGGCTTGAAGCTGCAAAAAGATGATTACCGTGTTCACTGTGAAGAAGCTTGAAAAGCAGC 60
P17_ClonH24     CAAGGCTTGAAGCTGCAAAAAGATGATTACCGTGTTCACTGTGAAGAAGCTTGAAAAGCAGC 60
*****

Hook1_ Ex10      TAATCGAATTCAGCATAGGAATGATGAATTGACTAGTCTTGCAGAAGAAACAAGAGCCC 120
P17_ClonA2      TAATCGAATTCAGCATAGGAATGATGAATTGACTAGTCTTGCAGAAGAAACAAGAGCCC 120
P17_ClonA3      TAATCGAATTCAGCATAGGAATGATGAATTGACTAGTCTTGCAGAAGAAACAAGAGCCC 120
P17_ClonB4      TAATCGAATTCAGCATAGGAATGATGAATTGACTAGTCTTGCAGAAGAAACAAGAGCCC 120
P17_ClonB6      TAATCGAATTCAGCATAGGAATGATGAATTGACTAGTCTTGCAGAAGAAACAAGAGCCC 120
P17_ClonG19     TAATCGAATTCAGCATAGGAATGATGAATTGACTAGTCTTGCAGAAGAAACAAGAGCCC 120
P17_ClonG21     TAATCGAATTCAGCATAGGAATGATGAATTGACTAGTCTTGCAGAAGAAACAAGAGCCC 120
P17_ClonH23     TAATCGAATTCAGCATAGGAATGATGAATTGACTAGTCTTGCAGAAGAAACAAGAGCCC 120
P17_ClonH24     TAATCGAATTCAGCATAGGAATGATGAATTGACTAGTCTTGCAGAAGAAACAAGAGCCC 120
*****

Hook1_ Ex10      TGAAAGATGAAATAGATGTTCTTAG 145
P17_ClonA2      TGAAAGATGAAATAGATGTTCTTAG 145
P17_ClonA3      TGAAAGATGAAATAGATGTTCTTAG 145
P17_ClonB4      TGAAAGATGAAATAGATGTTCTTAG 145
P17_ClonB6      TGAAAGATGAAATAGATGTTCTTAG 145
P17_ClonG19     TGAAAGATGAAATAGATGTTCTTAG 145
P17_ClonG21     TGAAAGATGAAATAGATGTTCTTAG 145
P17_ClonH23     TGAAAGATGAAATAGATGTTCTTAG 145
P17_ClonH24     TGAAAGATGAAATAGATGTTCTTAG 145
*****

```

**Figure 3.5. DNA sequence alignment of *Hook1*-exon10 from patient n°17.** The alignment of the eight clones analyzed are identical to the wild type sequence. Sequences were compared to the reference sequence NC\_000001.11.

```

Hook1_ Ex10      CAAGGCTTGAAGCTGCAAAAAGATGATTACCGTGTTCACTGTGAAGAAGCTTGAAAAGCAGC 60
P19_ClonK1      CAAGGCTTGAAGCTGCAAAAAGATGATTACCGTGTTCACTGTGAAGAAGCTTGAAAAGCAGC 60
P19_ClonK2      CAAGGCTTGAAGCTGCAAAAAGATGATTACCGTGTTCACTGTGAAGAAGCTTGAAAAGCAGC 60
P19_ClonL6      CAAGGCTTGAAGCTGCAAAAAGATGATTACCGTGTTCACTGTGAAGAAGCTTGAAAAGCAGC 60
P19_ClonM7      CAAGGCTTGAAGCTGCAAAAAGATGATTACCGTGTTCACTGTGAAGAAGCTTGAAAAGCAGC 60
P19_ClonM8      CAAGGCTTGAAGCTGCAAAAAGATGATTACCGTGTTCACTGTGAAGAAGCTTGAAAAGCAGC 60
P19_ClonN10     CAAGGCTTGAAGCTGCAAAAAGATGATTACCGTGTTCACTGTGAAGAAGCTTGAAAAGCAGC 60
P19_ClonN11     CAAGGCTTGAAGCTGCAAAAAGATGATTACCGTGTTCACTGTGAAGAAGCTTGAAAAGCAGC 60
P19_ClonN12     CAAGGCTTGAAGCTGCAAAAAGATGATTACCGTGTTCACTGTGAAGAAGCTTGAAAAGCAGC 60
*****

Hook1_ Ex10      TAATCGAATTCAGCATAGGAATGATGAATTGACTAGTCTTGCAGAAGAAACAAGAGCCC 120
P19_ClonK1      TAATCGAATTCAGCATAGGAATGATGAATTGACTAGTCTTGCAGAAGAAACAAGAGCCC 120
P19_ClonK2      TAATCGAATTCAGCATAGGAATGATGAATTGACTAGTCTTGCAGAAGAAACAAGAGCCC 120
P19_ClonL6      TAATCGAATTCAGCATAGGAATGATGAATTGACTAGTCTTGCAGAAGAAACAAGAGCCC 120
P19_ClonM7      TAATCGAATTCAGCATAGGAATGATGAATTGACTAGTCTTGCAGAAGAAACAAGAGCCC 120
P19_ClonM8      TAATCGAATTCAGCATAGGAATGATGAATTGACTAGTCTTGCAGAAGAAACAAGAGCCC 120
P19_ClonN10     TAATCGAATTCAGCATAGGAATGATGAATTGACTAGTCTTGCAGAAGAAACAAGAGCCC 120
P19_ClonN11     TAATCGAATTCAGCATAGGAATGATGAATTGACTAGTCTTGCAGAAGAAACAAGAGCCC 120
P19_ClonN12     TAATCGAATTCAGCATAGGAATGATGAATTGACTAGTCTTGCAGAAGAAACAAGAGCCC 120
*****

Hook1_ Ex10      TGAAAGATGAAATAGATGTTCTTAG 145
P19_ClonK1      TGAAAGATGAAATAGATGTTCTTAG 145
P19_ClonK2      TGAAAGATGAAATAGATGTTCTTAG 145
P19_ClonL6      TGAAAGATGAAATAGATGTTCTTAG 145
P19_ClonM7      TGAAAGATGAAATAGATGTTCTTAG 145
P19_ClonM8      TGAAAGATGAAATAGATGTTCTTAG 145
P19_ClonN10     TGAAAGATGAAATAGATGTTCTTAG 145
P19_ClonN11     TGAAAGATGAAATAGATGTTCTTAG 145
P19_ClonN12     TGAAAGATGAAATAGATGTTCTTAG 145
*****

```

**Figure 3.6. DNA sequence alignment of *Hook1*-exon10 from patient n°19.** The alignment of the eight clones analyzed are identical to the wild type sequence. Sequences were compared to the reference sequence NC\_000001.11.

Hook1_ Ex11	GGCTACCTCTGATAAAGCAAATAAACTGGAGTCAACAGTTGAGATATATCGTCAGAAGCT	60
P17_clon1	GGCTACCTCTGATAAAGCAAATAAACTGGAGTCAACAGTTGAGATATATCGTCAGAAGCT	60
P19_clon1	GGCTACCTCTGATAAAGCAAATAAACTGGAGTCAACAGTTGAGATATATCGTCAGAAGCT	60
	*****	
Hook1_ Ex11	ACAAGATCTGAATGACCTTCGCAAGCAGGTGAAAACCTTACAGGAAACCAACATGATGTA	120
P17_clon1	ACAAGATCTGAATGACCTTCGCAAGCAGGTGAAAACCTTACAGGAAACCAACATGATGTA	120
P19_clon1	ACAAGATCTGAATGACCTTCGCAAGCAGGTGAAAACCTTACAGGAAACCAACATGATGTA	120
	*****	
Hook1_ Ex11	TATGCATAATACAGTCAGCTTAGAAGAAGAATTAAGCAAAATGCAGCACGTACACA	180
P17_clon1	TATGCATAATACAGTCAGCTTAGAAGAAGAATTAAGCAAAATGCAGCACGTACACA	180
P19_clon1	TATGCATAATACAGTCAGCTTAGAAGAAGAATTAAGCAAAATGCAGCACGTACACA	180
	*****	
Hook1_ Ex11	ATTAGAAACATACAAAAGGCAG	202
P17_clon1	ATTAGAAACATACAAAAGGCAG	202
P19_clon1	ATTAGAAACATACAAAAGGCAG	202
	*****	

**Figure 3.7. DNA sequence alignment of *Hook1*-exon11 from patient n°17 and 19.** The alignment of the two clones analyzed are identical to the wild type sequence. Sequences were compared to the reference sequence NC\_000001.11.

### 3.1.3 Patients with decapitated spermatozoa carried normal sequences of exons 6 and 8 of the gene *Spag4l* compared to the reference wild-type sequence

*Spag4l* consists of 13 exons in humans that encode the nuclear membrane protein SPAG4L/SUN5 of a size of 43 kDa. SUN5 localizes at the implantation fossa of mature spermatozoa (Yassine et al., 2015) and is essential for the attachment of the sperm head to the tail. Given that SPAG4L is an essential protein of the HTCA, I explored the sequences of exons 6 and 8, which have a size of 50 bp and 109 bp, respectively.

Mutations of *Spag4l* in humans cause the abnormal attachment of the sperm flagellum to the nucleus. The disassembly is triggered by the absence of the implantation fossa and the basal plate. Previous analyses in patients with the acephalic spermatozoan syndrome have identified 11-point mutations. These mutations caused nonsense, missense, and one intron modification and can affect the protein structure (Zhu et al., 2016; Elkhatib et al., 2017), e.g., the mutations c.340G→A (p.Gly114Arg), c.425 + 1G →A (c.1043A>T) and c.475C→T (p.Arg159\*) (Fig. 3.8).

The mutation c.340G→A (p.Gly114Arg) localizes in the predicted transmembrane domain, specifically to the last nucleotide of exon 5. According to a computational prediction, the replacement c.340G→A resulted in a missense mutation that affects the exon 5 and the expression of the SUN5 protein. Hence, the mutation c.340G→A might disrupt the localization of SUN5 at the nuclear envelope because of the impairment of the transmembrane domain (Zhu et al., 2016; Elkhatib et al., 2017; Shang et al., 2018).

The intronic mutation c.425 + 1G →A in humans localizes in the first base of intron 7 and introduces a premature stop codon. The induction of this mutation in the mouse testicular teratoma cell line F9 truncates the protein translation, which ends at Arg-142. Furthermore, this point mutation localizes upstream of the coiled-coil domain (Zhu et al., 2016; Elkhatib et al., 2017; Shang et al., 2018). Therefore, it might affect the protein conformation. According to a previous report, this protein alteration might disrupt the ability of SUN5 to interact with other proteins, especially with DNAJB13 (Shang et al., 2018).

A similar effect is caused by the mutation c.475C→T (p.Arg159\*). It localizes to exon 8, inside the coiled-coil domain. This mutation introduces a premature stop codon and affects the secondary structure of the SUN5 protein. Furthermore, this premature protein termination increases the number of acephalic spermatozoa. Therefore, it has been suggested that this mutation disrupts the ability of SUN5 to interact with its counterparts (Shang et al., 2018).

Altogether, these data strongly indicate that impairments of the SUN5 function leads to the acephalic spermatozoa syndrome. Therefore, I analyzed different exons of the two unrelated infertile patients to identify possible mutations in *Spag4l*.

Exon 6 (50 bp length) was amplified using the primer pair Sun5-Ex7-For and Sun5-Ex7-Rev. This primer pair amplified a fragment of 200 bp, which includes part of the upstream and downstream introns. However, no mutations were found (Fig. 3.9 – 3.10 – 3.11). Thus, exon 6 seems not to be implicated in the acephalic spermatozoa syndrome in the two patients analyzed here. Exon 8 (109bp) was amplified using the primer pair suggested by Zhu et al. (2016), here named Sun5-Ex8-Zhu-For and Sun5-Ex8-Zhu-Rev. This primer pair amplified a fragment of 284 bp, which includes part of the upstream and downstream introns (Fig. 3.9). However, these primers turned out to be unspecific, amplifying a fragment of chromosome 17, whereas *Spag4l* localizes to chromosome 20. I also started to investigate exons 11 and 13 using the primer sequences specified by Zhu et al., Sun5-E11-Zhu-For/Sun5-E11-Zhu-Rev, and Sun5-E13-Zhu-For/Sun5-E13-Zhu-Rev. However, amplification of both exons was unsuccessful (Fig. 3.9).

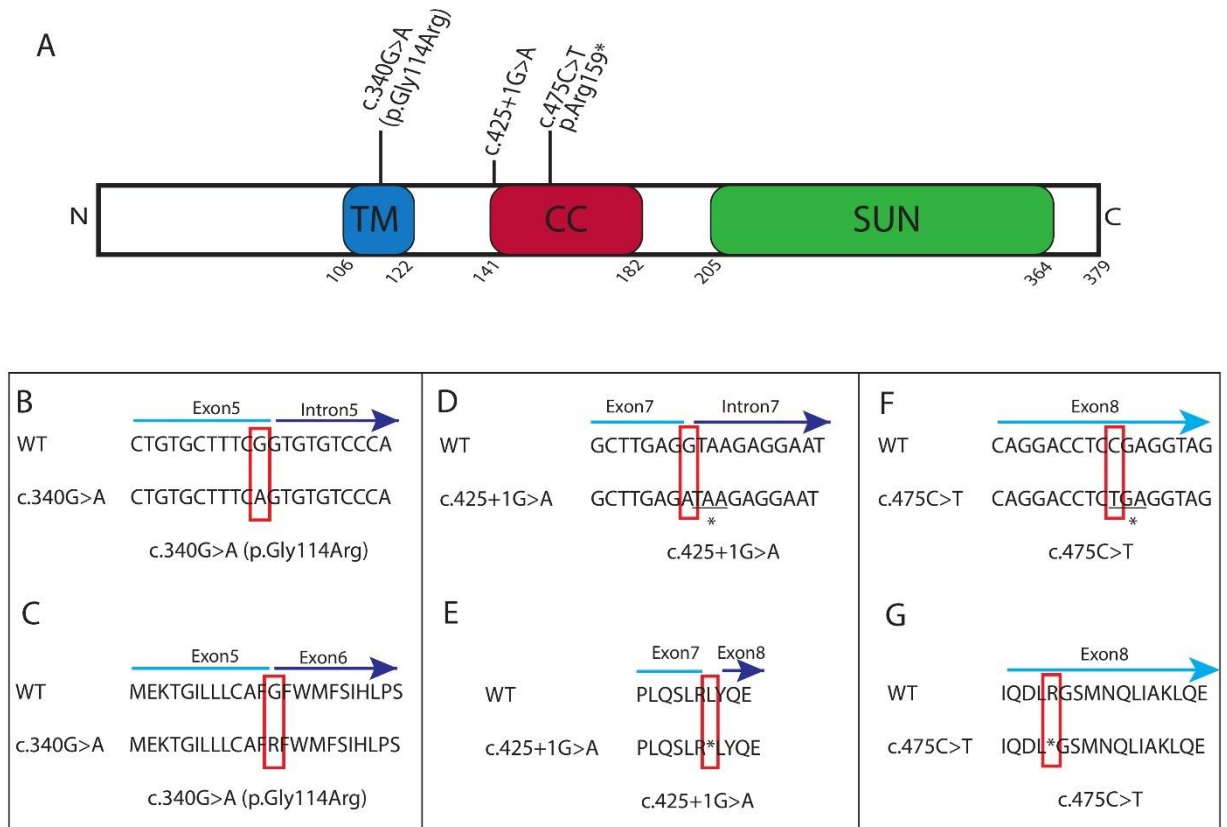


**Figure 3.8. Mutations in TM and coiled-coil domain of the human *Spag4L*.** (A) Distribution of mutations in *Spag4L*. c.340G>A affects the transmembrane domain (TM), c.425+1G>A situates upstream of the coiled-coil domain and c.475C>T situates in the coiled-coil domain. (B) c.340G>A mutation localizes in the last nucleotide of exon 5 (red square). (C) c.340G>A mutation produces a missense change, p.Gly114Arg (red square). (D) c.425+1G>A situates in the first nucleotide of intron 7 (red square), introducing a premature stop codon (asterisk) and retaining partially 18 bp of the intron 7. (E) c.425+1G>A produces a splicing-site mutation by the introduction of a stop codon (asterisk). (F) c.475C>T introduces a stop codon in exon 8 (red square and asterisk). (G) c.475C>T truncates the secondary structure of SPAG4L (asterisk). (Adapted from Zhu et al., 2016; Shang et al., 2018).

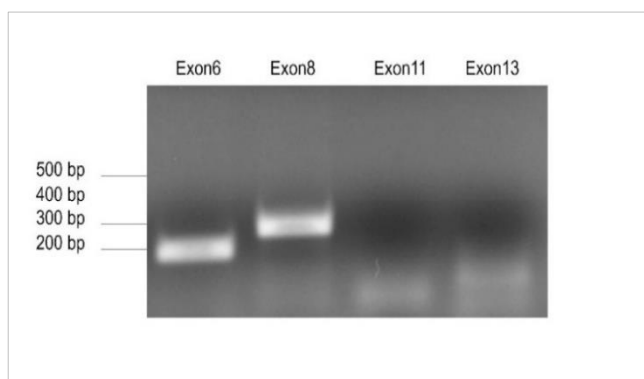


**Figure 3.9. DNA amplification of exons 6, 8, 11, and 13 of *Sun5*.** PCR was performed on DNA from patient n°19. Primers to amplify exon 6 generated the expected product size of ~ 200 bp (50 bp of exon 6 + introns). Primers to amplify exon 8 generated a product of ~300 bp (109 bp of exon 8 + introns) as expected. Primers to amplify exon 11 and 13 failed in the amplification. The expected product was not obtained.

Sun5-Ex6	GATTCTGGATGTTTTCTATTCACCTTACCATCGAAAATGAAAGTCTGGCAG	50
Pat17-Clon25	GATTCTGGATGTTTTCTATTCACCTTACCATCGAAAATGAAAGTCTGGCAG	50
Pat17-Clon26	GATTCTGGATGTTTTCTATTCACCTTACCATCGAAAATGAAAGTCTGGCAG	50
Pat17-Clon28	GATTCTGGATGTTTTCTATTCACCTTACCATCGAAAATGAAAGTCTGGCAG	50
	*****	

**Figure 3.10. DNA sequence alignment of *Sun5*-exon6 from patient n°17.** The alignment of the three clones analyzed are identical to the wild type sequence. Sequences were compared to the reference sequence NG\_054760.1.

Sun5-Ex6	GATTCTGGATGTTTTCTATTCACCTTACCATCGAAAATGAAAGTCTGGCAG	50
Pat19-Clon2	GATTCTGGATGTTTTCTATTCACCTTACCATCGAAAATGAAAGTCTGGCAG	50
Pat19-Clon5	GATTCTGGATGTTTTCTATTCACCTTACCATCGAAAATGAAAGTCTGGCAG	50
Pat19-Clon7	GATTCTGGATGTTTTCTATTCACCTTACCATCGAAAATGAAAGTCTGGCAG	50
Pat19-Clon10	GATTCTGGATGTTTTCTATTCACCTTACCATCGAAAATGAAAGTCTGGCAG	50
	*****	

**Figure 3.11. DNA sequence alignment of *Sun5*-exon6 from patient n°19.** The alignment of the four clones analyzed are identical to the wild type sequence. Sequences were compared to the reference sequence NG\_054760.1.

## 3.2 Characterization of the SUN-domain proteins SPAG4 and SPAG4L

### 3.2.1 Localization of the SUN domain proteins SPAG4L and SPAG4L2 at the nuclear membrane

SPAG4 and SPAG4L play essential roles in the formation of the HTCA. The depletion of SPAG4 in mice weakens the attachment of the basal plate to the implantation fossa affecting the HTCA formation (Yang et al., 2018). Similarly, the partial disruption of *Spag4l* in mice interferes with the correct attachment of the sperm head to the tail (Shang et al., 2017). Additionally, the disruption of the exons that encode the SUN domain of SPAG4L results in acephalic spermatozoa by affecting the implantation fossa as observed in infertile men (Shang et al., 2017). Altogether, these data confirm the role of SPAG4 and SPAG4L in the formation of the head to the tail coupling apparatus. Therefore, the topological analysis of SPAG4L and its variant SPAG4L2 contributes to a better comprehension of their ability to recruit proteins to the nuclear envelope. Moreover, it could improve the understanding of the mechanisms to link the sperm head to the flagellum.

SPAG4L and SPAG4L2 are nuclear membrane proteins that share a similar structure. Both proteins are composed of one or two transmembrane domains in the N-terminal region,



respectively, a coiled-coil domain in the middle and a SUN domain in the C-terminal region. *Spag4l* and *Spag4l2* are transcribed in testis, and their expression is correlated with the emergence of round spermatids during spermiogenesis (Xing et al., 2004; Frohnert et al., 2011).

*Spag4l2* is a longer isoform of *Spag4l* that encodes two predicted transmembrane domains in its N-terminal region. In contrast, *Spag4l* encodes solely one. In both isoforms, transmembrane domains are followed by a coiled-coil region and the conserved SUN domain at the C-terminal (Xing et al., 2004; Frohnert et al., 2011). Moreover, SPAG4L2 has been described as nuclear membrane protein, with a N-terminal region oriented towards the nucleoplasm, and a C-terminal domain oriented towards the cytoplasm (Frohnert et al., 2011). Despite that fact, SPAG4L has been also identified as interacting partner of the cytoplasmic protein ODF1 (Shao et al., 2001). Given the localization of SPAG4L at the nuclear envelope (NE) it raises the question of how SPAG4L is able to interact with ODF1. Thus, I reevaluate the localization of SPAG4L2 domains and the impact of a truncated SUN-domain on the recruitment of the full-length protein to the NE.

To figure out in more detail the contribution of the diverse protein domains for the distribution of the whole protein, I generated a series of plasmids encoding specific parts of the protein fused to either the HA-, myc-, or EGFP-tag (Fig. 3.12). Plasmids were transfected into NIH3T3 cells, and their expression and protein localization were investigated by tag-specific antibodies.

Moreover, I investigated whether the disruption of the SUN domain affects the localization of SPAG4L2 at the nuclear membrane. It has been reported that a CRISPR-mediated disruption of the exons 10-12 encoding the SUN domain caused acephalic spermatozoa in mice (Shang et al., 2017). Thus, an expression plasmid encoding the truncated protein reported by Shang et al. (2017) was generated.

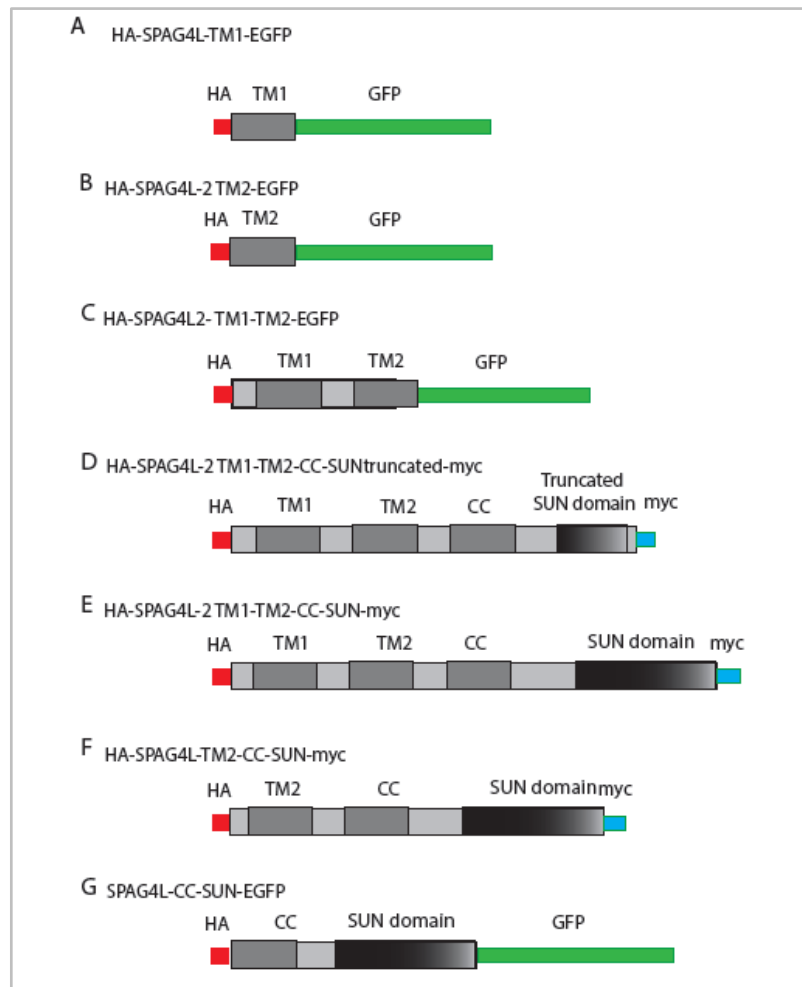


**Figure 3.12. Schematic representation of *Spag4l2* expression plasmids.** Transmembrane domain 1 (TM1); transmembrane domain 2 (TM2); coiled-coil domain (CC); SUN domain (SUN). (A) TM1 is tagged with HA at the N-terminal and GFP at the C-terminal. (B) TM2 is tagged with HA at the N-terminal and GFP at the C-terminal. (C) TM1 and TM2 tagged with HA at the N-terminal and GFP at the C-terminal. (D) Truncated *Spag4l2* with a deletion of exon 10-12 encoding the SUN domain. Truncated *Spag4l2* was tagged with HA at the N-terminal and with the myc epitope at the C-terminal. (E) Full-length *Spag4l2* was tagged with HA at the N-terminal and with the myc epitope at the C-terminal. (F) Full-length *Spag4l*, which contains only TM2, tagged with HA at the N-terminal and with the myc epitope at the C-terminal. (G) The Coiled-coil region and SUN domain were tagged with HA at the N-terminal and the EGFP epitope at the C-terminal.

Immunocytological analyses showed that the full-length SPAG4L2 protein localizes at the nuclear membrane as well as in the cytoplasm (Fig. 3.13 A-C). The TM1 tagged to HA at the N-terminal and EGFP at the C-terminal is highly expressed in the cytoplasm and at the nuclear membrane (Fig. 3.13 D-G). In contrast, the TM2 tagged to HA at the N-terminal and GFP at the C-terminal was detected at the nuclear membrane and cytoplasm by its HA-tag. However, its EGFP-tag was only detected in the region that seems to be the endoplasmic reticulum.

Additionally, the localization of the recombinant protein HA-TM2-EGFP was detected by its HA and EGFP tags in the region that corresponds to the Golgi apparatus endoplasmic reticulum by analogy to previous reports (Frohnert et al., 2011) (Fig. 3.13 H-K). Expression of the combined TMs (TM1 and TM2), tagged with HA and EGFP, revealed a clear nuclear membrane localization (Fig. 3.13 L-O). Ectopic expression of the truncated *Spag4l2*, comprising TM1, TM2, and the coiled-coil region but without the SUN domain, demonstrated a clear nuclear membrane localization (Fig. 3.13 P-R). By contrast, the C-terminal region containing the coiled-coil region and the SUN domain showed only a cytoplasmatic distribution (Fig. 3.13 S-U). These results strongly indicate that the transmembrane domain I (TM1) is essential for SPAG4L2 localization at the nuclear envelope. Furthermore, the transmembrane domain II (TM2) seems not to be required for the localization of SPAG4L2 at the nuclear membrane. Moreover, the coiled-coil region and SUN-domain displayed a cytoplasmatic localization and they appear not to be responsible for SPAG4L recruitment to the nuclear envelope.

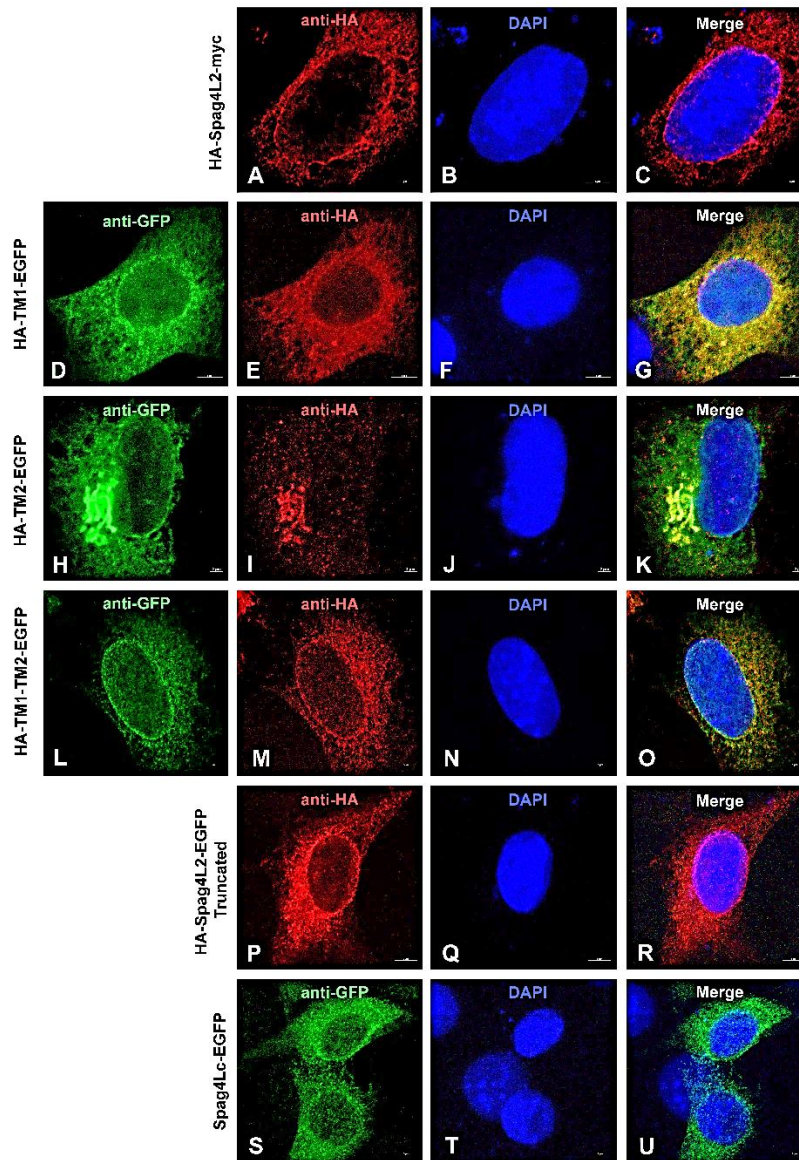


**Figure 3.13. The protein domain organization of SPAG4L2 and their individual cellular distribution.** Different expression plasmids were transfected into NIH3T3 cells and analyzed immunocytologically. (A-C) Full-length *Spag4l2* (tagged with HA at the N-terminal and with the myc epitope at the C-terminal) localizes to the nuclear envelope and shows a mild distribution in the cytoplasm. (D-G) TM1 (tagged with HA at the N-terminal and EGFP at the C-terminal) exposes a strong distribution in the cytoplasm and at the nuclear membrane. (H-K) TM2 (tagged with HA at the N-terminal and EGFP at the C-terminal) was detected at the nuclear membrane and the cytoplasm by its EGFP-tag, whereas the HA-tag was only detected in the cytoplasm. (L-O) TM1 and TM2 (tagged with HA at the N-terminal and EGFP at the C-terminal) expose a consistent localization at the nuclear envelope as well as a distribution to the cytoplasm. (P-R) The truncated SUN domain of *Spag4l2* (tagged with HA at the N-terminal and with the myc epitope at the C-terminal) reveals a strong distribution in the cytoplasm and the nuclear membrane. (S-U) The Coiled-coil region and SUN domain (tagged with HA at the N-terminal and with the EGFP at the C-terminal) localizes in the cytoplasm. Nuclear counterstain with DAPI (blue). Bars are of 2  $\mu\text{m}$  (A-L) and 5  $\mu\text{m}$  (M-P).

### 3.2.2 Impact of *Spag4*- deficiency on gene expression during mouse spermatogenesis

In mice, the expression of the *Spag4* gene is restricted to testes, and its transcription starts in post-meiotic stages, around 18 days after birth. SUN4/SPAG4 is exclusively expressed in round and elongated spermatids. At the beginning of spermiogenesis, SPAG4 localizes at the nucleus of round spermatids, while in elongated spermatids, SPAG4 is situated close to the manchette. At the late stages of spermiogenesis, the manchette disassembles and SPAG4 is placed at the distal pole of the nuclear envelope. Here, it contributes to the linkage of head to tail in sperm (Yang et al., 2018). Thus, SPAG4 is essential for the correct sperm head shape, manchette organization, and anchorage of the sperm head to the flagellum (Calvi et al., 2015; Pasch et al., 2015; Yang et al., 2018).

SUN domain proteins reside in the nuclear envelope and participate in the linkage of the cytoskeleton to the nucleoskeleton (LINC) by their interaction with the conserved KASH domain proteins. Besides that, SUN domain proteins are involved in many cellular functions as telomere attachment to the inner nuclear membrane and chromosomes movements during meiosis (Malone et al., 1999; Padmakumar, 2005; Crisp et al., 2006; Ding et al., 2007; Razafsky & Hodzic, 2009; Starr & Fridolfsson, 2010).

In mice, spermatogenesis requires around 35 days (Oakberg, 1956). The process starts with the proliferation of spermatogonial stem cells (SSC). SSC undergo spermatogonia differentiation to produce A-, intermediate and B-spermatogonia. After the differentiation phase, B-spermatogonia produces pre-leptotene spermatocytes, which go through meiosis in ~8.6 days old mice (Oakberg, 1956; Nebel et al., 1961; De Rooij & Grootegoed, 1998; Eddy, 1998). Primary spermatocytes undergo the first meiotic division, including leptotene, zygotene, pachytene, diplotene. Once the first meiotic phase is completed, secondary spermatocytes experience a fast second meiotic division to produce round spermatids (RS) at 18 dpp. Finally, RS undergo spermiogenesis, which is completed after 30 dpp and elongated spermatids are detected (Oakberg, 1956; Nebel et al., 1961; Clermont, 1972; Frank et al., 1986; Russell, 1990).

In the first step of spermatogenesis, the stimulated by retinoic acid gene (*Stra8*), a spermatogonial marker, is involved in spermatogonial proliferation and spermatocyte transition (Ma et al., 2018). Spermatocytes then enter meiosis and proteins as SYCP1 and SYCP3 regulate chromosome synapsis during zygotene-pachytene (Meuwissen et al., 1992; Yuan et al., 2000; Costa et al., 2005). Once round spermatids are produced, cells start the nuclear shaping and DNA packaging. During this process remodeling of the chromatin takes place that involves the replacement of somatic histones by testis-specific histones followed by transition proteins and

finally by protamines (Balhorn, 1982). The male germ cell-specific expressed histone Hanp1/H1T2/H1-7 is one of the early replacement histones (Balhorn, 1982; Tanaka et al., 2005), whereas protamine 1 is first transcribed in round spermatids (Braun, 1990).

During spermiogenesis, two  $\alpha$ -tubulin isotypes restricted to testis, *Ma3* and *Ma7*, start their transcription (Villasante et al., 1986). *Odf1* initiates its transcription in round spermatids before condensation and elongation of the spermatid nucleus (Burmester et al., 1996). *Spag4* starts its transcription in postmeiotic spermatids (Pasch et al., 2015; Yang et al., 2018).

Given that SPAG4, a member of the SUN domain proteins, localizes at the nuclear membrane and interacts with proteins inside the nucleus, disruption of *Spag4* might affect the transcription and spermatogenic progression. Hence, to evaluate a possible influence of the deletion of *Spag4* in male germ cells, I investigated the expression pattern of molecular marker genes that characterize the progression of spermatogenesis (Fig. 3.14). To achieve this purpose, RNA was isolated from adult testes of wild type mice as well as of heterozygous and homozygous *Spag4*-deficient mice using animals aged 10-months (wild-type and *Spag4*<sup>+/-</sup> #319), 3-months (*Spag4*<sup>-/-</sup> #343), and 8-weeks (wild-type #393, *Spag4*<sup>+/-</sup> #371, *Spag4*<sup>-/-</sup> #363). Total RNA was first treated with DNase and thereafter reverse transcribed into cDNA.

After the verification of the *Spag4*-genotype, the expression of meiotic and post-meiotic marker genes was investigated. Amplification of cDNA from wild-type versus *Spag4*-deficient mice showed a slight difference in *Hanp1* and *Prm1* gene expression. *Hanp1* exhibits a weaker band in the amplified cDNA from *Spag4*<sup>-/-</sup> testis compared to wild-type samples, whereas *Prm1* shows a stronger band in the amplification of the cDNA from *Spag4*<sup>-/-</sup> testis in comparison to wild-type (Fig. 3.15 A). Therefore, both genes were analyzed by qRT-PCR to quantify their expression.

First, specific primers were designed (Table 6.1.3), and their efficiencies and melting curves were tested by serial dilutions. The marker genes *Stra8*, *Hanp1*, *Prm1*, and *Odf1*, were quantified and their expression was calculated by the double delta Ct method. The housekeeping gene *Hrpt* was used as an internal reference gene (Fig. 3.15 B).

Two independent qRT-PCRs were performed. The first one included animals between 3 and 10 months old, whereas the second one included 8-weeks old animals. Thus, the experiment was performed using 2 biological replicates and 3 technical replicates. The results of the qRT-PCR expression analyses confirmed the previous results obtained by RT-PCR. These results suggest that *Spag4*-depletion affects the expression of the post-meiotic gene *Hanp1* and *Prm1*. It was

observed that *Spag4*-deficiency reduced the expression of *Hanp1* and increased the expression of *Prm1* (Fig. 3.15 B).

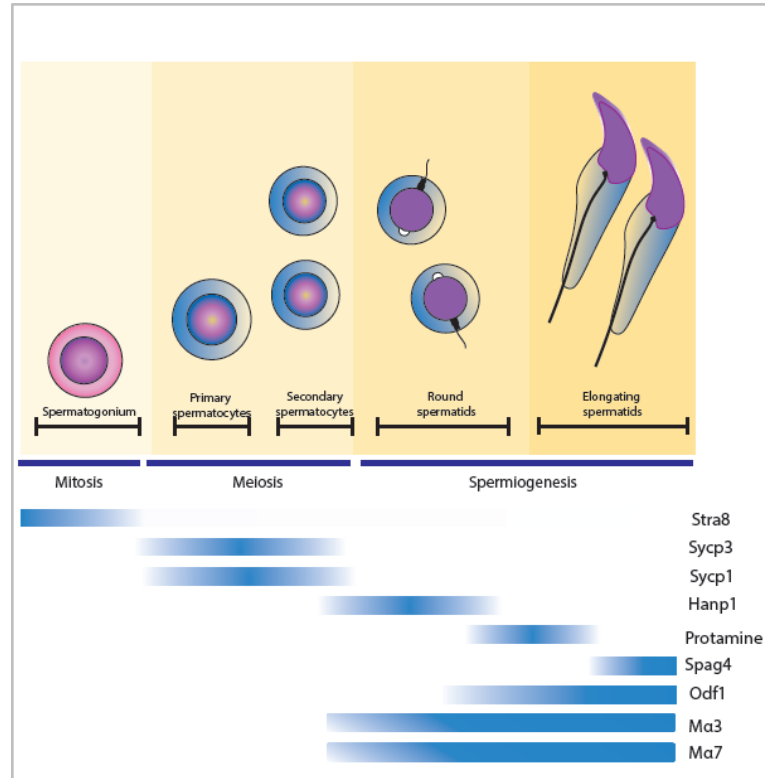


**Figure 3.14. Schematic representation of the expression of gene markers during spermatogenesis.** Spermatogonia are mitotically active cells that are characterized by the expression of *Stra8*. During meiosis, homologous chromosomes undergo synapsis. This process is assisted by synaptonemal complex proteins as SYCP1 and SYCP3. Chromatin remodeling starts in post-meiotic round spermatids with the replacement of somatic histones by testis-specific histones as HANP1. Afterward, histones are replaced by protamines. The transformation of round spermatids to mature spermatozoa includes the transcription of *Spag4*, *Odf1*, and the  $\alpha$ -tubulin isotypes *Ma3* and *Ma7*. These genes encode essential proteins required for the head reshaping and the connection of the sperm head and tail.

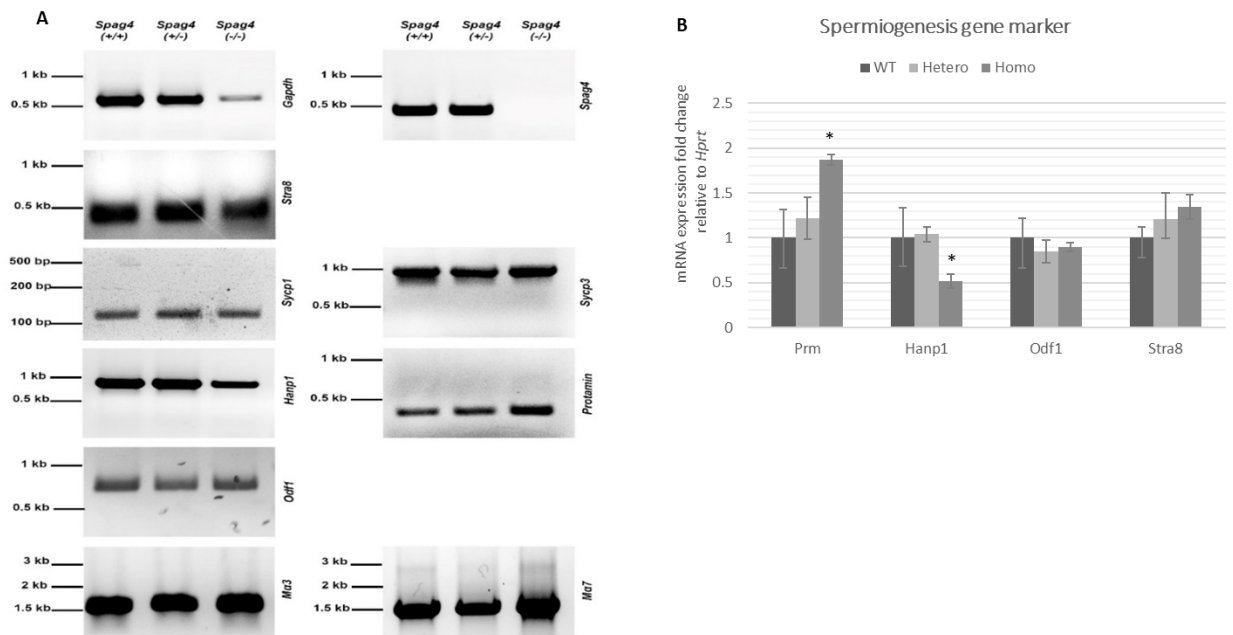


**Figure 3.15. Gene expression profiling of marker genes for spermatogenic progression in *Spag4*-deficient mice.** (A) RT-PCR was performed on cDNA generated from testes of 8-weeks old mice. The correct genotype was verified by amplifying *Spag4*. Amplification of *Gapdh* was used to confirm cDNA quality. RT-PCR shows normal expression of the premeiotic marker gene *Stra8* and the meiotic marker genes *Sycp1* and *Sycp3*. The early post-meiotic marker gene *Hanp1* shows a reduced transcription in *Spag4*<sup>-/-</sup> mice, whereas *Prm1* increases its transcription. The late post-meiotic marker genes *Odf1*, *Ma3*, and *Ma7*, display a homogeneous expression. (B) qRT-PCR analysis for gene markers during spermatogenesis. The expression of *Prm1*, *Hanp1*, *Odf1* and *Stra8* was evaluated using testicular cDNA obtained from wild type, *Spag4*<sup>+/-</sup> and *Spag4*<sup>-/-</sup> mice. Relative expression values were calculated by normalizing to *Hprt* expression. *Spag4*-depletion caused increased expression of *Prm1* and reduction of *Hanp1* expression. Significance is indicated with \* $p \leq 0.05$ .

### 3.2.3 The amber suppression method and its suitability for the identification of SPAG4 binding proteins

Identifying novel SPAG4 binding partners is essential for a better understanding of the sperm decapitation syndrome and male infertility to increase our knowledge about the molecular components of the HTCA. Considering that SPAG4 is a SUN domain protein that mediates the linkage between the nucleoskeleton and the cytoskeleton via binding KASH domain proteins, it is important to investigate currently unknown KASH domain proteins and lamins that could be specific for the male germ cell (Starr & Han, 2003; Crisp et al., 2006; Razafsky & Hodzic, 2009). Identification of novel interaction partners by taking advantage of the native topology and orientation of SUN domain proteins inside the nuclear membrane is a challenging task but



avoids severe artificial conditions that are present in Co-IP or pull-down assays (Choi et al., 2019). I, therefore, explored whether the amber suppression method is suitable for this purpose.

The amber suppression method takes advantage of an expansion of the genetic code. The genetic code comprises 64 three-base codons. Of these codons, 61 encode for 20 canonical amino acids, whereas the other 3 are the nonsense or termination codons (UAA-Ochre, UAG-Amber, and UGA-Opal). The genetic code was considered universal and “frozen” because it remained invariable in all organisms (Hinegardner and Engelberg, 1963; Woese et al., 1964; Sharp and Bulmer, 1988). However, in mitochondrial and nuclear genomes, the genetic code has evolved, e.g., in *Mycoplasma sp.*, which translates UGA as Trp, and in *Acetabularia acetabulum* that reassigns the stop codons UAA and UAG to Gln (Osawa et al., 1992; Knight et al., 2001). These expansions of the genetic code enable the artificial incorporation of unnatural amino acids into proteins.

To incorporate unnatural amino acids (UAAs) into proteins and expand the genetic code of mammalian cells, new tRNA and its corresponding aminoacyl tRNA synthetase (tRNA-aaRS) are required (Xie & Schultz, 2005). First, a stop codon should be incorporated into the protein-coding sequence of interest. Then, the corresponding tRNA anticodon must be engineered to be orthogonal to the aaRS. The aaRS must be modified to solely recognize the UAA and not any other natural amino acid. Next, the aminoacyl tRNA synthetase, tRNA, and construct of interest are introduced into cells. Once all components have been transfected and in the presence of the UAA, the aaRS covalently links the tRNA with the UAA. Then, tRNA charged with the anticodon recognizes the complementary three-base termination codon in the mRNA incorporating the UAA into the protein (Knight et al., 2001; Xie & Schultz, 2005).

Among the stop codons, the amber codon (UAG) is not used frequently by organisms as *E.coli* (9%) and yeast (23%). Therefore, its incorporation into mRNA does not significantly perturb the host growth (Xie & Schultz, 2005). Furthermore, the amber tRNA anticodon can be expressed in mammalian cells and can be aminoacylated by the mutant aaRS. Beyond that, it is also possible to incorporate a photoreactive amino acid into proteins. The incorporation of a photoreactive amino acid enables the identification of protein interacting partners that are near to the photo-labeled protein of interest. The *p*-benzoyl-L-phenylalanine (*p*Bpa) is an unnatural amino acid that contains a photoreactive side chain (Kauer et al., 1986; Xie et al., 2005). The benzophenone group of *p*Bpa is an efficient photo-crosslinker. It reacts with peptides close to the target protein, specifically with nearby C-H bonds, when cells are exposed to UV light of 350–365 nm. This reaction produces covalent cross-links between interacting proteins. *p*Bpa can be incorporated in vivo into proteins using an orthogonal aminoacyl-tRNA

synthetase/tRNA-pair that translates the amber codon (Kauer et al., 1986; Chin et al., 2003; Hino et al., 2005, Das and Oliver et al., 2011).

Thus, to first validate and explore the method, an orthogonal aminoacyl-tRNA synthetase/tRNA (p4XtRNA<sub>pBpa</sub>) that exclusively recognizes the amber stop codon, UAG, was generated. Furthermore, different plasmids encoding for lamin C were generated. Lamin C consists of an amino-terminal head, a helical rod domain (coiled-coil), and a carboxy-terminal tail domain. The C-terminal tail is highly conserved among lamins and adopts an immunoglobulin (Ig) fold (Dhe-Paganon et al., 2002; Krimm et al., 2002; Dittmer and Misteli 2011). Therefore, this region is supposed to be a hot spot for protein interactions. Thus, three different plasmids were designed in which amber codons were incorporated into the Ig-fold region of lamin C. An amber codon replaced the codons corresponding to Arg-470, Thr- 488, and Thr-534 in the coding region for the lamin C protein. The plasmids were named as pLMNC-R470-3X-FLAG, pLMNC-T488-3X-FLAG, and pLMNC-T534-3X-FLAG. Dr. Petra Neumann-Staubitz kindly provided all plasmids.

First, I evaluated the effective incorporation of the unnatural amino acid *pBpa*. NIH3T3 cells were transfected with plasmids that encode the orthogonal tRNA-aaRS (p4XtRNA<sub>pBpa</sub>) and one of the plasmids containing the specific amber mutation. As expected, the orthogonal tRNA-aaRS (p4XtRNA<sub>pBpa</sub>) incorporated *pBpa* into lamin C amino-acid sequence. Cells transfected with p4XtRNA<sub>pBpa</sub>/pLMNC-R470-3X-FLAG, p4XtRNA<sub>pBpa</sub>/pLMNC-T488-3X-FLAG, or p4XtRNA<sub>pBpa</sub>/pLMNC-T534-3X-FLAG were grown in media with or without supplementation of *pBpa*. After transfection, translation of LMNC comprising the amber codon was analyzed by immunofluorescence using the antibody anti-Flag.

The results revealed that the ectopic expression of pLMNC-R470-3X-Flag and p4XtRNA<sub>pBpa</sub> in NIH3T3 cells showed an abnormal expression of LMNC. Lamins generally reside at the nuclear membrane; however, the genetically engineered LMNC localized inside the nucleus (Fig. 3.16 A-C). In contrast, supplementation of 1mM of *pBpa* in the cell growth media enables the correct translation of the protein and its location at the nuclear membrane (Fig. 3.16 D-F). Similar results were obtained when cells were transfected with the following combinations: either p4XtRNA<sub>pBpa</sub>/pLMNC-T488-3X-FLAG or p4XtRNA<sub>pBpa</sub>/pLMNC-T534-3X-FLAG (Fig. 3.16 G-R). This experiment confirmed the efficient incorporation of the unnatural amino acid *pBpa* into the genetically engineered LMNC sequence. The addition of *pBpa* seemed neither to affect the protein sequence nor its localization at the nuclear membrane.

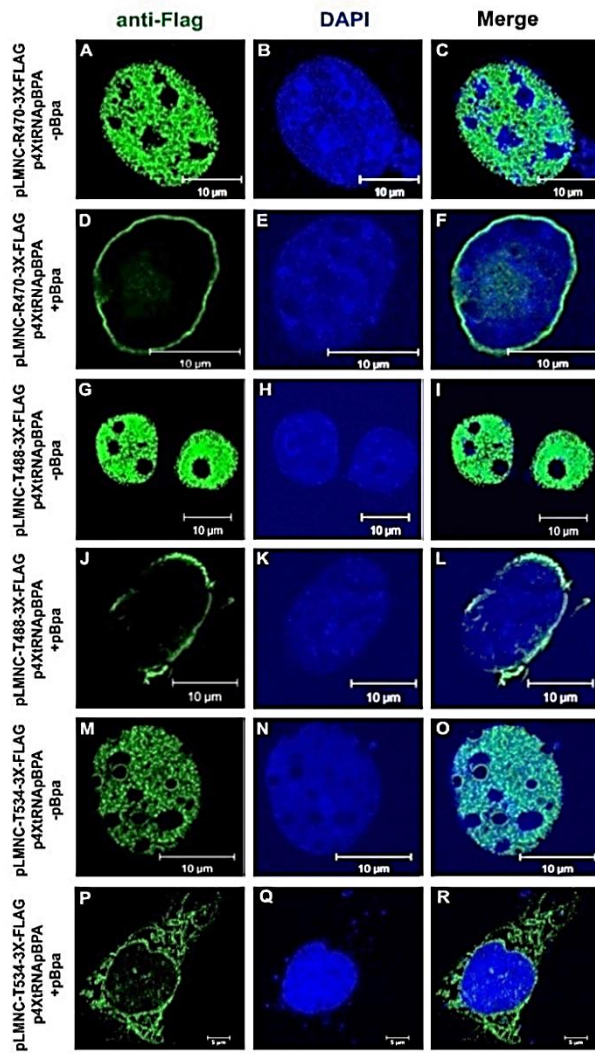


**Figure 3.16 Incorporation of the unnatural amino acid *pBpa* into LMNC sequences.**

Three different *Lmnc* expression plasmids were co-transfected with the orthogonal tRNA-aaRS in NIH3T3 in the following order: (A-F) *pLMNC-R470-3X-FLAG/ p4XtRNApBpa*, (G-I) *pLMNC-T488-3X-FLAG/p4XtRNApBpa*, (M-R) *pLMNC-T534-3X-FLAG/ p4XtRNApBpa*. NIH3T3 cells were either incubated in the absence of the unnatural amino acid *pBpa* (A-C; G-I; M-O) or with the addition of *pBpa* (D-F; J-L; P-R). Twenty-four hours post-transfection, cells were fixed and permeabilized. LMNC was detected using the anti-Flag antibody (green). Nuclei were stained using DAPI (blue). Scale bar, 10  $\mu$ m (A-O), and 5  $\mu$ m (P-R).

In the next step, I attempted to reevaluate the interaction of the SUN domain proteins with LMNC. Previously, it has been reported that SUN1 interacts with lamin A (LMNA) but not with lamin C, B1, or B2 (Haque et al., 2006). Therefore, I expected that SPAG4 would not interact with LMNC either. The first experiment performed served as a negative control experiment to exclude any false positive interactions.

For this purpose, we used the plasmid *HA-Spag4-MYC*. HEK293 cells were transfected in triplicate with the orthogonal tRNA-aaRS (4XtRNApBpa) and *HA-Spag4-MYC*, and either one or the other *Lmnc* expression plasmid carrying the amber codon. One group of transfected cells was not treated with *pBpa*. The second and third groups were incubated with the unnatural amino acid (*pBpa*). Twenty-four hours after transfection, the third group of transfected cells (previously incubated with *pBpa*) was treated with UV-light of  $\sim$ 365 nm. In this case, UV-light acts as a linking agent causing covalent cross-linking of closely associated proteins. Proteins were isolated from all cells and analyzed by western blotting.

To sum-up the experimental setting:

Group 1: HEK293 cells transfected with *pLMNC-R470-3X-Flag*, *p4XtRNApBpa* and *HA-Spag4-MYC*.

Group 2: HEK293 cells transfected with *pLMNC-R470-3X-Flag*, *p4XtRNApBpa* and *HA-Spag4-MYC*. Cells were incubated with 1 mM *pBpa*.

Group 3: HEK293 cells transfected with *pLMNC-R470-3X-Flag*, *p4XtRNApBpa* and *HA-Spag4-MYC*. Cells were incubated with 1 mM *pBpa*.

Exposition to ~365 nm UV light

Negative control: Untreated HEK293 cells

The results are shown in Fig. 3.17. The first lane of the images A and B shows the proteins isolated and detected from group 1 of samples. The second lane corresponds to group 2. The third lane corresponds to group 3, and lane four to untreated HEK293 cells. On the one hand, image A shows that HA-SPAG4-myc was successfully overexpressed in HEK293 cells. SPAG4 was detected using the mouse anti-HA antibody. The electrophoretic band was detected at ~55 kDa, consistent with the expected molecular weight of SPAG4.

Further, SPAG4 was detected in the three different groups of transfected cells. On the other hand, several unspecific bands were detected by the antibody in the image-A. One of these bands is at ~100 kDa and it is present in all the samples, including the negative control (lane four). Moreover, there are protein bands at ~130 kDa and ~180 kDa in the first lane. These unspecific bands do not correspond to a potential cross-linked complex between SPAG4 and LMNC, which has an expected molecular mass of ~110 kDa corresponding to the sum of SPAG4 (55 kDa) and LMNC (62 kDa) (Fig. 3.16, A). To elucidate the origin of these unexpected protein bands, I transfected HEK293 cells with *pLMNC-R470-3X-Flag*, exclusively. However, the same unspecific protein bands were detected with the anti-HA antibody (data are not shown).

Regarding LMNC, the same protein lysates were immunoblotted and probed with mouse IgM anti-laminA/C antibody. The expected electrophoretic bands at ~70 kDa and ~62 kDa, corresponding to LMNA and LMNC, respectively, were detected. This result was somehow unexpected because the third lane corresponds to proteins translated without *pBpa* supplementation. It was, therefore, expected that no recombinant LMNC would be generated (Fig. 3.17, B). The same protein lysates were immunoblotted with rabbit anti-Flag. However, the antibody detected unspecific bands even in the negative control (data are not shown). These data indicate that the endogenous expression of lamin A and lamin C seems to interfere with the

detection of the recombinant LMNC. Besides that, no interaction between SPAG4 and LMNC was detected.

To sum-up, the incorporation of the unnatural amino acid *pBpa* into LMNC sequences was successful, as shown by immunocytological analyses. However, the detection of the genetically engineered LMNC protein by Western blotting was unsuccessful.

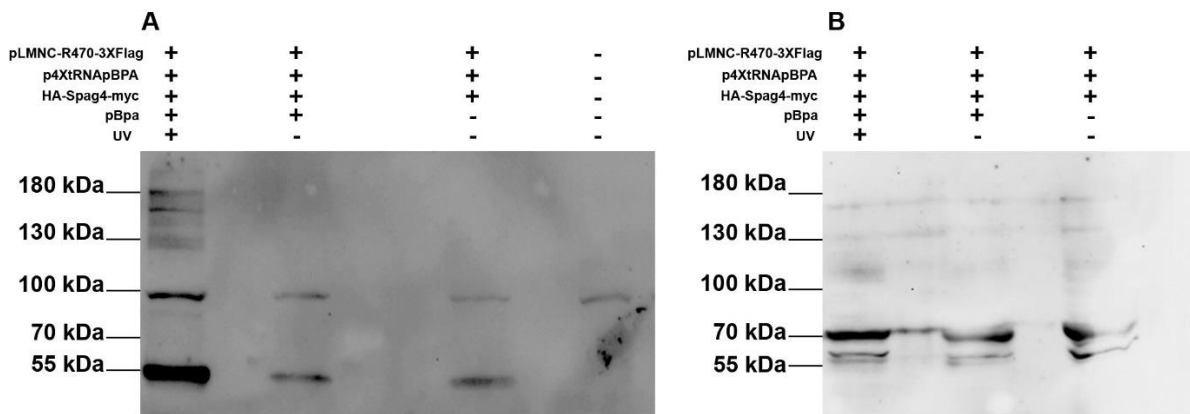


**Figure 3.17 Evaluation of the amber suppression method by immunoblotting.** HEK293 cells were transfected with *pLMNC-R470-3X-FLAG*, *p4XtRNApBpa*, and *HA-Spag4-MYC*, followed by *pBpa* addition or exclusion and UV exposure or omission. Proteins were detected using either mouse anti-HA to identify *HA-Spag4-MYC* (A) or mouse IgM anti-laminaA/C to identify LMNC (B). *HA-Spag4-MYC* was detected in all samples in the expected molecular mass of ~55 kDa. Besides, an unspecific band was detected around 100 kDa (A). LaminaA/C antibody detected two bands corresponding to LMNA of ~70 kDa and LMNC of ~62 kDa (B).

### 3.2.4 Reevaluation of the topology of SPAG4 and SPAG4L across the nuclear envelope by drug-induced protein recruitment

The SUN-domain proteins reside in the nuclear envelope. As anticipated from somatic SUN-domain proteins, their N-terminal region is located in the nucleus and their SUN domains in the perinuclear space (Crisp et al., 2006). The N-terminal contains up to two transmembrane domains, which recruit the full-length protein to the nuclear membrane. Beyond that, the orientation of testicular SUN-domain proteins, as e.g. SPAG4, is unknown. Considering that the C-terminal ends of SUN-domain proteins, including that of SPAG4 and SPAG4L, are inside the perinuclear space, it is completely unclear how they can directly interact with cytoskeletal proteins, as e.g. ODF1. Therefore, determining the topology of SPAG4 or SPAG4L in relation

to the nuclear membrane requires a sophisticated analysis. To this end, I established the rapamycin system.

Rapamycin is a small molecule that binds to both FKBP and FRB to induce dimerization. In the absence of rapamycin, FKBP and FRB proteins do not interact (Fegan et al., 2010; Inobe & Nukina, 2016). Thus, by the generation of fusion proteins that are either linked to FKBP or FRB, rapamycin induces their dimerization and, therefore, the recruitment of the fusion proteins.

The following sets of expression plasmids were designed to achieve this purpose: *FRB-ECFP-SUN4*, *FRB-ECFP-SUN5*, *Luciferase-mRFP-FKBP*, *pLCK-ECFP-FRB*, and *FKBP-mRFP*. Here, it is important to remark that the N-terminal region of *Sun4/Spag4* and *Sun5/Spag4l* were fused to the C-terminal region of *FRB-ECFP*. Given that the SUN-domain of SUN4 and SUN5 reside in the perinuclear space, their N-terminal coupled to FRB-ECFP could be oriented towards the nucleoplasm or to the cytoplasm. Thus, if the N-terminal region of FRB-ECFP-SUN4 or FRB-ECFP-SUN5 is oriented towards the cytoplasm, FRB will be available to interact with its counterpart FKBP. This might indicate that the N-terminal of SUN4 and SUN5 might interact with cytoplasmic proteins, e.g. ODF1. It was expected that Luciferase-mRFP-FKBP localized in the cytoplasm and not in the nucleoplasm. The proteins Luciferase-mRFP-FKBP, pLCK-ECFP-FRB, and FKBP-mRFP were used as controls.

Plasmids were pairwise transfected into NIH3T3 cells:

- a) *FRB-ECFP-SUN4* and *Luciferase-mRFP-FKBP*: Luciferase-mRFP-FKBP should predominantly be expressed in the cytoplasm, whereas FRB-ECFP-SUN4 in the nuclear envelope. Rapamycin should enable the interaction of Luciferase-mRFP-FKBP and FRB-ECFP-SUN4, causing the recruitment of the Luciferase-mRFP-FKBP protein from the cytoplasm to the nuclear membrane.
- b) *FRB-ECFP-SUN5* and *Luciferase-mRFP-FKBP*: the localization and reaction of these proteins should be the same as in a).
- c) *FRB-ECFP-SUN4* and *mRFP-FKBP*: FRB-ECFP-SUN4 should be expressed in the nuclear membrane, whereas mRFP-FKBP should localize in both cytoplasm and nucleoplasm. Rapamycin should induce the dimerization and relocalization of mRFP-FKBP to the nuclear membrane.
- d) *FRB-ECFP-SUN5* and *mRFP-FKBP*: the localization and reaction of these proteins should be the same as described in a).
- e) *pLCK-ECFP-FRB* and *Luciferase-mRFP-FKBP*: Luciferase-mRFP-FKBP should mostly be expressed in the cytoplasm, whereas pLCK-ECFP-FRB should localize in

both cytoplasm and nucleoplasm. Rapamycin may induce the relocalization of pLCK-ECFP-FRB from the nucleoplasm to the cytoplasm (control).

- f) *pLCK-ECFP-FRB* and *mRFP-FKBP*: Control. Both proteins should be expressed in the cytoplasm and nucleoplasm. Rapamycin addition should induce dimerization of both proteins but without changing their localization (control).

Rapamycin-induced heterodimerization of FKBP-rapamycin-FRB was started 24 hrs post-transfection by addition of 1 mM rapamycin for 20 minutes.

Since SUN4 and SUN5 are nuclear envelope proteins, I expected that the recombinant proteins FRB-ECFP-SUN4 and FRB-ECFP-SUN5 would be likewise localized in the nuclear membrane. In contrast, Luciferase-mRFP-FKBP was expected to be cytoplasmic. Rapamycin-induced heterodimerization between Luciferase-mRFP-FKBP and the FRB-fusion protein, either FRB-ECFP-SUN4 or FRB-ECFP-SUN5, should cause a re-localization and recruitment of Luciferase-mRFP-FKBP to the nuclear membrane (Fig. 3.18).

As expected, FRB-ECFP-SUN4 localizes at the nuclear membrane, whereas Luciferase-mRFP-FKBP resides in the cytoplasm (Fig.3.19 A-H). The addition of rapamycin triggered the re-localization of Luciferase-mRFP-FKBP from the cytoplasm to the nuclear membrane which is visible by the red fluorescent rim at the nuclear membrane (Fig. 3.19 I-P).

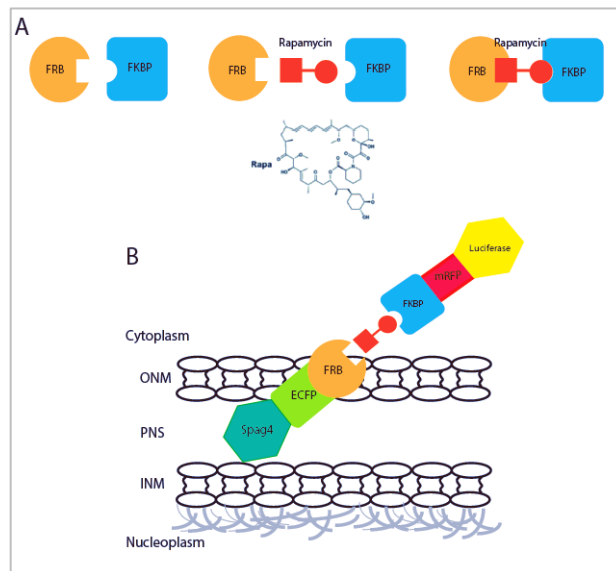


**Figure 3.18. Schematic representation of the rapamycin system.** (A) The interaction between FRB and FKBP is mediated by rapamycin. (B) FRB-ECFP-SUN4 resides in the nuclear envelope, whereas Luciferase-mRFP-FKBP localizes in the cytoplasm. Rapamycin induces the relocation of Luciferase-mRFP-FKBP to the nuclear membrane by affinity binding between FKBP-Rapamycin-FRB.

Luciferase-mRFP-FKBP is highly concentrated in the cytoplasm and at the area that seems to be the endoplasmic reticulum. The ER is an extension of the outer nuclear membrane (Lee et al., 1988). Therefore, it is difficult to clearly identify whether the proteins studied localize in the ER or at the nuclear membrane. Hence to inhibit protein translation, cells were incubated with puromycin for 4 hours before adding rapamycin. Thus, I expected that nuclear proteins would be recruited to the NE and would not be associated with the ER. However, cells treated with puromycin did not show considerable changes compared to the untreated cells (Fig. 3.19 Q- X).

Similar results were obtained by co-transfection of *FRB-ECFP-Sun5* and *Luciferase-mRFP-FKBP*. SUN5/SPAG4L resides at the nuclear membrane, while Luciferase-mRFP-FKBP is mostly localized in the cytoplasm without rapamycin incubation (Fig. 3.20 A-H). In contrast, rapamycin addition induces FKBP and FRB interaction, and hence the recruitment of Luciferase-mRFP-FKBP to the nuclear membrane via FRB-ECFP-SUN5 (Fig. 3.20 I-P).

As is known for the topology of the somatic SUN-domain proteins, SUN1 and SUN2, their N-terminal regions span the inner nuclear membrane and directly interact with lamin A and B (Hodzic et al., 2004; Padmakumar, 2005). Accordingly, the N-terminus is orientated towards the nucleoplasm. Therefore, I expected that the N-terminal fusion part FRB-ECFP linked to the N-terminal end of either SUN4 or SUN5 would be likewise exposed to the nucleoplasm and therefore not available for the rapamycin-induced dimerization when the FKBP-containing fusion protein localizes to the cytoplasm. However, the results demonstrate the ability of FRB-ECFP-SUN4 and FRB-ECFP-SUN5 to recruit Luciferase-mRFP-FKBP to the nuclear envelope, suggesting that the N-terminal end localizes in the cytoplasm.

To further validate the results, two control plasmids were used, mRFP-FKBP and pLCK-ECFP-FRB. Both plasmids encode fusion proteins of ~50 kDa, that are, due to their small size, able to passively diffuse through the nuclear envelope and enter the nucleus (Paine et al. 1972). Thus, mRFP-FKBP should be easily recruited by FRB-ECFP-SUN4 or FRB-ECFP-SUN5 to the inner nuclear membrane in the presence of rapamycin. *FRB-ECFP-Sun4* and *FRB-ECFP-Sun5* were each co-transfected with *mRFP-FKBP*. FRB-ECFP-SUN4 localized at the nuclear membrane, whereas mRFP-FKBP has a strong expression in the nucleus (Fig. 3.21 A-D, I-L). The addition of rapamycin caused recruitment of mRFP-FKBP to the nuclear membrane by both, either FRB-ECFP-SUN4 as well as FRB-ECFP-SUN5. However, a substantial amount of mRFP-FRB remained in the nucleoplasm and the cytoplasm (Fig. 3.21 E-H; M-P). These results demonstrate that the N-terminal ends of SUN4 or SUN5, fused to the FRB-ECFP, are exposed to the nucleoplasm, and can therefore recruit mRFP-FKBP.



Additionally, the cellular distribution of the recombinant proteins pLCK-ECFP-FRB and mRFP-FKBP were used as controls. Due to their small size, both proteins can pass the nuclear membrane and are therefore found in the nucleoplasm (Fig.3.21 Q-T). These data support the view that the luciferase fusion protein Luciferase-mRFP-FKBP localizes mainly in the cytoplasm. To finally demonstrate the rapamycin-induced heterodimerization, *Luciferase-mRFP-FKBP* was co-transfected with *pLCK-ECFP-FRB* into NIH3T3 cells. The addition of Rapamycin induced heterodimerization visible by the strong cytoplasmatic fluorescence (Fig.3.21 U-X).

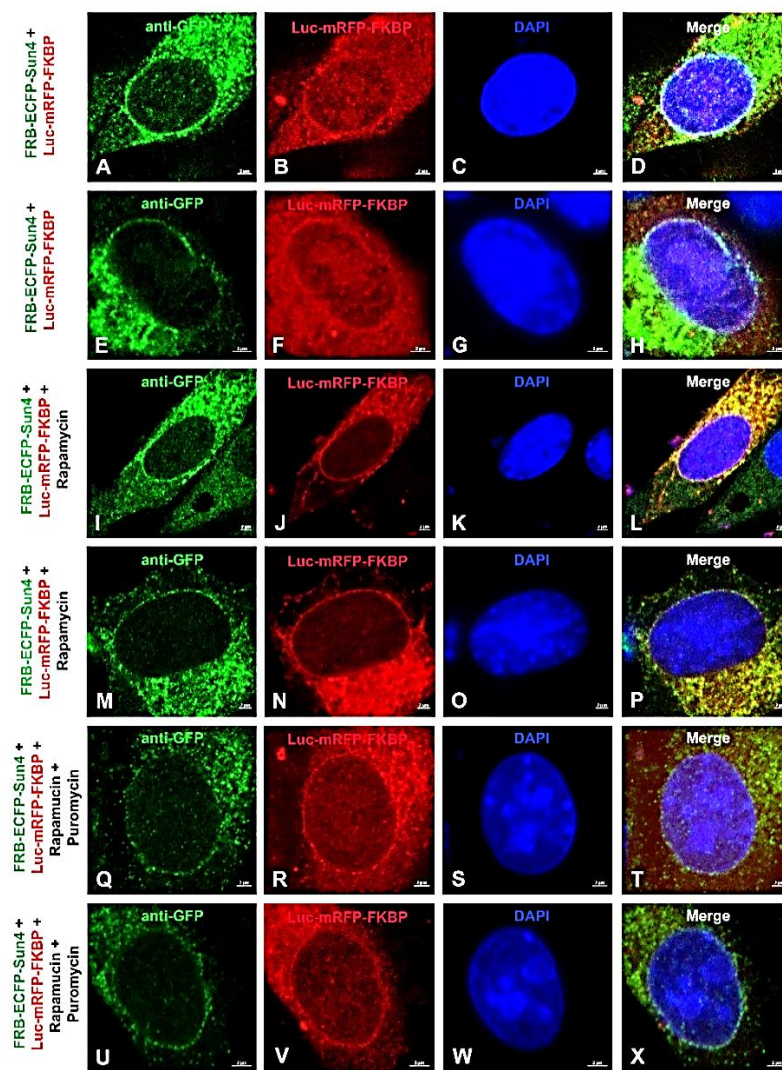


**Figure 3.19. Rapamycin-induced recruitment of Luciferase-mRFP-FKBP to the nuclear envelope via FRB-ECFP-SUN4.** *Luciferase-mRFP-FKBP* and *FRB-ECFP-Sun4* were co-transfected into NIH3T3 cells and analyzed by immuno-cytology. FRB-ECFP-SUN4 was immunodecorated by anti-GFP antibody (green), and Luciferase-mRFP-FKBP was detected by its fluorescent tag (Luciferase-mRFP FKBP, red). (A-H) FRB-ECFP-SUN4 is located at the nuclear envelope, whereas Luciferase-mRFP-FKBP is found mostly in the

cytoplasm and weakly in the nucleoplasm. (I-P) The addition of rapamycin induces the recruitment of Luciferase-mRFP-FKBP to the nuclear membrane resulting in a distinct red rim (Q-X). Pre-incubation with puromycin only weakened the cytoplasmic distribution of Luciferase-mRFP-FKBP and FRB-ECFP-SUN4. Nuclear counterstain with DAPI (blue). Bars are of 2  $\mu\text{m}$ .

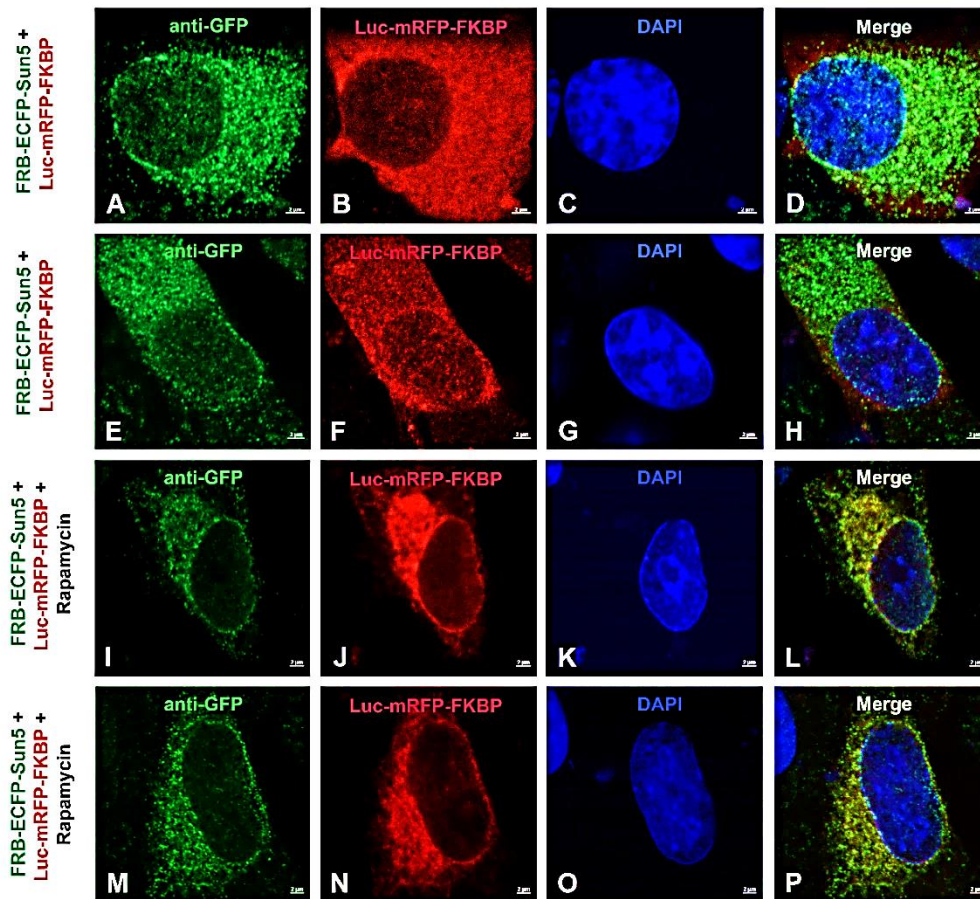


**Figure 3.20. Rapamycin-induced recruitment of Luciferase-mRFP-FKBP to the nuclear envelope via FRB-ECFP-SPAG4L/SUN5.** *Luciferase-mRFP-FKBP* and *FRB-ECFP-Sun5* were co-transfected into NIH3T3 cells and analyzed by immuno-cytology. FRB-ECFP-SUN5 was immunodecorated with anti-GFP antibody (green), and Luciferase-mRFP-FKBP was detected by its red fluorescent tag (Luciferase-mRFP-FKBP, red). (A-H) FRB-ECFP-SUN5 is located at the nuclear envelope without rapamycin, whereas Luciferase-mRFP-FKBP is mostly cytoplasmic. (I-P) The addition of rapamycin induces the re-localization of Luciferase-mRFP-FKBP to the nuclear membrane by heterodimerization of FRB-rapamycin-FKBP. Nuclear counterstain with DAPI (blue). Bars are of 2  $\mu\text{m}$ .

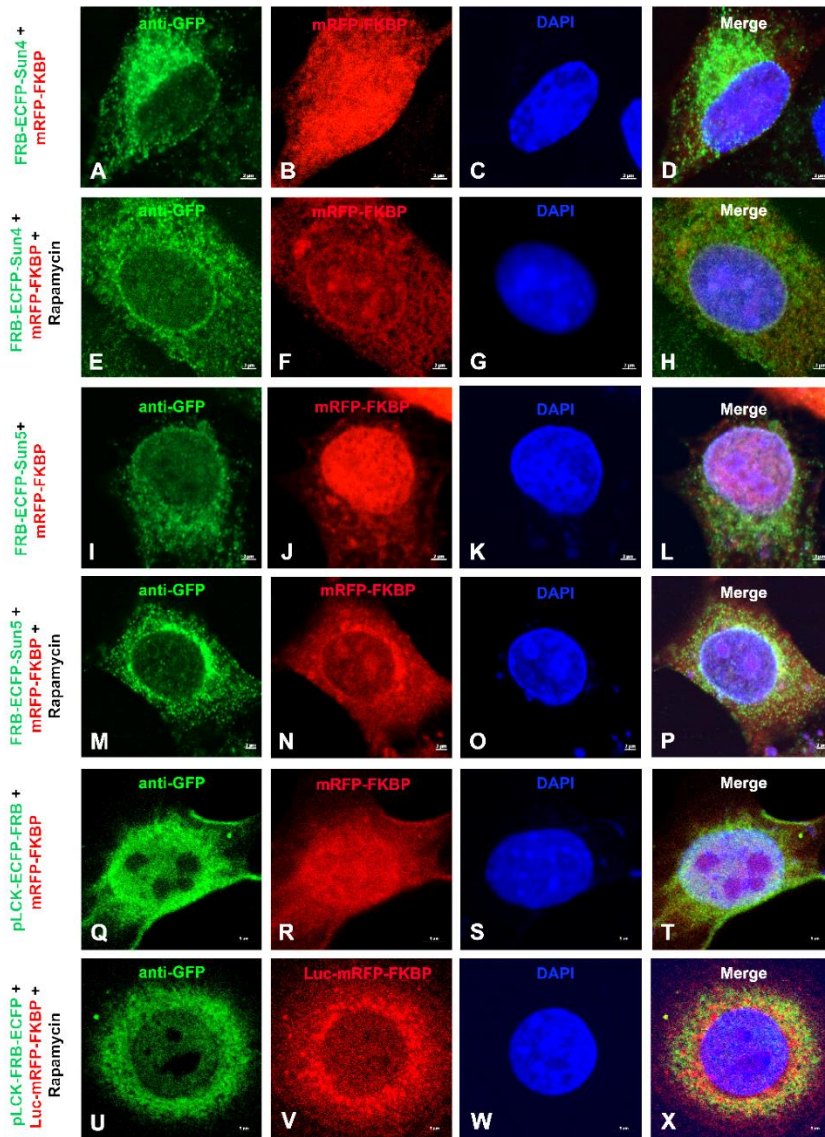


**Figure 3.21. Controls for the Rapamycin system.** FRB-ECFP-SUN4, FRB-ECFP-SUN5 and pLCK-FRB-ECFP were immunodecorated with anti-GFP antibody (green). Luciferase-mRFP-FKBP was detected by its red fluorescent protein, mRFP (red). (A-H) Co-expression of *FRB-ECFP-Sun4* and *mRFP-FKBP*. (A-D) FRB-ECFP-SUN4 localizes at the nuclear envelope, whereas mRFP-FKBP is strongly expressed in the nucleoplasm. (E-H) Rapamycin addition induces the heterodimerization of FRB with FKBP recruiting mRFP-FKBP to the nuclear membrane. (I-P) FRB-ECFP-SUN5 and mRFP-FKBP were co-transfected into NIH3T3 cells. (I-L) FRB-ECFP-SUN5 resides at the nuclear membrane, whereas mRFP-FKBP has a high expression in the nucleus. (M-P) The addition of rapamycin induces mRFP-FKBP recruitment to the nuclear membrane. (Q-X) Co-expression of *pLCK-ECFP-FRB* and *Luciferase-mRFP-FKBP*. (Q-T) Cytoplasmic and nuclear localization of Luciferase-mRFP-FKBP and pLCK-ECFP-FRB in the absence of rapamycin. (U-X) Rapamycin induces the heterodimerization of both proteins in the cytoplasm. Nuclear counterstain with DAPI (blue). Bars are of 2 µm.

### 3.3 Generation of *Spag4l/Sun5* knock out mice

#### 3.3.1 Genotyping of ES cells

To investigate the function of the *Sun5* gene, the project attempted to generate *Sun5* deficient mice using the knockout strategy. Homologous recombinant ES cells (*Sun5*tm1(KOMP)Vlcg, KOMP/Velocigene project: VG16078) were obtained from Velocigene Regeneron Pharmaceuticals Inc. The gene *Spag4L/Sun5* was completely disrupted and replaced by the reporter gene *LacZ* and the resistant gene *Neomycin* (Fig. 3.22). Recombinant embryonic stem cells were evaluated by PCR and qPCR, according to the method described in 2.2.5.4 and 2.2.5.5.

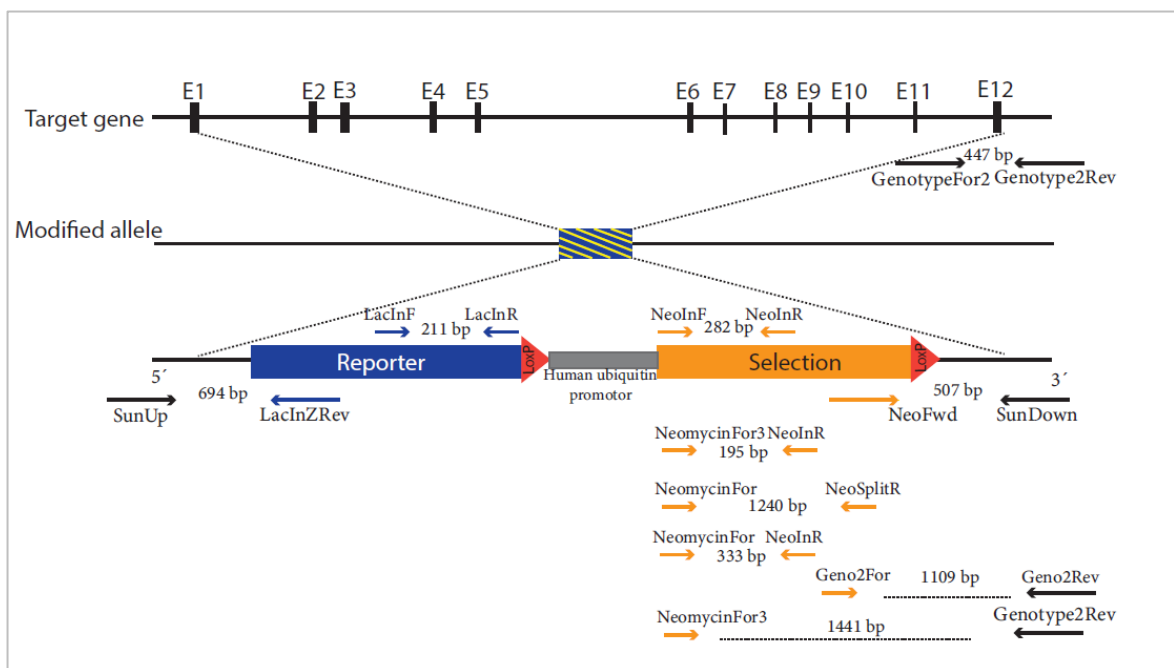


**Figure 3.22: Scheme of the *Sun5* knockout targeting vector.** The mouse *SUN5* gene consists of 12 exons. The targeted allele consists of the reporter gene *LacZ* (blue), followed by *LoxP*, human ubiquitin promoter, the selection gene neomycin (orange), and another *LoxP* site. This replacement cassette was integrated between the middle area of exon 1 and exon 12 of *Sun5*, leading to the complete depletion of *Sun5* coding sequences. Positions and sizes of primers required for genotyping are illustrated. The primer pairs SunUp/*LacInZRev* and Neofwd/*SunDown* enable the identification of the correct genomic insertion of the modified allele. The primer SunUp is situated in the upstream region of *Sun5*, whereas the primer *LacInZRev* is situated in the 5' region of the *LacZ* reporter gene. On the other side, Neofwd situates in the 3' region of neomycin cassette, whereas *SunDown* is situated in the downstream region of *Sun5*. Different pairs of primers served for genotyping and are shown as blue and orange arrows. The primer pair *GenotypeFor2/Genotype2Rev* detects the wild type allele, whereas Neofwd/*SunDown*, *Geno2For/Geno2Rev*, and NeomycinFor3/*Genotype2Rev* identified the recombinant allele.

DNA from ES cells was isolated using DirectPCR Lysis Reagent-Tail as described in 2.2.5.3 and the cassette insertion was verified by PCR using the primer pair SunUp and LacZRev. The primer SunUp amplified the intronic region upstream of the *Sun5* coding region. The cassette was inserted 88 bp downstream in the exon1. The primer LacInZRev situates at the beginning of the insertion cassette *LacZ* (Fig. 3.22). As expected, the PCR product had a size of ~602 bp (Fig. 3.23, A). Further, the fragment obtained was isolated and the DNA was sequenced with the primer LacInZRev to verify the cassette insertion in the genome. Sequences obtained confirm the insertion of the cassette in the genome (Fig. 3.23, B).

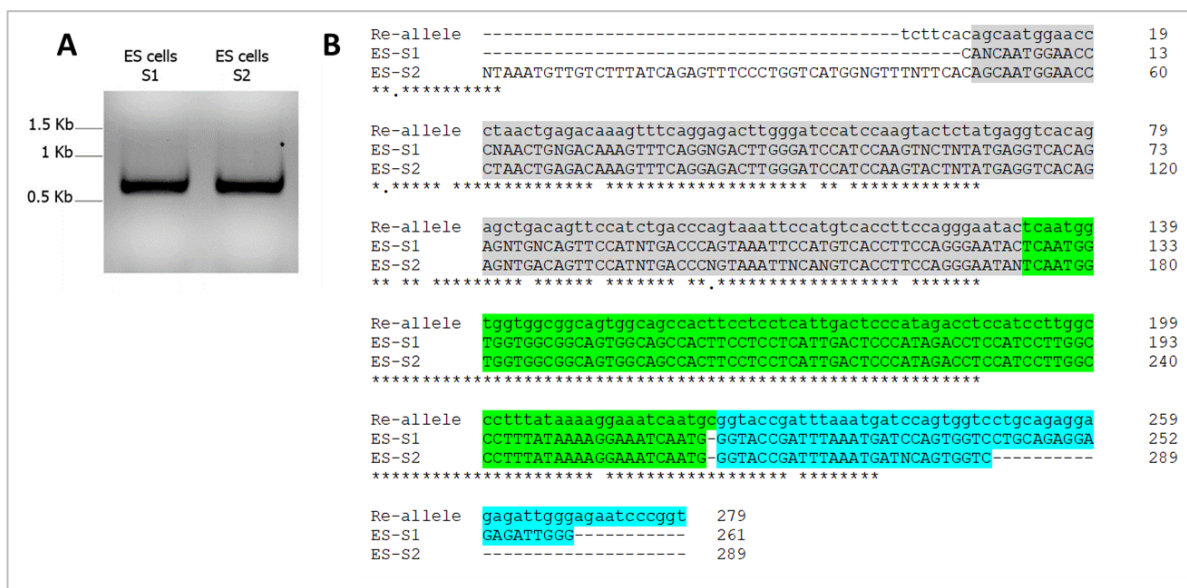


**Figure 3.23 Positive genotyping of ES cells.** (A) Recombinant ES cells confirm the correct LacZ-Neomycin cassette insertion in the mouse genome. The insertion was verified using the pairs of primers SunUp and LacZInRev, which amplify a fragment of ~602 bp. The primer SunUp is situated in the intronic region of the wild type allele ~ 562 bp upstream of the LacZ region (sequence highlighted in gray and green). Primer LacZInRev is situated in the 5' region of the LacZ reporter gene and recognize a fragment of ~40 bp (light blue). ES cells-sample 1 (S1), ES cells-sample 2 (S2). (B) Multiple alignment of the recombinant allele and recombinant embryonic stem cell sequences. Recombinant allele sequence (Re-allele), ES cells -sample 1 (S1), ES cells-sample 2 (S2). The intronic sequence of the wild type allele (gray), exon1 (green), LacZ sequence (light blue).

Once the correct insertion of the cassette LacZ-Neomycin in ES cells was confirmed, the deletion of *Sun5* was confirmed by qPCR before microinjection. To check the reduction of the expression of exon 7 and 9 of the *Sun5* gene, the following pair of primers were used: Sun5-mus-E5-For/ Sun5-mus-E5-Rev (to amplify exon7) and Sun5-mus-E8-For/ Sun5-mus-E8-Rev (to amplify exon 9) (Tab. 6.1.8). For this objective, the expression differences of the Ct value

obtained from the wild-type mouse was compared with the Ct value from recombinant ES cells using the double delta Ct method. *Odf1* and *protamine* genes were used as internal reference.

The relative Ct value of exons 7 and 9 was set as 1 in DNA from the wild-type mouse. The DNA from ES cells demonstrated a reduction of ~ 50%. These results demonstrate that the *Sun5* knock-out ES cells contain only one allele of *Sun5* exons 7 and 9 and are therefore heterozygous for the wild-type allele (Fig. 3.24). Therefore, qPCR confirmed the proper cassette insertion and disruption of the *Sun5* gene. After confirmation of the correct homologous recombination by PCR and qPCR, ES cells were used to generate chimeras.

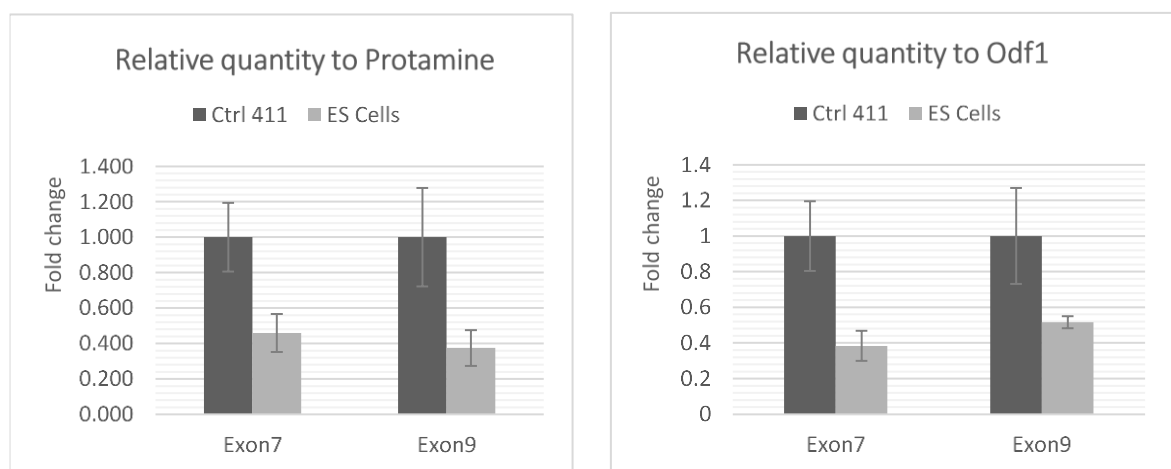


**Figure 3.24. Recombinant *Sun5* embryonic stem cells are heterozygous for the wild-type allele.** Quantification of exons 7 and 9 of *Sun5* in wild-type and recombinant ES cells, either related to the quantity of *Prm1* or *Odf1*, respectively, always in the same probe. The relative amount of the wild-type allele (Ctrl 411) is 1. In contrast, in the recombinant ES cells, the relative quantities of exons 7 and 9 are close to 0.5 when related to the quantity of either *Prm1* or *Odf1*.

### 3.3.2 Genotyping of chimeras

Genomic DNA was prepared using KAPA™ Mouse Genotyping Kit as described in 2.2.5.3. The genotyping of chimeras was performed using the primer pair NeomycinFor and NeoSplitRev (Tab. 6.1.7), which amplify a fragment of the neomycin selection gene (Fig. 3.22). An expected fragment size of ~1240 bp was amplified in 4 out of 61 chimeric mice (Fig. 3.25).

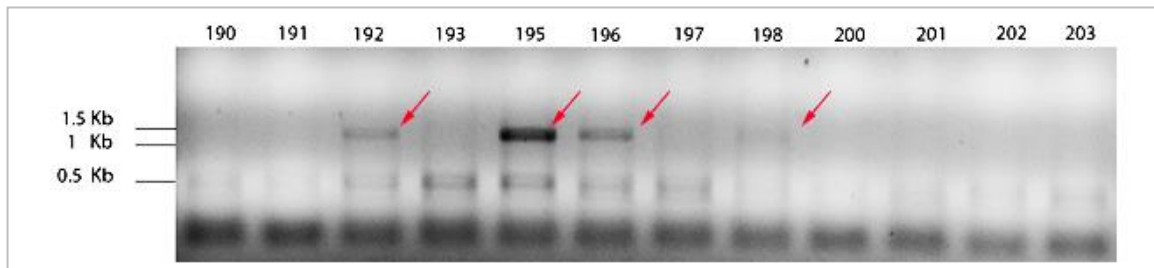


**Figure 3.25. Genotyping of *Sun5* chimeras.** DNA obtained from chimeras was tested by PCR using the primer pair NeomycinFor and NeoSplitRev. A fragment of ~1240 bp was obtained from chimeric mice #192, #195, #196, and #198.

### 3.3.3 Genotyping of chimeras' offspring

Positive chimeras were crossed with C57Bl/N mice. In the first generation, 29 animals were born, which were genotyped by nested PCR. First PCR was prepared using the primer pair Geno2For and Geno2Rev (Tab.6.1.7). The primer pair amplifies part of the resistant cassette and the targeted region (Fig. 3.22). No PCR product was visibly obtained when separated by agarose gel electrophoresis (not shown). The first PCR reaction product was used as a template for the secondary PCR, and a product of 507 bp was generated using the primers NeoFwd and Sundown (Fig. 3.26). NeoFwd is situated in the *neomycin* gene, whereas Sundown localizes in the 3' region flanking the cassette insertion. Two females, #336 and #360, were identified to carry the recombinant allele. Both females were selected for breeding with wild-type mice to establish the *Spag4l/Sun5*-deficient strain.

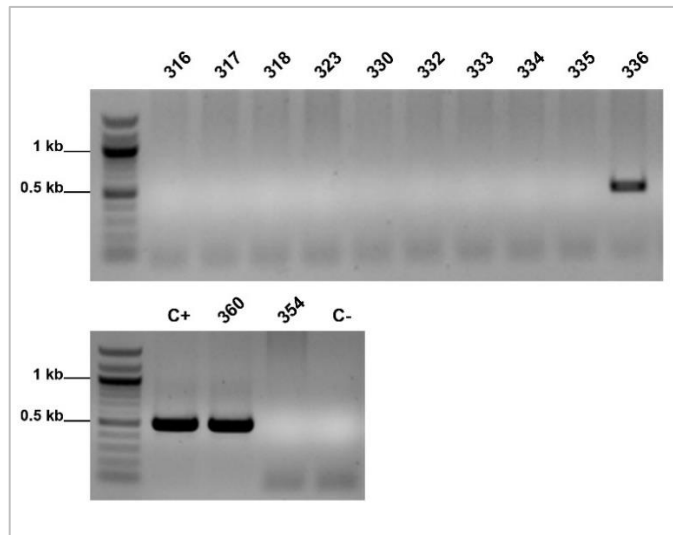


**Figure 3.26. Genotyping of the first generation of *Spag4l*-deficient mice by nested PCR.** F1 mice were genotyped by nested PCR. The first PCR reaction was performed with the primer pair Geno2For/Geno2 Rev. The second PCR was performed with primer pair NeoFwd/Sundown. The expected fragment of 507 bp was obtained in DNA from the females #336 and #360. C+ corresponds to the ES cells carrying the cassette, whereas in C-, ddH<sub>2</sub>O was used as template.

Both females were fertile and gave birth to the F2-generation. All mice of F2-generation were genotyped by nested PCR, using the primer pair NeomycinFor and NeoSplitRev for the first PCR and primers NeomycinFor3 and NeoInRev for the secondary PCR. A product of ~195 bp was obtained as expected in some samples. To confirm the correct transmission of the insertion cassette, some PCR products were sequenced, confirming the presence of the *neomycin* gene (Fig. 3.27).

Heterozygous animals, that tested positive for the presence of the insertion cassette and wild-type allele by genotyping, were intercrossed to generate homozygous *Spag4*-deficient mice. The breeding scheme and the progenies genotyped positive for the presence of the insertion cassette is shown in figure 3.28. Genotyping was performed using DNA isolated by three different methods. For the PCR reactions, different combinations of primers were used, which are described in figure 3.22.



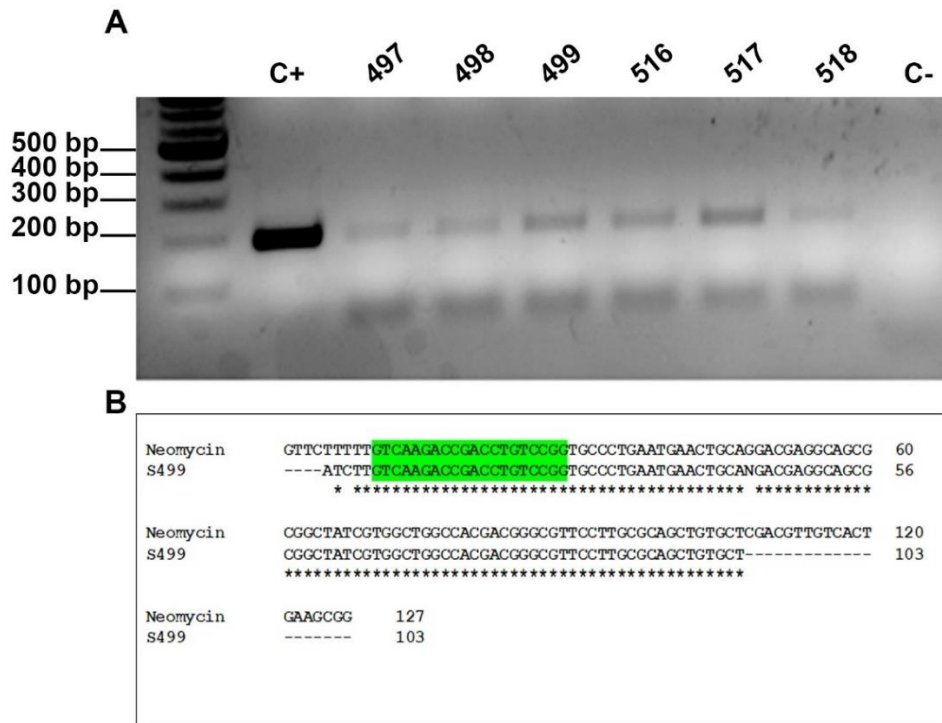


**Figure 3.27. Genotyping of the second generation of *Spag4l*-deficient mice** (A) Genotyping was performed by nested PCR using the primer pair NeomycinFor/NeoSplitRev for the first PCR reaction, and the primer pair NemoycinFor3/NeoInRev for the secondary PCR reaction. The expected fragment of 195 bp was amplified. The PCR product was sequenced (B) Alignment of DNA sequence from sample #499 with the neomycin sequence revealed amplification of the *neomycin* gene. The primer sequence of NemoycinFor3 is shown in green.

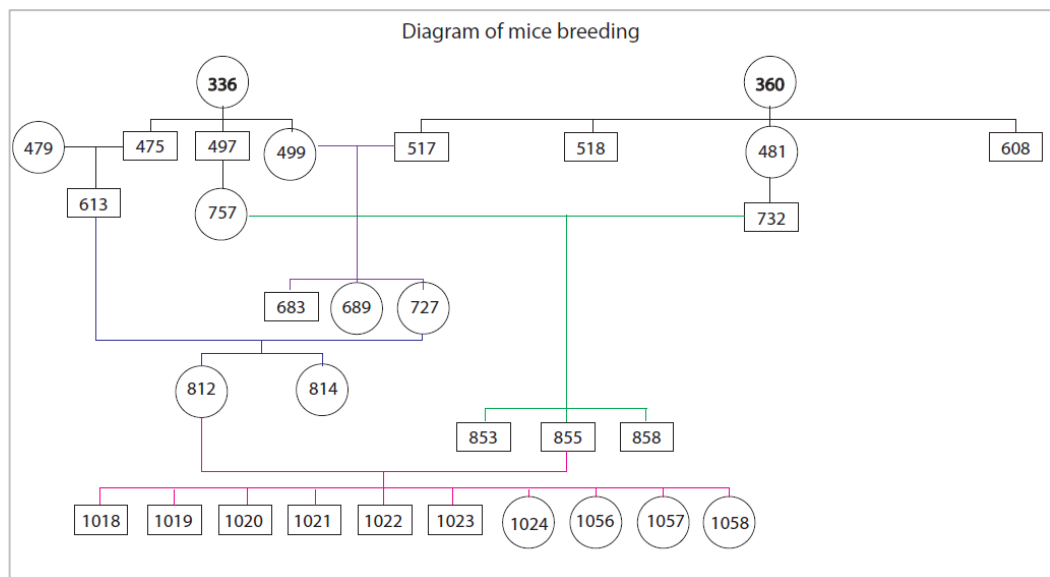


**Figure 3.28. Breeding scheme to generate homozygous-deficient *Spag4l*<sup>-/-</sup> mice.** Heterozygous animals were intercrossed to generate homozygous *Spag4*-deficient mice. Five generations of mice are represented in the current scheme.

Additionally, to confirm heterozygosity, samples were analyzed by qPCR to check whether the quantity of exons 7 and 9 of *Spag4l* are reduced. qPCR was performed using the same conditions as described for ES cells (2.2.5.5). The primer pairs Sun5-mus-E5-For/ Sun5-mus-E5-Rev and Sun5-mus-E8-For/ Sun5-mus-E8-Rev were used to amplify exon 7 and 9, respectively. DNA from a wild-type mouse was used as reference and protamine was used as an internal control gene. Relative quantity was calculated using the  $2^{-\Delta\Delta C_t}$  method. As shown in Fig. 3.29, a notable reduction of the exon 7 and 9 was found in some samples. Therefore, those animals that were positive genotyped for heterozygosity by PCR and qPCR were selected for breeding (Fig. 3.28).

After four generations of mice breeding, several animals were positive for the selection gene neomycin. However, all mice obtained were heterozygous since the wild-type allele was detected in all animals by using the primer pair GenotypeFor2 and GenotypeRev2 (Fig. 3.30). Thus, besides intercrossing of heterozygous animals, no homozygous *Spag4*-deficient mice could be obtained. After reevaluation of genotyping results, we concluded that transmission failed. The project was therefore stopped.

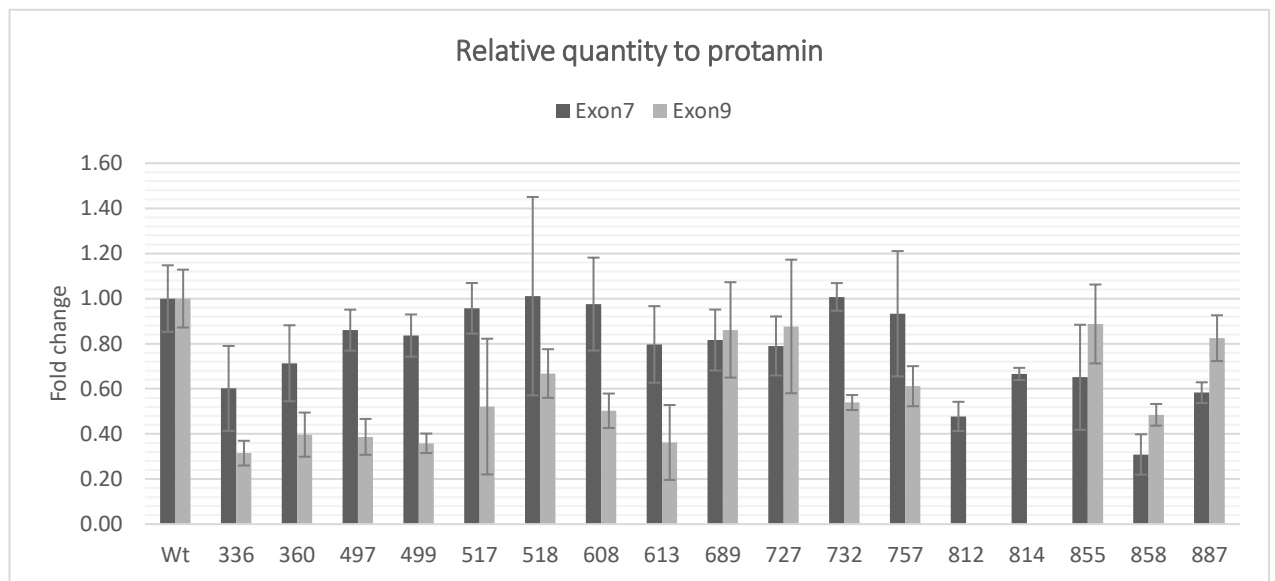


**Figure 3.29. Relative quantity of exon 7 and 9 of the offspring from heterozygous mice.** The quantity of exons 7 and 9 relative to protamine was calculated using DNA from a wild type as reference. Exon 9 shows a reduction in most of the animals analyzed (336, 360, 497, 499, 517, 518, 608, 613, 732, 757 and 858), whereas exon 7 is reduced in a few samples 336, 812, 855, 858, 887. Relative gene quantity was calculated using the  $2^{-\Delta\Delta C_t}$  method.

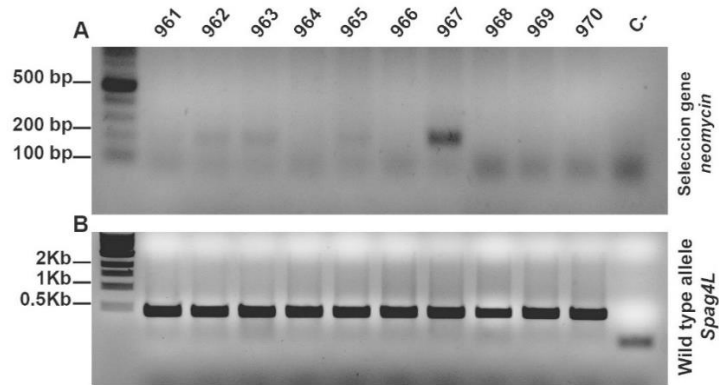


**Figure 3.30. Genotyping example of the fourth generation.** Offspring generated after mating of heterozygous mice #732 and #812. (A) Primers NeomycinFor3 and NeoInRev amplified the neomycin fragment ~195 bp, confirming *Spag4l* deficiency. (B) Primers GenotypeFor2 and GenotypeRev2 amplified a fragment of 447 bp of the wild type allele and was used to detect the wild-type allele. Both pairs of primers amplified a fragment in sample #967, thus confirming the heterozygosity of this mouse.

### **3.4 Identification of proteins that collaborate in the formation of the HTCA**

#### **3.4.1 CCDC42 localizes to manchette, HTCA and tail and interacts with ODF1 and ODF2 in the formation of the male germ cell cytoskeleton**

This chapter describes the identification of CCDC42 as an interacting partner of ODF1 and ODF2, suggesting its collaboration in the HTCA formation. The coiled-coil domain containing 42 (CCDC42) is an essential protein involved in the formation of the HTCA and sperm flagella. In early elongating spermatids, CCDC42 localizes to the manchette and perinuclear ring. In the later stages of spermiogenesis, CCDC42 locates in the connecting piece and to the sperm tail. Furthermore, CCDC42 interacts physically with ODF1, and both proteins exhibit a similar distribution in the sperm tail.

Moreover, CCDC42 interacts with the outer dense fiber protein 2 (ODF2). ODF2 is a known component of the sperm tail and centrosome/basal body in somatic cells. Similarly, CCDC42 has been identified as a centrosomal component in somatic cells, albeit previous reports restricted *Ccdc42* expression to testis and brain. However, these results indicate that another *Ccdc42* isoform is expressed in somatic cells. Hence, CCDC42 interacts with the cytoskeletal proteins ODF1 and ODF2, suggesting its potential role as a scaffold protein in the formation of the connecting piece and sperm tail.

Constanza Tapia Contreras and Sigrid Hoyer-Fender

**Author Contributions:** CTC did the experiments and prepared the figures. SH-F was the project leader and wrote the manuscript.

**Status of manuscript:** Published in *Frontiers in Cell and Developmental Biology* in 2019.



# CCDC42 Localizes to Manchette, HTCA and Tail and Interacts With ODF1 and ODF2 in the Formation of the Male Germ Cell Cytoskeleton

Constanza Tapia Contreras and Sigrid Hoyer-Fender\*

Johann-Friedrich-Blumenbach-Institute of Zoology and Anthropology – Developmental Biology, Göttingen Center for Molecular Biosciences (GZMB), Georg-August-University of Göttingen, Göttingen, Germany

## OPEN ACCESS

### Edited by:

Tomer Avidor-Reiss,  
The University of Toledo,  
United States

### Reviewed by:

Mania Eugenia Teves,  
Virginia Commonwealth University,  
United States  
Bénédicte Durand,  
Université Claude Bernard Lyon 1,  
France

### \*Correspondence:

Sigrid Hoyer-Fender  
shoyer@gwdg.de

### Specialty section:

This article was submitted to  
Cell Growth and Division,  
a section of the journal  
Frontiers in Cell and Developmental  
Biology

**Received:** 31 May 2019

**Accepted:** 18 July 2019

**Published:** 14 August 2019

### Citation:

Tapia Contreras C and  
Hoyer-Fender S (2019) CCDC42  
Localizes to Manchette, HTCA  
and Tail and Interacts With ODF1  
and ODF2 in the Formation of the  
Male Germ Cell Cytoskeleton.  
*Front. Cell Dev. Biol.* 7:151.  
doi: 10.3389/fcell.2019.00151

Terminal differentiation of male germ cells into functional spermatozoa requires shaping and condensation of the nucleus as well as the formation of sperm-specific structures. A transient microtubular structure, the manchette, is mandatory for sperm head shaping and the development of the connecting piece and the sperm tail. The connecting piece or head-to-tail coupling apparatus (HTCA) mediates the tight linkage of sperm head and tail causing decapitation and infertility when faulty. Using mice as the experimental model, several proteins have already been identified affecting the linkage complex, manchette or tail formation when missing. However, our current knowledge is far too rudimentary to even draft an interacting protein network. Depletion of the major outer dense fiber protein 1 (ODF1) mainly caused decapitation and male infertility but validated binding partners collaborating in the formation of sperm-specific structures are largely unknown. Amongst all candidate proteins affecting the HTCA when missing, the structural protein CCDC42 attracted our attention. The coiled-coil domain containing 42 (CCDC42) is important for HTCA and sperm tail formation but is otherwise largely uncharacterized. We show here that CCDC42 is expressed in spermatids and localizes to the manchette, the connecting piece and the tail. Beyond that, we show that CCDC42 is not restricted to male germ cells but is also expressed in somatic cells in which it localizes to the centrosome. Although centrosomal and sperm tail location seems to be irrespective of ODF1 we asked whether both proteins may form an interacting network in the male germ cell. We additionally considered ODF2, a prevalent protein involved in the formation of spermatid-specific cytoskeletal structures, as a putative binding partner. Our data depict for the first time the subcellular location of CCDC42 in spermatids and deepen our knowledge about the composition of the spermatid/sperm-specific structures. The presence of CCDC42 in the centrosome of somatic cells together with the obvious restricted male-specific phenotype when missing strongly argues for a compensatory function by other still unknown proteins most likely of the same family.

**Keywords:** spermiogenesis, HTCA, tail, CCDC42, centrosome, ODF2, ODF1

## INTRODUCTION

The transformation of spermatids into terminally differentiated sperm is a key event in spermatogenesis. Meiosis II generates spermatids of spherical shape that are then gradually transformed by shaping and condensation of the nucleus and the formation of acrosome and sperm tail, finally resulting in the mature spermatozoon (Fawcett, 1975; Russell et al., 1990; Jan et al., 2012). There is circumstantial evidence indicating that the shaping of the nucleus and the assembly of the sperm tail is provoked by a transient microtubular structure, the manchette (Clermont et al., 1993; Kierszenbaum, 2002; Kierszenbaum et al., 2011). The manchette forms during the acrosomal phase of spermiogenesis and disassembles during the maturation phase (Clermont et al., 1993). In mice, it is first seen in step 8 spermatids and disassembles prior to the formation of the sperm mid-piece around steps 13–14 (O'Donnell and O'Bryan, 2014; Lehti and Sironen, 2016). The manchette consists of a perinuclear mantle of microtubules emanating from the perinuclear ring (Fawcett et al., 1971; Rattner and Brinkley, 1972; Doohar and Bennett, 1973; Rattner and Olson, 1973; Wolosewick and Bryan, 1977; Clermont et al., 1993). However, detection of plus-end tracking proteins as EB3 and CLIP-170 at the perinuclear ring together with the absence of the minus-end binding protein  $\gamma$ -tubulin strongly argues against the perinuclear ring as the microtubule nucleation site (Akhmanova et al., 2005; Kierszenbaum et al., 2011; Lehti and Sironen, 2016). Instead, supporting evidence indicates that the centriolar adjunct serves as a nucleator of manchette microtubules with their plus ends reaching toward the perinuclear ring (Fawcett and Phillips, 1969; Lehti and Sironen, 2016; Fishman et al., 2018). The manchette is linked to the nuclear membrane and this is essential for nuclear shaping. The presence of rod-like elements that link the manchette to the nuclear envelope has first been demonstrated by electron microscopy studies (Russell et al., 1991). Supportively, deletion of SUN4, a testis-specific nuclear membrane protein and component of the linker of nucleoskeleton and cytoskeleton complex (LINC) caused detachment of the manchette and consequently round-headed sperm (Calvi et al., 2015; Pasch et al., 2015; Yang et al., 2018a). The importance of the manchette for nuclear shaping and male fertility is furthermore exemplified by the seminal discovery of the genetic cause underlying the *azh* phenotype in mice. Male *azh* mice are infertile due to a malformed manchette, abnormal spermatozoon head morphology, tail abnormalities and decapitation all caused by a deletion in the *Hook1* gene (Mendoza-Lujambio et al., 2002). (Review in: Chen et al., 2016). However, *Hook1* is a microtubule-binding protein and most likely responsible for the cross-linking of the manchette microtubules, whereas SUN4 is expected to be an inner nuclear membrane protein. Thus, the true nature of the rod-like elements that link the manchette to the nucleus is still unknown.

The observation of sperm decapitation indicated that the manchette is involved in sperm head to tail coupling and/or development of the sperm tail. Consequently, it was suggested that molecules required for the developing basal body/connecting piece and the sperm tail were delivered via intra-manchette transport meaning that the manchette functions as a track in

supporting the delivery of molecules (Kierszenbaum, 2001, 2002; Kierszenbaum et al., 2011). Contradictory, however, are the observations that the manchette is assembled when the axoneme is already developed and that the sperm tail develops irrespective of the detachment of the manchette in SUN4-deficient spermatids (Lehti and Sironen, 2017; Yang et al., 2018a).

The sperm tail develops from the basal body that itself is a derivative of the former centrosome. In spermatids, the daughter centriole of the centrosome is transformed into the proximal centriole, which acts as a seed for the formation of the connecting piece, and inserts into the nuclear indentation (Fawcett and Phillips, 1969). The perpendicular positioned mother centriole is transformed into the distal centriole, which acts as the basal body to initiate sperm tail development. Later on, the distal centriole disintegrates leaving the centriolar vault. The axoneme, the microtubule-based core structure, is the prolongation of the distal centriole that is surrounded by accessory structures as the nine prominent outer dense fibers (ODFs) and the fibrous sheath (FS) in the sperm tail. The ODFs are descending from the segmented columns formed at the proximal centriole of the head-to-tail coupling apparatus (HTCA). They accompany the microtubule doublets of the axoneme throughout the length of the tail whereas the FS is present only in the principal piece. The accessory fibers are important for stiffening the sperm tail thus supporting the elastic recoil of the sperm tail and protecting against shearing forces (Baltz et al., 1990; Lindemann, 1996). At the proximal region of the sperm tail, at the mid-piece, the mitochondrial sheath surrounds axoneme and ODFs.

The HTCA or connecting piece develops from the centrosome. It is an articular structure at the neck region mediating the tight connection between the sperm tail and the nucleus. Although the protein composition of the HTCA is far from being known, a couple of proteins have already been identified that are essential for the formation of the HTCA and/or the sperm tail. One protein essential for the tight connection of sperm head and tail is the outer dense fiber protein 1 (ODF1; also named HSPB10) (Burfeind and Hoyer-Fender, 1991; Schalles et al., 1998; Fontaine et al., 2003). Depletion of ODF1 caused sperm decapitation and male infertility in mice (Yang et al., 2012, 2014). A few interacting proteins have been identified, e.g., the outer dense fiber protein 2 (ODF2), which is a major protein of the sperm tail accessory fibers (Shao et al., 1997). Beyond that, validated ODF1 interacting proteins that are supposed to collaborate in the formation of sperm-specific structures are currently unknown. Proteins known to affect the HTCA or the sperm tail when missing are ideal candidates as putative interaction partners. We, therefore, focused on structural proteins with a reported effect on HTCA and sperm tail formation as putative interaction partners of ODF1. We asked here, whether the coiled-coil domain containing 42 (CCDC42) protein acts as a node in the ODF1 network. *Ccdc42* is specifically expressed in testis and brain and its deletion causes male sterility in mice with malformation of the HTCA and the sperm tail. Beyond that, no further phenotypes are evident (Pasek et al., 2016). CCDC42 (coiled-coil domain containing 42) belongs to the CFAP73 family and is a paralog of CFAP73. It contains the DUF4200, the domain of unknown function

that is shared by a couple of coiled-coil domain proteins and cilia-and flagella-associated proteins as CFAP73. The phenotype of *Ccdc42*-deficient mice suggested a male germ cell-specific function, but its expression and sub-cellular location is so far unknown. We explored here putative interacting proteins of CCDC42 in male germ cells and analyzed its expression and sub-cellular location. We show that CCDC42 is recruited to the manchette and the sperm tail and is specifically enriched in the perinuclear ring of the manchette and the HTCA. Pull down and co-IP experiments both indicated binding to ODF1 and ODF2. Furthermore, CCDC42 localizes to the centrosome/basal body not only in male germ cells but also in somatic cells. Revision of *Ccdc42* expression by RT-PCR demonstrated wide-spread expression in somatic tissues. The co-localization of CCDC42 with microtubule-based structures as the manchette and the centrosome/HTCA suggests that CCDC42 is involved in their formation by generating a rigid scaffold. However, as no further phenotypes are evident when *Ccdc42* is missing its function in somatic cells most likely might be taken over by other members of the family.

## MATERIALS AND METHODS

### Ethics Statement

All mouse experiments were reviewed and approved by the local ethic commission. License for animal experiments has been obtained by the Institute of Human Genetics and the Max-Planck-Institute for Experimental Medicine, Göttingen. The guidelines of the German Animal Welfare Act (German Ministry of Agriculture, Health and Economic Cooperation) were strictly followed in all aspects of mouse work.

### cDNA Synthesis and RT-PCR

Total RNA was prepared from adult mouse tissues as well as from NIH3T3 mouse fibroblasts using peqGOLD RNAPure™ (PeqLab, Erlangen, Germany) following the recommendations of the manufacturer. Total RNA was digested with Ambion® TURBO DNA-free™ DNase (Life Technologies) followed by cDNA synthesis using Maxima First Strand cDNA Synthesis (Thermo Fisher Scientific). RT-PCR for detection of transcribed sequences was performed using the following primer combinations: *Ccdc42*-Nterm\_For (GTGGCACTGTCACCTCACC) and C-terminal-*Ccdc42*-Rev (GGCTCACCAGGAACCTTCTC) generating the full-length product of 1093 bp, *Ccdc42*-For2 (GGAGACCGAGAATCCA GCC) and *Ccdc42*-Rev2 (CCGTTGGAATGCCTCCTTCT) for amplification of 305 bp of the 5' region (exons 1 + 2), C-terminal-*Ccdc42*-For (GGAATCCACCCAAGTGTC) and C-terminal-*Ccdc42*-Rev (GGCTCACCAGGAACCTTCTC) generating a fragment of 203 bp of the conserved 3' region (exons 6 + 7), *Ccdc42*-Exon5-For (GAAGAGATCCACGAGGTG) and C-terminal-*Ccdc42*-Rev for amplification of exons 5-7 (expected fragment size 535 bp), *Gapdh*-For (GTATGACTCCACTCACGGCA) and *Gapdh*-Rev (GTCAGATCCACGACGGACAC) generating a fragment of 594 bp.

### Plasmid Constructs

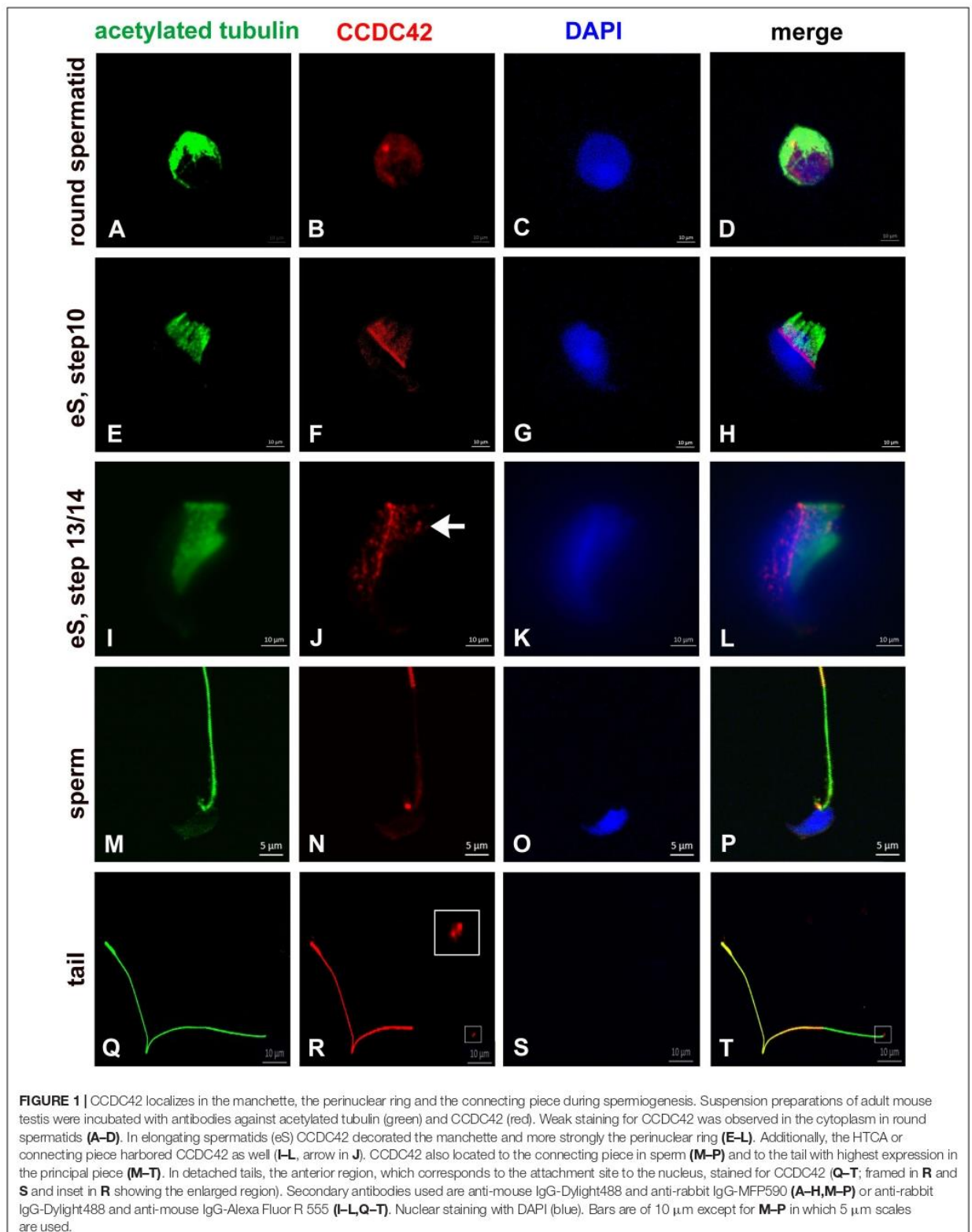
PCR amplification based on the Ensembl reference sequence NM\_177779 by using the following primers: *Ccdc42*-*NheI*-For (5'-GGCTGTTAGGTAGCTAGCGCAAC CATGAGTTTGGG-3') and *Ccdc42*-*HindIII*-Rev (5'-GTTCCTTAAGCTTGCCATCCGGACTTGCTGTGTG-3'), each primer containing restriction enzyme recognition sites. The full-length coding sequence of the *Ccdc42* isoform 203 was first cloned into pJET1.2/blunt (Thermo Fisher Scientific) followed by *NheI*/*HindIII* digestion and sub-cloning into pCR3.1-Cherry resulting in an in-frame fusion with the C-terminal Cherry-tag (pCR3.1, Invitrogen). The full-length coding region of *Odf1* was N-terminally fused to *ECFP* in *pECFP-C1* (Clontech Lab.). *Odf2* was C-terminally fused to *EGFP* in *pEGFP-N1* (Clontech Lab., #U55762) generating the full length construct *13.8NC-EGFP* (Donkor et al., 2004). Sequencing always revealed correct reading frames.

### Cell Culture and Immunocytochemistry

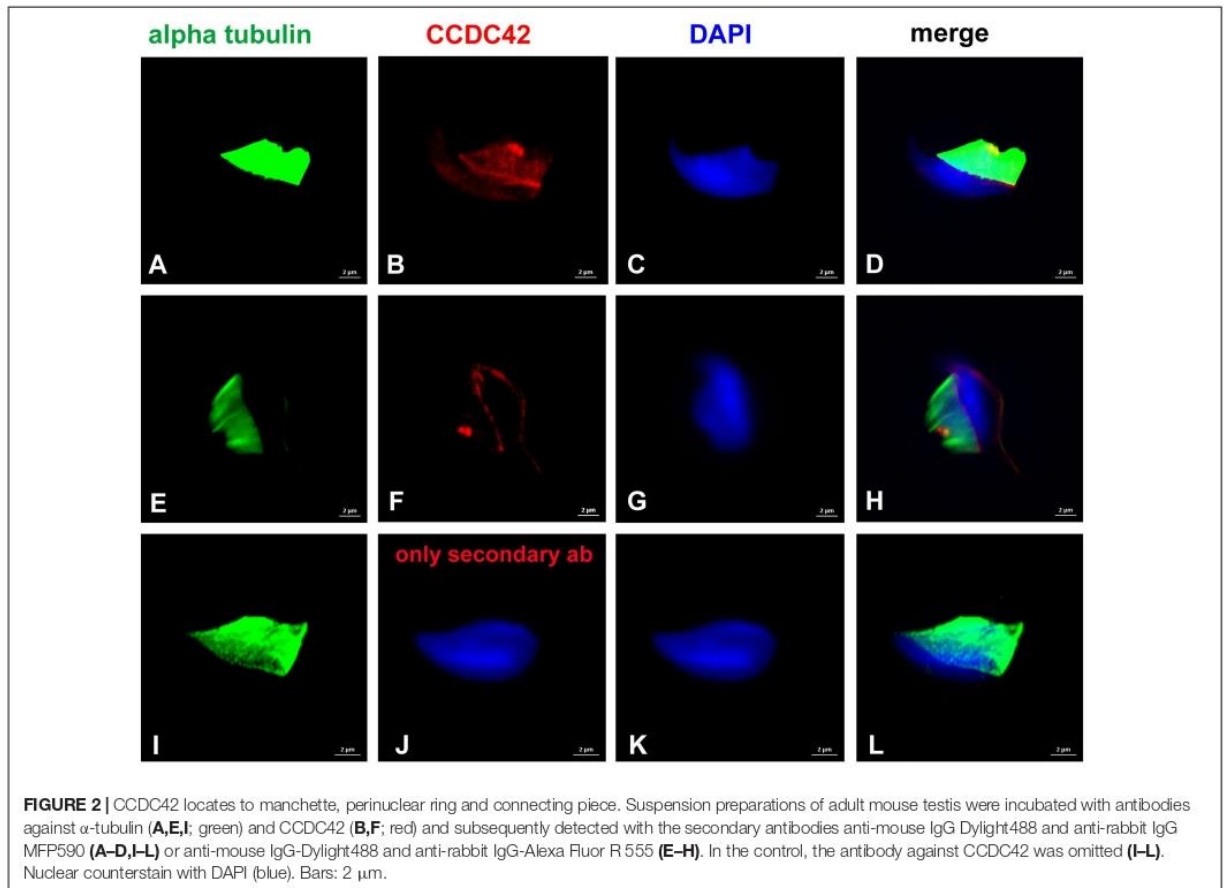
NIH3T3 (ATCC CRL-1658) or HEK-293 cells (ATCC CRL-1573) were maintained in Dulbecco's Modified Eagle's Medium (DMEM) supplemented with 10% (v/v) fetal bovine serum (FBS), 1000 U/ml penicillin, 1000 µg/ml streptomycin, and 20 mM L-Glutamine (all Gibco) at 37°C and 5% CO<sub>2</sub>. NIH3T3 cells were grown on coverslips in 6-well plates and transfected using EndoFectin™ Max Transfection Reagent, following the recommendations of the manufacturer (GeneCopoeia). Twenty-four hours after transfection, cells were washed in phosphate-buffered saline (PBS) and fixed in methanol for 10 min at -20°C. Specimens were then permeabilized in 0.3% TritonX-100 in PBS for 10 min at room temperature and blocked for 1 h using blocking solution (PBS containing 1% BSA and 0.3% TritonX-100). Samples were incubated with primary antibodies toward CCDC42 (ARP52735\_P050, antibodies-online ABIN2785068), Pericentrin (PRB432C, Covance), acetylated tubulin (6-11B-1; Sigma-Aldrich), gamma-tubulin (GTU-88, Sigma-Aldrich), ODF1 (ABIN4341345, antibodies-online), and GFP (raised in rabbit, self-made) at 37°C for 1 h. Secondary antibodies used are goat anti-mouse-IgG DyLight 488 (#35503, Thermo Fisher Scientific), and goat anti-rabbit MFP590 (#MFP-A1037, Mobitec). DNA was counterstained with DAPI. Images were taken by confocal microscopy (LSM 780, Zeiss) and processed using Adobe Photoshop 7.0.

### Immunocytology on Testicular Cell Suspensions

Fresh testes from laboratory mice of strain C57/Bl6, or frozen epididymides from wild-type mice or *Odf1*-ko mice (Yang et al., 2012) were minced in PBS, transferred onto superfrost slides, and fixed either in 2% or 3.7% paraformaldehyde in PBS for 20 min. Cells were permeabilized afterward in 0.3% Triton X-100 in PBS for 10 min, followed by blocking for 1 hr in blocking solution (PBS containing 1% BSA and 0.3% Triton X-100). The following antibodies were used for immunocytology: anti- $\alpha$ -tubulin (mouse monoclonal, DM1A, Calbiochem), anti-acetylated tubulin (6-11B-1, Sigma-Aldrich), anti-CCDC42







(ARP52735\_P050; antibodies-online ABIN2785068), anti-ODF1 (antibodies-online, ABIN4341345), guinea pig anti-SUN4 (self-made, Manfred Alsheimer, Würzburg). Primary antibodies were detected using different combinations of secondary antibodies as goat anti-mouse-IgG Alexa Fluor 555 IgG (H + L) (A21422, Molecular Probes) and goat anti-rabbit-IgG DyLight 488 (#35553, Thermo Fisher Scientific), goat anti-mouse-IgG DyLight 488 (#35503, Thermo Fisher Scientific) and goat anti-rabbit-MFP590 (#MFP-A1037, Mobitec), goat anti-mouse-IgG DyLight 488 (#35503, Thermo Fisher Scientific) and goat anti-rabbit-IgG (H + L) Alexa Fluor R 555 (F[ab]2 fragment; #A21430, Life Technologies), and goat anti-guinea pig-IgG Cy3 (Dianova #106-166-003). DNA was counterstained with DAPI (4', 6-Diamidino-2-phenylindole; Sigma D-9542), and the acrosome was decorated with FITC-labeled peanut lectin (PL-FITC). Images were taken by confocal microscopy (LSM 510, Zeiss) and processed using Adobe Photoshop 7.0. In some pictures, the fluorescent colors are replaced by pseudo-colors.

### Co-immunoprecipitation

HEK-293 cells were transfected using EndoFectin™ Max Transfection Reagent (GeneCopoeia), and 24 h post-transfection

harvested by trypsinization followed by two rinses in PBS. The cell pellet was resuspended in 1 ml lysis buffer (150 mM NaCl, 1% Nonidet P40, 0.5% sodium deoxycholate, 0.1% SDS, 50 mM Tris-HCl, pH 7.6, containing protease inhibitor cocktail (Halt Protease Inhibitor Cocktail 100x, Thermo Fisher Scientific, #78438). Subsequently, cell lysates were passed 10x through a syringe with a 21-gauge needle, followed by 3-times sonication for 45 s each. The soluble fraction was obtained by centrifugation at  $15,000 \times g$  for 15 min at 4°C. The supernatant was split into three parts and incubated with different antibodies for co-IP, either with rabbit anti-GFP (self-made), rat anti-RedFP (5F8, Chromotek), or rabbit anti-GAL4 (DBD) (sc-577, Santa Cruz Biotechnology). Protein G agarose beads (Thermo Fisher Scientific) were washed three times with lysis buffer and the antibody/supernatant mixture was then added. Samples were incubated overnight at 4°C on a rotating wheel. Afterward, beads were washed four times with lysis buffer, and bound proteins obtained by suspension of beads in SDS sample buffer and heating at 95°C for 10 min. Proteins were fractionated on SDS-PAGE and transferred onto nitrocellulose membrane (Amersham Hybond-ECL, GE Healthcare) (Laemmli, 1970; Towbin et al., 1979). The membrane was incubated in blocking solution [5% dry milk in TBST (10 mM Tris-HCl, pH 7.6, 150 mM NaCl 0.05%

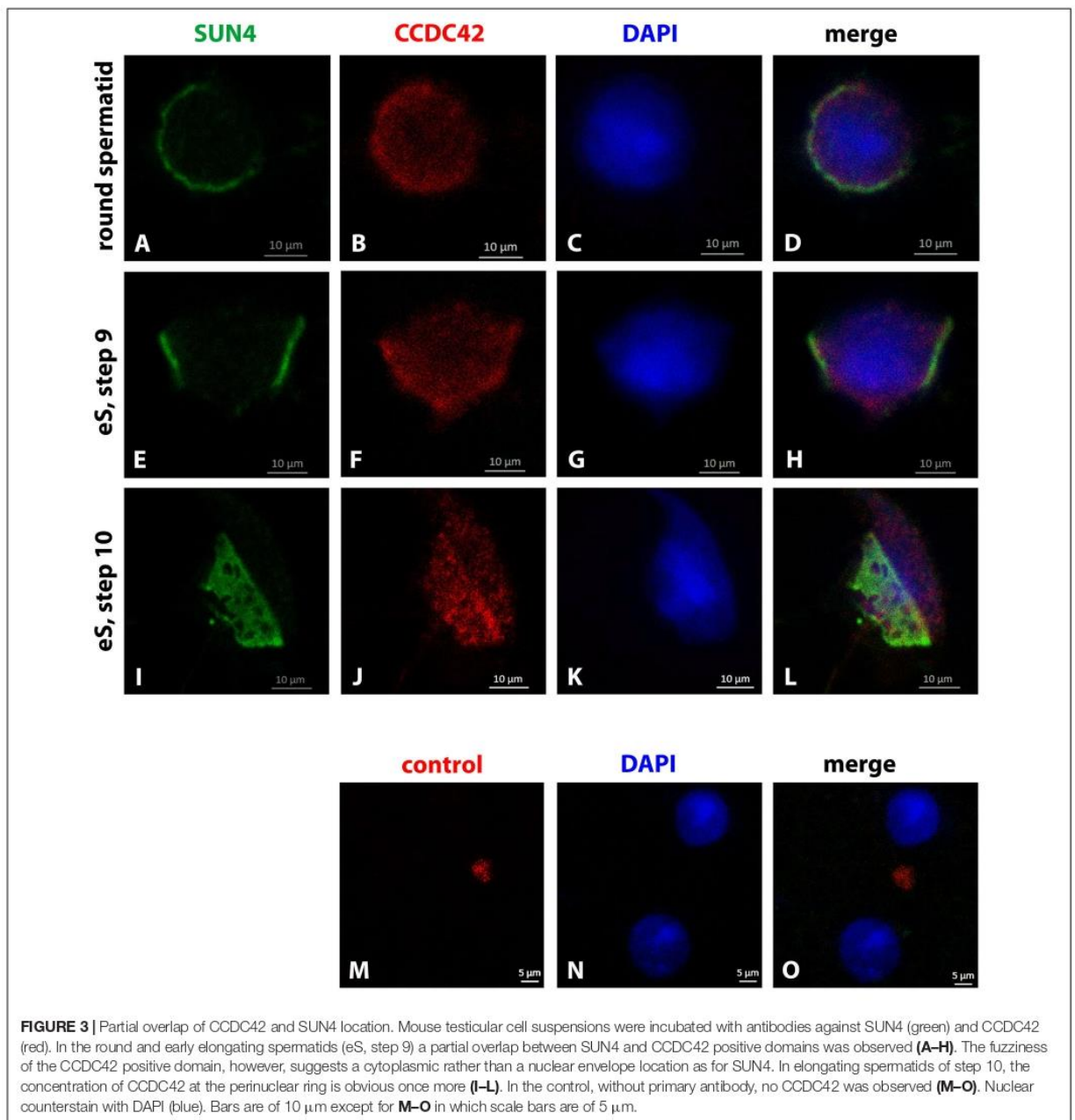


**FIGURE 3 |** Partial overlap of CCDC42 and SUN4 location. Mouse testicular cell suspensions were incubated with antibodies against SUN4 (green) and CCDC42 (red). In the round and early elongating spermatids (eS, step 9) a partial overlap between SUN4 and CCDC42 positive domains was observed (A–H). The fuzziness of the CCDC42 positive domain, however, suggests a cytoplasmic rather than a nuclear envelope location as for SUN4. In elongating spermatids of step 10, the concentration of CCDC42 at the perinuclear ring is obvious once more (I–L). In the control, without primary antibody, no CCDC42 was observed (M–O). Nuclear counterstain with DAPI (blue). Bars are of 10 μm except for M–O in which scale bars are of 5 μm.

Tween 20)] for 1 h. Membranes were incubated overnight at 4°C with primary antibodies either rabbit anti-GFP (self-made), mouse anti-GFP (MAB3580, Chemicon), or rat anti-RedFP (5F8, Chromotek) in blocking solution. Following washing of membranes in TBST, they were incubated with horseradish peroxidase-conjugated secondary antibodies either anti-rabbit IgG, anti-mouse IgG, or anti-rat IgG (Jackson ImmunoResearch, WestGrove, PA, United States or Sigma Biosciences, St Louis), respectively. Chemiluminescence detection was performed using

ClarityMax Western ECL Substrate (Bio-Rad, #1705062) and images captured with Chemdoc (Bio-Rad).

### Pull Down Assay

Preparation of bacterially expressed and refolded His-tagged ODF2-fusion protein (6xHis-13.8NC) was essentially as described in Yang et al. (2018b). Ni-NTA agarose (Qiagen GmbH, Hilden) was washed in wash buffer (50 mM NaPi, 500 mM NaCl, 30 mM imidazole, pH 7.6, containing protease

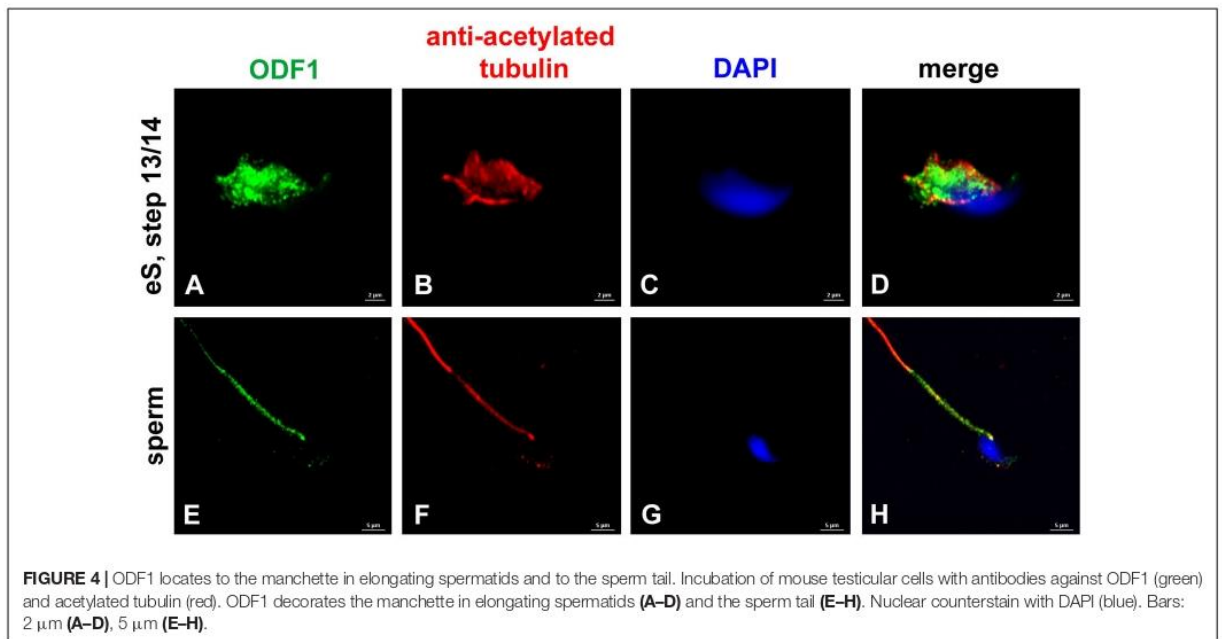


**FIGURE 4** | ODF1 localizes to the manchette in elongating spermatids and to the sperm tail. Incubation of mouse testicular cells with antibodies against ODF1 (green) and acetylated tubulin (red). ODF1 decorates the manchette in elongating spermatids (**A–D**) and the sperm tail (**E–H**). Nuclear counterstain with DAPI (blue). Bars: 2 µm (**A–D**), 5 µm (**E–H**).

inhibitors (Halt Protease Inhibitor Cocktail 100x, Thermo Fisher Scientific, #78438) and 0.2 mM PMSF). For *in vitro* interaction, 6xHis-ODF2 proteins were added to the washed Ni-NTA agarose and incubated for 1 h at 4°C in constant agitation. NIH3T3 cell lysate containing CCDC42-Cherry proteins was split into halves and one half added to the resin followed by incubation for 2 h at 4°C and constant agitation. The second half was used for the negative control. The beads were washed four times in wash buffer, followed by a final overnight washing step. To elute bound proteins, Ni-NTA agarose was incubated for 10 min at 4°C in elution buffer (50 mM NaPi, 500 mM NaCl, 500 mM imidazole, 0.2 mM PMSF). Eluates were boiled in SDS-sample buffer and analyzed by Western-blotting using rabbit anti-ODF2 antibodies (ESAP 15572, ABIN2430582, antibodies-online) and rat anti-RedFP antibodies (5F8, Chromotek). As negative control, the resin was incubated with one half of the NIH3T3 cell lysate containing CCDC42-Cherry proteins but without 6xHis-ODF2 proteins and processed as described.

## RESULTS

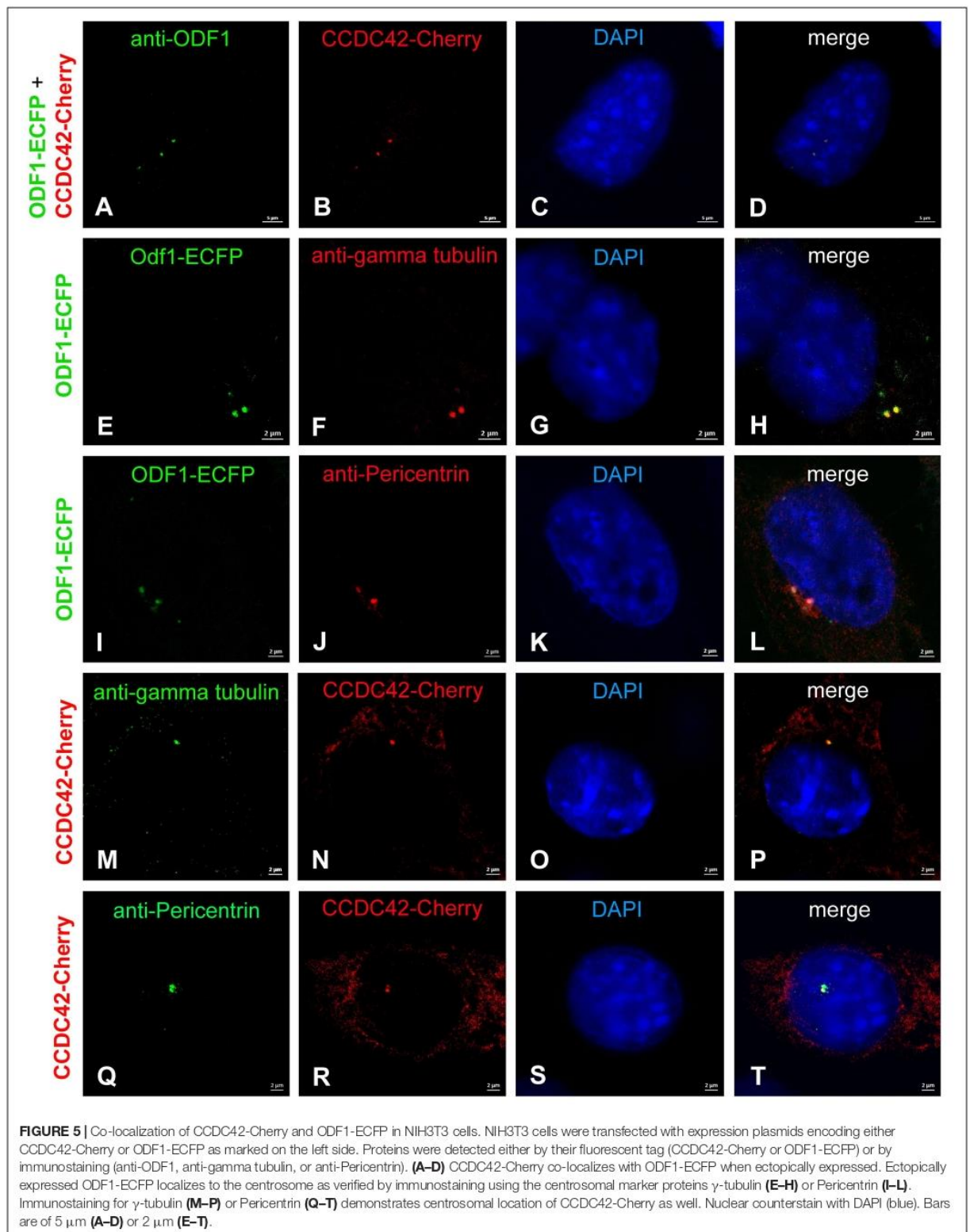
### CCDC42 Localizes to Manchette, Perinuclear Ring, Connecting Piece and Sperm Tail

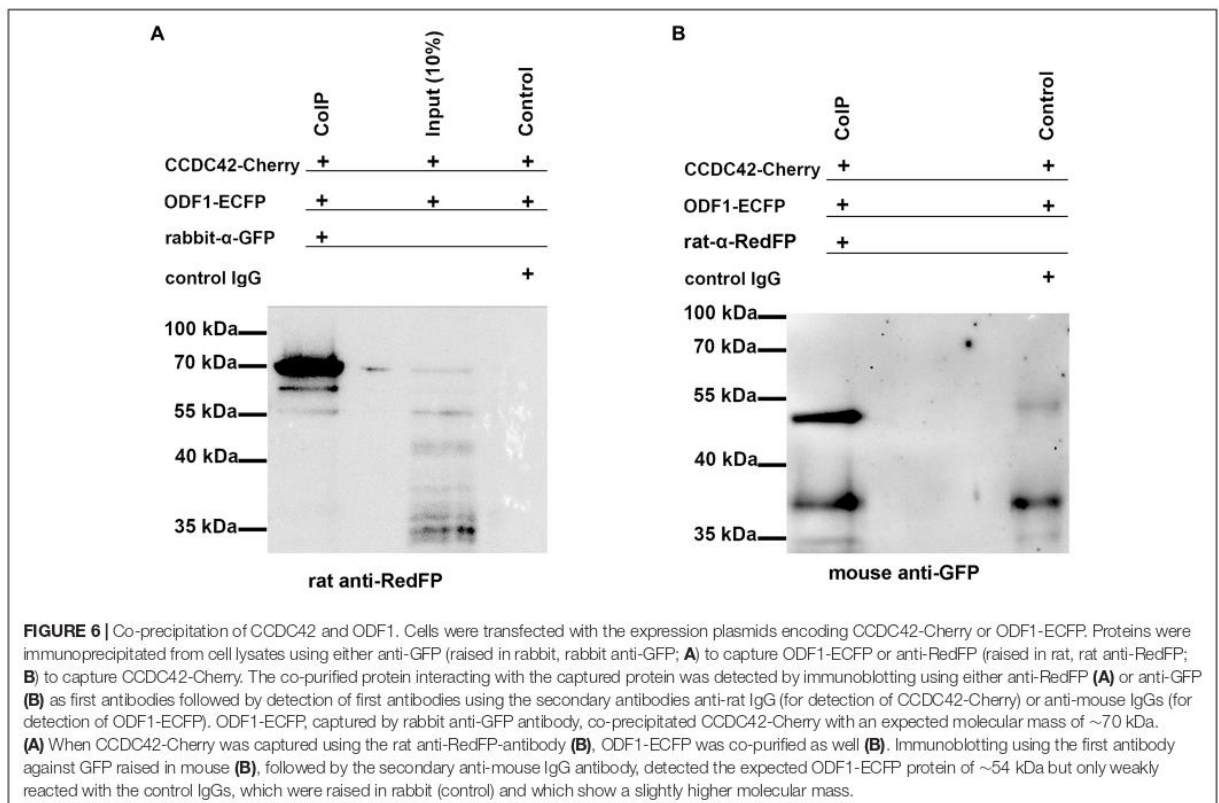
The coiled-coil domain containing protein of 42 kDa (CCDC42) belongs to the DUF4200 family of proteins containing the domain of unknown function 4200. Important paralogs of CCDC42 are CFAP73, CCDC38, and CFAP100, also known as CCDC37/MIA1. CCDC42 orthologs are present in most organisms from vertebrates to choanoflagellates

(Ruan et al., 2008; Guindon et al., 2010). Despite their widespread occurrence, information is currently scarce. *Ccdc42* is specifically expressed in testis and brain but deletion of *Ccdc42* seems to affect exclusively male germ cells resulting in infertility (Pasek et al., 2016). *Ccdc42*-deficient spermatids developed malformed HTCA and sperm tail that are functionally insufficient. However, beyond that no further information about CCDC42 is available. We first studied the subcellular localization of CCDC42 during spermatogenesis in the mouse using a commercially available antibody. The antibody was first validated by immunocytochemistry and Western blotting using the *Ccdc42*-expression construct (validation results are online at antibodies-online and are shown in Figure 9<sup>1</sup>).

Weak expression of CCDC42 was first observed in the cytoplasm of round spermatids (Figures 1A–D). In elongating spermatids CCDC42 co-localized with the manchette microtubules decorated by acetylated tubulin and more strongly with the perinuclear ring which marks the anterior border of the manchette (Figures 1E–L). Additionally, CCDC42 localized to the connecting piece detectable as two adjacent spots at the posterior end of the nucleus (Figures 1I–L, arrow in J). In sperm, CCDC42, again, was found at the connecting piece region and located to the sperm tail. CCDC42 strongly decorated the principal piece but only weakly the middle piece whereas acetylated tubulin marked the whole tail (Figures 1M–P). Labeling of detached sperm tails confirmed prevalent localization of CCDC42 in the principal piece whereas acetylated tubulin marked the whole tail. However, the anterior region of detached sperm tails, which corresponds to the former attachment site of the tail to the head, showed presence of CCDC42 visible by

<sup>1</sup><https://www.antibodies-online.com>





two adjacent spots (**Figures 1Q–T**; framed in R, S and enlarged inset in R). A stronger staining of the principal piece of the sperm tail than of the mid-piece might either reflect an unequal distribution of CCDC42 along the sperm tail or is caused by different accessibilities of the antibodies due to the presence of the mitochondrial sheath in the mid-piece.

Decoration of the manchette, the perinuclear ring, and the connecting piece was also demonstrated by using anti- $\alpha$ -tubulin antibody staining in conjunction with anti-CCDC42, both antibodies subsequently detected by varying secondary antibodies (**Figure 2**). The control, with anti- $\alpha$ -tubulin antibody incubation but omitting anti-CCDC42 antibody, followed by both secondary antibodies subsequently, revealed only  $\alpha$ -tubulin staining thus supporting specificity of anti-CCDC42 staining (**Figures 2I–L**).

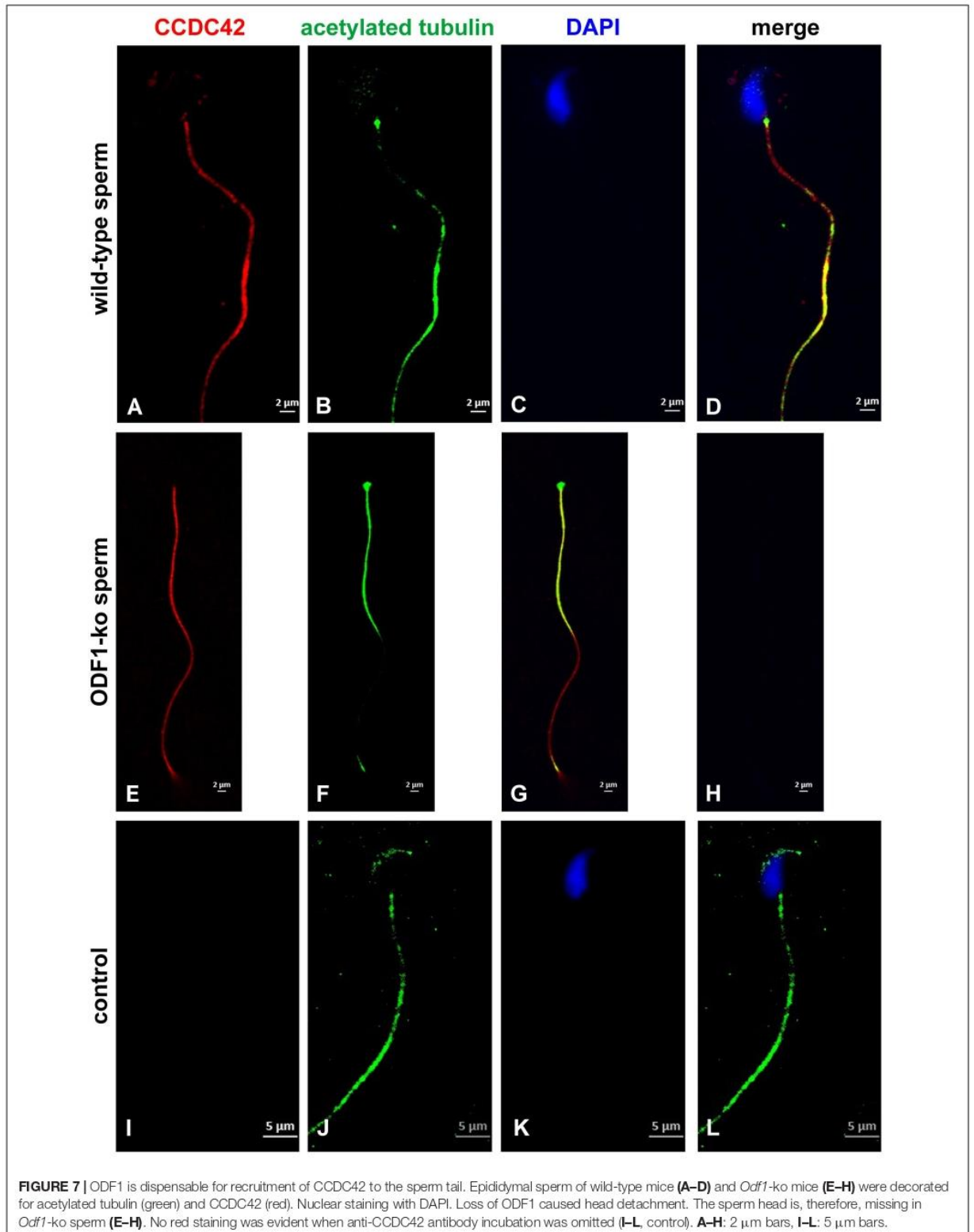
When concurrently stained for the nuclear envelope protein SUN4, the weak CCDC42 staining of the cytoplasm in round and early elongating spermatids was confirmed (**Figures 3A–H**). The SUN4 positive domain partially overlapped with the CCDC42 positive region as this is the region where the manchette develops. In early elongating spermatids, the SUN4 and CCDC42 localization domains seemingly overlapped corresponding most likely to the region where the manchette has formed and to which SUN4 locates (I–L) (Yang et al., 2018a). Again, CCDC42 more strongly decorated the perinuclear ring (I–L). The weak cytoplasmic staining for CCDC42 in the round spermatid seemed

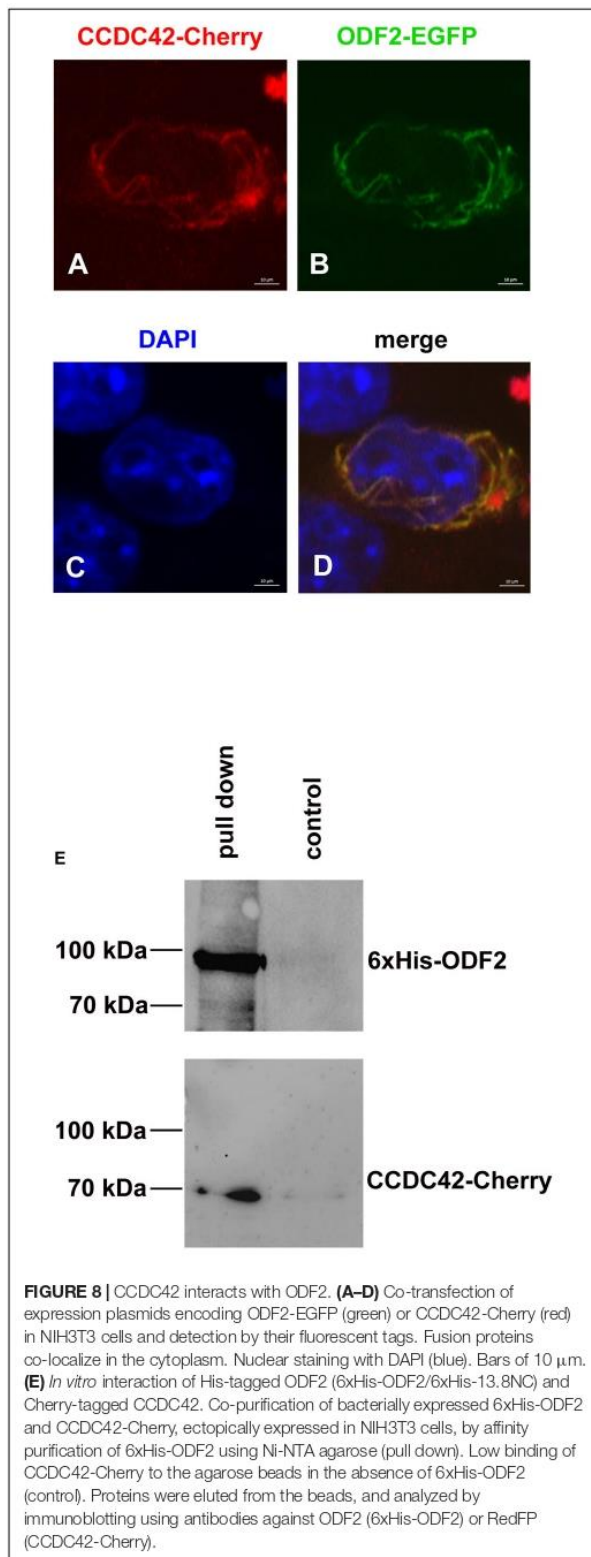
to be beyond background staining as demonstrated by the control experiment (**Figures 3M–O**).

### CCDC42 Interacts With ODF1 and ODF2

The small heat shock protein ODF1/HSPB10 is a main protein component of the sperm tail ODFs. Beyond that, it locates to the connecting piece and is essential for the tight connection between head and tail (Schalles et al., 1998; Yang et al., 2012, 2014). Immunocytological inspection confirmed sperm tail location of ODF1 and, additionally, showed expression in the manchette of elongating spermatids (**Figure 4**). Location of ODF1 thus resembled that of CCDC42 raising the question whether both proteins also physically interact.

We first investigated whether the location of ODF1 and CCDC42 is interdependent when ectopically expressed in NIH3T3 mouse fibroblasts. Cells were transfected with expression plasmids encoding either CCDC42 fused to Cherry (CCDC42-Cherry) or ODF1 fused to ECFP (ODF1-ECFP) and the proteins detected either by their fluorescent tags or by immunostaining (**Figure 5**). Ectopic expression of CCDC42-Cherry revealed bright staining of one or two dots close to the nucleus that overlap with ODF1-ECFP expression (**Figures 5A–D**). Since twin-dots are a typical signature of the centrosome, we verified centrosomal location of ODF1-ECFP (**Figures 5E–L**) as well as of CCDC42-Cherry (**Figures 5M–T**) using immunostaining for the

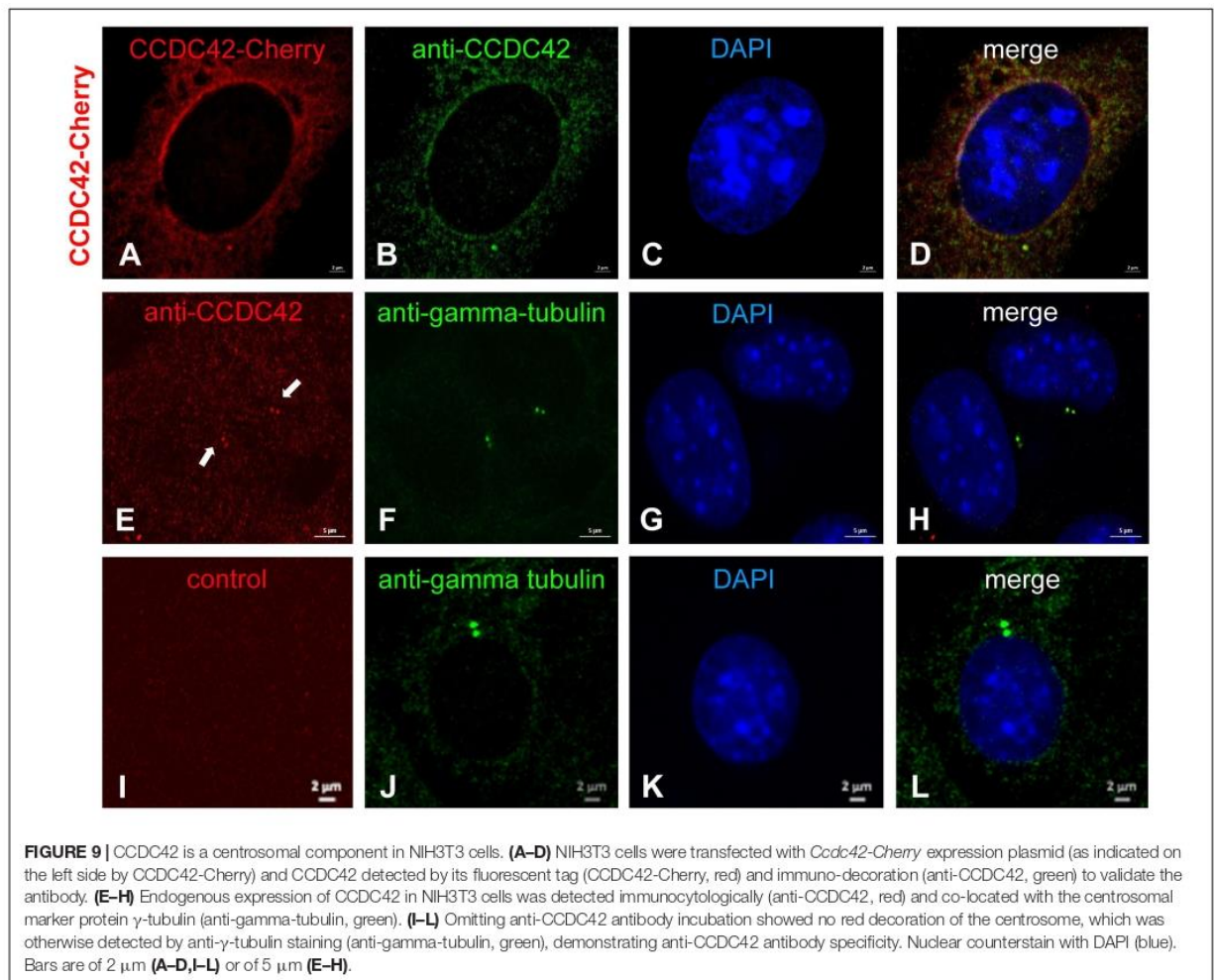




centrosomal marker proteins  $\gamma$ -tubulin (Figures 5E–H,M–P) or Pericentrin (Figures 5I–L,Q–T) (Doxsey et al., 1994). Our results show that CCDC42-Cherry co-localizes with ODF1-EGFP, when both proteins are ectopically expressed in NIH3T3 cells, notably at the centrosome. However, recruitment of CCDC42-Cherry to the centrosome is independent of ODF1 due to the fact that ODF1 is not at all expressed in somatic cells and CCDC42 locates to the centrosome despite absence of ODF1-EGFP (Figures 5M–T) (Yang et al., 2012).

Nevertheless, the physical interaction between CCDC42-Cherry and ODF1-EGFP was proven by co-immunoprecipitation. Both proteins were ectopically expressed in cultured cells by transient transfection of expression plasmids, and one of either protein immunoprecipitated out of the cell lysate. The immunoprecipitate was analyzed by immunoblotting detecting the protein that co-precipitated with the fished protein (Figure 6). Co-immunoprecipitation of CCDC42-Cherry and ODF1-EGFP was verified in either direction, capturing either CCDC42-Cherry or ODF1-EGFP. Our data thus indicate physical interaction between CCDC42 and ODF1. However, ODF1 is not only dispensable for recruitment of CCDC42 to the centrosome but also to the sperm tail. Immunocytochemistry on epididymal sperm of *Odf1*-ko mice showed decoration for CCDC42 similar as in wild-type sperm (Figure 7, wild-type sperm in A–D, *Odf1*-ko sperm in E–H). Acetylated tubulin staining identified the sperm tail. As ODF1 is essential for the anchorage of the sperm head to the tail causing head detachment when missing, the sperm head is absent in *ODF1*-ko sperm (Figures 7E–H) (Yang et al., 2012). In the control staining, when omitting anti-CCDC42 incubation but subsequent incubation with both secondary antibodies, the sperm tail is clearly visible by acetylated tubulin decoration but missed any red staining (Figures 7I–L).

Another important protein of the sperm tail and the connecting piece is ODF2. ODF2, furthermore, is an essential component of the centrosome and the basal body in somatic cells (Brohmann et al., 1997; Schalles et al., 1998; Nakagawa et al., 2001; Hüber et al., 2008). We, therefore, asked whether ODF2 is another binding partner of CCDC42. Co-transfection assays of expression plasmids in NIH3T3 cells revealed similar location of ODF2-EGFP and CCDC42-Cherry. ODF2 fused to EGFP (13.8NC-EGFP) often generated fibrous structures to which CCDC42-Cherry proteins localize (Figures 8A–D). Additionally, a physical interaction between CCDC42-Cherry and ODF2 was proven by pull-down assays (Figure 8E). Bacterially expressed and refolded 6xHis-tagged ODF2 was affinity purified using Ni-NTA agarose in the presence of CCDC42-Cherry, ectopically expressed in cell culture. Thereafter, eluates were immunoblotted for detection of the target protein 6xHis-ODF2 and its putative binding partner CCDC42-Cherry. CCDC42-Cherry co-purified with 6xHis-ODF2 (Figure 8E, pull down), whereas almost no binding of CCDC42-Cherry to the beads was observed in the absence of 6xHis-ODF2 (Figure 8E control). Our data, therefore, indicate ODF2 as another binding partner of CCDC42.



### CCDC42 Is a Centrosomal Protein in Somatic Cells

By ectopic expression of CCDC42-Cherry in NIH3T3 cells we have observed a predominant centrosomal location (Figure 5). This prompted us to investigate whether CCDC42 is endogenously expressed in somatic cells being a novel component of the centrosome. We first transfected cells with the CCDC42-Cherry expression plasmid for validation of the anti-CCDC42 antibody (Figures 9A–D). The antibody specifically decorated only transfected cells and co-localized with the fusion protein CCDC42-Cherry thus demonstrating its validity (Figures 9A–D). We next incubated untransfected NIH3T3 cells with the anti-CCDC42 antibody. Immunostaining of the endogenous CCDC42 decorated a twin-spot near the nucleus that additionally stained for the centrosomal marker  $\gamma$ -tubulin (Figures 9E–H). The centrosome was exclusively decorated by  $\gamma$ -tubulin staining but did not show a red fluorescence when omitting anti-CCDC42 antibody incubation (Figures 9I–L, control). Immunocytological data thus indicate expression of

CCDC42 in somatic cells, which is contradictory to its reported restricted expression pattern.

### Expression of *Ccdc42* Isoforms

According to Pasek et al. (2016), *Ccdc42* is expressed in testis and brain. In mouse testes, weak expression was first observed at 10-days of age that raised in 15-days old testis and maintained into adulthood. Testicular expression thus corresponds with the onset of meiosis around day 10 and its increase roughly coincides with the progression of spermatid differentiation during spermiogenesis (Nebel et al., 1961). However, three putative CCDC42 isoforms have been reported in mice (UniProtKB – Q5SV66) produced by alternative splicing (Figure 10). The longest isoform 203 (Q5SV66) consists of 316 amino acids (aa). In isoform 201 (Q5SV65) the sequence encoded by exon 5 is missing resulting in a putative protein of 238 aa. Isoform 202 (Q5SV66-2) has a postulated length of 169 aa since the N-terminal end encoded by exons 1-4 is completely missing. Instead, translation of the protein starts at the 3' end of



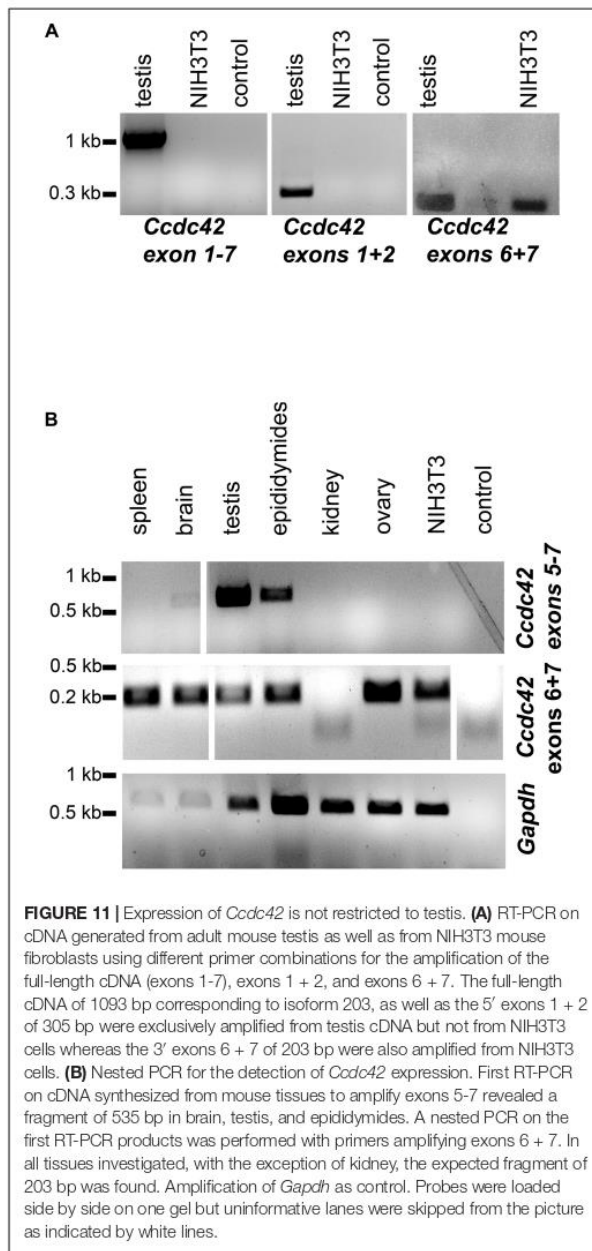


intron 4 encoding sequence MALGSQLFSDPSPLIPQ upstream of exon 5 encoded sequences. According to Interpro, the domain of unknown function 4200 (DUF4200) comprises aa 44-161 at the N-terminal half of isoform 203 and is therefore present in both, isoform 203 as well as in isoform 201, albeit shortened in the latter, but is largely missing in isoform 202 (Figure 10, depicted in violet). The coiled-coil region at the C-terminal end is present in all three isoforms (according to SMART; in Figure 10 highlighted in yellow). The antibody ABIN2785068, used for immunocytology, detects the epitope of 50 aa in the DUF4200, which is present in isoforms 203 and 202 but not in 201 (Figure 10, enframed in red).

Expression of *Ccdc42* was reported to be restricted to testis. In somatic tissues, with the only exception being the brain, *Ccdc42* seems to be not expressed. We confirmed testicular expression by RT-PCR using different primer combinations (Figure 11). The full-length product of isoform *Ccdc42-203* was expected to be of

1093 bp, which was confirmed by RT-PCR (Figure 11A, exons 1-7). However, for the putative isoform *Ccdc42-201*, a length of 729 bp was expected since exon 5 was skipped but we could not amplify the expected fragment (Figure 11A). Amplification of 305 bp of the 5' region (exons 1 + 2) again confirmed testicular expression of *Ccdc42* (Figure 11A, exons 1 + 2). When amplifying 203 bp of the conserved 3' region, *Ccdc42* expression was also demonstrated in NIH3T3 mouse fibroblasts (Figure 11A, exons 6 + 7).

Our results thus indicate that expression of *Ccdc42* isoforms is not restricted to testis. This prompted us to revise *Ccdc42* expression in other tissues (Figure 11B). We performed a nested PCR in order to detect even low expression levels. The first RT-PCR was performed to amplify exons 5-7 encoding part of the DUF domain with the epitope detected by the antibody, and the conserved coiled-coil region. We found strong expression in testis and epididymides and weak expression in the brain.



Sequencing of the RT-PCR products generated from testis and epididymides confirmed *Ccdc42*. *Gapdh* amplification, albeit demonstrating successful cDNA synthesis in all tissues, also indicated low amounts of cDNA in spleen and brain, which most likely accounts for the weak RT-PCR band found in brain cDNA. When performing a nested PCR on the first PCR products by amplifying exons 6 + 7 a fragment of the expected size was found in all tissues, with the exception of kidney. The RT-PCR fragments generated in ovary and NIH3T3 cDNA were sequenced confirming *Ccdc42* amplification. Our results,

therefore, indicate that *Ccdc42* expression is not restricted to testis. However, since the full-length product and the 5' region (exons 1 + 2) were found only in testis but not in NIH3T3 cells it is most likely that in somatic cells another isoform than the full-length CCDC42 isoform 203 is predominantly expressed, and that this isoform was detected by immunocytoLOGY in the centrosome.

## DISCUSSION

The HTCA is a complex structure present in the neck region of the sperm interconnecting the head and the tail. It develops from the centrosome that itself is composed of a pair of centrioles and associated components. During spermiogenesis, the proximal centriole inserts into a nuclear indentation, known as the implantation fossa, opposed to the acrosomal cap, and the linkage complex and the longitudinal columns of the connecting piece are formed (Fawcett and Phillips, 1969). The sperm tail starts outgrowing from the distal centriole of the former centriole that is now the basal body. In order to transmit only one centriole during fertilization, sperm of most vertebrates have disintegrated the distal centriole leaving only the proximal centriole. In contrast to centriole reduction in most vertebrates, in mice and other rodents, both distal and proximal centrioles degenerate during spermiogenesis leaving the centriolar vaults (Schatten, 1994; Hoyer-Fender, 2011). The current dogma of centrosome reduction in sperm was recently revisited by investigating the centrosomal protein inventory in human sperm. These data showed that the distal centriole is remodeled into an atypical centriole surrounded by a pericentriolar matrix instead of being completely vanished (Fishman et al., 2018). It is, therefore, feasible to view the neck structure as a specialized form of the pericentriolar matrix, and the centrioles as nucleation site for both the sperm tail and the manchette MTs. Few proteins are currently known that affect the head to tail linkage when missing, in between ODF1 and CCDC42 (Yang et al., 2012; Pasek et al., 2016). ODF1 is located in the sperm tail ODFs and in the connecting piece (Schalles et al., 1998). It interacts with ODF2, the major outer dense fiber protein, but no further interacting proteins have been confirmed (Shao et al., 1997). To figure out the interrelationship of HTCA proteins, and how they function in the formation of the HTCA, ODF1 interacting proteins are of utmost importance.

The coiled-coil domain containing 42 protein CCDC42 is highly conserved in evolution with orthologs existing in most organisms from vertebrates to choanoflagellates (Ruan et al., 2008; Guindon et al., 2010). Additionally, important paralogs of CCDC42 (also named CCDC42A) exist as CFAP73 (also named CCDC42B and MIA2), CCDC38 and CFAP100 (also named CCDC37 and MIA1). They altogether constitute the CFAP73 protein family. These proteins are in essential coiled-coil domain proteins and share the domain of unknown function DUF4200. Coiled-coil domain containing proteins are often involved in ciliary motility (Inaba and Mizuno, 2016; Zur Lage et al., 2019). In *C. reinhardtii* the gene product of the CCDC42 homolog MIA2 is a dynein regulator and necessary for ciliary motility

(Yamamoto et al., 2013). Further coiled-coil domain proteins as CCDC39 and CCDC40 are essential for ciliary motility by assembly of the dynein regulatory complex (Becker-Heck et al., 2011; Merveille et al., 2011; Blanchon et al., 2012). *Ccdc42*-ko mice are phenotypically normal but males are sterile. Sterility of *Ccdc42*-deficient male mice is most likely caused by the malformation of the HTCA and the sperm tail resulting in functional insufficiency (Pasek et al., 2016). These data suggest that CCDC42 has an important function in male germ cells but is otherwise dispensable (Pasek et al., 2016). Since CCDC42-deficiency affected exclusively the male germ cell, CCDC42 seems not to be involved in ciliary motility because otherwise, a more generalized phenotype has to be expected. CCDC42-deficient spermatids are characterized by a multiplicity of the HTCA, defective nuclear shaping despite presence of a manchette, dislocation of the HTCA from its implantation site and a loss of flagellar outgrowth from the HTCA (Pasek et al., 2016).

We have demonstrated by immunocytology that CCDC42 co-localizes with ODF1- and ODF2-fusion proteins when ectopically expressed, and with structures comprising these proteins endogenously. Furthermore, co-precipitation by pull-down and co-immunoprecipitation experiments indicated binding of CCDC42 to ODF1 as well as to ODF2. However, recruitment of CCDC42 to the sperm tail and the centrosome in somatic cells does not require ODF1. CCDC42 consists in essential of coiled-coil domains, which is also the main feature of ODF2. Coiled-coil domains are important oligomerization domains mediating homodimerization as well as heterodimerization (Mason and Arndt, 2004). It is, therefore, most likely that ODF2 and CCDC42 interact by means of their coiled-coil domains. This mutual interaction might contribute to the stabilization of important cytoskeletal structures potentially mediated by ODF1. Although the true molecular function of ODF1 is not known, it belongs to the small heat shock protein family and might, therefore, act as a chaperone in protein folding (Fontaine et al., 2003). The protein complex consisting of the core proteins ODF2/ODF1/CCDC42 may thus build the rigid scaffold essential for the formation of the connecting piece and the sperm tail. When missing any one of these proteins the rigid scaffold is damaged causing failure of the linkage complex and the sperm tail. Whether CCDC42 interacts with any of those proteins that have a reported function in HTCA formation, as Centrin 1, Centrobilin, Spata6, or Azi1/Cep131 awaits further investigation (Liska et al., 2009; Avashti et al., 2013; Hall et al., 2013; Yuan et al., 2015). However, since CCDC42-deficient sperm often show two instead of one basal body inserted into the nuclear membrane, centriole duplication, as well as correct attachment of the centrioles to the implantation fossa seem to be affected (Pasek et al., 2016). As similar phenotypes have been observed concerning mutations in Centrobilin, Centrin 1, and Azi/Cep131 a functional interaction with CCDC42 is likely (Liska et al., 2009; Avashti et al., 2013; Hall et al., 2013). Our observation that CCDC42 is expressed in the manchette and in particular in the perinuclear ring illuminates its involvement in the acrosome-acroplaxome complex formation and nuclear shaping

that are both affected when CCDC42 is missing. Since loss of CCDC42 did not prevent manchette formation, it is most likely involved in stabilizing the manchette or is a passenger protein transported via the manchette. Its accumulation in the perinuclear ring, however, points toward a stabilizing function and its involvement in the attachment of the manchette to the nuclear membrane.

Our data show that CCDC42 expression is not restricted to testis and brain but instead is found also in somatic tissues. We detected the endogenous protein in the centrosome of somatic NIH3T3 cells and hence identified CCDC42 as a novel component of the centrosome and the sperm tail not found before by large scale proteomics screens (Amaral et al., 2013; centrosome database Centrosome:DB). However, albeit RT-PCR experiments confirmed expression of *Ccdc42* in somatic tissues, the full-length sequence could only be amplified from testis cDNA. It is therefore probable that the full-length isoform 203 is restricted to testis or more specifically to male germ cells whereas another isoform is expressed in somatic tissues. We could not verify expression of isoform 202, which starts with translated sequences encoded by intron 4 since a primer that binds to these 5' sequences has amplified an unrelated almost unknown sequence (C6H1orf158). Furthermore, we got no indications by RT-PCR of isoform 201, which was expected to be encoded by a smaller cDNA due to skipping of exon 5. Our data additionally show that CCDC42 is a component of the centrosome in somatic cells and most likely functions in scaffolding the centrosome via interaction with ODF2/Cenexin. However, since the only obvious phenotype of CCDC42-deficient mice is male infertility, CCDC42 is either dispensable for the somatic centrosome or its function has been taken over by other members of the CFAP73 family.

## DATA AVAILABILITY

The datasets generated for this study are available on request to the corresponding author.

## AUTHOR CONTRIBUTIONS

CTC did the experiments and prepared the figures. SH-F was the project leader and wrote the manuscript. Both authors read and approved the final manuscript.

## FUNDING

CTC got a Ph.D. grant of the DAAD/CONICYT BECAS Chile program.

## ACKNOWLEDGMENTS

We thank Manfred Alsheimer (Würzburg) for the kind gift of  $\alpha$ -SUN4 antibody.

## REFERENCES

- Akhmanova, A., Mausset-Bonnefont, A. L., van Cappellen, W., Keijzer, N., Hoogenraad, C. C., Stepanova, T., et al. (2005). The microtubule plus-end-tracking protein CLIP-170 associates with the spermatid manchette and is essential for spermatogenesis. *Genes Dev.* 19, 2501–2515. doi: 10.1101/gad.344505
- Amaral, A., Castillo, J., Estanyol, J. M., Ballesca, J. L., Ramalho-Santos, J., and Oliva, R. (2013). Human sperm proteome suggests new endogenous metabolic pathways. *Mol. Cell. Proteomics* 12, 330–342. doi: 10.1074/mcp.M112.020552
- Avashiti, P., Scheel, J. F., Ying, G., Frederick, J. M., Baehr, W., and Wolfrum, U. (2013). Germline deletion of *Cetn1* causes infertility in male mice. *J. Cell Sci.* 126, 3204–3213. doi: 10.1242/jcs.128587
- Baltz, J. M., Williams, P. O., and Cone, R. A. (1990). Dense fibers protect mammalian sperm against damage. *Biol. Reprod.* 43, 485–491. doi: 10.1095/biolreprod43.3.485
- Becker-Heck, A., Zohn, I. E., Okabe, N., Pollock, A., Lenhart, K. B., Sullivan-Brown, J., et al. (2011). The coiled-coil domain containing protein CCDC40 is essential for motile cilia function and left-right axis formation. *Nat. Genet.* 43, 79–84. doi: 10.1038/ng.727
- Blanchon, S., Legendre, M., Copin, B., Duquesnoy, P., Montantin, G., Kott, E., et al. (2012). Delineation of CCDC39/CCDC40 mutation spectrum and associated phenotypes in primary ciliary dyskinesia. *J. Med. Genet.* 49, 410–416. doi: 10.1136/jmedgenet-2012-100867
- Brohm, H., Pinnecke, S., and Hoyer-Fender, S. (1997). Identification and characterization of new cDNAs encoding outer dense fiber proteins of rat sperm. *J. Biol. Chem.* 272, 10327–10332. doi: 10.1074/jbc.272.15.10327
- Burfeind, P., and Hoyer-Fender, S. (1991). Sequence and developmental expression of a mRNA encoding a putative protein of rat sperm outer dense fibers. *Dev. Biol.* 148, 195–204. doi: 10.1016/0012-1606(91)90329-2
- Calvi, A., Wong, A. S., Wright, G., Wong, E. S., Loo, T. H., Stewart, C. L., et al. (2015). SUN4 is essential for nuclear remodeling during mammalian spermiogenesis. *Dev. Biol.* 407, 321–330. doi: 10.1016/j.ydbio.2015.09.010
- Chen, S. R., Batool, A., Wang, Y. Q., Hao, X. X., Chang, C. S., Cheng, C. Y., et al. (2016). The control of male fertility by spermatid-specific factors: searching for contraceptive targets from spermatozoon's head to tail. *Cell Death Dis.* 7:e2472. doi: 10.1038/cddis.2016.344
- Clermont, Y., Oko, R., and Hermo, L. (1993). "Cell biology of mammalian spermiogenesis," in *Cell and Molecular Biology of the Testis*, eds C. Desjardins and L. Ewing (New York, NY: Oxford University Press), 332–376.
- Donkor, F. F., Mönnich, M., Czirr, E., Hollemann, T., and Hoyer-Fender, S. (2004). Outer dense fiber protein 2 (ODF2) is a self-interacting centrosomal protein with affinity for microtubules. *J. Cell. Sci.* 117, 4643–4651. doi: 10.1242/jcs.01303
- Dooher, G. B., and Bennett, D. (1973). Fine structural observations on the development of the sperm head in the mouse. *Am. J. Anat.* 136, 339–362.
- Doxsey, S. J., Stein, P., Evans, L., Calarco, P. D., and Kirschner, M. (1994). Pericentriolar, a highly conserved centrosome protein involved in microtubule organization. *Cell* 76, 639–650. doi: 10.1016/0092-8674(94)90504-5
- Fawcett, D. W. (1975). The mammalian spermatozoon. *Dev. Biol.* 44, 394–436. doi: 10.1016/0012-1606(75)90411-x
- Fawcett, D. W., Anderson, W. A., and Phillips, D. M. (1971). Morphogenetic factors influencing the shape of the sperm head. *Dev. Biol.* 26, 220–251. doi: 10.1016/0012-1606(71)90124-2
- Fawcett, D. W., and Phillips, D. M. (1969). The fine structure and development of the neck region of the mammalian spermatozoon. *Anat. Rec.* 165, 153–164.
- Fishman, E. L., Jo, K., Nguyen, Q. P. H., Kong, D., Royfma, N. R., Cekic, A. R., et al. (2018). A novel atypical sperm centriole is functional during human fertilization. *Nat. Commun.* 9:2210.
- Fontaine, J.-M., Rest, J. S., Welsh, M. J., and Benndorf, R. (2003). The sperm outer dense fiber protein is the 10th member of the superfamily of mammalian small stress proteins. *Cell Stress Chaperones* 8, 62–69.
- Guindon, S., Dufayard, J.-F., Lefort, V., Anisimova, M., Hordijk, W., and Gascuel, O. (2010). New algorithms and methods to estimate maximum-likelihood phylogenies: assessing the performance of PhyML 3.0. *Syst. Biol.* 59, 307–321. doi: 10.1093/sysbio/syq010
- Hall, E. A., Keighren, M., Ford, M. J., Davey, T., Jarman, A. P., Smith, L. B., et al. (2013). Acute versus chronic loss of mammalian *Azil1/Cep131* results in distinct ciliary phenotypes. *PLoS Genet.* 9:e1003928. doi: 10.1371/journal.pgen.1003928
- Hoyer-Fender, S. (2011). "Centrosomes in fertilization, early embryonic development, stem cell division, and cancer," in *Deep Insight for The Atlas of Genetics & Cytogenetics in Oncology and Haematology*, ed. J. L. Huret (Vandœuvre-lès-Nancy: Institute of Scientific and Technical).
- Hüber, D., Geisler, S., Monecke, S., and Hoyer-Fender, S. (2008). Molecular dissection of ODF2/Cenexin revealed a short stretch of amino acids necessary for targeting to the centrosome and the primary cilium. *Eur. J. Cell Biol.* 87, 137–146. doi: 10.1016/j.ejcb.2007.10.004
- Inaba, K., and Mizuno, K. (2016). Sperm dysfunction and ciliopathy. *Reprod. Med. Biol.* 15, 77–94. doi: 10.1007/s12522-015-0225-5
- Jan, S. Z., Hamer, G., Repping, S., de Rooij, D. G., van Pelt, A. M. M., and Vormer, T. L. (2012). Molecular control of rodent spermatogenesis. *Biochim. Biophys. Acta* 1822, 1838–1850. doi: 10.1016/j.bbadis.2012.02.008
- Kierszenbaum, A. L. (2001). Spermatid manchette: plugging proteins to zero into the sperm tail. *Mol. Reprod. Dev.* 59, 347–349. doi: 10.1002/mrd.1040
- Kierszenbaum, A. L. (2002). Intramanchette transport (IMT): managing the making of the spermatid head, centrosome, and tail. *Mol. Reprod. Dev.* 63, 1–4. doi: 10.1002/mrd.10179
- Kierszenbaum, A. L., Rivkin, E., and Tres, L. L. (2011). Cytoskeletal track selection during cargo transport in spermatids is relevant to male fertility. *Spermatogenesis* 1, 221–230. doi: 10.4161/spmg.1.3.18018
- Laemmli, U. K. (1970). Cleavage of structural proteins during assembly of the head of the bacteriophage T4. *Nature* 227, 680–685. doi: 10.1038/227680a0
- Lehti, M. S., and Sironen, A. (2016). Formation and function of the manchette and flagellum during spermatogenesis. *Reproduction* 151, R43–R54. doi: 10.1530/REP-15-0310
- Lehti, M. S., and Sironen, A. (2017). Formation and function of sperm tail structures in association with sperm motility defects. *Biol. Reprod.* 97, 522–536. doi: 10.1093/biolre/iox096
- Lindemann, C. B. (1996). Functional significance of the outer dense fibers of mammalian sperm examined by computer simulation with the geometric clutch model. *Cell. Motil. Cytoskeleton* 34, 258–270. doi: 10.1002/(sici)1097-0169(1996)34:4<258::aid-cm1>3.0.co;2-4
- Liska, F., Gosele, C., Rivkin, E., Tres, L. L., Cardoso, M. C., Domaing, P., et al. (2009). Rat hd mutation reveals an essential role of centrin in spermatid head shaping and assembly of the head-tail coupling apparatus. *Biol. Reprod.* 81, 1196–1205. doi: 10.1095/biolreprod.109.078980
- Mason, J. M., and Arndt, K. M. (2004). Coiled coil domains: stability, specificity, and biological implications. *ChemBiochem* 5, 170–176. doi: 10.1002/cbic.200300781
- Mendoza-Lujambio, I., Burfeind, P., Dixkens, C., Meinhardt, A., Hoyer-Fender, S., and Neesen, J. (2002). The *Hook1* gene is non-functional in the abnormal spermatozoon head shape (*azh*) mutant mouse. *Hum. Mol. Genet.* 11, 1647–1658. doi: 10.1093/hmg/11.14.1647
- Merveille, A. C., Davis, E. E., Becker-Heck, A., Legendre, M., Amirav, I., Bataille, G., et al. (2011). CCDC39 is required for assembly of inner dynein arms and the dynein regulatory complex and for normal ciliary motility in humans and dogs. *Nat. Genet.* 43, 72–78. doi: 10.1038/ng.726
- Nakagawa, Y., Yamane, Y., Okanou, T., Tsukita, S., and Tsukita, S. (2001). Outer dense fiber 2 is a widespread centrosome scaffold component preferentially associated with mother centrioles: its identification from isolated centrosomes. *Mol. Biol. Cell* 12, 1687–1697. doi: 10.1091/mbc.12.6.1687
- Nebel, B. R., Amarose, A. P., and Hackett, E. M. (1961). Calendar of gametogenic development in the prepubertal male mouse. *Science* 134, 832–833. doi: 10.1126/science.134.3482.832
- O'Donnell, L., and O'Bryan, M. K. (2014). Microtubules and spermatogenesis. *Semin. Cell. Dev. Biol.* 30, 45–54. doi: 10.1016/j.semdb.2014.01.003
- Pasch, E., Link, J., Beck, C., Scheuerle, S., and Alsheimer, M. (2015). The LINC complex component Sun4 plays a crucial role in sperm head formation and fertility. *Biol. Open* 4, 1792–1802. doi: 10.1242/bio.015768
- Pasek, R. C., Malarkey, E., Berbari, N. F., Sharma, N., Kesterson, R. A., Tres, L. L., et al. (2016). Coiled-coil domain containing 42 (*Ccdc42*) is necessary for proper sperm development and male fertility in the mouse. *Dev. Biol.* 412, 208–218. doi: 10.1016/j.ydbio.2016.01.042

- Rattner, J. B., and Brinkley, B. R. (1972). Ultrastructure of mammalian spermiogenesis. III. The organization and morphogenesis of the manchette during rodent spermatogenesis. *J. Ultrastruc. Res.* 41, 209–218. doi: 10.1016/s0022-5320(72)90065-2
- Rattner, J. B., and Olson, G. (1973). Observations on the fine structure of the nuclear ring of the mammalian spermatid. *J. Ultrastruc. Res.* 43, 438–444. doi: 10.1016/s0022-5320(73)90020-8
- Ruan, J., Li, H., Chen, Z., Coghlan, A., Coin, L. J. M., Guo, Y., et al. (2008). TreeFam: 2008 Update. *Nucleic Acids Res.* 36, D735–D740.
- Russell, L. D., Ettlin, R. A., Sinha Hikim, A. P., and Clegg, E. D. (1990). *Histological and Histopathological Evaluation of the Testis*. Clearwater, FL: Cache River Press, 120. doi: 10.1111/j.1365-2605.1993.tb01156.x
- Russell, L. D., Russell, J. A., MacGregor, G. R., and Meistrich, M. L. (1991). Linkage of manchette microtubules to the nuclear envelope and observations of the role of the manchette in nuclear shaping during spermiogenesis in rodents. *Am. J. Anat.* 192, 97–120. doi: 10.1002/aja.1001920202
- Schalles, U., Shao, X., van der Hooft, F., and Oko, R. (1998). Developmental expression of the 84-kDa ODF sperm protein: localization to both the cortex and medulla of outer dense fibers and to the connecting piece. *Dev. Biol.* 199, 250–260. doi: 10.1006/dbio.1998.8931
- Schatten, G. (1994). The centrosome and its mode of inheritance: the reduction of the centrosome during gametogenesis and its restoration during fertilization. *Dev. Biol.* 165, 299–335. doi: 10.1006/dbio.1994.1256
- Shao, X., Tarnasky, H. A., Schalles, U., Oko, R., and van der Hoorn, F. (1997). Interactional cloning of the 84-kDa major outer dense fiber protein Odf84. Leucine zippers mediate associations of Odf84 and Odf27. *J. Biol. Chem.* 272, 6105–6113. doi: 10.1074/jbc.272.10.6105
- Towbin, H., Staehelin, T., and Gordon, J. (1979). Electrophoretic transfer of proteins from polyacrylamide gels to nitrocellulose sheets: procedure and some applications. *Proc. Natl. Acad. Sci. U.S.A.* 76, 4350–4354. doi: 10.1073/pnas.76.9.4350
- Wolosewick, J. J., and Bryan, J. H. D. (1977). Ultrastructural characterization of the manchette microtubule in the seminiferous epithelium of the mouse. *Am. J. Anat.* 150, 301–332.
- Yamamoto, R., Song, K., Yanagisawa, H. A., Fox, L., Yagi, T., Wirschell, M., et al. (2013). The MIA complex is a conserved and novel dynein regulator essential for normal ciliary motility. *J. Cell Biol.* 201, 263–278. doi: 10.1083/jcb.201211048
- Yang, K., Adham, I. A., Meinhardt, A., and Hoyer-Fender, S. (2018a). Ultrastructure of the sperm head-to-tail linkage complex in the absence of the spermatid-specific LINC component SPAG4. *Histochem. Cell Biol.* 150, 49–59. doi: 10.1007/s00418-018-1669-7
- Yang, K., Tylkowski, M. A., Hüber, D., Tapia Contreras, C., and Hoyer-Fender, S. (2018b). ODF2/Cenexin maintains centrosome cohesion by restricting  $\beta$ -catenin accumulation. *J. Cell Sci.* 131:jcs220954. doi: 10.1242/jcs.220954
- Yang, K., Grzmil, P., Meinhardt, A., and Hoyer-Fender, S. (2014). Haplo-deficiency of ODF1/HSPB10 in mouse sperm causes relaxation of head-to-tail linkage. *Reproduction* 148, 499–506. doi: 10.1530/REP-14-0370
- Yang, K., Meinhardt, A., Zhang, B., Grzmil, P., Adham, I. M., and Hoyer-Fender, S. (2012). The small heat shock protein ODF1/HSPB10 is essential for tight linkage of sperm head to tail and male fertility in mice. *Mol. Cell. Biol.* 32, 216–225. doi: 10.1128/MCB.06158-11
- Yuan, S., Stratton, C. J., Bao, J., Zheng, H., Bhetwal, B. P., Yanagimachi, R., et al. (2015). Spata6 is required for normal assembly of the sperm connecting piece and tight head-tail junction. *Proc. Natl. Acad. Sci. U.S.A.* 112, E430–E439. doi: 10.1073/pnas.1424648112
- Zur Lage, P., Newton, F. G., and Jarman, A. P. (2019). Survey of the ciliary motility machinery of *Drosophila* sperm and ciliated mechanosensory neurons reveals unexpected cell-type specific variations: a model for motile ciliopathies. *Front. Genet.* 10:24. doi: 10.3389/fgene.2019.00024

**Conflict of Interest Statement:** The authors declare that the research was conducted in the absence of any commercial or financial relationships that could be construed as a potential conflict of interest.

Copyright © 2019 Tapia Contreras and Hoyer-Fender. This is an open-access article distributed under the terms of the Creative Commons Attribution License (CC BY). The use, distribution or reproduction in other forums is permitted, provided the original author(s) and the copyright owner(s) are credited and that the original publication in this journal is cited, in accordance with accepted academic practice. No use, distribution or reproduction is permitted which does not comply with these terms.

### **3.4.2 The WD40-protein CFAP52/WDR16 is a centrosome/basal body protein and localizes to the manchette and the flagellum in male germ cells**

This chapter reports the cilia and flagella-associated protein 52, CFAP52, as a new structural component of male germ cells located at the manchette and sperm tail. Initially, CFAP52 was related to the presence of motile cilia, while in *Chlamydomonas*, it contributes to the stabilization of the axoneme. *Cfap52* transcription has been detected in testes and the ependymal layer of the brain. However, the subcellular localization of CFAP52 had not been described. Thus, we have investigated CFAP52 localization in somatic and male germ cells. Here, we show that CFAP52 localizes to the transient manchette in round and elongating spermatids and the sperm tail. Further, our results reveal that CFAP52 expression is not restricted to male germ cells but instead that CFAP52 is a novel centrosome/basal body protein that also resides in the mitotic spindle poles and the mid-body. Thus, these data indicate that CFAP52 is associated with a subset of microtubular structures, especially centrosome/centriole derived structures.

Beyond that, CFAP52 is a member of the WD-repeat proteins, which mediate protein interactions. Therefore, CFAP52 might likewise act in the assembly or stabilization of protein complexes constituting the centrosomal/basal body matrix, the manchette, and the sperm tail. Furthermore, the location of CFAP52 to the sperm tail but not to the axoneme of primary cilia implies that CFAP52 fulfills specific functions in the stability or maintenance of the sperm tail.

Constanza Tapia Contreras and Sigrid Hoyer-Fender

**Author Contributions:** Conceived and designed experiments: SH-F. Performed experiments: CTC. Prepared figures and wrote the manuscript: SH-F and CTC. Both authors read and approved the final manuscript.

**Status of manuscript:** Published in Scientific Reports in 2020.



# OPEN The WD40-protein CFAP52/WDR16 is a centrosome/basal body protein and localizes to the manchette and the flagellum in male germ cells

Constanza Tapia Contreras & Sigrid Hoyer-Fender

Development of spermatozoa requires remodelling and formation of particular structures. In elongating spermatids, the transient microtubular manchette contributes to the formation of the head–tail coupling apparatus (HTCA) and the sperm tail. The HTCA derives from the centrosome in that the proximal centriole inserts into the nuclear indentation and the distal centriole gives rise to the sperm flagellum. Although impairments in the formation of HTCA and sperm tail cause male infertility their molecular constituents are only partially known. The WD40-protein CFAP52 is implicated in motile cilia, but its relevance for male germ cell differentiation is not known. Here we show that CFAP52 is widespread expressed and localizes to a subset of microtubular structures. In male germ cells, CFAP52 is a component of the transient manchette and the sperm tail. However, expression of *Cfap52* is not restricted to motile cilia-bearing cells. In NIH3T3 cells, CFAP52 localizes to the centrosome, the basal body, and the mitotic spindle poles, but not to the primary cilium. Our results demonstrate that CFAP52 is not restricted to motile cilia but instead most likely functions in constituting the centrosome/basal body matrix and the sperm tail.

The cilia and flagella associated protein 52, CFAP52 (also named WDR16, WD repeat domain 16, WDRPUH, FLJ37528) is a member of the large WD40-repeat protein family and is widely expressed in eukaryotes. WD40-repeats, which are also known as WD or beta-transducin repeats, are short motifs of 40–60 amino acids often terminating in the dipeptide WD. The WD40-domain often comprises several of the WD40-repeats each forming a beta-pleated sheet in a propeller blade<sup>1,2</sup>. WD40 proteins are crucially involved in several physiological functions as diverse as signal transduction, RNA processing, remodeling the cytoskeleton, regulation of vesicular traffic, and cell cycle control<sup>3–5</sup>. Their immediate purpose most likely is to serve as platforms for the assembly of protein complexes and to mediate protein–protein interactions<sup>6</sup>.

The WD40 protein family member WDR16 is highly conserved having homologs in invertebrates and vertebrates including flies and humans<sup>7</sup>. In rat, expression of WDR16 was mainly observed in testis and in ependymal cells of the brain, and with reduced expression in lungs. Its expression profile, especially during ependymal development, indicated a correlation to the presence of motile cilia whereas in cells harboring primary cilia WDR16 could not be detected<sup>7</sup>. By immunofluorescence, WDR16 was found in the cytosol of rat testicular cells, especially in early spermatocytes and pachytene spermatocytes showing a uniform and unspecific localization. Sperm flagella stained negative for WDR16 but in Western blots the tail fraction of bull sperm revealed WDR16<sup>7</sup>. Overall, these results indicated that WDR16 is a marker for motile cilia-bearing cells. WDR16 depletion in zebrafish caused hydrocephalus, however, ciliary movement remained intact. Similarly, the ependymal layer did not display visible alteration<sup>7</sup>. WDR16, furthermore, seems to be involved in the establishment of the left–right symmetry in humans as the homozygous deletion caused laterality disorders<sup>8</sup>. Taken together, these data indicated, that WDR16 is functionally associated with motile cilia, either in the ependym or in the embryonic node albeit cilia

Johann-Friedrich-Blumenbach-Institute of Zoology and Anthropology – Developmental Biology, GZMB, Ernst-Caspari-Haus, Justus-Von-Liebig-Weg11, Georg-August-Universität Göttingen, 37077 Göttingen, Germany. email: shoyer@gwdg.de

seem not to be directly affected. Nevertheless, WDR16 might be involved in the stabilization of microtubular structures, as observed for the *Chlamydomonas* WDR16 ortholog FAP52 that plays an important role in axoneme stability<sup>9</sup>. Our intention was therefore, to elucidate the association of WDR16 with cilia in more detail by investigating its expression and localization at the subcellular level. We were interested in both motile and immotile cilia/flagella firstly taking advantage of flagella formation in mammalian spermatogenesis.

Haploid spermatids derived from the second meiotic division differentiated into functional spermatozoa in spermiogenesis. This process is characterized by reshaping of spermatids including elongation and condensation of the nucleus, and the development of specific structures as the acrosome, the transient manchette and the flagellum, and eventually the shedding of the cytoplasm<sup>10,11</sup>. These morphological changes produce highly polarized cells determined by the apical acrosome and the flagellum at the opposite pole. The functionality of the spermatozoon, that is propelling the sperm nucleus towards the oocyte, depends on the tight linkage between sperm tail and nucleus mediated by the head-to-tail coupling apparatus (HTCA)<sup>10</sup>. The HTCA and its morphological equivalent the connecting piece develops from the centrioles. During spermiogenesis, the acrosome and the paired centrioles migrate to opposite poles of the nucleus<sup>12</sup>. The proximal centriole inserts into the caudal area of the nucleus forming the implantation fossa whereas the distal centriole constitutes the basal body that gives rise to the axoneme<sup>10,13,14</sup>. The sperm flagellum, furthermore, contains additional so-called accessory structures as the outer dense fibres (ODFs) that went laterally to the microtubule (MT) doublets of the axoneme and provide elasticity and stiffness to the flagellum<sup>15,16</sup>.

Spermatid elongation is characterized by the formation of a transient microtubular structure, the manchette. The manchette MTs are connected to the perinuclear ring, which is closely associated to the acrosomal border, and extend progressively towards the caudal region thus forming a skirt-like structure surrounding the nucleus<sup>17,18</sup>. The manchette is essential for nuclear reshaping and considered as a track for the delivery of cargos to assemble HTCA and sperm tail<sup>19,20</sup>.

Besides being far from figured out in detail up to now, knock out mouse models were useful in shedding light on the underlying genetic causes responsible for impaired spermiogenesis and male infertility<sup>21–23</sup>. In this regard, several genes were identified affecting manchette formation and reshaping of the spermatid when mutated, e.g. the abnormal spermatozoon head shape (*azh*) phenotype is caused by a mutation in the *Hook1* gene<sup>24–27</sup>. *Hook1*-depletion, furthermore, disrupted the tight connection between flagellum and nucleus causing sperm decapitation<sup>26</sup>. Sperm decapitation and male infertility were also observed when the outer dense fibre protein ODF1 or one of its interacting proteins centrosomal protein coiled-coil domain containing 42 (CCDC42) or the testis-specific SUN-domain protein SPAG4L/SUN5 were mutated<sup>28–31</sup>. SUN-domain proteins are integral nuclear membrane proteins and are part of the linker of nucleoskeleton and cytoskeleton (LINC) complex responsible for bridging the nuclear envelope and the cytoskeleton<sup>32</sup>. In contrast, deficiency of SPAG4/SUN4, the second testis-specific SUN-domain protein and reported ODF1-binding protein caused disjunction of the manchette and male infertility but not decapitation<sup>33–37</sup>.

In order to figure out the protein interaction network responsible for HTCA and sperm tail formation we focused here on the cilia and flagella associated protein 52 (CFAP52). We used RT-PCR for expression analyses, and investigated its sub-cellular localization by immunocytochemistry in transfected cells and in male germ cells. We found that CFAP52 is not restricted to motile cilia bearing cells but instead most likely is ubiquitously expressed. Our data indicate that CFAP52 is associated with a subset of MT structures especially centriole/centrosome derived structures, and the manchette and the axoneme in the sperm flagellum.

## Results

**Widespread expression of *Cfap52*.** In order to verify the reported expression of *Cfap52*, we performed RT-PCR using total RNA isolated from mouse tissues, and in addition from the mouse fibroblast cell line NIH3T3. Amplification of exons 1–14 of *Cfap52* revealed the expected fragment of 1871 bp in testis and ovary but not in any of the other probes (Fig. 1a), whereas amplification of *Gapdh* in all probes verified the quality of cDNAs (Fig. 1c). These results confirmed the previous observation of a testicular expression of *Cfap52* but additionally demonstrated that *Cfap52* is also highly expressed in ovary, which to the best of our knowledge do not harbor cells with motile cilia. However, to detect even low expression levels we performed a nested PCR on the first PCR product amplifying a region comprising parts of exons 4 to 6. A DNA fragment of the expected size of 255 bp was found in all samples (Fig. 1b). Sequencing of the PCR products obtained from brain, ovary and epididymis confirmed amplification of *Cfap52*. The different intensities obtained for the secondary PCR product are caused by differing amounts of first PCR used as template. These results demonstrate that *Cfap52* is expressed in all tissues investigated including the fibroblast cell line. *Cfap52*, therefore, seems to be ubiquitously expressed, including somatic tissues and cells that do not generate motile cilia, although at a low level. Expression of *Cfap52* is therefore not restricted to motile cilia bearing cells.

**CFAP52 localizes to the spermatid manchette and to the sperm tail.** Testicular expression of *Cfap52*, previously reported in the rat, was confirmed by our investigation in the mouse. However, besides an overall and unspecific cytoplasmic distribution of CFAP52 in spermatocytes no further specification is currently available<sup>7</sup>. We therefore intended to investigate the subcellular localization of CFAP52 during mouse spermatogenesis using mouse testicular cell suspensions decorated by a commercially available antibody. We first validated the anti-CFAP52 antibody for immunocytochemistry by generating a CFAP52::EGFP fusion construct, transfected the plasmid into NIH3T3 cells, and decorated the expressed fusion protein with the anti-CFAP52 antibody (Fig. 2a–d). Antibody staining was exclusively found in transfected cells, identified by their green auto-fluorescence of the CFAP52::EGFP fusion. Furthermore, the antibody co-localized with the green fluorescent CFAP52::EGFP fusion protein.



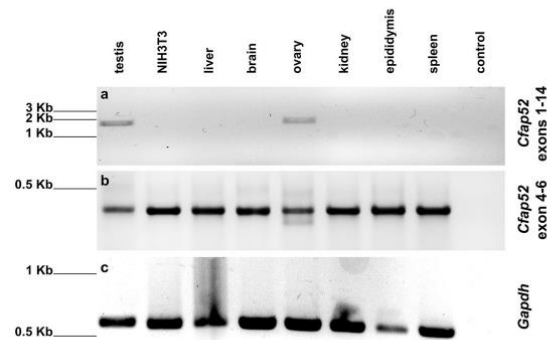


**Figure 1.** *Cfap52* expression is not correlated with the presence of motile cilia. RT-PCR on cDNA synthesized from different mouse tissues and from the fibroblast cell line NIH3T3. (a) Amplification of exon 1 to exon 14 of *Cfap52*. The expected fragment size of 1871 bp is found in testis and ovary. (b) Nested PCR on the first RT-PCR products was performed to amplify parts of exon 4 to exon 6 of *Cfap52*. The expected fragment size of 255 bp is present in all probes. (c) *Gapdh* amplification as quality check. Control is the PCR reaction without template.

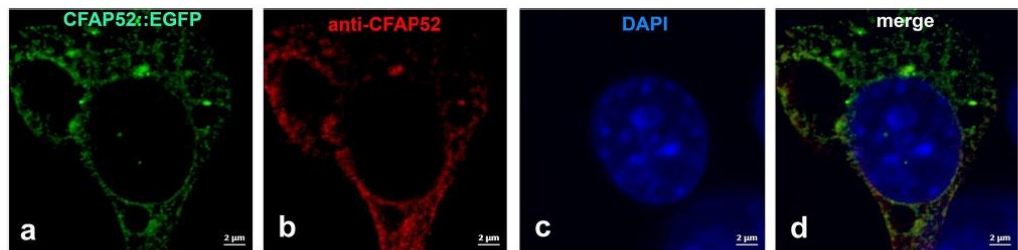


**Figure 2.** Validation of anti-CFAP52 antibody. NIH3T3 cells were transfected with the *pCfap52::Egfp* expression plasmid encoding the fusion protein CFAP52::EGFP. Proteins were detected either by their auto-fluorescence (green) or by the commercial anti-CFAP52 antibody (red). Colocalization of the inherent green fluorescence and the antibody decoration demonstrated antibody specificity (a–d). Nuclear counterstain with DAPI (blue). Bars: 2  $\mu$ m.

Having the anti-CFAP52 antibody validated, we performed immunocytochemistry on mouse testicular cell suspensions (Fig. 3). The acrosome was decorated by peanut lectin-FITC staining to enable identification of spermatid differentiation steps (Fig. 3). A weak expression of CFAP52 with a few strong dots and a shallow indication of fibrous structures at the nuclear surroundings was first found in early round spermatids (Fig. 3a–d). These weak structures are most likely the first indications of the forming manchette, as fibre like structures with a strong CFAP52 reactivity are present in round spermatids of a more advanced step (Fig. 3e–h). Thereafter, a clear manchette with its characteristic parallel bundles was visible in round spermatids (Fig. 3i–l) and elongating spermatids (Fig. 3m–x) that is strongly stained for CFAP52 indicating an association of CFAP52 with microtubules. In mature spermatozoa, CFAP52 located to the sperm tail with a somehow stronger intensity in the principal piece than in the mid-piece (Fig. 3y–y’). No antibody staining was detected in elongating spermatids when anti-CFAP52 antibody was omitted (Fig. 3z–z’’).

Colocalization of CFAP52 with the manchette microtubules was demonstrated by alpha-tubulin decoration in round and elongating spermatids (Fig. 4a–h). Furthermore, CFAP52 showed a similar distribution as the LINC components SUN3 and SUN4 (Fig. 4i–p). Enrichment of CFAP52 at the head-to-tail coupling apparatus (HTCA), which was decorated by  $\gamma$ -tubulin staining, was not found (Fig. 4q–t). Additionally, CFAP52 is not enriched at the perinuclear ring, which was decorated for the microtubule plus-end binding protein EB3 (Fig. 4u–x), but showed a faint ring-like concentration anteriorly to the perinuclear ring (Fig. 4u, x, arrows)<sup>23</sup>.

A similar distribution in the manchette and the sperm tail was observed for the outer dense fibre protein 1, ODF1<sup>31</sup>, posing the question whether the observed colocalization indicates interaction or interdependency. We, therefore, investigated CFAP52 localization in testicular sections using both wild-type as well as *Odf1*-deficient mice<sup>28</sup>. In testis-sections of *Odf1*<sup>+/+</sup>-mice we observed CFAP52-decoration in the manchette (Fig. 5a–d, i–l, arrows). *Odf1*-deficient testis-sections exhibited the same strong CFAP52-staining in the manchette (Fig. 5e–h,

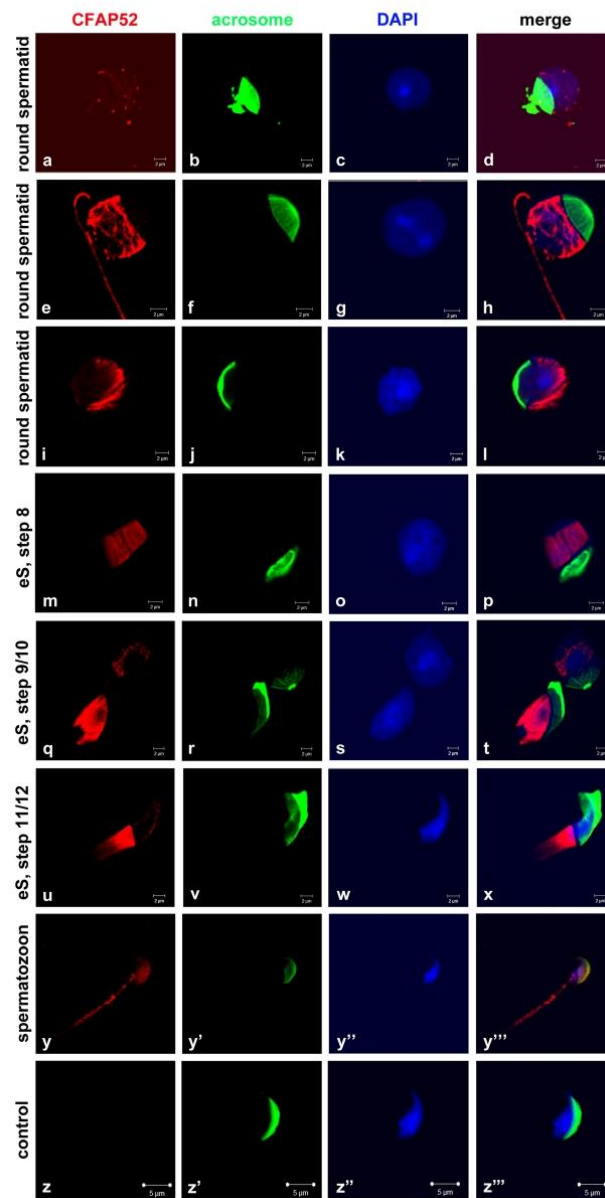


**Figure 3.** Subcellular localization of CFAP52 in male germ cells. CFAP52 is located to manchette and sperm tail in mouse male germ cells. Suspension preparations of adult mouse testis were incubated with a commercial antibody against CFAP52 (red) and the acrosome decorated with PL-FITC. The developing manchette is decorated with CFAP52 in round and elongating spermatids (a–x). In spermatozoa, CFAP52 localizes to the tail with a more intense staining of the principal piece than the mid-piece (z–z’’’). No staining of elongating spermatozoa was evident when the anti-CFAP52 antibody was omitted (control, y–y’’’).

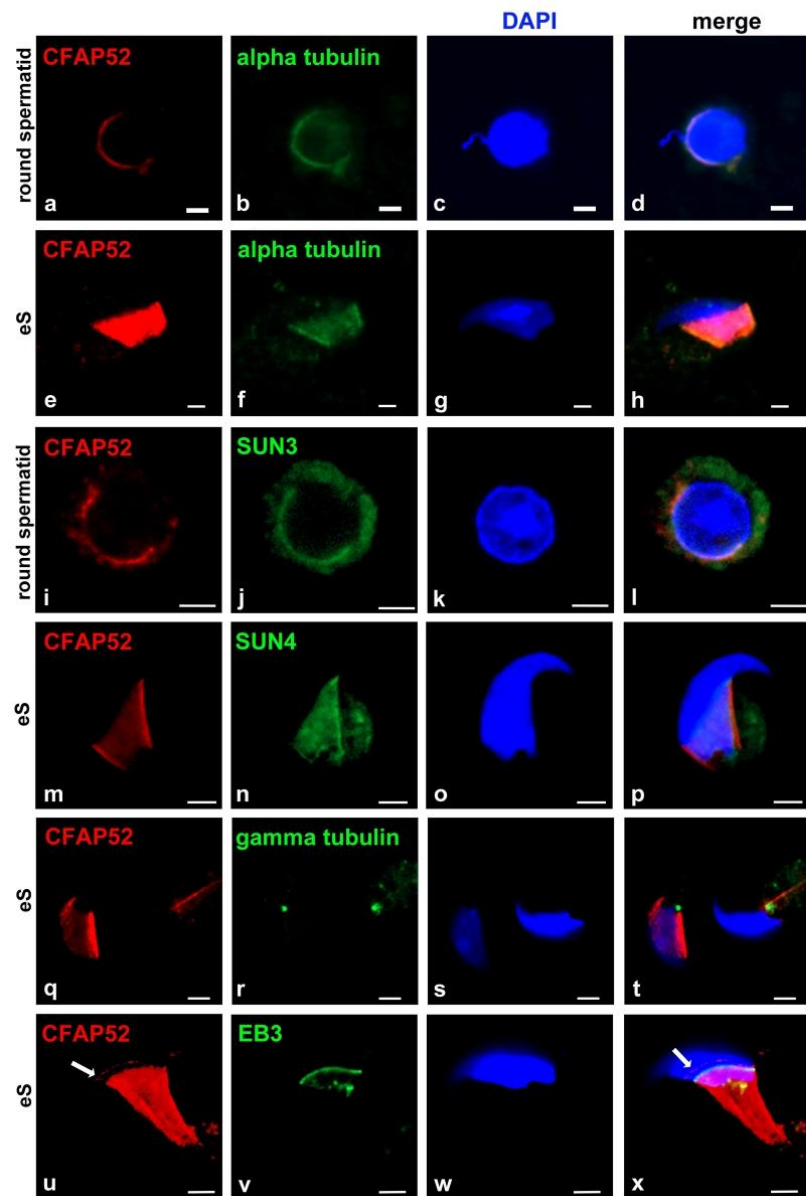


**Figure 4.** CFAP52 localizes to the manchette but not the perinuclear ring in spermatids. CFAP52 colocalizes with alpha-tubulin in the manchette in round (a–d) and elongating spermatids (e–h), and shows a similar distribution as the LINC components SUN3 (i–l) and SUN4 (m–p). Highlighting the basal body of the sperm tail by staining for gamma-tubulin could not demonstrate enrichment of CFAP52 (q–t). The microtubule plus-end tracking protein EB3 decorates the perinuclear ring that is not enriched for CFAP52 (u–x). The arrow points to the faint ring-like concentration of CFAP52 anteriorly to the perinuclear ring. CFAP52 in red (a, e, i, m, q, u), all other antibodies decorated in green (b, f, j, n, r, v). Nuclear counterstain with DAPI in blue (c, g, k, o, s, w) and merged images (d, h, l, p, t, x). eS: elongating spermatids. Bars: 2  $\mu$ m (a–h) or 2.5  $\mu$ m (i–x).

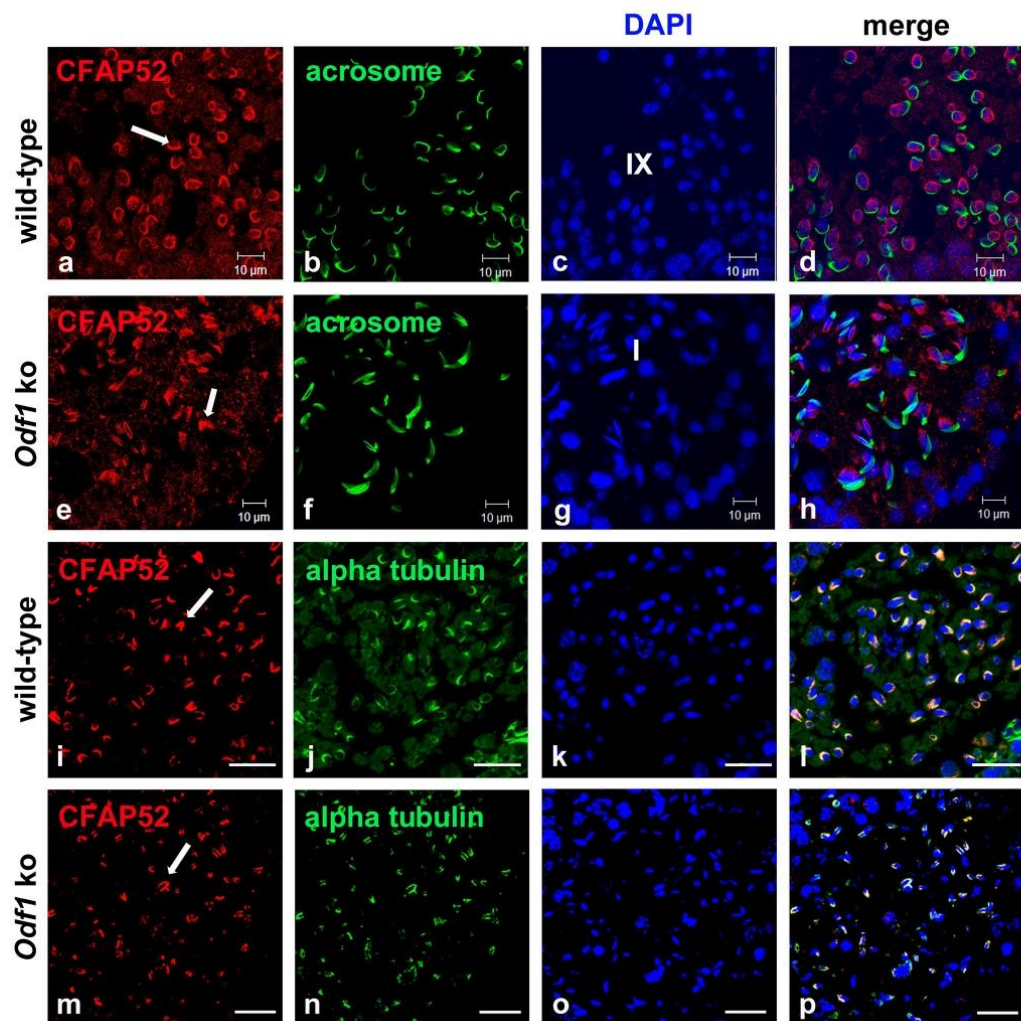


**Figure 5.** Depletion of ODF1 does not affect manchette location of CFAP52. CFAP52 decorates the manchette (arrows) in wild-type (a–d, i–l) as well as in *Odf1* ko testis sections (e–h, m–p) (in red). (a–h) Decoration of the acrosome by PL-FITC (green). Spermatogenic stages according to the acrosome formation are indicated (stage IX for the wild-type and stage I for the *Odf1* ko). (i–p) Double immunofluorescence with both, anti-CFAP52 (red) and anti-alpha-tubulin (green). Nuclear stain with DAPI (blue). (a, e, i, m) anti-CFAP52 antibody decoration (red), (b, f) PL-FITC (green), (j, n) detection of alpha-tubulin (green), (c, g, k, o) DAPI (blue), (d, h, l, p) merge. Bars: 10  $\mu$ m (a–h), 20  $\mu$ m (i–p).

m–p, arrows) demonstrated by alpha-tubulin decoration. Thus, depletion of *Odf1* neither affected the formation of the manchette nor the recruitment of CFAP52. Localization of CFAP52 to the manchette microtubules is therefore not mediated by ODF1.

**Endogenous CFAP52 localizes to centrosome/basal body, intercellular bridge and spindle poles in somatic cells.** We have proven prevalent low-level expression of *Cfap52* by nested RT-PCR. In order to substantiate these findings, we performed immunoblotting using total proteins obtained from mouse tissues as well as from NIH3T3 cells. CFAP52, in the expected molecular mass of ~68 kDa, was clearly detectable in all probes demonstrating once more that CFAP52 is not restricted to specific tissues (Fig. 6). Our results are corroborated by Western blot validation of anti-CFAP52 ([www.cusabio.com](http://www.cusabio.com)). Next, we used NIH3T3 cells

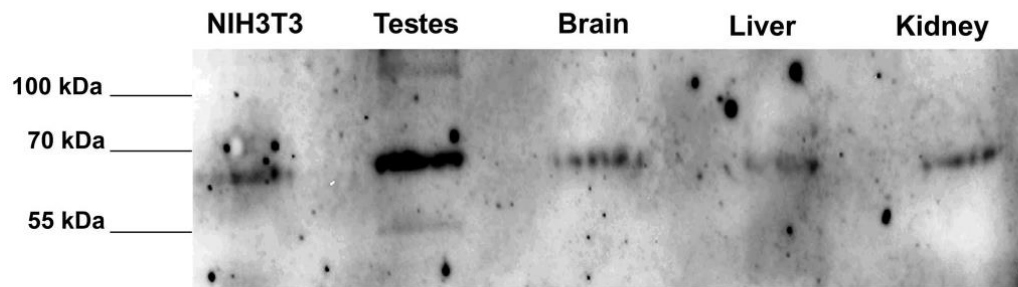


**Figure 6.** Detection of CFAP52 in mouse tissues. Total proteins of mouse tissues and of NIH3T3 cells were separated on a denaturing SDS-gel, transferred to Hybond ECL, and incubated with the anti-CFAP52 antibody. Chemiluminescence detection of the antibody. In all probes, CFAP52 with the predicted molecular mass of 68 kDa was detected.

to isolate the coding sequence of *Cfap52* and generated a fusion protein with EGFP by cloning *Cfap52* in frame to the N-terminal end of *Egfp* in plasmid *pEgfp-N1*. The plasmid *pCfap52::egfp* was transfected into NIH3T3 cells, and its distribution analyzed. Besides a more or less uniform background fluorescence we found a specific concentration of the CFAP52::EGFP fusion protein in two closely associated spots in the vicinity of the nucleus. Immunodecoration with anti- $\gamma$ -tubulin antibodies as a centrosomal marker revealed that CFAP52::EGFP colocalized with the centrosome in NIH3T3 cells (Fig. 7A a–d). We then asked whether the centrosomal location is caused by overexpression of the fusion protein, or otherwise is a feature of the endogenous protein characterizing CFAP52 as a novel centrosomal protein. To this end, NIH3T3 cells were treated for immunodecoration and double stained with anti-CFAP52, and either anti- $\gamma$ -tubulin or anti-acetylated tubulin antibodies (Fig. 7B). We detected the endogenous CFAP52 protein in the centrosome by colocalization with the centrosomal marker protein  $\gamma$ -tubulin (Fig. 7B a–d). Furthermore, CFAP52 is found in the cytoplasmic bridge linking the two daughter cells (Fig. 7B e–h). In this case, the cytoplasmic bridge is highlighted by acetylated tubulin. CFAP52 did not colocalize with acetylated tubulin but instead seemed to be concentrated at the tip of the cytoplasmic bridge near the plasma membrane. NIH3T3 cells generate non-motile, solitary cilia known as primary cilia that are also easily identifiable by immunodecoration for acetylated tubulin. The primary cilium as well as its associated daughter centriole at its base were identified by acetylated tubulin (Fig. 7B i–l). CFAP52 was not found in the ciliary axoneme but is highly concentrated at the basal body and at the daughter centriole. Additionally, CFAP52 is concentrated at the spindle poles that are highlighted by acetylated tubulin staining when captured at low intensity (Fig. 7B m–p). Omitting the anti-CFAP52 antibody and using both secondary antibodies for incubation in the controls demonstrated decoration of the centrosome with anti-acetylated tubulin antibodies (in red) but did not show any green fluorescence (Fig. 7B q–t).

**Centrosomal recruitment of CFAP52 isoforms.** We have identified CFAP52 as a novel centrosomal protein in NIH3T3 cells. CFAP52 is encoded by the *Wdr16/Cfap52* gene on chromosome 11 (11B3) in mice. The gene consists of 14 exons, and encodes three isoforms by alternative splicing. The longest isoform (NP\_082239.2) consists of 620 amino acids (aa) encoded by exons 1–14. The isoform denominated X1 (XP\_006534328.1) consists of 577 aa by skipping of exon 4. Isoform 203 (Q5F201) has a postulated length of 342 aa and is encoded by exons 1–8. We cloned the isoforms from NIH3T3 cells and generated in fusion plasmids to *Egfp*. Additionally, we generated another fusion protein named isoform X1-Nterm that consists of 309 aa of CFAP52 by skipping exons 4 and all C-terminal exons 9–14 (Fig. 8). According to ProSite (<https://prosite.expasy.org>) the full-length sequences CFAP52 and CFAP52-X1 contain two WD-repeats regions comprising aa 60–195, and 328–620 (related to the full-length isoform), and five WD-repeats-2. Referring to the full-length isoform, the WD-repeats-2 sequences comprise aa 107–142, 413–446, 457–490, 541–582, and 583–620. The isoform 203 contains one WD-repeat region and one WD-repeat-2, comprising aa 107–142. The WD-region of the isoform X1-Nterm differs from that of isoform 203 by a deletion of 43 aa (Fig. 8). To investigate the impact of the WD-domains for centrosomal recruitment of CFAP52 the *egfp*-fusion plasmids were transfected into NIH3T3 cells and the fusion proteins detected by their green auto-fluorescence (Fig. 9). The centrosome was decorated by immunostaining for their marker proteins either  $\gamma$ -tubulin or pericentrin. As observed previously for the full-length CFAP52::EGFP fusion protein (Fig. 7A) both, the EGFP-fusion proteins of isoform 203 as well as of the N-terminal end of isoform X1 (X1-Nterm), are concentrated in the centrosome (Fig. 9). Taken together, our data indicate that (1) the C-terminal region comprising the second WD-repeats domain is not essential for centrosomal recruitment and that (2) parts of the first WD-repeats domain encoded by exon 4 are also not essential for centrosomal recruitment. Thus, a centrosomal targeting sequence, if at all present, must reside in the N-terminal end of CFAP52, represented by isoform X1-Nterm, or most likely the WD-repeats domains taken as a whole are responsible to direct CFAP52 to the centrosome.

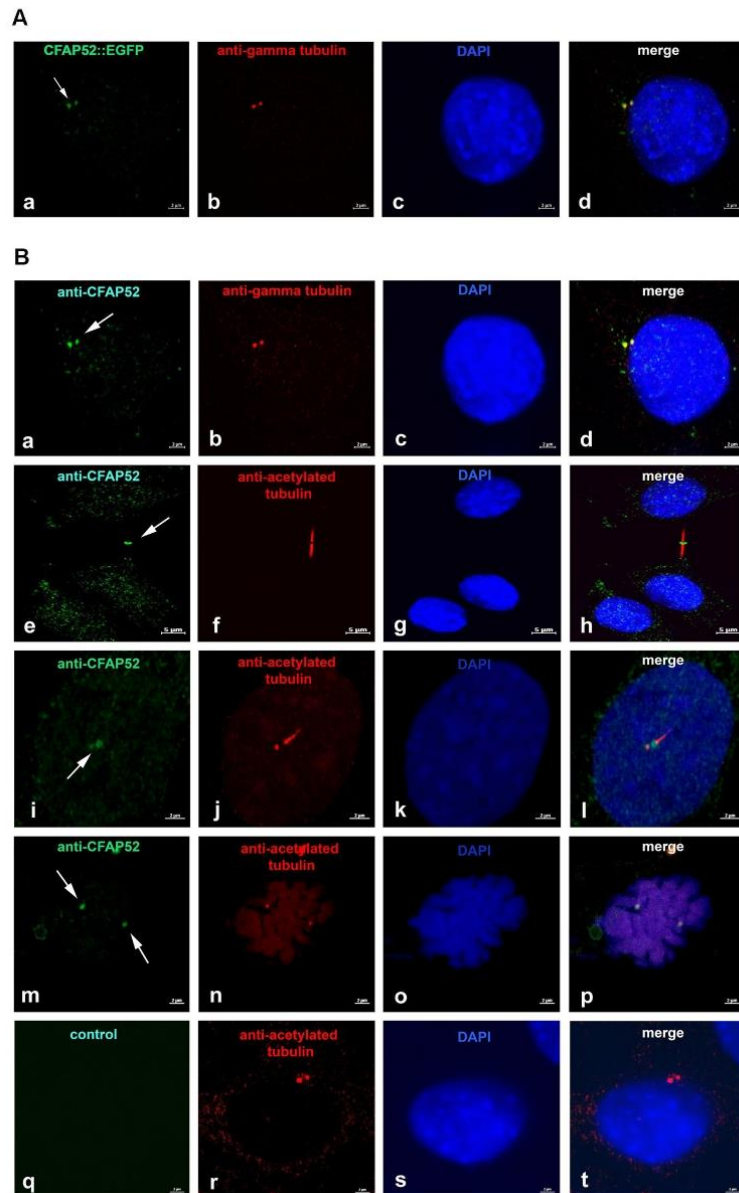


**Figure 7.** CFAP52 localizes to the centrosome, the basal body, the intercellular bridge, and the spindle poles in NIH3T3 cells. (A) The full-length *pCfap52::Egfp* expression plasmid was transfected into NIH3T3 cells and detected by auto-fluorescence (green) (a). Immuno-decoration of the centrosome with the centrosomal marker  $\gamma$ -tubulin (red) revealed localization of CFAP52 in the centrosome (b–d). Bars are of 2  $\mu\text{m}$ . (B) Endogenous expression of CFAP52 in NIH3T3 cells was detected by double immunostaining with anti-CFAP52 (green) and either anti- $\gamma$ -tubulin (red) or anti-acetylated tubulin (red).  $\gamma$ -tubulin and acetylated tubulin decoration for detection of the centrosome, acetylated tubulin for decoration of the basal body, the spindle poles, the intercellular bridge, and the primary cilium. The endogenous CFAP52 (arrows) localizes to the centrosome (a–d), the intercellular bridge (e–h), the basal body and its associated daughter centriole (i–l), and the spindle poles (m–p). Omitting anti-CFAP52 showed decoration of the centrosome by anti-acetylated tubulin staining (red) but no false CFAP52 staining (q–t). Nuclear counterstain with DAPI (blue). Bars are of 2  $\mu\text{m}$  except for (e–h), which are of 5  $\mu\text{m}$ .

CFAP52 (NP_082239.2)	MEEQVLPELDVAELELQAVIGFNHVPNGLKCHPDQEHLIYPLGCTVLIQAINTEQNF	60
CFAP52-X1 (XP_006534328.1)	MEEQVLPELDVAELELQAVIGFNHVPNGLKCHPDQEHLIYPLGCTVLIQAINTEQNF	60
CFAP52-203 (Q5F201)	MEEQVLPELDVAELELQAVIGFNHVPNGLKCHPDQEHLIYPLGCTVLIQAINTEQNF	60
CFAP52-X1-Nterm	MEEQVLPELDVAELELQAVIGFNHVPNGLKCHPDQEHLIYPLGCTVLIQAINTEQNF	60
CFAP52 (NP_082239.2)	HGHGNNVSCVTISKEGDYIASGQVTFMGFKADIILWDFKRELIARLSLHKGIKALAFS	120
CFAP52-X1 (XP_006534328.1)	HGHGNNVSCVTISKEGDYIASGQVTFMGFKADIILWDFKRELIARLSLHKGIKALAFS	120
CFAP52-203 (Q5F201)	HGHGNNVSCVTISKEGDYIASGQVTFMGFKADIILWDFKRELIARLSLHKGIKALAFS	120
CFAP52-X-Nterm	HGHGNNVSCVTISKEGDYIASGQVTFMGFKADIILWDFKRELIARLSLHKGIKALAFS	120
CFAP52 (NP_082239.2)	PNDLYLVSLGGPDDGSVVVWSIAKRDAICGSPAAGLNVGNATSVVFSRCRDEMFTAGNG	180
CFAP52-X1 (XP_006534328.1)	PNDLYLVSLGGPDDG-----SG	137
CFAP52-203 (Q5F201)	PNDLYLVSLGGPDDGSVVVWSIAKRDAICGSPAAGLNVGNATSVVFSRCRDEMFTAGNG	180
CFAP52-X1-Nterm	PNDLYLVSLGGPDDG-----SG	137
CFAP52 (NP_082239.2)	TIRVWELDLNPKKIWPTECQTGMKRIVLSTGMADDDSFYLGTTTGDILKMNPKTKLLA	240
CFAP52-X1 (XP_006534328.1)	TIRVWELDLNPKKIWPTECQTGMKRIVLSTGMADDDSFYLGTTTGDILKMNPKTKLLA	197
CFAP52-203 (Q5F201)	TIRVWELDLNPKKIWPTECQTGMKRIVLSTGMADDDSFYLGTTTGDILKMNPKTKLLA	240
CFAP52-X-Nterm	TIRVWELDLNPKKIWPTECQTGMKRIVLSTGMADDDSFYLGTTTGDILKMNPKTKLLA	197
CFAP52 (NP_082239.2)	DTGPVKDRFSLGVSALRCLKMGGLLVGSGAGLLIFCKSPSPYKPIKVVQLGGGITSITLRG	300
CFAP52-X1 (XP_006534328.1)	DTGPVKDRFSLGVSALRCLKMGGLLVGSGAGLLIFCKSPSPYKPIKVVQLGGGITSITLRG	257
CFAP52-203 (Q5F201)	DTGPVKDRFSLGVSALRCLKMGGLLVGSGAGLLIFCKSPSPYKPIKVVQLGGGITSITLRG	300
CFAP52-X1-Nterm	DTGPVKDRFSLGVSALRCLKMGGLLVGSGAGLLIFCKSPSPYKPIKVVQLGGGITSITLRG	257
CFAP52 (NP_082239.2)	EGHQFFVGTTEESHYIRVNFDFKTELIATCFEAVQDIVFFPGTAELEFATCARCKDIRVWH	360
CFAP52-X1 (XP_006534328.1)	EGHQFFVGTTEESHYIRVNFDFKTELIATCFEAVQDIVFFPGTAELEFATCARCKDIRVWH	317
CFAP52-203 (Q5F201)	EGHQFFVGTTEESHYIRVNFDFKTELIATCFEAVQDIVFFPL-----	342
CFAP52-X1-Nterm	EGHQFFVGTTEESHYIRVNFDFKTELIATCFEAVQDIVFFLVPRARDPEVA-----	309
CFAP52 (NP_082239.2)	TMSKRELLRITVPMNTCHGIDFMRDGRSIIISAWDDGKIRAFAPESGRMLYTIMSAHRIIV	420
CFAP52-X1 (XP_006534328.1)	TMSKRELLRITVPMNTCHGIDFMRDGRSIIISAWDDGKIRAFAPESGRMLYTIMSAHRIIV	377
CFAP52-203 (Q5F201)	-----	342
CFAP52-X1-Nterm	-----	309
CFAP52 (NP_082239.2)	TALATTSDCRKRIISGGGEGEVRVWQVGCQTKLEALREHKSSVSCIRVKKNEECVTAS	480
CFAP52-X1 (XP_006534328.1)	TALATTSDCRKRIISGGGEGEVRVWQVGCQTKLEALREHKSSVSCIRVKKNEECVTAS	437
CFAP52-203 (Q5F201)	-----	342
CFAP52-X1-Nterm	-----	309
CFAP52 (NP_082239.2)	TDGTCI IWDLVRLRRNQMI LANTLFQCVCYHPPEFQI IITSGTDRKIAYWEVFDGVSIREL	540
CFAP52-X1 (XP_006534328.1)	TDGTCI IWDLVRLRRNQMI LANTLFQCVCYHPPEFQI IITSGTDRKIAYWEVFDGVSIREL	497
CFAP52-203 (Q5F201)	-----	342
CFAP52-X1-Nterm	-----	309
CFAP52 (NP_082239.2)	EGSLSGSINGMDITQEGGHFVTGGHDHLVKVVDYNEGEVTHVGVGHSGNIMAMRISPGNQ	600
isoformX1 (XP_006534328.1)	EGSLSGSINGMDITQEGGHFVTGGHDHLVKVVDYNEGEVTHVGVGHSGNIMAMRISPGNQ	557
CFAP52-203 (Q5F201)	-----	342
CFAP52-X1-Nterm	-----	309
CFAP52 (NP_082239.2)	YIVSVSADGAILRWKYPPAS	620
CFAP52-X1 (XP_006534328.1)	YIVSVSADGAILRWKYPPAS	577
CFAP52-203 (Q5F201)	-----	342
CFAP52-X1-Nterm	-----	309

**Figure 8.** CFAP52 isoforms. *Wdr16/Cfap52* encodes three isoforms by alternative splicing. The full-length isoform CFAP52 (NP\_082239.2) consists of 620 amino acids. The isoform denominated CFAP52-X1 (XP\_006534328.1) consists of 577 amino acids, and the isoform CFAP52-203 (Q5F201) has a postulated length of 342 amino acids. The sequence denominated CFAP52-X1-Nterm is the N-terminal end of isoform X1 consisting of 309 aa and was artificially cloned. The WD40 repeats regions (according to Prosite circular profile) comprise aa 60 to 195 and 328 to 620 (enframed in red). The WD40 repeats (according to Prosite WD-repeats-2) are colour-coded.

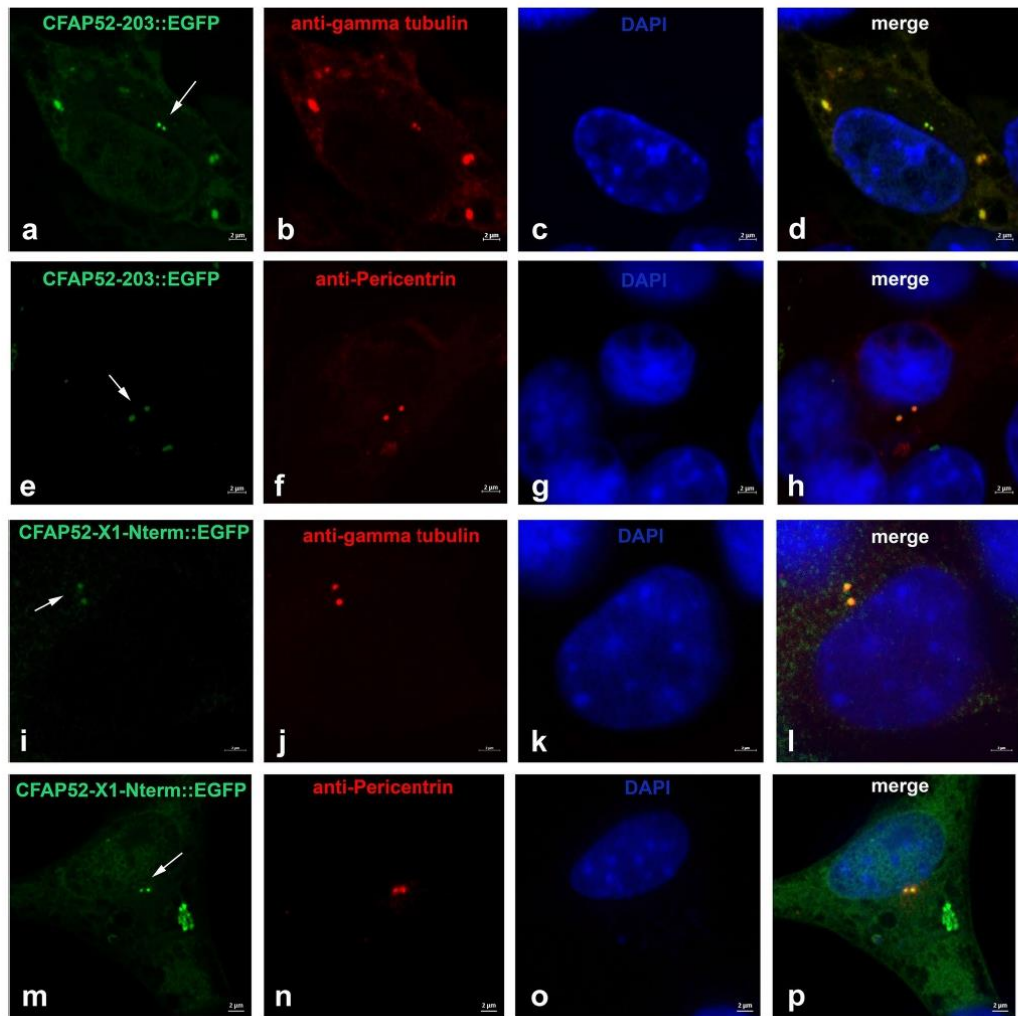


**Figure 9.** Centrosomal location of EGFP-fusion proteins of CFAP52 isoforms 203 (CFAP52-203::EGFP) and the N-terminal end of isoform X1 (CFAP52-X1-Nterm::EGFP). Expression plasmids for the isoform 203, *pCfap52-203::Egfp* (a–h), and the N-terminal sequence of CFAP52-isoform-X1, *pCfap52-X1-Nterm::Egfp* (i–p) were transfected into NIH3T3 cells and detected by the EGFP auto-fluorescence (green, a, e, i, m). Decoration of the centrosomes by immunostaining for the centrosomal marker proteins either  $\gamma$ -tubulin (anti-gamma-tubulin, b, j) or Pericentrin (anti-Pericentrin, f, n) (both in red). Nuclear counterstain with DAPI (blue). Arrows pointing to the centrosomal location of the fusion proteins. Bars are of 2  $\mu$ m (a–p).

### Discussion

WDR16/CFAP52 is a member of the WD40-protein family characterized by the WD-repeat domain. The WD40-repeats, also known as GH-WD repeats, are repetitive motifs consisting of a conserved core bracketed by GH (Gly-His) and WD, and additional sequences of variable lengths<sup>1,38</sup>.

The WD40-domains were first described in  $\beta$  subunits of transducin and other G proteins isolated from bovine tissues, and in the SCF (SKP1-CUL1-F-box protein) ubiquitin ligase complex component CDC4. WD-repeat proteins fulfill diverse biological functions including RNA synthesis/processing, signal transduction, cytoskeleton assembly, mitotic spindle formation, vesicular trafficking and cell growth<sup>6,39</sup>. WD-repeat domains are hence widespread and highly conserved in eukaryotes. Particularly, the WD40-repeat protein CFAP52/WDR16/WDRPUH was initially identified and found to be upregulated in human hepatocellular carcinomas.



Its overexpression in NIH3T3 cells accelerated cell growth, whereas inhibition of WDR16/CFAP52 reduced the growth of human liver carcinoma cells and induced apoptosis<sup>3,7</sup>.

Previous investigation of *Cfap52* indicated that its expression correlated with the presence of motile cilia<sup>7</sup>. Furthermore, WDR16/CFAP52 was annotated in the Ciliome Database and was identified in mouse ciliated tissues<sup>40</sup>. Moreover, the *Wdr16* gene was identified as FOXJ effector gene altogether indicating a correlation of WDR16/CFAP52 with ciliation especially with the generation of motile cilia<sup>41</sup>. Proteins containing specific domains, especially coiled-coil domains, WD40-repeat domains, or tetratricopeptide repeat domains have all been linked to cilia<sup>40,42,43</sup>. In this regard, the intraflagellar transport component IFTA-1 is a WD repeat-containing protein<sup>44</sup>. However, WDR16/CFAP52 is not annotated in Syscilia Gold Standard (<https://www.syscilia.org/goldstandard.shtml>) and therefore seems not to be an essential ciliary component.

The reported association of the cilia and flagella associated protein 52 (CFAP52/WDR16) with ciliation and its high expression in testis offered the unique opportunity to investigate its sub-cellular distribution in more detail. The formation of the flagellum starts in haploid spermatids and is well known step-by-step from the migration of the paired centrioles towards the caudal end of the nucleus, their insertion into the implantation fossa, and their progressive transformation into the basal body, the connecting piece, and eventually the outgrowth of the flagellum. The proximal centriole inserts into the implantation fossa and mediates the proper linkage between head and tail by the head-to-tail coupling apparatus (HTCA). The distal centriole, on the other hand, gives rise to the basal body that in turn will seed flagellum formation<sup>10,45</sup>. Furthermore, flagellum and connecting piece are both discernable at light-microscopic resolution and are easily identifiable using immuno-decoration.

Formation of HTCA and sperm tail requires many proteins that are presumably transported by a transient microtubular structure, the manchette<sup>24,27</sup>. The HTCA is essential for functional sperm, and its malformation causes acephalic spermatozoa and male infertility due to fragile attachment of sperm head and tail or even detachment<sup>12,46</sup>. Albeit essential for fertilisation, the knowledge of the molecular composition of the HTCA is just in the beginning. We therefore asked, whether CFAP52 as an annotated ciliary component is associated with the flagellum or its development. We found that, opposed to previous reports, CFAP52 localises to the transient manchette in round and elongating spermatids. CFAP52 might thus be involved in the stabilization of the structure or in supporting delivery of cargos, or is a cargo protein itself. Later on, CFAP52 was found in the sperm tail with the strongest staining in the principal piece. A weaker decoration was observed in the middle piece that might be explained by a reduced antibody accessibility due to the fact that mitochondria and outer dense fibres encapsulate the central region of the axoneme. Although, location of CFAP52 to manchette microtubules and sperm tail resembles that of the major outer dense fibre protein ODF1, recruitment of CFAP52 to these structures is independent of ODF1.

Expression analyses of *Cfap52* by RT-PCR, notably nested RT-PCR, revealed transcription in all tissues investigated including those that do not harbour motile cilia, e.g. ovary. Additionally, *Cfap52* was also expressed in the fibroblast cell line NIH3T3. *Cfap52* cDNAs were isolated from NIH3T3 cells and cloned in frame to *egfp* to generate EGFP-fusion proteins when ectopically expressed. Investigations of the subcellular distributions of CFAP52::EGFP-fusion proteins as well as of the endogenous CFAP52 protein demonstrated location of CFAP52 in the centrosome, the mitotic spindle poles, the tip of the mid-bodies, and at the base of primary cilia. However, the primary cilium axoneme was not decorated by CFAP52. We observed centrosomal location of full-length CFAP52 and its isoforms including its N-terminal part comprising a single truncated WD40-domain. We propose that centrosomal recruitment most likely is mediated by the WD40-domain that generally functions in mediating protein-protein interactions<sup>9</sup>.

Our data indicate, that CFAP52 associates with a subset of microtubular structures, especially centrosome/centriole derived structures. As WD-repeat proteins mediate protein interactions, CFAP52 might likewise act in assembly or stabilization of protein complexes constituting the centrosomal/basal body matrix and the sperm tail<sup>6</sup>. Furthermore, the location of CFAP52 to the sperm tail but not to the axoneme of primary cilia suggests that CFAP52 fulfils specific functions related to the stability, maintenance, or motility of the sperm tail. A loss-of-function of CFAP52 might therefore primarily affect the sperm tail and in turn male fertility. It is currently not known whether mutations in CFAP52 affect male fertility although mutations in WD-repeat proteins, as e.g. in WDR66/CFAP251, WDR96/CFAP43, and WDR52/CFAP54, causing human male infertility due to the sperm flagella defects have been reported<sup>17–19</sup>. Knock down or mutation studies of CFAP52 in zebrafish and humans, respectively, indicated impaired motile cilia in the ependym causing hydrocephalus, and impaired motile, solitary cilia in the node causing left-right symmetry disorders<sup>7,8</sup>. However, it has not been investigated whether primary cilia and the sperm tail are also affected, causing ciliopathies and male infertility due to sperm motility disorders, respectively. We anticipate our results to be a starting point for a more sophisticated analysis of the role CFAP52 plays in the formation of centrosome-derived structures and in male germ cells using knock out approaches.

## Materials and methods

**cDNA synthesis and RT-PCR.** Total RNA from adult mouse tissues (testis, liver, brain, ovary, kidney, spleen, epididymides) as well as from NIH3T3 mouse fibroblasts was prepared using peqGOLD RNAPure™ (PeqLab, Erlangen, Germany) following the recommendations of the manufacturer. Total RNA was digested with Ambion® TURBO DNA-free™ DNase (Life Technologies). cDNA was synthesized using Maxima First Strand cDNA Synthesis (ThermoFisher Scientific)<sup>31</sup>. Detection of transcribed sequences was performed by RT-PCR using the following primer pairs: CFAP52-NheI-X1-For (GCTAGCATGGAAGAACAAGTTTACC) and CFAP52-X1-BamHI-R (GGATCCGAAGCAAATGGTATTTC) generating a product of 1871 bp. After first PCR, the following primers were used to perform a nested PCR: CFAP52-For (CCAGCGTGGTCTCTCTA GG) and CFAP52-Rev (CCTTCACAGGCCAGTATC) generating a fragment of 255 bp. Gaphd was amplified

using Gapdh-For (GTATGACTCCACTCAGGCA) and Gapdh-Rev (GTCAGATCCACGACGGACAC) generating a fragment of 594 bp. PCR products were sequenced.

**Plasmid constructs.** Four different *Cfap52* coding sequences were amplified by PCR. *Cfap52* full-length (NP\_082239.2) and *Cfap52* isoform X1 (XP\_006534328.1) were amplified using the primer pair CFAP52-NheI-X1-For (5'-GCTAGCATGGAAGAACAAGTTTACC-3') and CT-CFAP52-X1-BamHI-R (5'-GGATCCGAA GCAAATGGGTATTTC-3'). The isoform *Cfap52-203* (Q5F201) and the N-terminal region of the isoform X1 were amplified using the following primer pair: CFAP52-NheI-For (5'-GCTAGCCATGGAAACAAGTTTAC-3') and CFAP52-KpnI-203-Rev (5'-GGTACCAATGGAAAGACAATGTCCTGG-3'). PCR products were cloned into *pJET1.2/blunt* (ThermoFisher Scientific) followed by NheI/BamHI or NheI/KpnI digestion and sub-cloning into *pEGFP-N1* (Clontech Lab., #U55762). Correct reading frames were confirmed by sequencing.

**Cell culture and immunocytochemistry.** NIH3T3 cells (ATCC CRL-1658) were maintained in Dulbecco's Modified Eagle's Medium (DMEM), 10% (v/v) fetal bovine serum (FBS), 1000 U/ml penicillin, 1000 µg/ml streptomycin, and 20 mM L-Glutamine (all Gibco) at 37 °C and 5% CO<sub>2</sub>. NIH3T3 cells were grown on glass coverslips in 6-well plates and the plasmid DNA was transfected using EndoFectin™ Max Transfection Reagent, using the manufacturer's instructions (GeneCopoeia). Twenty-four hours post transfection, cells were rinsed with phosphate-buffered saline (PBS) and fixed either in methanol for 10 min at -20 °C or in 3.7% paraformaldehyde (PFA) for 20 min at 4 °C. Samples were then permeabilized with 0.3% Triton X-100 in PBS for 10 min at room temperature. Cells were rinsed in PBS, and non-specific binding sites were blocked by incubation in PBS containing 1% BSA and 0.3% Triton X-100 for 1 h<sup>31</sup>. Samples were incubated with primary antibodies: anti-CFAP52 (CSB-PA839781LA01HU; Wuhan Huamei Biotech Co., Ltd., Wuhan, China, Cusabio), anti-Pericentrin (PRB432C, Covance), anti-acetylated tubulin (6-11B-1; Sigma-Aldrich), anti-γ tubulin (GTU-88, Sigma-Aldrich) at 37 °C for 1 h. Secondary antibodies used are goat anti-mouse-IgG DyLight 488 (#35503, ThermoScientific), and goat anti-rabbit-MFP590 (#MFP-A1037, Mobitec). DNA was counterstained with DAPI. Images were taken by confocal microscopy (LSM 780, Zeiss) and processed using Adobe Photoshop 7.0.

**Immunocytology on testicular cell suspensions.** Fresh testes from laboratory mice of strain C57/Bl6 were minced in PBS containing 2% paraformaldehyde, 0.02% SDS, and 0.15% Triton X-100, and transferred onto superfrost slides. Cells were blocked for 1 h in PBS containing 1% BSA and 0.3% Triton X-100. Anti-CFAP52 (CSB-PA839781LA01HU; Wuhan Huamei Biotech Co., Ltd., Wuhan, China, Cusabio) was used as 1:100 dilution and incubated at 4 °C overnight. CFAP52 was detected using the secondary antibody goat anti-rabbit-IgG (H+L) Alexa Fluor R 555 (F[ab]2 fragment; #A21430, Life Technologies) used as 1:1,000 dilution. Additionally, the following first antibodies were used: anti-α-tubulin (DM1A, Calbiochem, #CP06), anti-γ-tubulin (GTU-88, Sigma-Aldrich, #T6557), anti-EB3 (EB3(7), Santa Cruz, sc-136405), anti-SUN3 and anti-SUN4<sup>36,50</sup>, and detected using goat anti-mouse-IgG DyLight488 (Thermo Scientific, #35503) or goat anti-guinea pig-IgG Alexa Fluor 488 (Life Technologies, #A11073). DNA was counterstained with DAPI (4',6-Diamidino-2-phenylindole; Sigma D-9542), and the acrosome was decorated with FITC-labelled peanut lectin (PL-FITC). Images were taken by confocal microscopy (LSM 510, Zeiss) and processed using Adobe Photoshop 7.0.

**Histology.** Testes were fixed in 4% paraformaldehyde in phosphate-buffered saline (145 mM NaCl, 7 mM Na<sub>2</sub>HPO<sub>4</sub>, and 3 mM NaH<sub>2</sub>PO<sub>4</sub>; PBS) and embedded in paraffin. 4 µm sections were cut and placed onto Superfrost slides. After deparaffinization and rehydration probes were treated for enzymatic epitope retrieval by incubation with 0.5% Trypsin for 10–20 min at 37 °C. Specimen were blocked in PBS containing 1% BSA and 0.3% Triton X-100 followed by antibody incubation with rabbit anti-CFAP52 (CSB-PA839781LA01HU) at 4 °C overnight. Anti-CFAP52 was detected with goat anti-rabbit-MFP590 (#MFP-A1037, Mobitec) (diluted 1:100). The acrosome was stained with FITC-labelled peanut-lectin (PL-FITC) and the DNA by DAPI (4', 6-Diamidino-2-phenylindole; Sigma D-9542).

**Western blotting.** Proteins were prepared from mice tissues (testes, brain, liver, kidney) and NIH3T3 cells. Tissues were homogenized with a Dounce homogenizer in lysis buffer [150 mM NaCl, 1% Nonidet P40, 0.5% sodium deoxycholate, 0.1% SDS, 50 mM Tris-HCl, pH 7.6, protease inhibitor cocktail (Halt Protease Inhibitor Cocktail 100X, Thermo Fisher Scientific, #78438)]. NIH3T3 cells were harvested by trypsinization followed by rinsing twice in phosphate-buffered saline (PBS). NIH3T3 cell pellet was resuspended in lysis buffer. Protein lysates were sonicated 3 times for 45 s each. Total protein lysates were resuspended in 2×SDS-sample buffer and heated to 95 °C for 10 min. Proteins were separated on SDS-PAGE and transferred onto nitrocellulose membrane (Amersham Hybond-ECL, GE Healthcare)<sup>51,52</sup>. The membrane was blocked in 5% dry milk in TBST (10 mM Tris-HCl pH 7.6, 150 mM NaCl, 0.05% Tween20) for one hour. Afterwards, the membrane was incubated with the primary antibody rabbit anti-CFAP52 (CSB-PA839781LA01HU) in blocking solution at 4 °C overnight. First antibodies were detected by incubation with HRP-conjugated secondary antibody goat anti-rabbit IgG (Jackson ImmunoResearch, West Grove, PA, USA). Signals were detected using ClarityMax Western ECL Substrate (Bio-Rad, #1705062) and images were captured with Chemdoc (Bio-Rad).

**Ethics statement.** All mouse experiments were reviewed and approved by the animal welfare commission of the University Medical Faculty and Niedersächsisches Landesamt für Verbraucherschutz und Lebensmittelsicherheit. Licence for animal experiments has been obtained by the Institute of Human Genetics. The guidelines

of the German Animal Welfare Act (German Ministry of Agriculture, Health and Economic Cooperation) were strictly followed in all aspects of mouse work. *Odf1*-ko mice has been previously described<sup>28</sup>.

### Data availability

All data generated or analysed during this study are included in this published article.

Received: 6 May 2020; Accepted: 7 August 2020

Published online: 28 August 2020

### References

1. Neer, E. J., Schmidt, C. J., Nambudripad, R. & Smith, T. F. The ancient regulatory-protein family of WD-repeat proteins. *Nature* **371**, 297–300. <https://doi.org/10.1038/371297a0> (1994).
2. Smith, T. F., Gaitatzes, C., Saxena, K. & Neer, E. J. The WD repeat: a common architecture for diverse functions. *Trends Biochem. Sci.* **24**, 181–185. [https://doi.org/10.1016/s0968-0004\(99\)01384-5](https://doi.org/10.1016/s0968-0004(99)01384-5) (1999).
3. Silva, F. P., Hamamoto, R., Nakamura, Y. & Furukawa, Y. WDRPUH, A Novel WD-repeat—containing protein, is highly expressed in human hepatocellular carcinoma and involved in cell proliferation. *Neoplasia* **7**, 348–355. <https://doi.org/10.1593/neo.04544> (2005).
4. Smith, T. F. Diversity of WD-repeat proteins. *Subcell. Biochem.* **48**, 20–30 (2008).
5. Atlas of Genetics and Cytogenetics in Oncology and Haematology [https://atlasgeneticsoncology.org/Genes/GC\\_CFAP52.html](https://atlasgeneticsoncology.org/Genes/GC_CFAP52.html)
6. Li, D. & Roberts, R. Human genome and diseases: review WD-repeat proteins: structure characteristics, biological function, and their involvement in human diseases. *CMLS Cell. Mol. Life Sci.* **58**, 2085–2097. <https://doi.org/10.1007/PL00000838> (2001).
7. Hirschner, W. *et al.* Biosynthesis of Wdr16, a marker protein for kinocilia-bearing cells, starts at the time of kinocilia formation in rat, and wdr16 gene knockdown causes hydrocephalus in zebrafish. *J. Neurochem.* **101**, 274–288. <https://doi.org/10.1111/j.1471-4159.2007.04500.x> (2007).
8. Ta-Shma, A. *et al.* A human laterality disorder associated with a homozygous WDR16 deletion. *Eur. J. Hum. Genet.* **23**, 1262–1265 (2015).
9. Owa, M. *et al.* Inner lumen proteins stabilize doublet microtubules in cilia and flagella. *Nat. Commun.* **10**, 1143. <https://doi.org/10.1038/s41467-019-2014-265> (2019).
10. Fawcett, D. W. The mammalian spermatozoon. *Dev. Biol.* **44**, 394–436. [https://doi.org/10.1016/0012-1606\(75\)90411-x](https://doi.org/10.1016/0012-1606(75)90411-x) (1975).
11. Russell, L. D., Russell, J. A., MacGregor, G. R. & Meistrich, M. L. Linkage of manchette microtubules to the nuclear envelope and observations of the role of the manchette in nuclear shaping during spermiogenesis in rodents. *Am. J. Anat.* **192**, 97–120. <https://doi.org/10.1002/aja.1001920202> (1991).
12. Chemes, H. E. Sperm centrioles and their dual role in flagellogenesis and cell cycle of the zygote. *Centrosome* [https://doi.org/10.1007/978-1-62703-035-9\\_2](https://doi.org/10.1007/978-1-62703-035-9_2) (2012).
13. Chemes, H. E. & Rawe, V. Y. The making of abnormal spermatozoa: cellular and molecular mechanisms underlying pathological spermiogenesis. *Cell Tissue Res.* **341**, 349–357. <https://doi.org/10.1007/s00441-010-1007-3> (2010).
14. Hoyer-Fender, S. Centrosomes in fertilization, early embryonic development, stem cell division, and cancer. *Atlas Genet. Cytogen. Oncol. Haematol.* **16**, 306–319. <https://doi.org/10.4267/2042/47311> (2012).
15. Baltz, J. M., Oneeka Williams, P. & Cone, R. A. Dense fibers protect mammalian sperm against damage. *Biol. Reprod.* **43**, 485–491. <https://doi.org/10.1095/biolreprod43.3.485> (1990).
16. Lindemann, C. B. Functional significance of the outer dense fibers of mammalian sperm examined by computer simulations with the geometric clutch model. *Cell Motil. Cytoskelet.* **34**, 258–270. [https://doi.org/10.1002/\(SICI\)1097-0169\(1996\)34:4%3c258::AID-CM1%3e3.0.CO;2-4](https://doi.org/10.1002/(SICI)1097-0169(1996)34:4%3c258::AID-CM1%3e3.0.CO;2-4) (1996).
17. Rattner, J. B. & Olson, G. Observations on the fine structure of the nuclear ring of the mammalian spermatid. *J. Ultrastruct. Res.* **43**, 438–444. [https://doi.org/10.1016/S0022-5320\(73\)90020-8](https://doi.org/10.1016/S0022-5320(73)90020-8) (1973).
18. Kierszenbaum, A. L., Rivkin, E. & Tres, L. L. Acroplaxome, an F-actin–keratin-containing plate, anchors the acrosome to the nucleus during shaping of the spermatid head. *Mol. Biol. Cell* **14**, 4628–4640. <https://doi.org/10.1091/mbc.e03-04-0226> (2003).
19. Rattner, J. B. & Brinkley, B. R. Ultrastructure of mammalian spermiogenesis. *J. Ultrastruct. Res.* **41**, 209–218. [https://doi.org/10.1016/s0022-5320\(72\)90065-2](https://doi.org/10.1016/s0022-5320(72)90065-2) (1972).
20. Kierszenbaum, A. L., Rivkin, E. & Tres, L. L. Cytoskeletal track selection during cargo transport in spermatids is relevant to male fertility. *Spermatogenesis* **1**, 221–230. <https://doi.org/10.4161/spmg.1.3.18018> (2011).
21. Yan, W. Male infertility caused by spermiogenic defects: lessons from gene knockouts. *Mol. Cell. Endocrinol.* **306**, 24–32. <https://doi.org/10.1016/j.mce.2009.03.003> (2009).
22. Chen, S. R. *et al.* The control of male fertility by spermatid-specific factors: Searching for contraceptive targets from spermatozoon's head to tail. *Cell Death Dis.* **7**, e2472–e2472. <https://doi.org/10.1038/cddis.2016.344> (2016).
23. Lehti, M. S. & Sironen, A. Formation and function of the manchette and flagellum during spermatogenesis. *Reproduction* **151**, R43–R54. <https://doi.org/10.1530/REP-15-0310> (2016).
24. Cole, A., Meistrich, M. L., Cherry, L. M. & Trostle-Weige, P. K. Nuclear and manchette development in spermatids of normal and *azh/azh* mutant mice. *Biol. Reprod.* **38**, 385–401. <https://doi.org/10.1095/biolreprod38.2.385> (1988).
25. Meistrich, M. L., Trostle-Weige, P. K. & Russell, L. D. Abnormal manchette development in spermatids of *azh/azh* mutant mice. *Am. J. Anat.* **188**, 74–86. <https://doi.org/10.1002/aja.1001880109> (1990).
26. Mendoza-Lujambio, I. *et al.* The Hook1 gene is non-functional in the abnormal spermatozoon head shape (*azh*) mutant mouse. *Hum. Mol. Genet.* **11**, 1647–1658. <https://doi.org/10.1093/hmg/11.14.1647> (2002).
27. Kierszenbaum, A. L. & Tres, L. L. The acrosome-acroplaxome-manchette complex and the shaping of the spermatid head. *Arch. Histol. Cytol.* **67**, 271–284. <https://doi.org/10.1679/aohc.67.271> (2004).
28. Yang, K. *et al.* The small heat shock protein ODF1/HSPB10 is essential for tight linkage of sperm head to tail and male fertility in mice. *Mol. Cell. Biol.* **32**, 216–225. <https://doi.org/10.1128/MCB.06158-11> (2012).
29. Yang, K., Grzmil, P., Meinhardt, A. & Hoyer-Fender, S. Haplo-deficiency of ODF1/HSPB10 in mouse sperm causes relaxation of head-to-tail linkage. *Reproduction* **148**, 499–506. <https://doi.org/10.1530/REP-14-0370> (2014).
30. Shang, Y. *et al.* Essential role for SUN5 in anchoring sperm head to the tail. *Elife* **6**, e28199. <https://doi.org/10.7554/eLife.28199> (2017).
31. Tapia Contreras, C. & Hoyer-Fender, S. CCDC42 localizes to manchette, HTCA and tail and interacts with ODF1 and ODF2 in the formation of the male germ cell cytoskeleton. *Front. Cell Dev. Biol.* **7**, 151. <https://doi.org/10.3389/fcell.2019.00151> (2019).
32. Starr, D. A. KASH and SUN proteins. *Curr. Biol.* **21**, R414–R415. <https://doi.org/10.1016/j.cub.2011.04.022> (2011).
33. Shao, X., Tarnasky, H. A., Lee, J. P., Oko, R. & van der Hoorn, F. A. Spag4, a novel sperm protein, binds outer dense-fiber protein Odf1 and localizes to microtubules of manchette and axoneme. *Dev. Biol.* **211**, 109–123. <https://doi.org/10.1006/dbio.1999.9297> (1999).
34. Shao, X., Xue, J. & van der Hoorn, F. A. Testicular protein Spag5 has similarity to mitotic spindle protein deepest and binds outer dense fiber protein Odf1. *Mol. Reprod. Dev.* **59**, 410–416. <https://doi.org/10.1002/mrd.1047> (2001).

35. Calvi, A. *et al.* SUN4 is essential for nuclear remodeling during mammalian spermiogenesis. *Dev. Biol.* **407**, 321–330. <https://doi.org/10.1016/j.ydbio.2015.09.010> (2015).
36. Pasch, E., Link, J., Beck, C., Scheuerle, S. & Alsheimer, M. The LINC complex component Sun4 plays a crucial role in sperm head formation and fertility. *Biol. Open* **4**, 1792–1802. <https://doi.org/10.1242/bio.015768> (2015).
37. Yang, K., Adham, I. M., Meinhardt, A. & Hoyer-Fender, S. Ultra-structure of the sperm head-to-tail linkage complex in the absence of the spermatid-specific LINC component SPAG4. *Histochem. Cell Biol.* **150**, 49–59. <https://doi.org/10.1007/s00418-018-1668-7> (2018).
38. Garcia-Higuera, I. *et al.* Folding of proteins with WD-repeats: comparison of six members of the WD-repeat superfamily to the G protein  $\beta$  subunit. *Biochemistry* **35**, 13985–13994. <https://doi.org/10.1021/bi9612879> (1996).
39. Fong, H. K. W., Hurley, J. B., Doolittle, R. F. & Simon, M. I. Repetitive segmental structure of the transducin Beta subunit: homology with the CDC4 gene and identification of related mRNAs. *Proc. Natl. Acad. Sci. USA* **83**, 2162–2166. <https://doi.org/10.1073/pnas.83.7.2162> (1986).
40. McClintock, T. S., Glasser, C. E., Bose, S. C. & Bergman, D. A. Tissue expression patterns identify mouse cilia genes. *Physiol. Genom.* **32**, 198–206. <https://doi.org/10.1152/physiolgenomics.00128.2007> (2008).
41. Stauber, M. *et al.* Identification of FOXJ1 effectors during ciliogenesis in the foetal respiratory epithelium and embryonic left–right organiser of the mouse. *Dev. Biol.* **423**, 170–188. <https://doi.org/10.1016/j.ydbio.2016.11.019> (2017).
42. Burkhard, P., Stetefeld, J. & Strelkov, S. V. Coiled coils: a highly versatile protein folding motif. *Trends Cell Biol.* **11**, 82–88. [https://doi.org/10.1016/s0962-8924\(00\)01898-5](https://doi.org/10.1016/s0962-8924(00)01898-5) (2001).
43. Pazour, G. J., Agrin, N., Leszyk, J. & Witman, G. B. Proteomic analysis of a eukaryotic cilium. *J. Cell Biol.* **170**, 103–113. <https://doi.org/10.1083/jcb.200504008> (2005).
44. Blacque, O. E. *et al.* The WD repeat-containing protein IFTA-1 is required for retrograde intraflagellar transport. *Mol. Biol. Cell* **17**, 5053–5062. <https://doi.org/10.1091/mbc.E06-06-0571> (2006).
45. Fawcett, D. W. & Phillips, D. M. The fine structure and development of the neck region of the mammalian spermatozoon. *Anat. Rec.* **165**, 153–183. <https://doi.org/10.1002/ar.1091650204> (1969).
46. Chemes, H., Carizza, C. & Scarinci, F. Lack of a head in human spermatozoa from sterile patients: a syndrome associated with impaired fertilization. *Int. J. Gynecol. Obstet.* **26**, 165–165. [https://doi.org/10.1016/s0015-0282\(16\)50011-9](https://doi.org/10.1016/s0015-0282(16)50011-9) (1988).
47. Tang, S. *et al.* Biallelic mutations in CFAP43 and CFAP44 cause male infertility with multiple morphological abnormalities of the sperm flagella. *Am. J. Hum. Genet.* **100**, 854–864. <https://doi.org/10.1016/j.ajhg.2017.04.012> (2017).
48. Coutton, C. *et al.* Mutations in CFAP43 and CFAP44 cause male infertility and flagellum defects in trypanosoma and human. *Nat. Commun.* **9**, 686. <https://doi.org/10.1038/s41467-017-02792-7> (2018).
49. Kherraf, Z. E. *et al.* Homozygous ancestral SVA-insertion-mediated Deletion in WDR66 induces multiple morphological abnormalities of the sperm flagellum and male infertility. *Am. J. Hum. Genet.* **103**, 400–412. <https://doi.org/10.1016/j.ajhg.2018.07.014> (2018).
50. Göb, E., Schmitt, J., Benavente, R. & Alsheimer, M. Mammalian sperm head formation involves different polarization of two novel LINC complexes. *PLoS ONE* **5**(8), e12072. <https://doi.org/10.1371/journal.pone.0012072> (2010).
51. Laemmli, U. K. Cleavage of structural proteins during the assembly of the head of bacteriophage T4. *Nature* **227**, 680–685. <https://doi.org/10.1038/227680a0> (1970).
52. Towbin, H., Staehelin, T. & Gordon, J. Electrophoretic transfer of proteins from polyacrylamide gels to nitrocellulose sheets: procedure and some applications. *Proc. Natl. Acad. Sci. U. S. A.* **76**, 4350–4354. <https://doi.org/10.1073/pnas.76.9.4350> (1979).

### Acknowledgments

We thank Manfred Alsheimer, Würzburg, for the kind gift of antibodies. CTC is supported by grants from DAAD/CONICYT BECAS Chile program and Department of Developmental Biology, GZMB, Georg-August-Universität Göttingen, Germany.

### Author contributions

Conceived and designed experiments: S.H.-F. Performed experiments: C.T.C. Prepared figures and wrote the manuscript: S.H.-F. and C.T.C. Both authors read and approved the final manuscript.

### Funding

Open Access funding provided by Projekt DEAL.

### Competing interests

The authors declare no competing interests.


### Additional information

Supplementary information is available for this paper at <https://doi.org/10.1038/s41598-020-71120-9>.

Correspondence and requests for materials should be addressed to S.H.-F.

Reprints and permissions information is available at [www.nature.com/reprints](http://www.nature.com/reprints).

**Publisher's note** Springer Nature remains neutral with regard to jurisdictional claims in published maps and institutional affiliations.

 **Open Access** This article is licensed under a Creative Commons Attribution 4.0 International License, which permits use, sharing, adaptation, distribution and reproduction in any medium or format, as long as you give appropriate credit to the original author(s) and the source, provide a link to the Creative Commons license, and indicate if changes were made. The images or other third party material in this article are included in the article's Creative Commons license, unless indicated otherwise in a credit line to the material. If material is not included in the article's Creative Commons license and your intended use is not permitted by statutory regulation or exceeds the permitted use, you will need to obtain permission directly from the copyright holder. To view a copy of this license, visit <http://creativecommons.org/licenses/by/4.0/>.

© The Author(s) 2020

## 4 Discussion

### 4.1 Relevance and impact of mutations of candidate genes involved in the linkage of sperm tail to its head

Infertility has been defined by the International Committee for Monitoring Assisted Reproductive Technology, World Health Organization (WHO), as a reproductive system disease defined by the failure to achieve a clinical pregnancy after 12 months or more of regular unprotected sexual intercourse (Zegers-Hochschild et al., 2009). This condition is a global issue and it affects approximately 15% of couples due to primary or secondary infertility. Thus, around 48.5 million couples worldwide suffer from infertility. At least 20%-30% and up to 40% of reproduction failure is based on male infertility (WHO, 2010; Sharlip et al., 2002; Sharma, 2017).

Male infertility has attracted more and more attention, along with the development of assisted reproductive technology (ART). Hence, identifying the causative factors of sperm pathologies, especially when they originate genetically, is mandatory for successful ART. Therefore, understanding the genetic causes of male infertility contribute to the efficacy, safety, and health of the progeny conceived by ART (Sharlip et al., 2002; Sharma, 2017).

Teratozoospermia is defined as a low percentage of spermatozoa with normal morphology (WHO, 2010). The acephalic spermatozoa syndrome is a type of teratozoospermia caused by an abnormal head-tail connection that arises during spermiogenesis (Chemes & Alvarez Sedo, 2012; Miyamoto et al., 2012). Moreover, the decapitated sperm syndrome has been reported in familial cases suggesting a genetic origin (Baccetti et al., 1989; Chemes et al., 1999). However, which genes are affected is still unclear.

Alterations of the head-neck attachment have been described in mice provoked by the experimental depletion of specific genes. Among these genes, *Odf1* and *Spag4l* are interesting candidates to analyze in humans because their disruption in mice produces relaxation of the head-tail junction and sperm decapitation (Yang et al., 2014; Yassine et al., 2015). Furthermore, in infertile men some *Spag4l* mutations have already been identified in infertile men with decapitated spermatozoa (Elkhatib et al., 2017; Zhu et al., 2016).

ODF1 is encoded by two slightly different alleles giving rise to two proteins that differ in the number of the C-terminal tripeptide motifs, CSP or CNP (Hofferbert et al., 1993). Both alleles

were also found in the two patients analyzed here. However, the variation of the expression of these alleles is not causative for spermatozoa decapitation. Beyond that, no additional variations were found in the coding region of the *Odf1*-gene in the two patients studied here.

The two exons that encode ODF1 are separated by a 7 kb intron (Hofferbert et al., 1993). Even though intronic sequences do not encode a protein, they contain conserved regulatory elements involved in pre-mRNA splicing. Thus, mutations in intronic regions might also alter gene expression (Gilbert 1978; Kelly et al., 2015). It is the case of the intronic mutation c.425 + 1G →A that affects the *Sun5*-gene leading to a premature stop codon (Zhu et al., 2016). So far, no mutations have been reported to affect either *Odf1* exons or intron. Nonetheless, exploring intronic variants that potentially affect *Odf1*-gene expression might be highly informative.

Since a mutation in *Odf1* was excluded, I turned to *Spag4l* as the next likely candidate. Based on the study conducted by Zhu et al. (2016), specific mutations in 8 of 17 infertile male patients were identified. The mutations described in that study affected the exons 4, 5, 6, 7, 8, 11 and 13. Therefore, I attempted to investigate these variants in two unrelated patients with the acephalic spermatozoa syndrome. The exons 6, 8 were successfully amplified, though their sequences displayed no differences compared to the wild-type sequence. In contrast, the amplification of exons 5, 11, and 13 failed due to unknown reasons, albeit the same primers were used as indicated by Zhu et al. (2016).

The unsuccessful identification of mutations in the gene *Sun5* in the patients studied here might be related to the inappropriate selection of exons. I centered the attention on the exons 6-8 and 11-13 because they encode either the coiled-coil or SUN domain of SUN5, respectively (Zhu et al., 2016). Although mutations in exons 6 and 8 have been reported in patients with decapitated spermatozoa (Zhu et al., 2016), they are not causative of the syndrome in the patients studied here.

Besides that, *Hook1* attracted my attention because a truncating mutation caused abnormal head shape and sperm decapitation in mice (Mendoza-Lujambio et al., 2002). Further, the missense mutation p.Q286R in exon 10 has been reported in infertile men that suffer from headless sperm (Chen et al., 2018). Moreover, HOOK1 localizes in the manchette, which is essential for the transport of molecules required for tail formation (Mendoza-Lujambio, 2002). Therefore, I investigated the *Hook1* gene in two unrelated patients with acephalic spermatozoa syndrome. Since deletion of exons 10 and 11 in mice caused *azh* (abnormal spermatozoon head shape) phenotype, and mouse exon 10 corresponds to the human exon 10, I concentrated on these

regions. Further, exon 10 encodes the VWFC domain that seems to be involved in the formation of protein complexes (Bork 1993). However, I found no evidence for mutation by sequencing the clones of the PCR products.

Our mutation screening using the genomic DNA of two unrelated infertile men that suffer from sperm decapitation excluded mutations in the coding region of *Odf1* as causative. Furthermore, I found no indications for mutation in exon 6 of *Spag4l* or in exons 10 and 11 of *Hook1*. The acephalic spermatozoa syndrome is a rare condition. Therefore, the failure in the identification of a mutation in the two patients investigated is not surprising. To demonstrate a causative mutation requires careful inspection of a large number of patients and genes. Besides that, Zhu et al. (2016) has described an intronic mutation that affects the coiled-coil structure of the SUN5. Therefore, it remains to explore the intronic sequences of the genes *Odf1* and *Hook1* that eventually affect the protein conformation. In mice, some genes have been identified as causative of sperm decapitation phenotype, but mutations affecting these genes in humans have rarely been demonstrated. The loss of function of *Ccdc42* in mice severely affects the formation of the HTCA. However, no mutations in *Ccdc42* were found in these two human patients (Hector Chemes, personal information).

A high number of genes are involved in male infertility, which not only disrupts male germ cells but also may cause genetic impairments in the offspring. These gene mutations may be autosomal recessive or dominant and highly variable between individuals (Hackstein et al., 2000; Matzuk et al., 2002). Even though many genes are involved in male infertility, few affect spermiogenesis (Vogt, 2004). Therefore, the individual's genetic constitution and the few known genes that affect the head-tail junction hamper the detection of mutations in patients. Here, I investigated specific regions of three promising candidate genes. However, identifying the cause of the sperm decapitation in the two patients analyzed requires an intensive screening of mutations in still unexplored genes. Further, DNA sequencing from infertile and fertile male patients that share a specific genetic background may enable identifying new genes involved in the acephalic spermatozoa syndrome.

Considering the complexity of the factors associated with male infertility and the limitation of performing studies in many patients, mouse models are particularly valuable. Therefore, to evaluate the impact of SUN5 on the spermatozoa ultrastructure, *Spag4l*-deficient mice were developed. Two female founders were mated with wild-type males. After genotyping of the offspring by PCR, ~38% of the F1 animals were heterozygous that is below the expected Mendelian ratio of 50%. Heterozygous F1 mice were mated with wild-type mice. Intriguingly, we obtained only a ~9% of heterozygous mice in F2 generation, whereas the expected number

of heterozygous mice was 50%. *Spag4l*<sup>+/-</sup> mice obtained from two independent founder animals were mated to obtain the F3 and F4 generations. Around 30% of heterozygous mice were detected by genotyping, albeit they carried only a small fragment of the integration cassette, but no homozygous *Spag4l*-deficient mice.

The gradual reduction of the cassette size over the generations was intriguing. In ES cells, the up and downstream regions of the recombinant allele were detected by genotyping, demonstrating the correct integration of the replacement cassette into the *Spag4l* gene. Afterward, only the resistant gene neomycin and the flanking region at the 3'-terminal were amplified. However, in further generations, only a small fragment of the neomycin insertion was amplified, whereas the amplification of the flanking regions and the reporter gene LacZ failed.

Multiple biological mechanisms may cause an unusual transmission ratio, including a faulty integration of the targeting allele into the genome, genomic instability of the ES cell, and late injection of ES cells into blastomeres (Martin, 1981; Palmiter et al., 1982). First, correct incorporation of the insertion is fundamental to ensure the stable transmission of the modified allele to the offspring (Palmiter et al., 1982). Further, if transgenic cells' contribution to the germline is low, the foreign DNA transmission frequency will be greatly reduced (Wilkie et al., 1986). Therefore, ES cell clones were carefully analyzed, and the sequencing of the PCR product confirmed the correct position of the cassette. The integration of the cassette replaced nearly the complete *Sun5*-gene, leaving only 89 bp of the N-terminal region. However, the founders were not able to fully transmit the transgene.

Moreover, females are mostly undesirable for a breeding scheme, only two female chimeras tested positive for the transgene and were selected as founders. Among the disadvantages of female founders are the duration of the breeding process as well as the uncertainty of a successful germline transmission (Longenecker et al., 2009). Even though female founders produced offspring, they did not efficiently transmit the cassette. Besides that, the first two generations were tested by nested PCR, given that the amplification of the 5'-region of the insertion cassette could not be amplified. Thus, it is possible that our genotyping results of F1 and further generations were mostly false positive.



## **4.2 Topology and localization of SPAG4 and SPAG4L2 at the nuclear membrane might mediate the connection of the sperm nucleus to its tail**

SPAG4 and SPAG4L/SPAG4L2 are members of the mammalian SUN domain protein family and reside in the nuclear membrane. The mammalian SUN domain protein family comprises at least five conserved SUN-domain proteins. SUN1 and SUN2 are widely expressed in somatic and germinal cells, while SUN3, SUN4/SPAG4, and SUN5/SPAG4L are restricted to male germ cells (Malone et al., 1999; Göb et al., 2010; Padmakumar, 2005; Frohnert et al., 2011). The SUN domain protein family shares a similar structure, consisting of an N-terminal region containing up to three transmembrane domains (TMs), followed by one or two coiled-coil regions and a conserved SUN domain at the C-terminal region. The N-terminus containing the transmembrane domains spans the inner nuclear membrane and interacts with the nuclear lamina and chromatin. Meanwhile, the C-terminus containing the SUN-domain resides in the perinuclear space. Here, the SUN-domain interacts with the KASH domain proteins located in the ONM, thus linking the cytoskeleton to the nucleoskeleton (Hodzic et al., 2004; Crisp et al., 2006; Haque et al., 2006; Razafsky & Hodzic, 2009)

In round spermatids, SPAG4L is recruited from the cytoplasm to the nuclear envelope except for the NE overlaying the acrosome. Meanwhile, in elongating spermatids, SPAG4L as well as SPAG4 locate to the posterior pole of the NE, and more specifically at the implantation fossa (Yassine et al., 2015; Yang et al., 2018). Previous analyses have confirmed that SPAG4 and SPAG4L interact with ODF1 in vitro (Shao et al., 1999; 2001). Further, the homozygous mutation c.381delA that affects the TM of *Sun5* in humans seems to change the expression and distribution of ODF1 (Sha et al., 2018). This data indicates that SPAG4 and SPAG4L are involved in the recruitment of ODF1 to the nuclear membrane. However, the localization of SPAG4 and SPAG4L at the NE does not explain their ability to interact with ODF1 that locates in the basal plate and capitulum. Therefore, this raises the question of whether the N-terminal region of SPAG4 might also localize at the outer nuclear membrane to enable the interaction with cytoskeletal proteins, as e.g. ODF1.

To obtain a clearer view of the orientation of SPAG4 and SPAG4L within the NE, their transmembrane segments and domains were analyzed. The localization pattern of different regions and domains of SPAG4L revealed a clear localization of TM1 and TM2 in the NE. TM1 also locates in the cytoplasm, and TM2 strongly concentrates in the area that seems to be the ER. In contrast to TM2, TM1 is widely distributed to the nuclear envelope and cytoplasm, whereas the combination of both TMs recruits the protein to the nuclear envelope. These results indicate that the TM1 is responsible for the recruitment of the protein to the nuclear membrane.

In contrast, the presence of the TM2 in the Golgi-apparatus might be associated with protein trafficking through membrane compartments. Analyses of the dynamics of SUN5 during spermiogenesis have indicated that SUN5 transits through the Golgi apparatus to experience post-translational modifications before reaching its final localization at the NE (Yassine et al., 2015). Additional data also indicate that TM2 does not recruit SPAG4L to the nuclear membrane. The mutation c.340G→A (p.Gly114Arg) affects the TM-domain of *Spag4l* in humans, whereas in mice the mutation localizes in the position c.334G>A (p.Gly114Arg) and affects the TM2 of *Spag4l2*. The overexpression of SUN5 carrying the p.Gly114Arg mutation in HeLa cells induces protein aggregation near the NE but does not prevent its localization at the nuclear membrane (Elkhatib et al., 2017; Shang et al., 2018).

The results also indicate that the coiled-coil and SUN domains are not involved in retaining SPAG4L at the NE. According to a previous study, the deletion of the SUN-domain coding region of *Spag4l* (exons 10, 11, and 12) leads to male infertility in mice (Shang et al., 2017). Therefore, I investigated whether the C-terminal truncation of SPAG4L2 affects its nuclear membrane localization. My results show that the truncated SPAG4L2 is localized in the nuclear membrane with a similar distribution as the full-length protein. These results coincide with Frohnert et al. (2011), who described the two TMs (TM1 and TM2) as mediators of SPAG4L2 recruitment to the NE. Besides, Hasan et al. (2006) and Hodzic et al. (2004) have also reported that the SUN-domain is not responsible for maintaining SUN1 and SUN2 at the NE, confirming the data obtained here.

These data suggest that the TM1 plays a major role in recruiting SPAG4L and SPAG4L2 at the NE. Thus, mutations affecting the coding sequence of TM1 and TM2 might impair nuclear membrane localization. On the other hand, mutations affecting the SUN-domain might disrupt the ability of SPAG4L2 to establish protein interactions, thus affecting the linkage to the cytoskeleton and perhaps the linkage of the sperm head to the tail. However, it remains the question how SPAG4 and SPAG4L interact with cytoplasmatic proteins.

Since SPAG4 and SPAG4L are nuclear membrane proteins in somatic cells and SUN proteins form the LINC complex, it is suggested that SPAG4 or SPAG4L might connect the NE to the capitulum via ODF1. For this reason, the orientation of the N-terminal region of SPAG4 and SPAG4L acquire great relevance and might explain the mechanism of these proteins to interact with ODF1. Thus, I used the rapamycin-based FKBP-FRB dimerization to analyze the orientation of SPAG4 and SPAG4L.

Rapamycin induces the formation of a ternary complex between FKBP and FRB (Banaszynski et al., 2005). Therefore, the binding domain FRB was coupled to the N-terminus of SUN4 (or SUN5)-ECFP, whereas Luciferase-mRFP was coupled to FKBP to its C-terminus. Luciferase-mRFP-FKBP was mostly distributed at the cytoplasm, whereas FRB-ECFP-SUN4 (SUN5) localized at the nuclear membrane. The addition of rapamycin induced the recruitment of Luciferase-mRFP-FKBP from the cytoplasm to the nuclear envelope.

Thus, the NH<sub>2</sub>-termini of SPAG4 and SPAG4L containing FRB were able to interact with their partner FKBP in the presence of rapamycin. Without rapamycin induction, Luciferase-mRFP-FKBP was exclusively cytoplasmatic. These results indicate that the N-terminal region of SPAG4 and SPAG4L was oriented to the outer nuclear membrane (ONM). On the contrary, if the NH<sub>2</sub>-termini of SPAG4 and SPAG4L were localized at inner nuclear membrane INM, FRB would not be able to recruit the cytoplasmic Luciferase to the nuclear envelope.

To sum up, these results support the view that the NH<sub>2</sub>-termini of the SUN-domain proteins SPAG4 and SPAG4L localize at the ONM as well as the INM. Thus, this model could explain the ability of SPAG4 and SPAG4L to interact with ODF1 and still unknown cytoplasmatic proteins to generate the coupling apparatus in sperm (Fig. 4.2, B).

So far, the only known interaction partner of SPAG4 is the HTCA protein ODF1, indicating its function in the establishment of a novel sperm-specific LINC complex. Additional SPAG4 interacting partners that collaborate in the formation of the connecting piece still await to be identified. Therefore, I have explored the application of the amber suppression strategy to identify in vitro new SPAG4 interacting partners that might collaborate in the formation of the HTCA. To identify potential protein interactions, it is necessary to overexpress candidate testis-specific proteins in somatic cells in combination with an engineered sequence able to encode a photoreactive amino acid.

The amber suppression method works by the reassignment of the stop-codon function that enables the expansion of the genetic code. Stop codons can encode unnatural amino acids (UAAs) and be incorporated into proteins. Further, the UAAs serve to label proteins to investigate their functionality in a native context (Xie & Schultz, 2005). The translation of UAAs can incorporate photo-crosslinking amino acids, e.g., p-benzoyl-phenylalanine (*p*Bpa). Once the amino acid *p*Bpa has been integrated into the protein chain, cross-linking to close C-H bonds of nearby proteins can be induced by illumination with UV-light of 350-360 nm (Kauer et al., 1986). Thus, the cross-linking of close-by proteins or peptides enables the identification of potential interacting proteins (Chin et al., 2002, 2003; Hino et al., 2005; Xie & Schultz, 2005).

In this study, I evaluated the feasibility of this method to identify LMNC interacting partners. First, the amber stop codon was incorporated into three different regions of LMNC, giving rise to three independent LMNC expression plasmids. Amber nonsense mutations were inserted into the C-terminal region of LMNC because this region contains immunoglobulin domains, which are supposed to be involved in protein-protein interactions (Dechat et al., 2000). Once the amber codon replaced the amino acid Arg-470, Thr-488, and Thr-534 in the LMNC sequence respectively, the amber codon was translated into the photo-activatable amino acid (*pBpa*) in the presence of the orthogonal tRNA-aaRS (*p4XtRNA<sub>pBpa</sub>*) and *pBpa*.

The correct incorporation of the unnatural amino acid in LMNC was confirmed immunocytologically. Cells that were exclusively transfected with *Lmnc* containing the nonsense sequence produced a truncated protein. Thus, LMNC was detected in the nucleoplasm forming aggregates. The incorporation of *pBpa* restored LMNC localization at the nuclear membrane. Considering that the use of the inducible crosslinking of LMNC containing a UAA can react with native proteins, it is mandatory to validate the system and avoid false positives. *Lmnc* was co-transfected with *Spag4*, confirming that their respective proteins do not interact. However, unspecific bands were detected by Western blotting. These protein bands could be explained by the unspecificity of the antibodies and the presence of endogenous LMNC expressed in NIH3T3 cells detected by the anti-laminA/C antibody.

To further evaluate the ability of the modified LMNC to interact with exogenous proteins, *Lmnc* was transfected with its known binding partners *Lmnb3* and *Lmnc2*, respectively (Ye & Worman, 1995). However, no cross-linking between these proteins was found, whereas LMNB3 and LMNC2 could be detected (data are not shown).

These results show that the amber suppression method is sensitive and susceptible to several experimental conditions, including the amount of RS/tRNA transfected and the appropriate protein translation. Furthermore, the modified LMNC is highly reactive with endogenous proteins complicating the detection of interacting proteins.

Even though this system is appropriate to detect weak and transient interactions with high specificity in mammalian cells (Hino et al., 2005), the identification of testicular protein interactions will only be possible by their ectopic expression. However, the protein that will be engineered to induce the photo-crosslinking should be carefully chosen to fit the specific purpose of the experiment. Considering this aspect, the amber suppression method should first be evaluated using the known interacting partners LMNA and SUN1 and SUN2 (Haque et al., 2006; Crisp et al., 2006). Furthermore, LMNA is a suitable candidate to evaluate its interaction

with the testes specific SUN-domain proteins SUN3, SUN4 and SUN5. For this goal, a site-specific UAA incorporation into *Lmna* and the addition of a tag for its posterior detection by Western-blotting is mandatory. LMNA contains the immunoglobulin Ig-fold in its C-terminal region, which may mediate specific intermolecular protein-protein, protein-DNA, and protein-phospholipid interactions (Dhe-Paganon et al., 2002). It is known that the region of LMNA that encompasses residues 430–545 adopts an Ig-like fold (Krimm et al., 2002). Therefore, this area is an interesting “hot-spot” to incorporate *pBPA*. Moreover, the modification of the amino acid R482 (R482W) alters the interaction of the LMNA with LAP2 $\alpha$  and emerin, among others (Gilchrist et al., 2004). Hence, it will be recommended to consider replacing the amino acid R482 with the amber stop codon.

### **4.3 Identification of proteins that collaborate in the formation of the HTCA**

The HTCA formation and its structure have acquired great relevance because its proper development ensures oocyte fertilization. The ultrastructure of the HTCA is formed by specific components such as the basal plate, capitulum, centrioles, and segmented columns. However, its molecular components are barely known.

ODF1 is a pivotal component of the HTCA, and its disruption in mice affects the thigh junction of the sperm head-to-tail, causing sperm decapitation. It localizes in the cytoskeletal portion of the HTCA (Yang et al., 2012; 2014), whereas its interacting partner SPAG4, localizes at the nuclear membrane of the sperm (Shao and van der Hoorn, 1996; Shao et al., 1997; 1999). Considering that the linkage between the nucleoskeleton and the cytoskeleton in somatic cells is mediated via interaction between SUN domain and KASH domain proteins, the HTCA might be established via interaction between male germ cell-specific SUN domain proteins and still to be identified KASH domain proteins or directly to cytoskeletal proteins, as, e.g., ODF1 (Starr, 2002; Starr & Fridolfsson, 2010). The SUN-domain proteins reside at the nuclear membrane. Therefore, the ability of SPAG4 and SPAG4L to interact with cytoskeletal proteins in sperm is far from being comprehended. SPAG4 and SPAG4L contain at least one transmembrane domain responsible for recruiting the full-length protein to the nuclear envelope. Further, from the five SUN-domain proteins encoded in mammals, SUN1 and SUN2 reside at the INM (Hodzic et al., 2004; Haque et al., 2006; Hasan et al., 2006). However, the data obtained here indicated that SPAG4 and SPAG4L also localize at the ONM. This suggests that the N-terminal region of SPAG4 and SPAG4L might recruit ODF1 to the nuclear membrane and thus link the sperm head to its tail (Fig. 4.2, B). Furthermore, the *Sun5* mutation c.381delA (p.Val128Serfs\*7) has

been described in 33.33% - 47.06% of Chinese patients affected by the acephalic spermatozoa syndrome. Particularly, this mutation localizes at the coding region of the transmembrane domain and reduces the expression of ODF1 in sperm from an infertile patient compared to the sperm control (Sha et al., 2018). In *Drosophila*, SPAG4 is involved in the linkage of the sperm head to the flagellum through the coiled-coil protein Yuri Gagarin. Yuri is a component of the basal body in elongated spermatids and its localization is altered by the absence of SPAG4 (Kracklauer et al., 2010). These data support the ability of SPAG4 and SPAG4L, to recruit cytoskeletal proteins such as ODF1 to the nuclear envelope.

ODFs are prominent components of the cytoskeletal structure of the sperm tail, and mostly located in the mid-piece of human spermatozoa (Okamoto, 1988; Petersen et al., 1999). From these proteins, the major components in human spermatozoa are ODF1, ODF2, and ODF3 (Petersen et al., 2002). ODF1 and ODF2 are interacting partners via their leucine zipper motif (Shao et al., 1997), whereas ODF3 is a cytoskeletal coiled-coil protein (Petersen et al., 2002). ODF1 (unpublished observation) and ODF2 are centrosomal components in somatic cells (Schweizer et al., 2009), and both are required to maintain a tight connection between the sperm head and its tail (Yang et al., 2012, 2014; Ito et al., 2019). These proteins are components of the cellular cytoskeleton and their structure may contribute to forming a scaffold of proteins involved in the formation of the HTCA. ODF3, also known as PMFBP1 or STAP, has a reported effect in the detachment of the sperm nuclear envelope to the connecting piece when it is faulty (Sha et al., 2019). In humans, six mutations that affect *Odf3/Pmfbp1* have been identified to be causative of the acephalic spermatozoa syndrome (Zhu et al., 2018; Sha et al., 2019). In humans and mice spermatozoa, polyamine-modulated factor 1-binding protein 1 “PMFBP1” localizes at the HTCA, specifically between SUN5 and SPATA6 (Zhu et al., 2018). SUN5 locates at the NE, whereas SPATA6 in the segmented columns and capitulum (Frohnert et al., 2010; Yuan et al., 2015). Thus, the complex formed by SUN5/PMFBP1/SPATA6 contributes to the junction of the sperm head to the tail. Moreover, the mutations c.425+1G>A and c.1043A>T in *Sun5* affect the localization of PMFBP1 in the implantation fossa, indicating their cooperative role in the HTCA formation (Zhu et al., 2018). The coiled-coil protein ODF3/PMFBP1/STAP may serve as platform of still unidentified protein that collaborate in the in the articulation of the sperm head to the tail.

Another protein also implicated in the formation of the HTCA is the coiled-coil domain-containing protein 42 (CCDC42). Genetic depletion of CCDC42 in mice affects sperm nuclear shaping and the implantation site leading to male infertility (Pasek et al., 2016). Our subcellular analyses have detected CCDC42 in the manchette and perinuclear ring in elongating spermatids,

whereas, in sperm, it localizes to the connecting piece and the sperm tail. The presence of CCDC42 in the manchette and sperm tail coincides with the localization of ODF1. Moreover, in somatic cells, ODF1 and CCDC42 colocalized in the centrosome, indicating an interaction between both proteins. The interaction between CCDC42 and ODF1 as well as ODF2 was probed by pull-down and Co-IP assays. These data indicate that the interaction between CCDC42 and ODF1 and ODF2 might serve as a scaffold in forming the HTCA and the sperm tail.

The current research has shown that CCDC42 and ODF1 as well as the coiled-coil protein HOOK1 localize at the microtubular manchette. Depletion of *Hook1* disrupts the formation of the HTCA leading to sperm decapitation (Mendoza-Lujambio, 2002). HOOK1 interacts with the manchette-associated protein RIMBP3. Disruption of *Rimbp3* results in abnormal sperm head shape, detached acrosome, abnormal manchette positioning, and disarranges the sperm head-to-tail linkage (Zhou et al., 2009). Furthermore, RIM-BP3 interacts with the microtubule-dependent motor protein KIF3B which is involved in the manchette function and sperm tail formation. KIF3B seems to be involved most likely in the intra-manchette transport of proteins towards the axoneme (Zhou et al., 2009). KIF3B forms a complex with KIF3A, another microtubule-based motor member of the kinesin family (Yamazaki et al., 1995). KIF3A localizes in the basal body, axoneme and manchette of elongating spermatids, whereas in mature spermatozoa it situates in the sperm tail (Lehti et al., 2013). In mice spermatids, KIF3A disruption affects the nuclear shaping, manchette organization and alters the axoneme organization and tail accessory structures (Lehti et al., 2013). Thus, KIF3A seems to be involved in the microtubule network of the manchette and flagellar assembly (Lehti et al., 2013). During axoneme formation, *Kif3a* expression correlates with the expression of *Odf3/Pmfbp1* and *Ccdc11/Cfap53* suggesting their interaction and collaboration in the formation of the flagellum (Lehti et al., 2013).

As another putative component of the HTCA, the cilia and flagella associated protein 52 (CFAP52) came into focus. CFAP52/WDR16 is a WD-repeat domain protein, which contains GH-WD repeats. These repetitive motifs have the property to support protein-protein interaction enabling CFAP52 to perform several biological functions. WD-repeat domain proteins are involved in RNA synthesis/processing, signal transduction, cytoskeleton assembly, mitotic spindle formation, vesicular trafficking, and cell growth (Neer et al., 1994; Li & Roberts, 2001). Therefore, I was interested first in the expression and localization of CFAP52 in somatic and male germ cells. I demonstrated for the first time that CFAP52 is a centrosomal protein in somatic cells. Furthermore, it localizes to the basal body, the mitotic spindle poles, and the

intercellular bridge. In male germ cells, CFAP52 is a component of the manchette and sperm tail as well as ODF1, although these proteins do not interact. Therefore, these results suggest that CFAP52 might be associated with microtubular structures and is involved in the traffic of proteins through the manchette. These data indicate that CFAP52 may be a suitable interacting partner of KIF3A which is also involved in the manchette and axoneme organization (Fig. 4.1).

In summary, ODF1 and CCDC42 are essential for HTCA formation since their deficiency causes sperm decapitation. Disruption of SPAG4 debilitates the tight junction between the sperm tail and head. SPAG4L is responsible for the attachment between the sperm nucleus and the flagellum, and mutations lead to the acephalic syndrome in humans. The proteins CFAP52 and CCDC42 were identified as centrosomal proteins in somatic cells and resided in specific structures of male germ cells where they colocalize with ODF1 (Fig. 4.2, A). These proteins may form a complex to stabilize the connecting piece, and their failure leads to sperm decapitation and thus human male infertility.

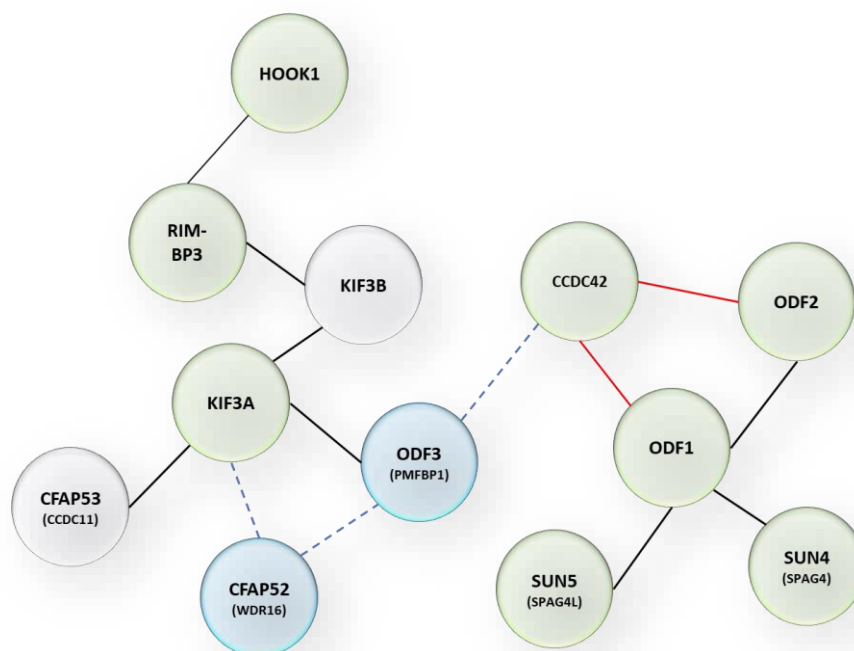


**Figure 4.1. Mapping of HTCA protein interaction network.** Green nodes represent proteins with a reported effect in the formation of the HTCA. Blue nodes represent structural proteins in mammalian spermatozoa. Gray nodes represent proteins associated with microtubular structures in mitotic or meiotic cells. Red lines represent the interactions identified in this study. Black lines represent proteins interactions previously published. Light blue dashed lines represent potential protein interactions.



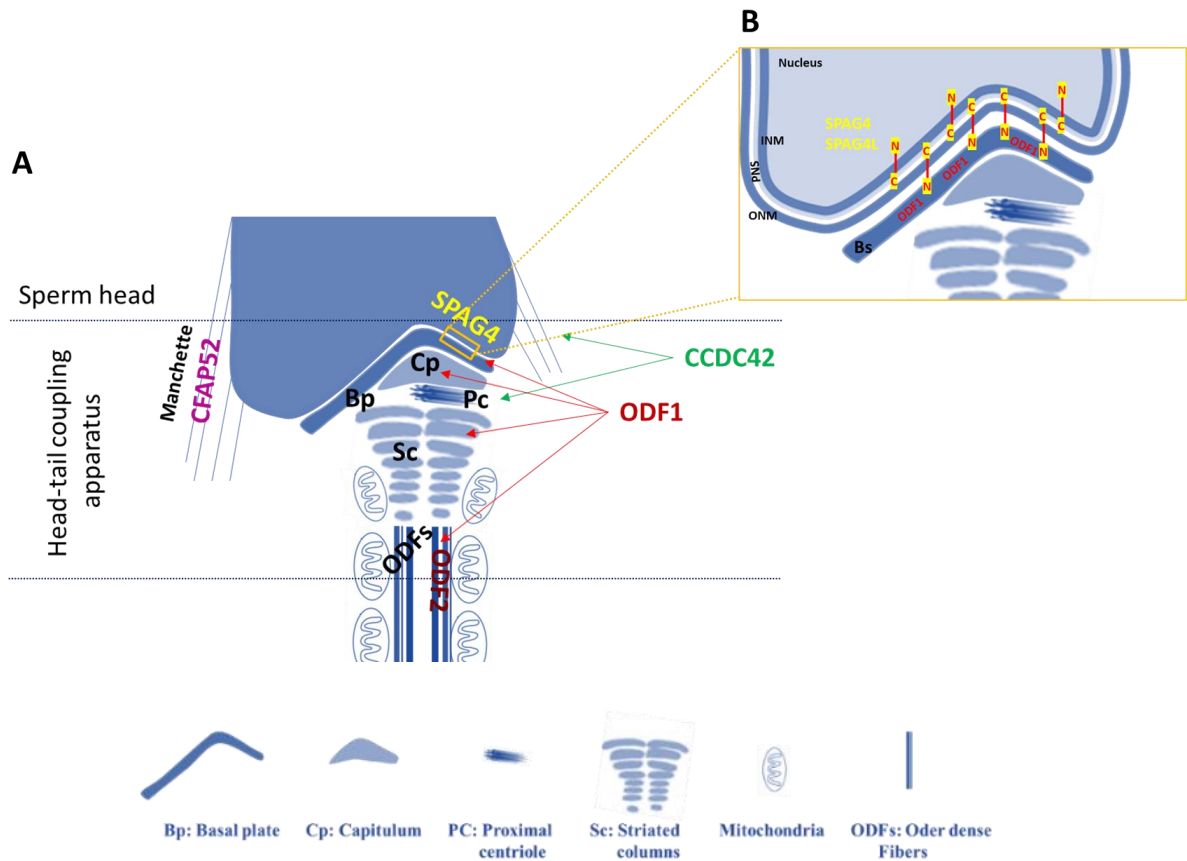


**Figure 4.2. Representative scheme of proteins associated with the HTCA in elongating spermatids.**

(A) The HTCA is composed of the basal plate (Bp), capitulum (Cp), proximal centriole (Pc) and striated columns (Sc). The sperm head is linked to the connecting piece via basal plate and capitulum. SPAG4 localizes at the nuclear envelope and interacts with the cytoskeletal protein ODF1. ODF1 localizes at the basal plate, capitulum, striated columns and ODFs. ODF1 interacts with ODF2 and CCDC42. CCDC42 localizes to the manchette and connecting piece. CFAP52 is a component of the manchette. (B) SPAG4 and SPAG4L localizes at the nuclear membrane. ODF1 localizes at the basal plate. The N-terminal region of SPAG4 and SPAG4L might be oriented towards the inner nuclear membrane (INM) or the outer nuclear membrane (ONM). In contrast, their C-terminal region localizes at the perinuclear space (PNS). The N-terminal region of SPAG4 and SPAG4L oriented to the ONM might enable the interaction with the cytoskeletal protein ODF1.

## 5 References

- Alsheimer, M., von Glasenapp, E., Schnolzer, M., Heid, H., & Benavente, R. (2000). Meiotic lamin C2: The unique amino-terminal hexapeptide GNAEGR is essential for nuclear envelope association. *Proceedings of the National Academy of Sciences*, 97(24), 13120–13125. <https://doi.org/10.1073/pnas.240466597>
- Alsheimer, M. & Benavente, R. (1996). Change of Karyoskeleton during Mammalian Spermatogenesis: Expression Pattern of Nuclear Lamin C2 and Its Regulation. *Experimental Cell Research*, 228(2), 181–188. <https://doi.org/10.1006/excr.1996.0315>
- Alvey, P. L. (1985). An investigation of the centriole cycle using 3T3 and CHO cells. *Journal of Cell Science*, 78(1), 147–162. <https://jcs.biologists.org/content/78/1/147>
- Avidor-Reiss, T., Mazur, M., Fishman, E. L., & Sindhvani, P. (2019). The Role of Sperm Centrioles in Human Reproduction - The Known and the Unknown. *Frontiers in cell and developmental biology*, 7, 188. <https://doi.org/10.3389/fcell.2019.00188>
- Baccetti, B., Burrini, A. G., Collodel, G., Magnano, A. R., Piomboni, P., Renieri, T. & Sensini, C. (1989). Morphogenesis of the decapitated and decaudated sperm defect in two brothers. *Gamete Research*, 23(2), 181–188. <https://doi.org/10.1002/mrd.1120230205>
- Balhorn, R. (1982). A model for the structure of chromatin in mammalian sperm. *The Journal of Cell Biology*, 93(2), 298–305. <https://doi.org/10.1083/jcb.93.2.298>
- Baltz, J. M., Oneeka Williams, P. & Cone, R. A. (1990a). Dense Fibers Protect Mammalian Sperm Against Damage. *Biology of Reproduction*, 43(3), 485–491. <https://doi.org/10.1095/biolreprod43.3.485>
- Baltz, J. M., Oneeka Williams, P. & Cone, R. A. (1990b). Dense Fibers Protect Mammalian Sperm Against Damage. *Biology of Reproduction*, 43(3), 485–491. <https://doi.org/10.1095/biolreprod43.3.485>
- Banaszynski, L. A., Liu, C. W., Wandless, T. J. (2005). Characterization of the FKBP.rapamycin.FRB ternary complex. *Journal of the American Chemical Society*, 127(13), 4715–4721. <https://doi:10.1021/ja043277y>
- Bhullar, B., Zhang, Y., Junco, A., Oko, R. & van der Hoorn, F. A. (2003). Association of Kinesin Light Chain with Outer Dense Fibers in a Microtubule-independent Fashion. *The Journal of biological chemistry*, 278(18), 16159–16168. <https://doi.org/10.1074/jbc.M213126200>

- Bork, P. (1993). The modular architecture of a new family of growth regulators related to connective tissue growth factor. *FEBS letters*, 327(2), 125–130. [https://doi.org/10.1016/0014-5793\(93\)80155-n](https://doi.org/10.1016/0014-5793(93)80155-n)
- Bornens, M. (2002). Centrosome composition and microtubule anchoring mechanisms. *Current Opinion in Cell Biology*, 14(1), 25–34. [https://doi.org/10.1016/S0955-0674\(01\)00290-3](https://doi.org/10.1016/S0955-0674(01)00290-3)
- Braun, R. E. (1990). Temporal translational regulation of the protamine 1 gene during mouse spermatogenesis. *Enzyme*, 44(1-4), 120–128. <https://doi.org/10.1159/000468752>
- Burfeind, P. & Hoyer-Fender, S. (1991). Sequence and developmental expression of a mRNA encoding a putative protein of rat sperm outer dense fibers. *Developmental Biology*, 148(1), 195–204. [https://doi.org/10.1016/0012-1606\(91\)90329-2](https://doi.org/10.1016/0012-1606(91)90329-2)
- Burke, B. & Stewart, C. L. (2002). Life at the edge: The nuclear envelope and human disease. *Nature Reviews Molecular Cell Biology*, 3(8), 575–585. <https://doi.org/10.1038/nrm879>
- Burke, B. & Stewart, C. L. (2013). The nuclear lamins: Flexibility in function. *Nature Reviews. Molecular Cell Biology*, 14(1), 13–24. <https://doi.org/10.1038/nrm3488>
- Burmester, S. & Hoyer-Fender, S. (1996). Transcription and translation of the outer dense fiber gene (Odf1) during spermiogenesis in the rat. A study by in situ analyses and polysome fractionation. *Molecular Reproduction and Development*, 45(1), 10–20. [https://doi.org/10.1002/\(SICI\)1098-2795\(199609\)45:1<10::AID-MRD2>3.0.CO;2-V](https://doi.org/10.1002/(SICI)1098-2795(199609)45:1<10::AID-MRD2>3.0.CO;2-V)
- Calvi, A., Wong, A. S. W., Wright, G., Wong, E. S. M., Loo, T. H., Stewart, C. L. & Burke, B. (2015). SUN4 is essential for nuclear remodeling during mammalian spermiogenesis. *Developmental Biology*, 407(2), 321–330. <https://doi.org/10.1016/j.ydbio.2015.09.010>
- Chemes, H. E., Carizza, C. & Scarinci, F. (1987). Lack of a head in human spermatozoa from sterile patients: A syndrome associated with impaired fertilization. *International Journal of Gynecology & Obstetrics*, 26(1), 165–165. [https://doi.org/10.1016/0020-7292\(88\)90230-5](https://doi.org/10.1016/0020-7292(88)90230-5)
- Chemes, H. E., Puigdomenech, E. T., Carizza, C., Olmedo, S. B., Zanchetti, F. & Hermes, R. (1999). Acephalic spermatozoa and abnormal development of the head–neck attachment: A human syndrome of genetic origin. *Human Reproduction*, 14(7), 1811–1818. <https://doi.org/10.1093/humrep/14.7.1811>
- Chemes, H. E. (2000). Phenotypes of Sperm Pathology: Genetic and Acquired Forms in Infertile Men. *Journal of Andrology*, 21(6), 799–808. <https://doi.org/10.1002/j.1939-4640.2000.tb03409.x>
- Chemes H. E. (2012) Sperm Centrioles and Their Dual Role in Flagellogenesis and Cell Cycle of the Zygote. In: Schatten H. (eds) The Centrosome. *Humana Press*, Totowa, NJ. [https://doi.org/10.1007/978-1-62703-035-9\\_2](https://doi.org/10.1007/978-1-62703-035-9_2)

- Chemes, H. E. & Alvarez Sedo, C. (2012). Tales of the Tail and Sperm Head Aches: Changing concepts on the prognostic significance of sperm pathologies affecting the head, neck and tail. *Asian Journal of Andrology*, *14*(1), 14–23. <https://doi.org/10.1038/aja.2011.168>
- Chemes, H. E. & Rawe, V. Y. (2003). Sperm pathology: A step beyond descriptive morphology. Origin, characterization and fertility potential of abnormal sperm phenotypes in infertile men. *Human Reproduction Update*, *9*(5), 405–428. <https://doi.org/10.1093/humupd/dmg034>
- Chemes, H. E. & Rawe, V. Y. (2010). The making of abnormal spermatozoa: Cellular and molecular mechanisms underlying pathological spermiogenesis. *Cell and Tissue Research*, *341*(3), 349–357. <https://doi.org/10.1007/s00441-010-1007-3>
- Chen, H., Zhu, Y., Zhu, Z., Zhi, E., Lu, K., Wang, X., Liu, F., Li, Z. & Xia, W. (2018). Detection of heterozygous mutation in hook microtubule-tethering protein 1 in three patients with decapitated and decaudated spermatozoa syndrome. *Journal of medical genetics*, *55*(3), 150–157. <https://doi.org/10.1136/jmedgenet-2016-104404>
- Chikashige, Y., Haraguchi, T. & Hiraoka, Y. (2007). Another way to move chromosomes. *Chromosoma*, *116*(6), 497–505. <https://doi.org/10.1007/s00412-007-0114-8>
- Chin, J. W., Cropp, T. A., Anderson, J. C., Mukherji, M., Zhang, Z. & Schultz, P. G. (2003). An expanded eukaryotic genetic code. *Science (New York, N.Y.)*, *301*(5635), 964–967. <https://doi.org/10.1126/science.1084772>
- Chin, J. W., Santoro, S. W., Martin, A. B., King, D. S., Wang, L. & Schultz, P. G. (2002). Addition of *p*-Azido-*L*-phenylalanine to the Genetic Code of *Escherichia coli*. *Journal of the American Chemical Society*, *124*(31), 9026–9027. <https://doi.org/10.1021/ja027007w>
- Choi, C. P., Moon, A. S., Back, P. S., Jami-Alahmadi, Y., Vashisht, A. A., Wohlschlegel, J. A., Bradley, P. J. (2019). A photoactivatable crosslinking system reveals protein interactions in the *Toxoplasma gondii* inner membrane complex. *PLoS Biology*, *17*(10): e3000475. <https://doi.org/10.1371/journal.pbio.3000475>
- Clermont, Y. (1972). Kinetics of spermatogenesis in mammals: Seminiferous epithelium cycle and spermatogonial renewal. *Physiological Reviews*, *52*(1), 198–236. <https://doi.org/10.1152/physrev.1972.52.1.198>
- Conrad, M. N., Lee, C. Y., Wilkerson, J. L. & Dresser, M. E. (2007). MPS3 mediates meiotic bouquet formation in *Saccharomyces cerevisiae*. *Proceedings of the National Academy of Sciences*, *104*(21), 8863–8868. <https://doi.org/10.1073/pnas.0606165104>
- Costa, Y., Speed, R., Ollinger, R., Alsheimer, M., Semple, C. A., Gautier, P., Maratou, K., Novak, I., Höög, C., Benavente, R. & Cooke, H. J. (2005). Two novel proteins recruited by synaptonemal complex protein 1 (SYCP1) are at the centre of meiosis. *Journal of cell science*, *118*(Pt 12), 2755–2762. <https://doi.org/10.1242/jcs.02402>

- Crisp, M., Liu, Q., Roux, K., Rattner, J. B., Shanahan, C., Burke, B., Stahl, P. D. & Hodzic, D. (2006). Coupling of the nucleus and cytoplasm: Role of the LINC complex. *The Journal of Cell Biology*, 172(1), 41–53. <https://doi.org/10.1083/jcb.200509124>
- Das, S. & Oliver, D. B. (2011). Mapping of the SecA·SecY and SecA·SecG interfaces by site-directed in vivo photocross-linking. *The Journal of biological chemistry*, 286(14), 12371–12380. <https://doi.org/10.1074/jbc.M110.182931>
- De Rooij, D. G. & Grootegoed, J. A. (1998). Spermatogonial stem cells. *Current Opinion in Cell Biology*, 10(6), 694–701. [https://doi.org/10.1016/s0955-0674\(98\)80109-9](https://doi.org/10.1016/s0955-0674(98)80109-9)
- Dechat, T., Korbei, B., Vaughan, O. A., Vlcek, S., Hutchison, C. J. & Foisner, R. (2000). Lamina-associated polypeptide 2alpha binds intranuclear A-type lamins. *Journal of cell science*, 113 Pt 19, 3473–3484.
- Dhe-Paganon, S., Werner, E. D., Chi, Y., Shoelson, S. E. (2002). Structure of the Globular Tail of Nuclear Lamin. *The Journal of Biological Chemistry*, 277, 17381–17384. <https://doi.org/10.1074/jbc.C200038200>
- Ding, X., Xu, R., Yu, J., Xu, T., Zhuang, Y. & Han, M. (2007). SUN1 Is Required for Telomere Attachment to Nuclear Envelope and Gametogenesis in Mice. *Developmental Cell*, 12(6), 863–872. <https://doi.org/10.1016/j.devcel.2007.03.018>
- Dittmer, T. A. & Misteli, T. (2011). The lamin protein family. *Genome biology*, 12(5), 222. <https://doi.org/10.1186/gb-2011-12-5-222>
- Dunleavy, J., O'Bryan, M. K., Stanton, P. G. & O'Donnell, L. (2019). The cytoskeleton in spermatogenesis. *Reproduction (Cambridge, England)*, 157(2), R53–R72. <https://doi.org/10.1530/REP-18-0457>
- Eddy, E. M. (1998). Regulation of gene expression during spermatogenesis. *Seminars in Cell & Developmental Biology*, 9(4), 451–457. <https://doi.org/10.1006/scdb.1998.0201>
- Elkhatib, R. A., Paci, M., Longepied, G., Saias-Magnan, J., Courbiere, B., Guichaoua, M. R., Lévy, N., Metzler-Guillemain, C. & Mitchell, M. (2017). Homozygous deletion of SUN5 in three men with decapitated spermatozoa. *Human Molecular Genetics*, 26, 3167–3171. <https://doi.org/10.1093/hmg/ddx200>
- Fawcett, D. W. (1975). The mammalian spermatozoon. *Developmental Biology*, 44(2), 394–436. [https://doi.org/10.1016/0012-1606\(75\)90411-X](https://doi.org/10.1016/0012-1606(75)90411-X)
- Fawcett, D. W. & Phillips, D. M. (1969). The fine structure and development of the neck region of the mammalian spermatozoon. *The Anatomical Record*, 165(2), 153–183. <https://doi.org/10.1002/ar.1091650204>
- Fegan, A., White, B., Carlson, J. C. T. & Wagner, C. R. (2010). Chemically Controlled Protein Assembly: Techniques and Applications. *Chemical Reviews*, 110(6), 3315–3336. <https://doi.org/10.1021/cr8002888>

- Fitzgerald, C. J., Oko, R. J. & van der Hoorn, F. A. (2006). Rat Spag5 associates in somatic cells with endoplasmic reticulum and microtubules but in spermatozoa with outer dense fibers. *Molecular Reproduction and Development*, 73(1), 92–100. <https://doi.org/10.1002/mrd.20388>
- Fontaine, J. M., Rest, J. S., Welsh, M. J. & Benndorf, R. (2003). The sperm outer dense fiber protein is the 10th member of the superfamily of mammalian small stress proteins. *Cell stress & chaperones*, 8(1), 62–69. [https://doi.org/10.1379/1466-1268\(2003\)8<62:tsodfp>2.0.co;2](https://doi.org/10.1379/1466-1268(2003)8<62:tsodfp>2.0.co;2)
- Frank, C. J., Lorna K. J., Donald P. E. (1986). Mouse Testicular and Sperm Cell Development Characterized from Birth to Adulthood by Dual Parameter Flow Cytometry, *Biology of Reproduction*, 4(4), 613–623. <https://doi.org/10.1095/biolreprod34.4.613>
- Frohnert, C., Schweizer, S. & Hoyer-Fender, S. (2011). SPAG4L/SPAG4L-2 are testis-specific SUN domain proteins restricted to the apical nuclear envelope of round spermatids facing the acrosome. *Molecular Human Reproduction*, 17(4), 207–218. <https://doi.org/10.1093/molehr/gaq099>
- Furukawa, K. & Hotta, Y. (1993). cDNA cloning of a germ cell specific lamin B3 from mouse spermatocytes and analysis of its function by ectopic expression in somatic cells. *The EMBO Journal*, 12(1), 97–106. <https://doi.org/10.1002/j.1460-2075.1993.tb05635.x>
- Gerace, L. & Burke, B. (1988). Functional organization of the nuclear envelope. *Annual Review of Cell Biology*, 4, 335–374. <https://doi.org/10.1146/annurev.cb.04.110188.002003>
- Gilbert, W. (1978). Why genes in pieces? *Nature* 271, 501. <https://doi.org/10.1038/271501a0>
- Gilchrist, S., Gilbert, N., Perry, P., Ostlund, C., Worman, H. J., Bickmore, W. A. (2004). Altered protein dynamics of disease-associated lamin A mutants. *BMC Cell Biology*, 5(1), 46. <https://doi.org/10.1186/1471-2121-5-46>
- Goto, M., O'Brien, D. A. & Eddy, E. M. (2010). Speriolin is a novel human and mouse sperm centrosome protein. *Human Reproduction*, 25(8), 1884–1894. <https://doi.org/10.1093/humrep/deq138>
- Göb, E., Schmitt, J., Benavente, R. & Alsheimer, M. (2010). Mammalian Sperm Head Formation Involves Different Polarization of Two Novel LINC Complexes. *PLoS ONE*, 5(8), e12072. <https://doi.org/10.1371/journal.pone.0012072>
- Graham, F. L., Smiley, J., Russell, W. C. & Nairn, R. (1977). Characteristics of a human cell line transformed by DNA from human adenovirus type 5. *The Journal of General Virology*, 36(1), 59–74. <https://doi.org/10.1099/0022-1317-36-1-59>
- Hackstein, J. H., Hochstenbach, R. & Pearson, P. L. (2000). Towards an understanding of the genetics of human male infertility: lessons from flies. *Trends in genetics: TIG*, 16(12), 565–572. [https://doi.org/10.1016/s0168-9525\(00\)02140-5](https://doi.org/10.1016/s0168-9525(00)02140-5)

- Hagan, I. & Yanagida, M. (1995). The product of the spindle formation gene *sad1+* associates with the fission yeast spindle pole body and is essential for viability. *The Journal of Cell Biology*, 129(4), 1033–1047. <https://doi.org/10.1083/jcb.129.4.1033>
- Haque, F., Lloyd, D. J., Smallwood, D. T., Dent, C. L., Shanahan, C. M., Fry, A. M., Trembath, R. C., & Shackleton, S. (2006). SUN1 Interacts with Nuclear Lamin A and Cytoplasmic Nesprins To Provide a Physical Connection between the Nuclear Lamina and the Cytoskeleton. *Molecular and Cellular Biology*, 26(10), 3738–3751. <https://doi.org/10.1128/MCB.26.10.3738-3751.2006>
- Hasan, S., Güttinger, S., Mühlhäusser, P., Anderegg, F., Bürgler, S. & Kutay, U. (2006). Nuclear envelope localization of human UNC84A does not require nuclear lamins. *FEBS letters*, 580(5), 1263–1268. <https://doi.org/10.1016/j.febslet.2006.01.039>
- Hermo, L., Pelletier, R.-M., Cyr, D. G., & Smith, C. E. (2009b). Surfing the wave, cycle, life history, and genes/proteins expressed by testicular germ cells. Part 3: Developmental changes in spermatid flagellum and cytoplasmic droplet and interaction of sperm with the zona pellucida and egg plasma membrane. *Microscopy Research and Technique*, 73(4), 320–363. <https://doi.org/10.1002/jemt.20784>
- Hermo, L., Pelletier, R. M., Cyr, D. G. & Smith, C. E. (2010). Surfing the wave, cycle, life history, and genes/proteins expressed by testicular germ cells. Part 1: Background to spermatogenesis, spermatogonia, and spermatocytes. *Microscopy Research and Technique*, 73(4), 241–278. <https://doi.org/10.1002/jemt.20783>
- Hinegardner, R. T., Engelberg, J. (1963). Rationale for a universal genetic code. *Science*, 142(3595), 1083-1085. <https://doi.org/10.1126/science.142.3595.1083>
- Hino, N., Okazaki, Y., Kobayashi, T., Hayashi, A., Sakamoto, K. & Yokoyama, S. (2005). Protein photo-cross-linking in mammalian cells by site-specific incorporation of a photoreactive amino acid. *Nature Methods*, 2(3), 201–206. <https://doi.org/10.1038/nmeth739>
- Hodzic, D. M., Yeater, D. B., Bengtsson, L., Otto, H. & Stahl, P. D. (2004). Sun2 Is a Novel Mammalian Inner Nuclear Membrane Protein. *Journal of Biological Chemistry*, 279(24), 25805–25812. <https://doi.org/10.1074/jbc.M313157200>
- Hofferbert, S., Burfeind, P., Hoyer-Fender, S., Lange, R., Haldl, G. & Engel, W. (1993). A homozygous deletion of 27 base pairs in the coding region of the human outer dense fiber protein gene does not result in a pathologic phenotype. *Human Molecular Genetics*, 2(12), 2167–2170. <https://doi.org/10.1093/hmg/2.12.2167>
- Horvitz, H. R. & Sulston, J. E. (1980). Isolation and genetic characterization of cell-lineage mutants of the nematode *Caenorhabditis elegans*. *Genetics*, 96(2), 435–454.
- Hoyer-Fender, S., Burfeind, P. & Hameister, H. (1995). Sequence of mouse *Odf1* cDNA and its chromosomal localization: Extension of the linkage group between human

- chromosome 8 and mouse chromosome 15. *Cytogenetics and Cell Genetics*, 70(3–4), 200–204. <https://doi.org/10.1159/000134033>
- Hoyer-Fender, S. (2010). Centriole maturation and transformation to basal body. *Seminars in Cell & Developmental Biology*, 21(2), 142–147. <https://doi.org/10.1016/j.semcd.2009.07.002>
- Hoyer-Fender, S. (2012). Centrosomes in fertilization, early embryonic development, stem cell division, and cancer. *Atlas of Genetics and Cytogenetics in Oncology and Haematology*, 16(4):306-319. <https://doi.org/10.4267/2042/47311>
- Inobe, T. & Nukina, N. (2016). Rapamycin-induced oligomer formation system of FRB–FKBP fusion proteins. *Journal of Bioscience and Bioengineering*, 122(1), 40–46. <https://doi.org/10.1016/j.jbiosc.2015.12.004>
- Ito, C., Akutsu, H., Yao, R., Yoshida, K., Yamatoya, K., Mutoh, T., Makino, T., Aoyama, K., Ishikawa, H., Kunimoto, K., Tsukita, S., Noda, T., Kikkawa, M. & Toshimori, K. (2019). Odf2 haploinsufficiency causes a new type of decapitated and decaudated spermatozoa, Odf2-DDS, in mice. *Scientific Reports*, 9(1), 14249. <https://doi.org/10.1038/s41598-019-50516-2>
- Iwashita, T. & Oura, C. (1980). A Three Dimensional Analysis of the Capitellum and Striated Columns in the Sperm Neck Region of the Mouse. *Okajimas Folia Anatomica Japonica*, 56(6), 361–381. [https://doi.org/10.2535/ofaj1936.56.6\\_361](https://doi.org/10.2535/ofaj1936.56.6_361)
- Kamal, A., Mansour, R., Fahmy, I., Serour, G., Rhodes, C. & Aboulghar, M. (1999). Easily decapitated spermatozoa defect: a possible cause of unexplained infertility. *Human reproduction (Oxford, England)*, 14(11), 2791–2795. <https://doi.org/10.1093/humrep/14.11.2791>
- Kauer, J. C., Erickson-Viitanen, S., Wolfe, H. R. & DeGrado, W. F. (1986). p-Benzoyl-L-phenylalanine, a new photoreactive amino acid. Photolabeling of calmodulin with a synthetic calmodulin-binding peptide. *The Journal of biological chemistry*, 261(23), 10695–10700.
- Kellogg, D. R., Moritz, M. & Alberts, B. M. (1994). The Centrosome and Cellular Organization. *Annual Review of Biochemistry*, 63(1), 639–674. <https://doi.org/10.1146/annurev.bi.63.070194.003231>
- Kelly, S., Georgomanolis, T., Zirkel, A., Diermeier, S., O'Reilly, D., Murphy, S., Längst, G., Cook, P. R. & Papantonis, A. (2015). Splicing of many human genes involves sites embedded within introns. *Nucleic acids research*, 43(9), 4721–4732. <https://doi.org/10.1093/nar/gkv386>
- Kierszenbaum, A. L., Rivkin, E. & Tres, L. L. (2003). Acroplaxome, an F-Actin–Keratin-containing Plate, Anchors the Acrosome to the Nucleus during Shaping of the Spermatid



Head. *Molecular Biology of the Cell*, 14(11), 4628–4640.  
<https://doi.org/10.1091/mbc.e03-04-0226>

- Kierszenbaum, A. L., Rivkin, E., Tres, L. L., Yoder, B. K., Haycraft, C. J., Bornens, M. & Rios, R. M. (2011). GMAP210 and IFT88 are present in the spermatid golgi apparatus and participate in the development of the acrosome-acroplaxome complex, head-tail coupling apparatus and tail. *Developmental Dynamics*, 240(3), 723–736.  
<https://doi.org/10.1002/dvdy.22563>
- Kierszenbaum, A. L. & Tres, L. L. (2002). Bypassing natural sperm selection during fertilization: The azh mutant offspring experience and the alternative of spermiogenesis in vitro. *Molecular and Cellular Endocrinology*, 187(1–2), 133–138.  
[https://doi.org/10.1016/S0303-7207\(01\)00692-X](https://doi.org/10.1016/S0303-7207(01)00692-X)
- Kierszenbaum, A. L. & Tres, L. L. (2004). The acrosome-acroplaxome-manchette complex and the shaping of the spermatid head. *Archives of Histology and Cytology*, 67(4), 271–284.  
<https://doi.org/10.1679/aohc.67.271>
- Kierszenbaum, A. L. & Tres, L. L. (2016). *Histology and Cell Biology: An Introduction to Pathology—4th Edition*. Philadelphia, PA: Elsevier Saunders.
- Kite, G. L. (1913). The Relative Permeability of the Surface and Interior Portions of the Cytoplasm of Animal and Plant Cells. (A Preliminary Paper). *Biological Bulletin*, 25(1), 1. <https://doi.org/10.2307/1536080>
- Knight, R., Freeland, S. & Landweber, L. (2001). Rewiring the keyboard: evolvability of the genetic code. *Nature Reviews. Genetics*, 2(1), 49–58. <https://doi.org/10.1038/35047500>
- Kochanski, R. S. & Borisy, G. G. (1990). Mode of centriole duplication and distribution. *The Journal of Cell Biology*, 110(5), 1599–1605. <https://doi.org/10.1083/jcb.110.5.1599>
- Kracklauer, M. P., Wiora, H. M., Deery, W. J., Chen, X., Bolival, B., Romanowicz, D., Simonette, R. A., Fuller, M. T., Fischer, J. A. & Beckingham, K. M. (2010). The Drosophila SUN protein Spag4 cooperates with the coiled-coil protein Yuri Gagarin to maintain association of the basal body and spermatid nucleus. *Journal of Cell Science*, 123(Pt 16), 2763–2772. <https://doi.org/10.1242/jcs.066589>
- Krimm, I., Ostlund, C., Gilquin, B., Couprie, J., Hossenlopp, P., Mornon, J. P., Bonne, G., Courvalin, J. C., Worman, H. J. & Zinn-Justin, S. (2002). The Ig-like structure of the C-terminal domain of lamin A/C, mutated in muscular dystrophies, cardiomyopathy, and partial lipodystrophy. *Structure (London, England: 1993)*, 10(6), 811–823.  
[https://doi.org/10.1016/s0969-2126\(02\)00777-3](https://doi.org/10.1016/s0969-2126(02)00777-3)
- Lee, C. & Chen, L. B. (1988). Dynamic behavior of endoplasmic reticulum in living cells. *Cell*, 54(1), 37–46. [https://doi.org/10.1016/0092-8674\(88\)90177-8](https://doi.org/10.1016/0092-8674(88)90177-8)

- Lehti, M. S., Kotaja, N. & Sironen, A. (2013). KIF3A is essential for sperm tail formation and manchette function. *Molecular and Cellular Endocrinology*, 377(1–2), 44–55. <https://doi.org/10.1016/j.mce.2013.06.030>
- Li, D. & Roberts, R. (2001). WD-repeat proteins: structure characteristics, biological function, and their involvement in human diseases. *Cellular and molecular life sciences : CMLS*, 58(14), 2085–2097. <https://doi.org/10.1007/pl00000838>
- Lindemann, C. B. (1996). Functional significance of the outer dense fibers of mammalian sperm examined by computer simulations with the geometric clutch model. *Cell Motility and the Cytoskeleton*, 34(4), 258–270. [https://doi.org/10.1002/\(SICI\)1097-0169\(1996\)34:4<258::AID-CM1>3.0.CO;2-4](https://doi.org/10.1002/(SICI)1097-0169(1996)34:4<258::AID-CM1>3.0.CO;2-4)
- Liška, F., Gosele, C., Popova, E., Chyliková, B., Křenová, D., Křen, V., Bader, M., Tres, L. L., Hubner, N. & Kierszenbaum, A. L. (2013). Overexpression of Full-Length Centrobin Rescues Limb Malformation but Not Male Fertility of the Hypodactylous (hd) Rats. *PLoS ONE*, 8(4), e60859. <https://doi.org/10.1371/journal.pone.0060859>
- Liška, F., Gosele, C., Rivkin, E., Tres, L., Cardoso, M. C., Domaing, P., Krejčí, E., Šnajdr, P., Lee-Kirsch, M. A., Rooij, D. G. de, Křen, V., Křenová, D., Kierszenbaum, A. L. & Hubner, N. (2009). Rat *hd* Mutation Reveals an Essential Role of Centrobin in Spermatid Head Shaping and Assembly of the Head-Tail Coupling Apparatus1. *Biology of Reproduction*, 81(6), 1196–1205. <https://doi.org/10.1095/biolreprod.109.078980>
- Liu, W., Brock, A., Chen, S., Chen, S. & Schultz, P. G. (2007). Genetic incorporation of unnatural amino acids into proteins in mammalian cells. *Nature Methods*, 4(3), 239–244. <https://doi.org/10.1038/nmeth1016>
- Longenecker, G. & Kulkarni, A. B. (2009). Generation of gene knockout mice by ES cell microinjection. *Current protocols in cell biology, Chapter 19*, Unit–19.14.36. <https://doi.org/10.1002/0471143030.cb1914s44>
- Łuksza, M., Queguigner, I., Verlhac, M.-H. & Brunet, S. (2013). Rebuilding MTOCs upon centriole loss during mouse oogenesis. *Developmental Biology*, 382(1), 48–56. <https://doi.org/10.1016/j.ydbio.2013.07.029>
- Ma, H. T., Niu, C. M., Xia, J., Shen, X. Y., Xia, M. M., Hu, Y. Q. & Zheng, Y. (2018). Stimulated by retinoic acid gene 8 (Stra8) plays important roles in many stages of spermatogenesis. *Asian journal of andrology*, 20(5), 479–487. [https://doi.org/10.4103/aja.aja\\_26\\_18](https://doi.org/10.4103/aja.aja_26_18)
- MacKinnon, E. A., Abraham, P. J. & Svatek, A. (1973). Long link induction between the microtubules of the manchette in intermediate stages of spermiogenesis. *Zeitschrift Für Zellforschung Und Mikroskopische Anatomie (Vienna, Austria: 1948)*, 136(4), 447–460. <https://doi.org/10.1007/BF00307363>

- Malone, C. J., Fixsen, W. D., Horvitz, H. R. & Han, M. (1999). UNC-84 localizes to the nuclear envelope and is required for nuclear migration and anchoring during *C. elegans* development. *Development*, *126*(14), 3171–3181. <https://dev.biologists.org/content/126/14/3171>
- Malone, C. J., Misner, L., Le Bot, N., Tsai, M.-C., Campbell, J. M., Ahringer, J. & White, J. G. (2003). The *C. elegans* Hook Protein, ZYG-12, Mediates the Essential Attachment between the Centrosome and Nucleus. *Cell*, *115*(7), 825–836. [https://doi.org/10.1016/S0092-8674\(03\)00985-1](https://doi.org/10.1016/S0092-8674(03)00985-1)
- Manandhar, G. & Schatten, G. (2000). Centrosome reduction during Rhesus spermiogenesis: Gamma-tubulin, centrin, and centriole degeneration. *Molecular Reproduction and Development*, *56*(4), 502–511. [https://doi.org/10.1002/1098-2795\(200008\)56:4<502::AID-MRD8>3.0.CO;2-Q](https://doi.org/10.1002/1098-2795(200008)56:4<502::AID-MRD8>3.0.CO;2-Q)
- Manandhar, G., Sutovsky, P., Joshi, H. C., Stearns, T. & Schatten, G. (1998). Centrosome Reduction during Mouse Spermiogenesis. *Developmental Biology*, *203*(2), 424–434. <https://doi.org/10.1006/dbio.1998.8947>
- Martin, G. R. (1981). Isolation of a pluripotent cell line from early mouse embryos cultured in medium conditioned by teratocarcinoma stem cells. *Proceedings of the National Academy of Sciences*, *78*(12), 7634–7638. <https://doi.org/10.1073/pnas.78.12.7634>
- Matzuk, M. M. & Lamb, D. J. (2002). Genetic dissection of mammalian fertility pathways. *Nature cell biology*, *4 Suppl*, s41-s49. <https://doi.org/10.1038/ncb-nm-fertilityS41>
- Mendoza-Lujambio, I. (2002). The Hook1 gene is non-functional in the abnormal spermatozoon head shape (azh) mutant mouse. *Human Molecular Genetics*, *11*(14), 1647–1658. <https://doi.org/10.1093/hmg/11.14.1647>
- Meuwissen, R. L., Offenberg, H. H., Dietrich, A. J., Riesewijk, A., van Iersel, M. & Heyting, C. (1992). A coiled-coil related protein specific for synapsed regions of meiotic prophase chromosomes. *The EMBO journal*, *11*(13), 5091–5100.
- Minn, I., Rolls, M. M., Hanna-Rose, W. & Malone, C. J. (2009). SUN-1 and ZYG-12, Mediators of Centrosome–Nucleus Attachment, Are a Functional SUN/KASH Pair in *Caenorhabditis elegans*. *Molecular Biology of the Cell*, *20*(21), 4586–4595. <https://doi.org/10.1091/mbc.E08-10-1034>
- Miyamoto, T., Tsujimura, A., Miyagawa, Y., Koh, E., Namiki, M. & Sengoku, K. (2012). Male Infertility and Its Causes in Human. *Advances in Urology*, *2012*, 1–7. <https://doi.org/10.1155/2012/384520>
- Morales, C. R., Oko, R. & Clermont, Y. (1994). Molecular cloning and developmental expression of an mRNA encoding the 27 kDa outer dense fiber protein of rat spermatozoa. *Molecular Reproduction and Development*, *37*(2), 229–240. <https://doi.org/10.1002/mrd.1080370215>

- Nebel, B. R., Amarose, A. P. & Hackett, E. M. (1961). Calendar of gametogenic development in the prepuberal male mouse. *Science*, *134*, 832–833. <https://doi.org/10.1126/science.134.3482.832>
- Neer, E. J., Schmidt, C. J., Nambudripad, R. & Smith, T. F. (1994). The ancient regulatory-protein family of WD-repeat proteins. *Nature*, *371*(6495), 297–300. <https://doi.org/10.1038/371297a0>
- Netzel-Arnett, S., Bugge, T. H., Hess, R. A., Carnes, K., Stringer, B. W., Scarman, A. L., Hooper, J. D., Tonks, I. D., Kay, G. F. & Antalis, T. M. (2009). The Glycosylphosphatidylinositol-Anchored Serine Protease PRSS21 (Testisin) Imparts Murine Epididymal Sperm Cell Maturation and Fertilizing Ability<sup>1</sup>. *Biology of Reproduction*, *81*(5), 921–932. <https://doi.org/10.1095/biolreprod.109.076273>
- Nozawa, Y. I., Yao, E., Gacayan, R., Xu, S.-M. & Chuang, P.-T. (2014). Mammalian Fused is essential for sperm head shaping and periaxonemal structure formation during spermatogenesis. *Developmental Biology*, *388*(2), 170–180. <https://doi.org/10.1016/j.ydbio.2014.02.002>
- Oakberg, E. F. (1956). A description of spermiogenesis in the mouse and its use in analysis of the cycle of the seminiferous epithelium and germ cell renewal. *American Journal of Anatomy*, *99*(3), 391–413. <https://doi.org/10.1002/aja.1000990303>
- O'Donnell, L., & O'Bryan, M. K. (2014). Microtubules and spermatogenesis. *Seminars in Cell & Developmental Biology*, *30*, 45–54. <https://doi.org/10.1016/j.semcdb.2014.01.003>
- Oko, R. (1988). Comparative Analysis of Proteins from the Fibrous Sheath and Outer Dense Fibers of Rat Spermatozoa<sup>1</sup>. *Biology of Reproduction*, *39*(1), 169–182. <https://doi.org/10.1095/biolreprod39.1.169>
- Osawa, S., Jukes, T. H., Watanabe, K. & Muto, A. (1992). Recent evidence for evolution of the genetic code. *Microbiological reviews*, *56*(1), 229–264. <https://doi.org/10.1128/MMBR.56.1.229-264.1992>
- Padmakumar, V. C. (2005). The inner nuclear membrane protein Sun1 mediates the anchorage of Nesprin-2 to the nuclear envelope. *Journal of Cell Science*, *118*(15), 3419–3430. <https://doi.org/10.1242/jcs.02471>
- Paine, P. L. & Feldherr, C. M. (1972). Nucleocytoplasmic exchange of macromolecules. *Experimental cell research*, *74*(1), 81–98. [https://doi.org/10.1016/0014-4827\(72\)90483-1](https://doi.org/10.1016/0014-4827(72)90483-1)
- Palmiter, R. D., Chen, H. Y. & Brinster, R. L. (1982). Differential regulation of metallothionein-thymidine kinase fusion genes in transgenic mice and their offspring. *Cell*, *29*(2), 701–710. [https://doi.org/10.1016/0092-8674\(82\)90186-6](https://doi.org/10.1016/0092-8674(82)90186-6)

- Pasch, E., Link, J., Beck, C., Scheuerle, S. & Alsheimer, M. (2015). The LINC complex component Sun4 plays a crucial role in sperm head formation and fertility. *Biology Open*, 4(12), 1792–1802. <https://doi.org/10.1242/bio.015768>
- Pasek, R. C., Malarkey, E., Berbari, N. F., Sharma, N., Kesterson, R. A., Tres, L. L., Kierszenbaum, A. L. & Yoder, B. K. (2016). Coiled-coil domain containing 42 (Ccdc42) is necessary for proper sperm development and male fertility in the mouse. *Developmental Biology*, 412(2), 208–218. <https://doi.org/10.1016/j.ydbio.2016.01.042>
- Perotti, M. E., Giarola, A. & Gioria, M. (1981). Ultrastructural study of the decapitated sperm defect in an infertile man. *Journal of Reproduction and Fertility*, 63(2), 543–549. <https://doi.org/10.1530/jrf.0.0630543>
- Petersen, C. (1999). Outer dense fibre proteins from human sperm tail: Molecular cloning and expression analyses of two cDNA transcripts encoding proteins of 70 kDa. *Molecular Human Reproduction*, 5(7), 627–635. <https://doi.org/10.1093/molehr/5.7.627>
- Petersen, C., Aumüller, G., Bahrami, M. & Hoyer-Fender, S. (2002). Molecular cloning of Odf3 encoding a novel coiled-coil protein of sperm tail outer dense fibers. *Molecular Reproduction and Development*, 61(1), 102–112. <https://doi.org/10.1002/mrd.1136>
- Qi, Y., Jiang, M., Yuan, Y., Bi, Y., Zheng, B., Guo, X., Huang, X., Zhou, Z. & Sha, J. (2013). ADP-ribosylation factor-like 3, a manchette-associated protein, is essential for mouse spermiogenesis. *Molecular Human Reproduction*, 19(5), 327–335. <https://doi.org/10.1093/molehr/gat001>
- Rattner, J. B. & Olson, G. (1973). Observations on the fine structure of the nuclear ring of the mammalian spermatid. *Journal of Ultrastructure Research*, 43(5), 438–444. [https://doi.org/10.1016/S0022-5320\(73\)90020-8](https://doi.org/10.1016/S0022-5320(73)90020-8)
- Razafsky, D. & Hodzic, D. (2009). Bringing KASH under the SUN: The many faces of nucleocytoskeletal connections. *The Journal of Cell Biology*, 186(4), 461–472. <https://doi.org/10.1083/jcb.200906068>
- Rober, R. A., Weber, K. & Osborn, M. (1989). Differential timing of nuclear lamin A/C expression in the various organs of the mouse embryo and the young animal: A developmental study. *Development*, 105(2), 365. <http://dev.biologists.org/content/105/2/365.abstract>
- Russell, L. D. (1990). *Histological and histopathological evaluation of the testis*. Clearwater, Fla.: Cache River Press. <https://agris.fao.org/agris-search/search.do?recordID=US201300697285>
- Salpingidou, G., Smertenko, A., Hausmanowa-Petrucewicz, I., Hussey, P. J. & Hutchison, C. J. (2007). A novel role for the nuclear membrane protein emerin in association of the centrosome to the outer nuclear membrane. *The Journal of Cell Biology*, 178(6), 897–904. <https://doi.org/10.1083/jcb.200702026>

- Schalles, U., Shao, X., van der Hoorn, F. A. & Oko, R. (1998). Developmental Expression of the 84-kDa ODF Sperm Protein: Localization to both the Cortex and Medulla of Outer Dense Fibers and to the Connecting Piece. *Developmental Biology*, 199(2), 250–260. <https://doi.org/10.1006/dbio.1998.8931>
- Schatten, H., Schatten, G., Mazia, D., Balczon, R. & Simerly, C. (1986). Behavior of centrosomes during fertilization and cell division in mouse oocytes and in sea urchin eggs. *Proceedings of the National Academy of Sciences*, 83(1), 105–109. <https://doi.org/10.1073/pnas.83.1.105>
- Schatten, H., & Sun, Q. Y. (2009). The role of centrosomes in mammalian fertilization and its significance for ICSI. *Molecular Human Reproduction*, 15(9), 531–538. <https://doi.org/10.1093/molehr/gap049>
- Schirmer, E. C., Florens, L., Guan, T., Yates, J. R. & Gerace, L. (2003). Nuclear Membrane Proteins with Potential Disease Links Found by Subtractive Proteomics. *Science*, 301(5638), 1380–1382. <https://doi.org/10.1126/science.1088176>
- Schmitt, J., Benavente, R., Hodzic, D., Höög, C., Stewart, C. L. & Alsheimer, M. (2007). Transmembrane protein Sun2 is involved in tethering mammalian meiotic telomeres to the nuclear envelope. *Proceedings of the National Academy of Sciences of the United States of America*, 104(18), 7426–7431. <https://doi.org/10.1073/pnas.0609198104>
- Schütz, W., Alsheimer, M., Öllinger, R. & Benavente, R. (2005). Nuclear envelope remodeling during mouse spermiogenesis: Postmeiotic expression and redistribution of germline lamin B3. *Experimental Cell Research*, 307(2), 285–291. <https://doi.org/10.1016/j.yexcr.2005.03.023>
- Schweizer, S. & Hoyer-Fender, S. (2009). Mouse Odf2 localizes to centrosomes and basal bodies in adult tissues and to the photoreceptor primary cilium. *Cell and Tissue Research* 338, 295. <https://doi.org/10.1007/s00441-009-0861-3>
- Sha, Y. W., Xu, X., Ji, Z. Y., Lin, S. B., Wang, X., Qiu, P. P., Zhou, Y., Mei, L. B., Su, Z. Y., Li, L. & Li, P. (2018). Genetic contribution of SUN5 mutations to acephalic spermatozoa in Fujian China. *Gene*, 647, 221–225. <https://doi.org/10.1016/j.gene.2018.01.035>
- Sha, Y. W., Wang, X., Xu, X., Ding, L., Liu, W. S., Li, P., Su, Z. Y., Chen, J., Mei, L. B., Zheng, L. K., Wang, H. L., Kong, S. B., You, M. & Wu, J. F. (2019). Biallelic mutations in PMFBP1 cause acephalic spermatozoa. *Clinical genetics*, 95(2), 277–286. <https://doi.org/10.1111/cge.13461>
- Shang, Y., Yan, J., Tang, W., Liu, C., Xiao, S., Guo, Y., Yuan, L., Chen, L., Jiang, H., Guo, X., Qiao, J. & Li, W. (2018). Mechanistic insights into acephalic spermatozoa syndrome-associated mutations in the human SUN5 gene. *The Journal of Biological Chemistry*, 293(7), 2395–2407. <https://doi.org/10.1074/jbc.RA117.000861>

- Shang, Y., Zhu, F., Wang, L., Ouyang, Y.-C., Dong, M.-Z., Liu, C., Zhao, H., Cui, X., Ma, D., Zhang, Z., Yang, X., Guo, Y., Liu, F., Yuan, L., Gao, F., Guo, X., Sun, Q.-Y., Cao, Y. & Li, W. (2017). Essential role for SUN5 in anchoring sperm head to the tail. *ELife*, 6, e28199. <https://doi.org/10.7554/eLife.28199>
- Shao, X., Tarnasky, H. A., Lee, J. P., Oko, R. & van der Hoorn, F. A. (1999). Spag4, a Novel Sperm Protein, Binds Outer Dense-Fiber Protein Odf1 and Localizes to Microtubules of Manchette and Axoneme. *Developmental Biology*, 211(1), 109–123. <https://doi.org/10.1006/dbio.1999.9297>
- Shao, X., Tarnasky, H. A., Schalles, U., Oko, R. & van der Hoorn, F. A. (1997). Interactional Cloning of the 84-kDa Major Outer Dense Fiber Protein Odf84: leucine zippers mediate associations of Odf84 and Odf27. *Journal of Biological Chemistry*, 272(10), 6105–6113. <https://doi.org/10.1074/jbc.272.10.6105>
- Shao, X. & van der Hoorn, F. A. (1996). Self-Interaction of the Major 27-Kilodalton Outer Dense Fiber Protein is in Part Mediated by a Leucine Zipper Domain in the Rat1. *Biology of Reproduction*, 55(6), 1343–1350. <https://doi.org/10.1095/biolreprod55.6.1343>
- Shao, X., Xue, J. & van der Hoorn, F. A. (2001). Testicular protein Spag5 has similarity to mitotic spindle protein Deepest and binds outer dense fiber protein Odf1. *Molecular Reproduction and Development*, 59(4), 410–416. <https://doi.org/10.1002/mrd.1047>
- Sharlip, I. D., Jarow, J. P., Belker, A. M., Lipshultz, L. I., Sigman, M., Thomas, A. J., Schlegel, P. N., Howards, S. S., Nehra, A., Damewood, M. D., Overstreet, J. W. & Sadovsky, R. (2002). Best practice policies for male infertility. *Fertility and Sterility*, 77(5), 873–882. [https://doi.org/10.1016/s0015-0282\(02\)03105-9](https://doi.org/10.1016/s0015-0282(02)03105-9)
- Sharma, A. (2017). Male Infertility: Evidences, Risk Factors, Causes, Diagnosis and Management in Human. *Annals of Clinical and Laboratory Research*, 05(03). <https://doi.org/10.21767/2386-5180.1000188>
- Sharp, P. M. & Bulmer, M. (1988). Selective differences among translation termination codons. *Gene*, 63 (1), 141-145. [https://doi.org/10.1016/0378-1119\(88\)90553-7](https://doi.org/10.1016/0378-1119(88)90553-7)
- Simerly, C., Wu, G.-J., Zoran, S., Ord, T., Rawlins, R., Jones, J., Navara, C., Gerrity, M., Rinehart, J., Binor, Z., Asch, R. & Schatten, G. (1995). The paternal inheritance of the centrosome, the cell's microtubule-organizing center, in humans, and the implications for infertility. *Nature Medicine*, 1(1), 47–52. <https://doi.org/10.1038/nm0195-47>
- Starr, D. A. (2002). Role of ANC-1 in Tethering Nuclei to the Actin Cytoskeleton. *Science*, 298(5592), 406–409. <https://doi.org/10.1126/science.1075119>
- Starr, D. A. (2003). ANChors away: An actin based mechanism of nuclear positioning. *Journal of Cell Science*, 116(2), 211–216. <https://doi.org/10.1242/jcs.00248>

- Starr, D. A. & Fridolfsson, H. N. (2010). Interactions Between Nuclei and the Cytoskeleton Are Mediated by SUN-KASH Nuclear-Envelope Bridges. *Annual Review of Cell and Developmental Biology*, 26(1), 421–444. <https://doi.org/10.1146/annurev-cellbio-100109-104037>
- Starr, D. A. & Han, M. (2003). ANChors away: An actin based mechanism of nuclear positioning. *Journal of Cell Science*, 116(2), 211. <https://doi.org/10.1242/jcs.00248>
- Tanaka, H., Iguchi, N., Isotani, A., Kitamura, K., Toyama, Y., Matsuoka, Y., Onishi, M., Masai, K., Maekawa, M., Toshimori, K., Okabe, M. & Nishimune, Y. (2005). HANP1/H1T2, a Novel Histone H1-Like Protein Involved in Nuclear Formation and Sperm Fertility. *Molecular and Cellular Biology*, 25(16), 7107–7119. <https://doi.org/10.1128/MCB.25.16.7107-7119.2005>
- Tapia Contreras, C. & Hoyer-Fender, S. (2019). CCDC42 Localizes to Manchette, HTCA and Tail and Interacts With ODF1 and ODF2 in the Formation of the Male Germ Cell Cytoskeleton. *Frontiers in Cell and Developmental Biology*, 7, 151. <https://doi.org/10.3389/fcell.2019.00151>
- Todaró, G. J. & Green, H. (1963). Quantitative studies of the growth of mouse embryo cells in culture and their development into established lines. *The Journal of Cell Biology*, 17, 299–313. <https://doi.org/10.1083/jcb.17.2.299>
- Tokuhiro, K., Isotani, A., Yokota, S., Yano, Y., Oshio, S., Hirose, M., Wada, M., Fujita, K., Ogawa, Y., Okabe, M., Nishimune, Y. & Tanaka, H. (2009). OAZ-t/OAZ3 Is Essential for Rigid Connection of Sperm Tails to Heads in Mouse. *PLoS Genetics*, 5(11), e1000712. <https://doi.org/10.1371/journal.pgen.1000712>
- Toyama, Y., Iwamoto, T., Yajima, M., Baba, K. & Yuasa, S. (2000). Decapitated and decaudated spermatozoa in man, and pathogenesis based on the ultrastructure. *International Journal of Andrology*, 23(2), 109–115. <https://doi.org/10.1046/j.1365-2605.2000.t01-1-00217.x>
- Tzur, Y. B., Wilson, K. L. & Gruenbaum, Y. (2006). SUN-domain proteins: “Velcro” that links the nucleoskeleton to the cytoskeleton. *Nature Reviews Molecular Cell Biology*, 7(10), 782–788. <https://doi.org/10.1038/nrm2003>
- Urbani, L. & Stearns, T. (1999). The centrosome. *Current Biology: CB*, 9(9), R315-317. [https://doi.org/10.1016/s0960-9822\(99\)80201-2](https://doi.org/10.1016/s0960-9822(99)80201-2)
- Van der Hoorn, F. A., Tarnasky, H. A. & Nordeen, S. K. (1990). A new rat gene RT7 is specifically expressed during spermatogenesis. *Developmental Biology*, 142(1), 147–154. [https://doi.org/10.1016/0012-1606\(90\)90158-F](https://doi.org/10.1016/0012-1606(90)90158-F)
- Vera, J. C., Brito, M., Zuvic, T. & Burzio, L. O. (1984). Polypeptide composition of rat sperm outer dense fibers. A simple procedure to isolate the fibrillar complex. *The Journal of Biological Chemistry*, 259(9), 5970–5977.



- Villasante, A., Wang, D., Dobner, P., Dolph, P., Lewis, S. A. & Cowan, N. J. (1986). Six mouse alpha-tubulin mRNAs encode five distinct isotypes: testis-specific expression of two sister genes. *Molecular and cellular biology*, 6(7), 2409–2419. <https://doi.org/10.1128/mcb.6.7.2409>
- Vogt, P. H. (2004). Molecular genetics of human male infertility: from genes to new therapeutic perspectives. *Current pharmaceutical design*, 10(5), 471–500. <https://doi.org/10.2174/1381612043453261>
- Vorobjev, I. A. & Chentsov, Y. S. (1980). The ultrastructure of centriole in mammalian tissue culture cells. *Cell Biology International Reports*, 4(11), 1037–1044. [https://doi.org/10.1016/0309-1651\(80\)90177-0](https://doi.org/10.1016/0309-1651(80)90177-0)
- Vorobjev, I. A., & Chentsov, Y. S. (1982). Centrioles in the cell cycle. I. Epithelial cells. *The Journal of Cell Biology*, 93(3), 938–949. <https://doi.org/10.1083/jcb.93.3.938>
- Walenta, J. H., Didier, A. J., Liu, X. & Krämer, H. (2001). The Golgi-Associated Hook3 Protein Is a Member of a Novel Family of Microtubule-Binding Proteins. *The Journal of Cell Biology*, 152(5), 923–934. <https://doi.org/10.1083/jcb.152.5.923>
- Wang, Q., Du, X., Cai, Z. & Greene, M. I. (2006). Characterization of the Structures Involved in Localization of the SUN Proteins to the Nuclear Envelope and the Centrosome. *DNA and Cell Biology*, 25(10), 554–562. <https://doi.org/10.1089/dna.2006.25.554>
- Watson, M. L. (1955). The nuclear envelope. *The Journal of Biophysical and Biochemical Cytology*, 1(3), 257–270. <https://www.ncbi.nlm.nih.gov/pmc/articles/PMC2223813/>
- Wilhelmsen, K., Ketema, M., Truong, H. & Sonnenberg, A. (2006). KASH-domain proteins in nuclear migration, anchorage and other processes. *Journal of Cell Science*, 119(24), 5021–5029. <https://doi.org/10.1242/jcs.03295>
- Wilkie, T. M., Brinster, R. L. & Palmiter, R. D. (1986). Germline and somatic mosaicism in transgenic mice. *Developmental Biology*, 118(1), 9–18. [https://doi.org/10.1016/0012-1606\(86\)90068-0](https://doi.org/10.1016/0012-1606(86)90068-0)
- Woese, C. R., Hinegardner, R. T., Engelberg, J. (1964). Universality in the Genetic Code. *Science*, 144(3621), 1030–1031. <https://doi.org/10.1126/science.144.3621.1030>
- World Health Organization. (2010). WHO laboratory manual for the examination and processing of human semen. (5th ed). World Health Organization. <https://apps.who.int/iris/handle/10665/44261>
- Xie, J. & Schultz, P. G. (2005). An expanding genetic code. *Methods*, 36(3), 227–238. <https://doi.org/10.1016/j.ymeth.2005.04.010>

- Xing, X. W., Li, L.-Y., Liu, G., Fu, J.-J., Tan, X.-J. & Lu, G.-X. (2004). Identification of a Novel Gene SRG4 Expressed at Specific Stages of Mouse Spermatogenesis. *Acta Biochimica et Biophysica Sinica*, 36(5), 351–359. <https://doi.org/10.1093/abbs/36.5.351>
- Yang, K., Meinhardt, A., Zhang, B., Grzmil, P., Adham, I. M. & Hoyer-Fender, S. (2012). The Small Heat Shock Protein ODF1/HSPB10 Is Essential for Tight Linkage of Sperm Head to Tail and Male Fertility in Mice. *Molecular and Cellular Biology*, 32(1), 216–225. <https://doi.org/10.1128/MCB.06158-11>
- Yang, K., Adham, I. M., Meinhardt, A., & Hoyer-Fender, S. (2018). Ultra-structure of the sperm head-to-tail linkage complex in the absence of the spermatid-specific LINC component SPAG4. *Histochemistry and Cell Biology*, 150(1), 49–59. <https://doi.org/10.1007/s00418-018-1668-7>
- Yang, K., Grzmil, P., Meinhardt, A., & Hoyer-Fender, S. (2014). Haplo-deficiency of ODF1/HSPB10 in mouse sperm causes relaxation of head-to-tail linkage. *Reproduction*, 148(5), 499–506. <https://doi.org/10.1530/REP-14-0370>
- Yassine, S., Escoffier, J., Nahed, R. A., Pierre, V., Karaouzene, T., Ray, P. F. & Arnoult, C. (2015). Dynamics of Sun5 Localization during Spermatogenesis in Wild Type and Dpy1912 Knock-Out Mice Indicates That Sun5 Is Not Involved in Acrosome Attachment to the Nuclear Envelope. *PloS one*, 10(3), e0118698. <https://doi.org/10.1371/journal.pone.0118698>
- Ye, Q. & Worman, H. J. (1995). Protein-protein interactions between human nuclear lamins expressed in yeast. *Experimental Cell Research*, 219(1), 292–298. <https://doi.org/10.1006/excr.1995.1230>
- Yuan, L., Liu, J. G., Zhao, J., Brundell, E., Daneholt, B. & Höög, C. (2000). The murine SCP3 gene is required for synaptonemal complex assembly, chromosome synapsis, and male fertility. *Molecular cell*, 5(1), 73–83. [https://doi.org/10.1016/s1097-2765\(00\)80404-9](https://doi.org/10.1016/s1097-2765(00)80404-9)
- Yuan, S., Stratton, C. J., Bao, J., Zheng, H., Bhetwal, B. P., Yanagimachi, R. & Yan, W. (2015). *Spata6* is required for normal assembly of the sperm connecting piece and tight head-tail conjunction. *Proceedings of the National Academy of Sciences*, 112(5), E430–E439. <https://doi.org/10.1073/pnas.1424648112>
- Zarsky, H. A., Cheng, M. & van der Hoorn, F. A. (2003). Novel RING Finger Protein OIP1 Binds to Conserved Amino Acid Repeats in Sperm Tail Protein ODF1. *Biology of Reproduction*, 68(2), 543–552. <https://doi.org/10.1095/biolreprod.102.009076>
- Zegers-Hochschild, F., Adamson, G. D., de Mouzon, J., Ishihara, O., Mansour, R., Nygren, K., Sullivan, E. & Vanderpoel, S. (2009). International Committee for Monitoring Assisted Reproductive Technology (ICMART) and the World Health Organization (WHO) revised glossary of ART terminology, 2009. *Fertility and Sterility*, 92(5), 1520–1524. <https://doi.org/10.1016/j.fertnstert.2009.09.009>

- Zeng, X., Li, K., Yuan, R., Gao, H., Luo, J., Liu, F., Wu, Y., Wu, G. & Yan, X. (2018). Nuclear Envelope-Associated Chromosome Dynamics during Meiotic Prophase I. *Frontiers in Cell and Developmental Biology*, 5, 121. <https://doi.org/10.3389/fcell.2017.00121>
- Zhen, Y. Y., Libotte, T., Munck, M., Noegel, A. A. & Korenbaum, E. (2002). NUANCE, a giant protein connecting the nucleus and actin cytoskeleton. *Journal of Cell Science*, 115(15), 3207–3222. <https://jcs.biologists.org/content/115/15/3207>
- Zhou, J., Du, Y. R., Qin, W. H., Hu, Y. G., Huang, Y. N., Bao, L., Han, D., Mansouri, A. & Xu, G. L. (2009). RIM-BP3 is a manchette-associated protein essential for spermiogenesis. *Development*, 136(3), 373–382. <https://doi.org/10.1242/dev.030858>
- Zhu, F., Liu, C., Wang, F., Yang, X., Zhang, J., Wu, H., Zhang, Z., He, X., Zhang, Z., Zhou, P., Wei, Z., Shang, Y., Wang, L., Zhang, R., Ouyang, Y.-C., Sun, Q.-Y., Cao, Y. & Li, W. (2018). Mutations in PMFBP1 Cause Acephalic Spermatozoa Syndrome. *The American Journal of Human Genetics*, 103(2), 188–199. <https://doi.org/10.1016/j.ajhg.2018.06.010>
- Zhu, F., Wang, F., Yang, X., Zhang, J., Wu, H., Zhang, Z., Zhang, Z., He, X., Zhou, P., Wei, Z., Gecz, J. & Cao, Y. (2016). Biallelic SUN5 Mutations Cause Autosomal-Recessive Acephalic Spermatozoa Syndrome. *The American Journal of Human Genetics*, 99(4), 942–949. <https://doi.org/10.1016/j.ajhg.2016.08.004>
- Zimmerman, W., Sparks, C. A. & Doxsey, S. J. (1999). Amorphous no longer: The centrosome comes into focus. *Current Opinion in Cell Biology*, 11(1), 122–128. [https://doi.org/10.1016/S0955-0674\(99\)80015-5](https://doi.org/10.1016/S0955-0674(99)80015-5)

## 6 Appendix

### 6.1 List of oligonucleotides

**Table 6.1.1** Oligonucleotides for mutation screening in patients with acephalic spermatozoon phenotype

Target gene	Primer	Sequence	Annealing temperature (°C)	Product size (bp)
<i>Odf1</i> Exon1	Odf1-Homo-Exon1-Forward Odf1-Homo-Exon1-Reverse	TGAGGTCATAGAACACAAGC CAGGGTCATTATCCTGAACC	54°C	590 bp
<i>Odf1</i> Exon2	Odf1-Homo-Exon2-Forward Odf1-Homo-Exon2-Reverse	GATTCTGAGGTCTGAGCTCCC GACTTTCACACAACACCAGCAG	54°C	635 bp
<i>Hook1</i> Exon10	Hook1-E10-N-for Exon10-Rev	CAAGGCTTGAAGCTGCAAAAG CTTGACCTCCCTGTACCTGTC	54°C	453 bp
<i>Hook1</i> Exon11	Hook1-E11-N-for Hook1-E11-N-Rev	CCTCTTCTCACTCACTCAC GCTTATTACATGCAACGCTTC	52°C	448 bp
<i>Sun5</i> Exon6	Sun5-Ex7-For Sun5-Ex7-Rev	CAATGCTGGCAAGTGGCATAG TGACTGGTTAGGGTGAGACCT	54°C	218 bp
<i>Sun5</i> Exon8	Sun5-Ex8-Zhu-For Sun5-Ex8-Zhu-Rev	ATGAATGGGTCCAGGGATGG AGATGTTTGGGGCAGAATGG	53°C	284 pb
<i>Sun5</i> Exon11	Sun5-E11-Zhu-For Sun5-E11-Zhu-Rev	AGGGGATCAAAGGTGGGATG ACTTCCAGCCTTAAACCAAGC	53°C	376bp
<i>Sun5</i> Exon13	Sun5-E13-Zhu-For Sun5-E13-Zhu-Rev	TGTCTGTCCTTCTGGCCTC TCAGATGTGAAAGGCTAGCC	52°C	437bp
<i>Arl3</i> Exon3	Arl3-E3-For Arl3-E3-Rev	CCACAACCTGGATGAAACAAGCA CAGTGGCATGATCTTCTGACTTCC	55°C	613 bp

**Table 6.1.2** Oligonucleotides for RT-PCR in *Spag4*-deficient mouse

Target gene	Primer	Sequence	Annealing temperature (°C)	Product size (bp)
<i>Gapdh</i>	rGAPDH-For3	GTCAGATCCACGACGGACAC	52°C	595 bp
	rGAPDH-Rev2	GTATGACTCCACTCACGGCA		
<i>Spag4</i>	Spag4-650for	TGCAGGGAAATCTGCTCC	55°C	546 bp
	Spag4C2-KpnI	GGTACCTTAGAGTCAGCATCTCCGTAGGTTC		
<i>Stra8</i>	Stra8 For	TCACAGCCTCAAAGTGGCAGG	56°C	444 bp
	Stra8 Rev	GCAACAGAGTGGAGGAGGAGT		
<i>Sycp1</i>	MmSycp1f	CGCTACAACCACATGCTTCG	52°C	200 bp
	MmSycp1r	GGAACGCTGGTTAGATCTCCTC		
<i>Sycp3</i>	MSycp3-5' KpnI	GACGGTACCATGCTTCGAGGGTGTGGG	52°C	900 bp
	MSycp3r	TTGACACAATCGTGGAGAGAA		
<i>Odf1</i>	Odf1C	CCGCGGTACCCAAGATCATCTTCCTACA	54°C	800 bp
	Odf1N-TomHindIII	AAGCTTATGGCCGCACTGAGTTG		
<i>Odf1</i>	Odf1N434	CCTCTACTACCCGTGCTG	52°C	548 b
	Odf1C	CCGCGGTACCCAAGATCATCTTCCTACA		
<i>Prm1</i>	mProtamin1f	TCCACCTGCTCACAGGTTGGC	52°C	407 bp
	mProtamin1r	GCAGGCTCCTGTTTTTCATCG		
<i>Hanp1</i>	Hanp1-HIT2-for	GCTGGCTACTTCAGGGTCT	50°C	800 bp
	Hanp1-HIT2-rev	TGTATGCTGGGAGCGTTG		
$\alpha$ -Tubulin	Ma3_For	TTGAGGACCAGTGGTGAGG	55°C	1464 bp
	Ma3_Rev	TTTCCAATGGTGGGGAAGACAT		
$\alpha$ -Tubulin	Ma7_For	CTCGTAGGATCGGCTGAGGTA	54°C	1400 bp
	Ma7_Rev	CCATGCGCTCAGTACTCCT		

**Table 6.1.3** Oligonucleotides for qRT-PCR in *Spag4*-deficient mouse

Target gene	Primer	Sequence
<i>HPRT</i>	mHPRT-For2	GGAGTCCTGTTGATGTTGCC
	mHPRT-Rev2	GGGACGCAGCAACTGACATT
<i>Protamin</i>	Protamin-p1-For	CCCTCTCACCACTTTTCTTACCTT
	Protamin-p1-For	GGCGAGATGCTCTTGAAGTCT
<i>Stra8</i>	Stra8 For	TCACAGCCTCAAAGTGGCAGG
	Stra8 Rev	GCAACAGAGTGGAGGAGGAGT
<i>Odf1</i>	ODF1-p1-Forward	CGGGGCTCTTTTAGTCTTGCTA
	ODF1-p1-Reverse	TTCAAAGCCGCACACATTAC
<i>Hanp1</i>	qHANP1-For	CTGCTGGCTACTTCAGGGTCTGG
	qHANP1-Rev	GGACCTTGTTCTGACCCTCTG

**Table 6.1.4** Oligonucleotides for amber suppression method

Target gene	Primer	Sequence	Annealing temperature (°C)	Product size (bp)
<i>Sun1</i>	Sun1-NheI-F	5`GGTCTGAGACGGTGCTAGCAACATGGACTTT	62°C	2200 bp
	Sun1-BamHI-Rev2	TCTC-3` CTAGGATCCTGGATGGGCTCTCCG		
<i>Sun3</i>	Sun3-NheI-For	CGCTAGCAATGTAACTCGATCATGGAAG	65°C	975 bp
	Sun3-KpnI-Rev	GGGTACCGCAGTGTAATCACTGGGGATG		
<i>Lamin C2</i>	LmnC2-XbaI-For	TCTAGAGGCCAGCCATGGGGAAC	58°C	1408 bp
	LmnC2-KpnI-Rev	CGGTACCAGCGGCGGCTGCCACTCAC		
<i>Lamin B3</i>	LmnB3-XbaI-For	CTCTAGAGCCATGGGGGAGTCGGAATC	58°C	1438 bp
	LmnB3-KpnI-Rev	TGGTACCATCAGTCGGCAGCCCCTTG		

**Table 6.1.5** Oligonucleotides for rapamycin system method

Target gene	Primer	Sequence	Annealing temperature (°C)	Product size (bp)
<i>mECFP-FRB</i>	ECFP-N-NheI FIASH-C-NheI	GCTAGCATGGGCTGCGTGTGCAGCAG GCTAGCGGGCTCCATGCAGCAGCCG	58°C	1100 bp
<i>Luciferase (pGL3)</i>	Luc-NheI-For2 Luc-AgeI-Rev2	GAGCTAGCATGGAAGACGCCAAAAACAT TAACCGGTGCCACGGCGATCTTTCCGCC	58°C	1668 bp
<i>Sun5</i>	Sun5-SacI-N-Rap Sun5-KpnI-C-Rap	GAGCTCATGCCCCGGACGAGGAAC CTTGGTACCGGATAGGGGCTCTAGGTGTG	60°C	1130 bp

**Table 6.1.6** Oligonucleotides for *Spag4l2* investigation

Oligonucleotide name	Oligonucleotides sequence
Primer1	CGGCTAGCGCCACCATGGCCTACCCCTACGACGTG
Primer2	GCCTACCCCTACGACGTGCCCGACTACGCCTCTAGA
primer 3 TM2	CCCGACTACGCCTCTAGAATGAAGATGGGCCTTCTGGTCTC
TM38-58r	GGAATTCGCTGGGTCTGAGTCCTCAGGAA
Spag77-95r EcoRI	GGAATTCGTAAGTGCATGGAAAACATCCA
Spag4XbaI for	GCTCTAGAGCAATGCCCCGGACGAGGAACATC
Spag4KpnI-frameshift	AGCTTGGTACCGACTGGCAAAGGCCCAGCAGTTC
Spag4lC-term-F-HindIII	CCAAGCTTATGCCATCAAAAGTGGAAGTCTGG
Spag4l C-term-rev-EcoRI	GGAATTCGGGATAGGGGCTCTAGGTGTGA

**Table 6.1.7** Oligonucleotides for *Spag4L2*-deficient mice genotyping.

Target gene	Primer	Sequence	Annealing temperature (°C)	Product size (bp)
<i>LacZ</i>	LacInZRev	GTCTGTCTAGCTTCCTCACTG	54°C	694 bp
	SunUp	TGGCATCCTCTGAGGGAG		
<i>LacZ</i>	LacInFor	GGTAAACTGGCTCGGATTAGGG	55°C	211 bp
	LacInRev	TTGACTGTAGCGGCTGATGTTG		
<i>Neomycin</i>	NeoInFor	TTCGGCTATGACTGGGCACAACAG	55°C	282 bp
	NeoInRev	TACTTTCTCGGCAGGAGCAAGGT		
<i>Neomycin</i>	NeoFwd	TCATTCTCAGTATTGTTTTGCC	52°C	507 bp
	SunDown	GAGACTGAGGCCCTAGGAGG		
<i>Neomycin</i>	NeomycinFor	GAACAAGATGGATTGCACG	50°C	1239 bp
	NeoSplitRev	GCAAAACAATACTGAGAATG		
<i>Neomycin</i>	NeomycinFor	GAACAAGATGGATTGCACG	48°C	333 bp
	NeoInRev	TACTTTCTCGGCAGGAGCAAGGT		
<i>Neomycin/Sun5 3'end</i>	NeomycinFor3	GTCAAGACCGACCTGTCCGG	56°C	1441 bp
	Genotype2Rev	GAGCGGTCCTGTCTCCTATG		
<i>Neomycin and Sun5 3'end</i>	Geno2For	AGGACATAGCGTTGGCTACC	52°C	1109 bp
	Geno2Rev	TAGCTGTCATCCTGCCCTA		
<i>Sun5</i> wild type allele	GenotypeFor2	GGAGCTGCTACACTCTGGCTC	57°C	447 bp
	GenotypeRev2	GAGCGGTCCTGTCTCCTATG		

**Table 6.1.8** Oligonucleotides for qPCR for *Spag4l2*-deficient mice and ES cells.

Target	Primer	Sequence
<i>Protamin</i>	Protamin-p1-For	CCCTCTCCACCACTTTTCTTACCTT
	Protamin-p1-Rev	GGCGAGATGCTCTTGAAGTCT
<i>Odf1</i>	ODF1-p1-Forward	CGGGGCTCTTTTAGTCTTGCTA
	ODF1-p1-Reverse	TTCAAAGCCGCACACATTCAC
<i>Exon7</i>	Sun5-mus-E5-For	GGTAGACCCAGGAGAGGGAA
	Sun5-mus-E5-Rev	TGGTAAAGGGTCTAACGGCA
<i>Exon 9</i>	Sun5-mus-E8-For	GGGTGCCCTCAGAACTTGTC
	Sun5-mus-E8-Rev	CCTCTTCTGGCCACCTCCTA



## 6. 2 List of abbreviations

°C	Degree centigrade
ASS	Acephalic spermatozoa syndrome
AnP	Antarctic Phosphatase
APS	Ammonium persulfate
Arl3	ADP-ribosylation factor-like protein 3
ART	Assisted reproductive technology
Bm	Mitosis of spermatogonia
bp	Base pair(s)
BSA	Bovine serum albumin
CCDC42	Coiled-coil domain containing 42
cDNA	complementary DNA
CFAP52/WDRPUH/WDR16	Cilia and flagella associated protein 52
Cntrob	Centrobin
CO <sub>2</sub>	Carbon dioxide
Co-IP	Co-immunoprecipitation
COOH-terminus/C-terminus	Carboxyl-terminal
Ct	Cycle threshold
C-X-P	Cysteine-X-proline
DAPI	4',6'-diamidino-2-phenylindole
ddH <sub>2</sub> O	ultra-pure and sterile water
DEPC	Diethyl pyrocarbonate
DH10b	10-beta competent E.coli
DH5 $\alpha$	5-alpha Competent E.coli
DMEM	Dulbecco's Modified Eagle's Medium
DMSO	Dimethyl sulfoxide
DNA	Deoxyribonucleic acid
Dnase	Deoxyribonuclease
dsDNA	double-stranded desoxyribonucleic acid
DTT	Dithiothreitol
ECFP	enhanced cyan fluorescent protein
ECL	enhanced chemiluminescence
EDTA	Ethylenediaminetetraacetic acid
ER	Endoplasmic reticulum
ES	Embryonic stem
et al.	et alii (and others)
FBS	Fetal bovine serum
Fig	Figure
FKBP	FK506 binding protein
FRB	FKBP rapamycin binding
Fu	Protein serine-threonine kinase Fused
G1-S	Transition phase

GAPDH	Glyceraldehyde-3-Phosphate Dehydrogenase
gDNA	Genomic deoxyribonucleic acid
HA	Human influenza hemagglutinin
HANP1/ HIT2	Human testis-specific H1 histone
HEK293	Human embryonic kidney cell line
HEPES	Hydroxyethyl piperazineethanesulfonic acid
HOOK1	Protein Hook homolog 1
HPRT	Hypoxanthine phosphoribosyltransferase
HPRT	Hypoxanthine phosphoribosyltransferase
HRP	Horseradish peroxidase
HSPB10	Heat shock protein B10
HTCA	Head-to-tail coupling apparatus
ICSI	Intracytoplasmic sperm injection
Ift88	Intraflagellar Transport 88
IgG	Immunoglobulin G
$^{in}_m$	Intermediate spermatogonia
INM	Inner nuclear membrane
IPTG	isopropil- $\beta$ -D-1-tiogalactopiranósido
KASH	Klarsicht/ANC-1/Syne-1 homology
kb	kilobase
kDa	kilodalton
KIF27	Kinesin protein
KLC3	Kinesin light chain 3
Ko	Knock out
KOAc	Potassium acetate
LB	Lysogeny broth
LINC	Linker of nucleoskeleton and cytoskeleton
LMNA	lamin A
LMNB1	lamin B1
LMNB2	lamin B2
LMNC	lamin C
LoxP	locus of X-over P1
LSM	Confocal laser scanning microscopy
M	molar
$m2^{\circ}m$	Second meiotic division
MBP	maltose-binding protein
mg	Milligram(s)
$m^{in}$	Mitosis of intermediate spermatogonia
mL	Millimeter(s)
MTOC	Microtubule-organizing center
MYL6	Myosin
$M\alpha 3$	mouse $\alpha 3$ -tubulin
$M\alpha 7$	mouse $\alpha 7$ -tubulin
NH2-terminal/N-terminal	Amino-terminal

NIH3T3	Mouse embryonic fibroblast
Oaz3	Ornithine Decarboxylase Antizyme 3
OD	optical density
ODF1	Outer Dense Fiber of Sperm Tails 1
ODF2	Outer Dense Fiber of Sperm Tails 2
ODFs	Outer dense fibers
ONM	Outer nuclear membrane
PAGE	Polyacrylamide gel electrophoresis
pBpa	Unnatural amino acid p-benzoyl-L-phenylalanine
PBS	Phosphate-buffered saline
PCM	Pericentriolar material
PCR	Polymerase chain reaction
PFA	Paraformaldehyde
PK	Protein kinase
PI	Preleptotene
PL-FITC	Fluorescein isothiocyanate-labeled peanut lectin
PMC	Dense pericentriolar matrix
PMFBP1	Polyamine modulated factor 1 binding protein 1
PMSF	Phenylmethanesulfonyl fluoride
Prm1	Protamine 1
Prss21	Glycosylphosphatidylinositol-Anchored Serine Protease
PS	Perinuclear space
qPCR	Real-time PCR
qRT-PCR	Real-Time Quantitative Reverse Transcription PCR
RIM-BP3	RIMS Binding Protein 3
RNA	Ribonucleic acid
rRNA	Ribosomal ribonucleic acid
RS	Round spermatids
RT-PCR	reverse transcription-PCR
S.O.C	Super Optimal broth with Catabolite repression
SDS-PAGE	Sodium dodecyl sulfate-polyacrylamide gel electrophoresis
sHSPs	Small heat shock proteins
SPAG4/SUN4	Sperm associated antigen 4
SPAG4L/SUN5	Sad1 and UNC84 domain containing 5-like
SPAG4L2	Sad1 and UNC84 domain containing 5
SPATA6	Spermatogenesis Associated 6
Stk36	Serine/Threonine Kinase 36
Stra8	Stimulated by retinoic acid gene 8
SUN	Sad1p, UNC-84 domains
SYCP1	Synaptonemal complex protein 1
SYCP3	Synaptonemal complex protein 3
SYNE-1	Synaptic nuclear envelope protein 1
TAE	Tris-acetate-EDTA
TBST	Tris-buffered saline with Tween 20
TEMED	Tetramethylethylenediamine

TM1	Transmembrane domain I
TM2	Transmembrane domain II
TMs	Transmembrane domains
tRNA	Transfer ribonucleic acid
tRNA-aaRS	Orthogonal aminoacyl tRNA synthetase-tRNA
TZI	Human teratozoospermia
U	Units
UAAs	Unnatural amino acids
UV	Ultraviolet
V	Volt
v/v	volume/volume
w/v	weight/volume
WD40	WD40 domain-containing proteins
WHO	World Health Organization
WT	Wild type
x g (or RFC)	relative centrifugal force
μg	microgram(s)
μl	microliter(s)
μM	micromolar
μm	micrometer(s)